Doctoral Thesis

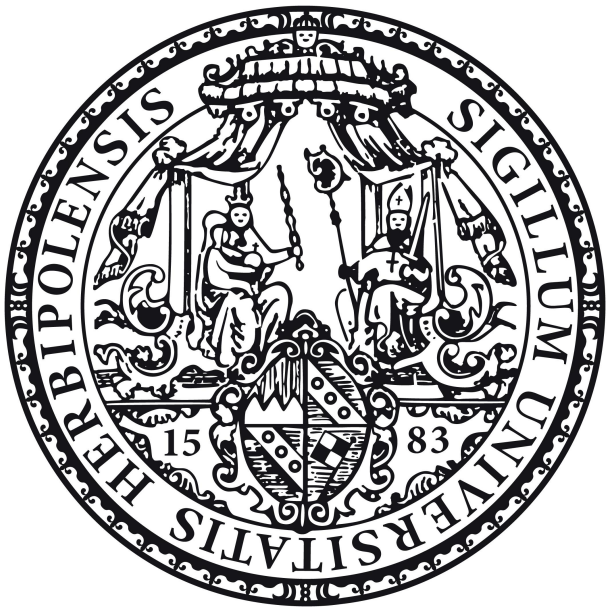

For a doctoral degree
doctor rerum naturalium (Dr. rer. nat.)
at the Graduate School of Life Sciences (Section Biomedicine),
Julius-Maximilians-Universität Würzburg

Tissue Engineering of a Vascularized Meniscus Implant

Tissue Engineering eines vaskularisierten Meniskus-Implantates

Submitted by

Antje Kremer

born in Bad Mergentheim

Würzburg 2019

Studienstiftung des deutschen Volkes

TERM Department Tissue Engineering & Regenerative Medicine

UK

Submitted on: .....

Members of the committee:
Chairperson: Prof. Dr. Thomas Dandekar
Primary supervisor: Prof. Dr. Heike Walles
Supervisor (second): Prof. Dr. Michael Raghunath
Supervisor (third): Dr. rer. nat. Jörg Teßmar
Supervisor (fourth): Dr. med. Kai Fehske
Supervisor (fifth): Dr. med. vet. PhD. Iris Ribitsch

Date of public defense: .....

Date of receipt of certificates: .....

Abstract

The knee joint is a complex composite joint containing the C-shaped wedge-like menisci composed of fibrocartilage. Due to their complex composition and structure, they provide mechanical resilience to the knee joint protecting the articular cartilage. Because of the limited repair potential, meniscal injuries do not only affect the meniscus itself but also lead to altered joint homeostasis and inevitably to secondary osteoarthritis.
The meniscus was characterized focusing on its anatomy, structure and meniscal markers such as aggrecan, collagen type I (Col I) and Col II. The components relevant for meniscus tissue engineering, namely cells, Col I scaffolds, biochemical and biomechanical stimuli were studied. Meniscal cells (MCs) were isolated from meniscus, mesenchymal stem cells (MSCs) from bone marrow and dermal microvascular endothelial cells (d-mvECs) from foreskin biopsies. For the human (h) meniscus model, wedge-shape compression of a hMSC-laden Col I gel was successfully established. During three weeks of static culture, the biochemical stimulus transforming growth factor β-3 (TGFβ-3) led to a compact collagen structure. On day 21, this meniscus model showed high metabolic activity and matrix remodeling as confirmed by matrix metalloproteinases detection. The fibrochondrogenic properties were illustrated by immunohistochemical detection of meniscal markers, significant GAG/DNA increase and increased compressive properties. For further improvement, biomechanical stimulation systems by compression and hydrostatic pressure were designed. As one vascularization approach, direct stimulation with ciclopirox olamine (CPX) significantly increased sprouting of hd-mvEC spheroids even in absence of auxiliary cells such as MSCs. Second, a cell sheet composed of hMSCs and hd-mvECs was fabricated by temperature triggered cell sheet engineering and transferred onto the wedge-shaped meniscus model. Third, a biological vascularized scaffold (BioVaSc-TERM®) was re-endothelialized with hd-mvECs providing a viable vascularized network. The vascularized BioVaSc-TERM® was suggested as wrapping scaffold of the meniscus model by using two suture techniques, the all-inside-repair (AIR) for the posterior horn, and the outside-in-refixation (OIR) for the anterior horn and the middle part.
This meniscus model for replacing torn menisci is a promising approach to be further optimized regarding vascularization, biochemical and biomechanical stimuli.

Zusammenfassung

Das Knie ist ein komplex zusammengesetztes Gelenk mit zwei C-förmigen Keilen aus Bindegewebsknorpel, die Menisken. Sie sorgen für die mechanische Belastbarkeit des Knies, wodurch der Gelenksknorpel geschützt wird. Aufgrund des limitierten Heilungspotentials beeinträchtigen Meniskusverletzungen nicht nur den Meniskus selbst, sondern schädigen auch das Gelenksgleichgewicht und führen zu sekundärer Osteoarthritis.
Der Meniskus wurde in seiner Anatomie, Struktur und Meniskusmarkern wie Aggrekan, Kollagen I und Kollagen II charakterisiert. Die Komponenten von Meniskus Tissue Engineering, Zellen, Kollagen I Materialien, biochemische und biomechanische Stimuli wurden untersucht. Meniskuszellen (MCs) wurden aus Meniskus isoliert, mesenchymale Stammzellen (MSCs) aus Knochenmark und dermale mikrovaskuläre Endothelzellen (d-mvECs) aus Vorhautbiopsien. Für das humane (h) Meniskus-Modell wurde die keilförmige Kompression eines hMSC-beladenen Kollagen I Gels erfolgreich etabliert. Während drei Wochen statischer Kultur führte der biochemische Stimulus transformierender Wachstumsfaktor β-3 (TGFβ-3) zu einer kompakten Kollagenstruktur. An Tag 21 zeigte dieses Meniskus-Modell eine hohe metabolische Aktivität und Matrixumbau durch die Detektion von Matrix-Metalloproteasen. Der Bindegewebsknorpel wurde durch immunhistochemische Detektion der Meniskusmarker, einem signifikanten GAG/DNA Anstieg und erhöhter Kompressionseigenschaften bestätigt. Für weitere Verbesserungen wurden biomechanische Stimulierungssysteme mittels Kompression und hydrostatischen Druck aufgebaut. Als Vaskularisierungsansatz führte die direkte Stimulierung mit Ciclopirox Olamine (CPX) sogar in Abwesenheit von Helferzellen wie MSCs zu einem erhöhten Sprouting der hd-mvEC Spheroide. Zweitens wurde ein hMSC/hd-mvEC Sheet mithilfe eines Temperatur-abhängigen Verfahrens produziert und auf das keilförmige Meniskus-Modell transferiert. Drittens wurde ein vaskularisiertes Biomaterial (BioVaSc-TERM®) mit hd-mvECs besiedelt, wodurch ein vitales Gefäßsystem bereitgestellt wurde. Die vaskularisierte BioVaSc-TERM® wurde als Hülle des Meniskus-Modells unter der Verwendung von zwei Nahttechniken vorgeschlagen: die All-Inside-Repair (AIR) für das Hinterhorn und die Outside-In-Refixation (OIR) für das Vorderhorn und den mittleren Teil.
Dieses Meniskus-Modell ist ein vielversprechender Ansatz für den Meniskusersatz, um in Vaskularisierung, biochemischer und biomechanischer Stimuli weiter optimiert zu werden.

Contents

List of Figures

List of Tables

List of Abbreviations

Abbreviation	**meaning**
2D	two-dimensional
3D	three-dimensional
AH	anterior horn
AIR	all-inside-repair
as	anti-sense
ASC	adipose tissue-derived mesenchymal stem cell
ATMP	advanced medicinal therapy product
bFGF	basic fibroblast growth factor
BioVaSc	biological vascularized scaffold
BM-MSC	bone marrow-derived mesenchymal stem cell
BSA	bovine serum albumin
C	carbon
CD	cluster of differentiation
cDNA	complementary DNA
CF	compression factor
CMI®	collagen meniscus implant®
CO_2	carbon dioxide
Col I	collagen type I
COLIA1	human pro-collagen I alpha 1
Col I gel	collagen type I hydrogel
Col II	collagen type II
Col IV	collagen type IV
Col X	collagen type X
CPX	ciclopirox olamine
CSL	cumulative sprouting length
CTGF	connective tissue growth factor
c_t-values	cycle threshold values
d	dermal
DAB	3,3'-diaminobencidine
DAPI	4',6-diamidino-2-phenylindole

DF	dermal fibroblast
DiI ($DiIC_{18}(3)$)	1,1'-dioctadecyl-3,3,3',3'-tetramethylindocarbocyanine perchlorate
DM	differentiation medium
DMEM	Dulbecco's modified eagle medium
DMSO	dimethyl sulfoxide
DNA	deoxyribonucleic acid
DS	decellularization solution
EC	endothelial cell
ECM	extracellular matrix
EDTA	ethylenediaminetetraacetic acid
EF1α	elongation factor 1α
E_{lin}	linear modulus
ELISA	enzyme-linked immunosorbent assay
em	emission
EPC	endothelial progenitor cell
eq	equine
EtOH	ethanol
ex	excitation
FBS	fetal bovine serum
FCM	flow cytometry
FCS	fetal calf serum
FDA	US Food and Drug Administration
FITC	fluorescein isothiocyanate
GAG	glycosaminoglycans
GAPDH	glyceraldehyde-3-phosphate dehydrogenase
GMP	good manufacturing practice
GNL	gel neutralizing solution
h	human
HCl	hydrochloric acid
HE	hematoxylin and eosin
HEPES	4-(2-hydroxyethyl)-1-piperazineethanesulfonic acid
HG	high glucose
HIF-1	hypoxia inducible factor-1
H_2O	water
H_2O_2	hydrogen peroxidase
HPRT	hypoxanthine-guanine phosphoribosyltransferase
HRE	hypoxia-response elements

HRP	horse radish peroxidase
HUVEC	human umbilical vein endothelial cell
IBMX	3-isobutyl-1-methylxanthine
IF	immunofluorescence
Ig	immunoglobulin
IHC	immunohistochemistry
IL	interleukin
ISC	Institute for Silicate Research
ISCT	International Society for Cellular Therapy
IT	isotype
ITS	insulin-transferrin-sodium selenite
LG	low glucose
MC	meniscal cell
Mg	magnesium
MHC	major histocompatibility complex
MMP	matrix metalloproteinase
mRNA	messenger ribonucleic acid
MSC	mesenchymal stem cell
MSC-CM	MSC-conditioned medium
MTT	3-(4,5-dimethyl-2-thiazolyl)-2,5-diphenyl-2H-tetrazolium bromide
mvEC	microvascular endothelial cell
NOS	number of spheroids
OA	osteoarthritis
OD	optical density
OIR	outside-in-refixation
o/n	overnight
P	passage
PBS^-	phosphate buffered saline, without divalent ions
PBS^+	phosphate buffered saline, with calcium chloride and magnesium chloride
PBST	PBS with 0.5 % (v/v) Tween-20
PCL	polycaprolactone
PCR	polymerase chain reaction
PCU	polycarbonate urethane
PDGF	platelet-derived growth factor
PDLLA	poly D/L lactide
PE	phycoerythrin
PenStrep	penicillin/streptomycin

PFA	paraformaldehyde
PGA	polyglycolic acid
PGE	polyglycidylether
PHD	prolyl hydroxylase domain containing enzyme
PHI	prolyl hydroxylase inhibitor
PH	posterior horn
PI	pars intermedia
PLA	polylactic acid
PLGA	polylactic co-glycolic acid
po	porcine
proMMP	proenzyme of MMP
PS	polystyrol
PU	polyurethane
pVHL	von Hippel Lindau tumor suppressor protein
qRT-PCR	qualitative real-time polymerase chain reaction
RNA	ribonucleic acid
RR	red-red
RT	room temperature
RW	red-white
SCF	stem cell factor
SD	standard deviation
SDS	sodium dodecyl sulfate
sGAG	sulfated glycosaminoglycans
SIS	small intestinal submucosa
SIS-ser	small intestinal submucosa without mucosal layer
SIS-muc	small intestinal submucosa with mucosa
SMSC	synovial membrane-derived mesenchymal stem cell
SOP	standard operating procedure
ss	single-stranded
TBS	Tris buffered solution
TBST	TBS with 0.5 % (v/v) Tween-20
TCPS	tissue culture polystyrol
TE	tissue engineering
TERM	Department Tissue Engineering & Regenerative Medicine
TGF	transforming growth factor
TGS	Tris/Glycine/SDS
TIMP	tissue inhibitor of metalloproteinases

VascuLife®	VEGF endothelial cell culture medium®
VE-cadherin	vascular endothelial cadherin
VEGF	vascular endothelial growth factor
VEGFR	VEGF receptor
vWF	van Willebrand factor
w/o	without
WW	white-white

Unit	**meaning**
°C	degree Celsius
A.U.	arbitrary unit(s)
d	day(s)
g	times gravity
g	gram(s)
h	hour(s)
Hz	hertz
kDa	kilodalton
kGγ	kilogray
kPa	kilopascal
L	liter
m	meter(s)
min	minute(s)
mmHg	millimeter(s) of mercury
N	normal
Pa	pascal
rpm	revolution(s) per minute
s	second(s)
U	unit(s)

Chapter 1

Introduction

In 1897, the meniscus was described as a functionless remnant tissue [1]. Thus, from the 19th century the recommended treatment for meniscal lesions caused by sport or age-related degeneration was the resection of the meniscus, namely total meniscectomy [2]. However, through total meniscectomy the anti-shock pad with spring function in the knee joint with its ability to absorb and to reduce pressure is lost [3]. The remaining articular cartilage can not compensate this function and the constant pressure loaded onto the knee joint will inevitably induce degeneration of the articular cartilage. The final consequence of this process is arthritis and osteoarthritis (OA). As reported in 2015, 50 % of women and 33 % of men in Germany with an age between 70 and 79 years suffered from arthritis with more than half related to the knee joint [4]. For the prevention of secondary cartilage degeneration, arthritis and OA, a sustainable treatment for meniscal lesions is required.

Up to the 20th century, total meniscectomy was the standard approach to treat meniscal injuries [5]. Serendipitously, negative long-term effects of total meniscectomy such as cartilage degeneration, arthritis and pain were reported [6]. Starting from the 1970s/80s, partial meniscectomy gained interest [7], as it was found to reduce the loading stress between femur and tibia by more than 50 % [8]. In addition, the first meniscus transplants dated back to 1989 [9]. Based on these studies, it became clear that the meniscus plays an important role in the knee joint. Thorough understanding and study of the meniscus anatomy, structure and biomechanics was and is still mandatory to treat meniscal lesions properly [3]. Until today, there is no optimal treatment for meniscal injuries. Meniscal sutures and partial meniscectomy are still the state of the art trying to maintain as much meniscal tissue as possible [5]. The two synthetic implants on the market, the Actifit® polyurethane (PU) meniscus scaffold and the collagen meniscus implant® (CMI®), are only for a small field of indication after partial meniscectomy. Alternatively, meniscus tissue engineering may offer the potential to build a personalized and vascularized meniscus implant with regenerative potential for sport-related injuries and the aging population

[3]. For successful tissue engineering of a meniscus implant, knowledge of the meniscus anatomy, structure, biochemical composition and biomechanics is necessary.

1.1. Meniscus physiology

Two menisci are located in the knee joint: the medial and the lateral meniscus (figure 1.1 A, B). The menisci are two crescent-shaped wedges of fibrocartilage located between the femur and the tibia [3]. The menisci are fixed in the knee joint by the horn attachments to the tibial plateau and the ligaments of Humphrey and Wrisberg to the femur (figure 1.1 B) [10]. Moreover, the transverse ligament attaches the medial and the lateral meniscus to each other [10]. Different forces such as shear, tension and compression act on the menisci (figure 1.1 C) [3]. During everyday activity, the menisci are compressed by axial tibiofemoral forces [3]. These vertical compressive forces are converted to horizontal hoop stresses by the wedge-shape and the horn attachments of the menisci [3]. In addition, the meniscus is deformed radially and shear stress acts between the collagen fibers [3]. Thus, the contact area between femur and tibia is enlarged for chondroprotection by weight distribution [5].

At birth, the meniscus is completely vascularized [11]. The neurovascularization decreases during life, with aging, weight bearing and knee motion as supposed reasons [11]. In adulthood, the meniscus has a gradual vascularization of approximately (approx.) 10 to 25 % of the meniscus (figure 1.1 D) with a vascularized abaxial part, namely the vascular/neural red-red (RR) zone [3]. The neurovascularization decreases in the red-white (RW) region until reaching the avascular/aneural white-white (WW) zone [3]. The healing capacity of each region correlates with the vascularization level [12].

The meniscus has a complex and heterogeneous collagen structure, cellular and biochemical composition. In general, meniscal tissue is a highly hydrated fibrocartilaginous tissue with a water content of approx. 72 % [3]. The 28 % organic material are composed of 75 % collagen, 17 % glycosaminoglycans (GAG), 2 % deoxyribonucleic acid (DNA), <1 % adhesion glycoproteins and <1 % elastin [13, 14]. The composition between individuals varies related to age, injury or pathological state [15].

The orientation of the collagen fibres in the meniscus directly correlates with its load bearing function. Petersen & Tillmann (1998) revealed three distinct layers in the meniscus by scanning electron microscopy (SEM) (figure 1.2 A) [16]. (1) The meniscus surfaces to the tibial and femoral sides represent a meshwork of thin collagen fibrils, named as superficial layer [16]. (2) The lamellar layer is located beneath the superficial layer and

contains radially oriented fibers in the external circumference of the anterior horn (AH) and the posterior horn (PH), whereas all other collagen fibril bundles are randomly oriented [16]. (3) The central main layer represents the main portion of the meniscus with circumferentially oriented collagen fibril bundles creating the high tensile strength of the meniscus [16].

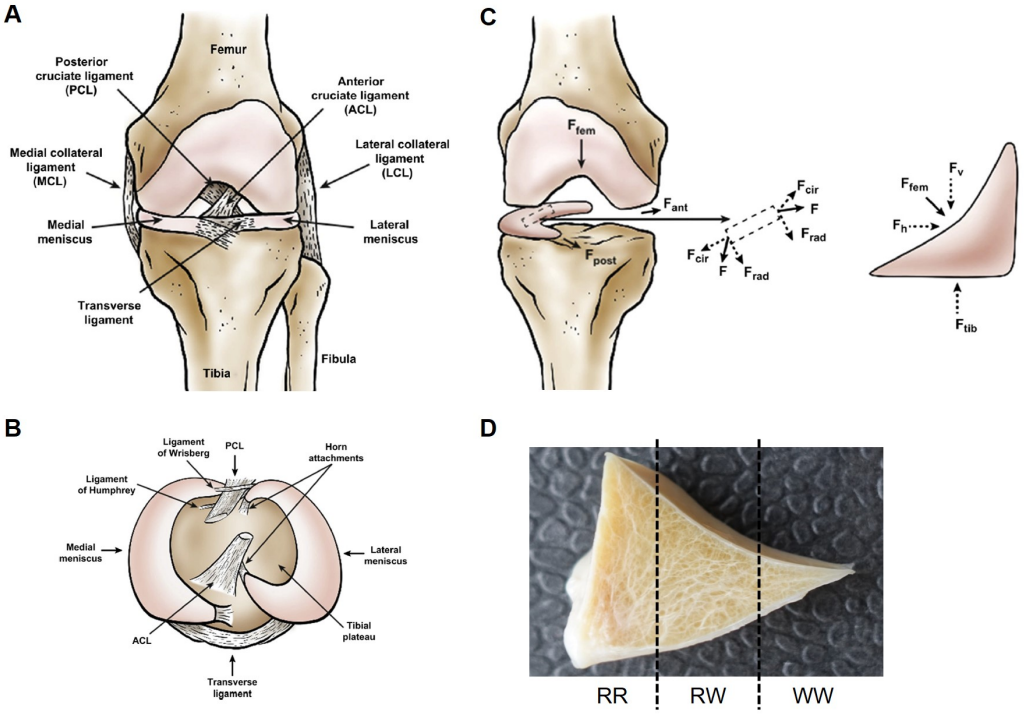

Figure 1.1.: Anatomy, force transduction and gradual vascularization of the menisci. A Anterior view of the knee joint with the menisci located between femur and tibia. Reprinted from [3] with permission from Elsevier. **B** Superior view of the tibial plateau with the medial and the lateral meniscus. Reprinted from [3] with permission from Elsevier. **C** During normal activity and loading, different forces are transduced upon and throughout the meniscus. For simplicity, the lateral meniscus is shown. Reprinted from [3] with permission from Elsevier. **D** Gradual vascularization: the meniscus is composed of the vascular RR, the RW and the avascular WW zone.

This special collagen structure defines the biomechanical properties of the meniscus such as a high circumferential tensile strength between 80 and 125 MPa, a radial tensile strength between 1.7 and 3.6 MPa, an aggregate modulus of approx. 0.15 MPa measured during compression and a permeability of approx. 1.9×10^{-15} $N^{-}s^{-}$ as defined as the ease of fluid flowing through the tissue [15, 17].

In addition to the complex collagen structure, the cellular distribution of the meniscal tissue shows three different cell morphologies of meniscal cells (MCs) (figure 1.2 B).

The superficial zone contains fusiform cells directly located beneath the tissue surface, the abaxial outer one-third contains fibroblast-like cells with elongated morphology and the axial inner two-thirds of RW and WW contain fibrochondrocytes with round or oval morphology [15, 18]. Moreover, different collagen types are found looking at the biochemical composition of the meniscus (figure 1.2 B). Collagen type I (Col I) is the main collagen of the meniscus, predominantly found in the abaxial one-third [18]. In contrast, the main collagen type of hyaline cartilage such as articular cartilage is Collagen type II (Col II) [19]. The axial two-thirds of the meniscus contain Col I and Col II. The WW zone is composed of 70 % collagen by dry weight with 60 % Col II and 40 % Col I [3]. Collagen type X (Col X) expression only occurs in osteoarthritic cartilage indicating chondrocyte hypertrophy [20]. Other important components of the meniscus extracellular matrix (ECM) are proteoglycans composed of a core protein decorated with GAG [3]. The major large proteoglycan of the meniscus is aggrecan and the main small proteoglycans are biglycan and decorin [21]. These proteoglycans especially located in the inner compressed two-thirds enable water absorption protecting the meniscus against compression and loading [15, 21].

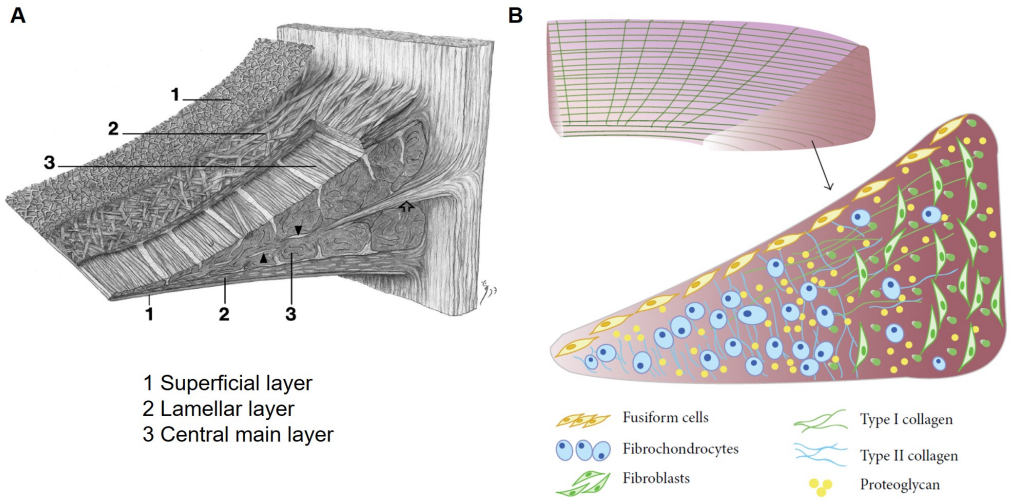

Figure 1.2.: Collagen structure, cellular and biochemical composition of the meniscus. A Synoptic drawing of the collagen structure: (1) the superficial network of thin collagen fibrils on the femoral and tibial surface, (2) the lamellar layer with radially arranged collagen fibers in the external circumference, (3) the central main layer with circular collagen fibril bundles. Arrowheads indicate radial collagen fibrils located between the circular fibril bundles. Penetration of connective tissue from the joint capsule is indicated by the arrow. Adapted from [16] with kind permission. **B** Schematic diagram of the cellular and biochemical composition: fibroblast-like cells in the RR zone are spindle-shaped, while cells in the RW and WW region are described as oval-shaped fibrochondrocytes. The cells of the superficial zone are fusiform. Col I is predominantly expressed in the RR part, while the ratio of Col I and Col II in the WW section is 2:3. Adapted from [18], open access article.

The meniscus anatomy, collagen microstructure, cellular and biochemical composition mediate its diverse functions. The crucial functions of the meniscus include shock absorption, load bearing and transmission resulting in a decreased stress on the articular cartilage and increased stability of the knee joint, as well as joint lubrication, articular cartilage nutrition and propioception [22]. Understanding the meniscus physiology is important for the next chapter: meniscus pathophysiology.

1.2. Meniscus pathophysiology

Meniscal injuries occur in young and old patients, typically resulting from twisting movements, shearing motion, hyperextension or actions of great forces [23]. In young patients, most of the meniscal injuries are sport-related, while the aging population faces meniscus degeneration [3]. It was shown that degenerated meniscal tissue has an increased water content, decreased collagen and GAG contents, reduced elasticity and compressive moduli [13, 24]. In general, tears of the medial meniscus are more frequent with a ratio of 2:1 compared to lateral meniscal tears, as the lateral meniscus is more mobile due to less tight ligament fixation [15].
The currently preferred meniscus repair aims at preserving as much meniscal tissue as possible [5]. Unfortunately not all meniscal injuries can be repaired leading inevitably to the formation of secondary OA [5]. Additionally, it is known that osteoarthritic changes of the knee joint effect the structure and functions of the meniscus [22]. Thus, there is a direct relationship between meniscal injuries and OA demonstrating the importance of a successful treatment for meniscal lesions.
The current strategies comprise conservative therapy with anti-inflammatory treatment and rehabilitation, and meniscus repair by suturing, partial and total meniscectomy, allografts or implants [15]. For meniscus repair strategies, open repair or arthroscopic techniques are known [3]. Today, open repair is obsolete as it requires the dissection of parts of the meniscus [15]. The arthroscopic techniques are divided in three groups inside-out, outside-in and all-inside techniques. The outside-in-refixation (OIR) technique passes the suture from outside to inside through the meniscus rim and then the meniscus body [25]. For the OIR it is a challenge to access the posterior part of the meniscus [22]. The all-inside-repair (AIR) technique is based on vertical sutures containing special suture anchors. These anchors are passed through the capsular bed and through the meniscus body followed by fixating them inside the knee joint [25]. However, the standard treatment for meniscal lesions is still meniscectomy: 65 % of all meniscal lesions are treated with

meniscectomy [26]. Today, partial meniscectomy preserving the peripheral rim of the meniscus is the gold standard [5]. Though, partial meniscectomy means a loss of meniscal tissue and induces an early onset of OA [27].
Implants such as the PU-based meniscus scaffold Actifit® (Orteq Sports Medicine) and the collagen-based scaffold CMI® (Ivy Sports Medicine) have proven to be safe implants following partial meniscectomy, as the implantation requires an intact meniscal rim, AH and PH for fixation [22]. Several studies have shown positive outcomes of these scaffolds. The Actifit® scaffold performed consistently on second-look arthroscopy indicated by good tissue in-growth and implant integration after 12 months [28]. A long-term study with a minimum of 10 years' follow-up of meniscus substitution with the CMI® scaffold showed significant pain reduction and functional improvement without development or progression of degenerative knee joint diseases for most cases [29]. However, both implants are appropriate only for a narrow window of indications: the knee joint has to be stable and well-aligned with only low grades of degeneration [27]. In contrast, transplantation of allografts is indicated for patients after a total meniscectomy [22]. An allograft is a transplantable tissue from a genetically different person. At early OA stages, allografts can be transplanted to contribute to a delay of joint degeneration [27]. However, allografts are limited by costs, fitting size, preservation of biomechanical properties and the risk of rejection [22, 27].
As the current treatment possibilities are limited and not optimal, there is high need for new treatment strategies. Meniscus tissue engineering is discussed in the next chapter introducing tissue engineering in general and its potential to build a personalized meniscus implant.

1.3. Tissue engineering to build a vascularized meniscus implant

Tissue engineering came up in context of transplantation. Due to the lack of donor tissue in the 1960s/70s, first tissue engineered skin products were developed [30, 31]. However, the modern term tissue engineering was only introduced in 1987 [31]. Tissue engineering was defined as '*an interdisciplinary field that applies the principles of engineering and life sciences toward the development of biological substitutes that restore, maintain, or improve tissue function*' by Langer and Vacanti in 1993 [30]. This chapter describes tissue engineering and its challenges regarding vascularization, matrix synthesis and remodeling.

1.3.1. Cycle of tissue engineering

Langer and Vacanti (1993) suggested three components to build new tissue: cells, scaffolds and chemical stimuli such as growth factors [30]. Later, mechanical stimuli as further component were added [31].
The interaction of the components relevant for tissue engineering are visualized in figure 1.3 showing the cycle of tissue engineering. For tissue engineering, a biopsy of a patient is taken. Cells are isolated from this biopsy and expanded in vitro. The expanded cells are combined with an appropriate scaffold or combination of scaffolds. 3D tissue is then generated by static or dynamic 3D culture in bioreactor systems imitating the physiologic environment by pulsatile flow or mechanical stimulation. The generated artificial tissue is usable as 3D in vitro test system or implant for the patient [32].

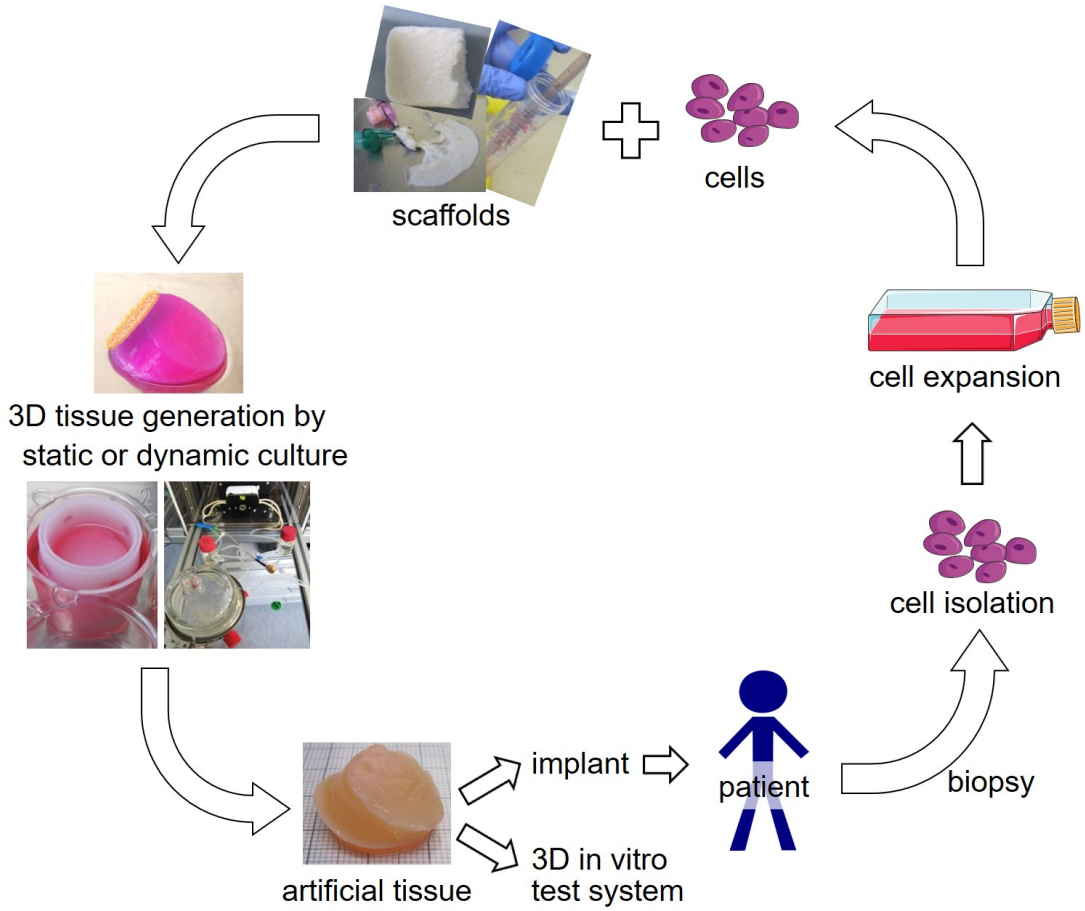

Figure 1.3.: The cycle of tissue engineering. Cells are isolated from a tissue biopsy of a patient. After cell expansion, the cells are combined with scaffolds to generate 3D tissue by static or dynamic culture in a bioreactor system. The generated artificial tissue is usable as 3D in vitro test system or to be implanted back into the patient.

A major problem of tissue engineering is the mass transfer limitation, as most of the tissue engineered constructs lack a vascular network [31]. Diffusion processes limit the supply of oxygen and nutrients within tissue engineered constructs to a distance of 100 to 200 μm from the next capillary [33]. Therefore, implementing vascularization to artificial tissue constructs is of high importance.

1.3.2. Angiogenesis and vascularization strategies in tissue engineering

1.3.2.1. Angiogenesis and its master regulator hypoxia

The formation of blood vessels in vivo is based on two processes: angiogenesis and vasculogenesis [34]. Vasculogenesis describes the de novo formation of a primitive vascular network normally occurring during embryogenesis [34]. Angiogenesis is the formation of capillaries from pre-existing blood vessels; it implies expansion and remodeling of the vascular network [35]. The underlying principle of angiogenesis is proliferation of endothelial cells (ECs) of existing blood vessels and involves two mechanisms: endothelial sprouting and intussusceptive microvascular growth. Sprouting comprises EC migration, proliferation and tube formation [35]. Usually, ECs are quiescent and divide less than once in 100 to 300 days [36]. However, they are activated in the presence of pro-angiogenic signals such as vascular endothelial growth factor (VEGF), platelet-derived growth factor (PDGF), angiopoietin and fibroblast growth factor (FGF) [36, 37]. Sprouting is initiated when a single EC becomes a tip cell and starts a new sprout in the direction of an angiogenic growth factor gradient [38]. To achieve this, the tip cell has to break through the basement membrane, whereas neighboring cells simultaneously act as stalk cells [38]. These sprouts do not contain a lumen. After tip cell selection and migration, sprouts from neighboring vessels fuse and build a functional vessel linkage, an anastomosis [38]. To provide vessel stabilization and to regulate vessel perfusion in parallel, mural cells such as pericytes in capillaries and vascular smooth muscle cells in larger blood vessels are recruited to the immature vasculature. Acting as mural cells, MSCs support the formation of microvascular networks by ECs [39]. MSCs secrete a variety of cytokines and growth factors which have paracrine and autocrine effects [40]. Through paracrine actions via extracellular microvesicles or secreted factors, MSCs are known to modulate angiogenesis [41], apoptosis [42], differentiation [43] and immune responses [44] of surrounding cells. It has been shown that interactions between MSCs and endothelial progenitor cells (EPCs)

induce differentiation towards a pericyte-like phenotype [45]. However, not all MSCs are able to act as pericyte [46]. Nevertheless, such interactions support the maturation of newly formed luminal structures [47].

The hypoxia-inducible factor-1α (HIF-1α) is a transcription factor and master switch of angiogenesis. Under normoxic conditions, HIF-1α is almost immediately degraded after synthesis by hydroxylation of one or two proline residues of HIF-1α by the prolyl hydroxylase domain containing enzymes (PHDs) (figure 1.4). The degradation of HIFs is inhibited by a hypoxic environment or pharmacologically by a prolyl hydroxylase inhibitor (PHI) (figure 1.4).

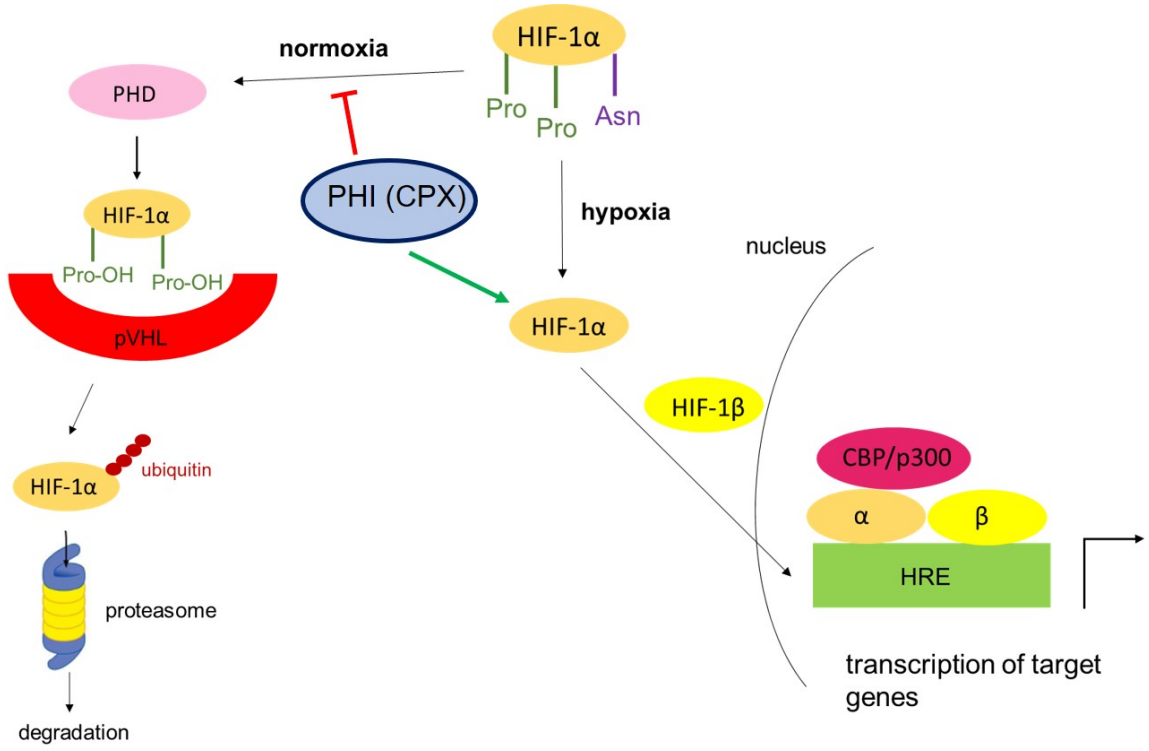

Figure 1.4.: Role of PHIs such as CPX in the oxygen-dependent regulation of HIF-1α pathway. Under normoxic condition, HIF-1α is almost immediately degraded after synthesis. Hydroxylation of one or two proline residues of HIF-1α by the PHDs initiates the degradation. Then, hydroxyprolines enable the binding of von Hippel Lindau tumor suppressor protein (pVHL) to HIF-1α. Thus, HIF-1α is tagged by ubiquitination and marked for degradation via the proteasome. Under hypoxic condition, which may also be pharmacologically induced by a PHI such as CPX, the prolyl hydroxylase is inhibited and fails to oxidize the two prolines of HIF-1α. As it is not marked for degradation and escapes from ubiquitination, levels of HIF-1α rapidly increase. Consequently, accumulated HIF-1α translocates to the nucleus, dimerizes with metabolically stable HIF-1β and binds to hypoxia-response elements (HREs) within the promoters of target genes. Thereby, gene expression of angiogenic factors such as VEGF, PDGF and FGF is induced. Adapted from [48] with kind permission.

Proline hydroxylases are iron-containing dioxygenases. Thus, they can be inhibited by substrate competition at the active site of the enzyme or iron chelation. Inhibition leaves two prolines of HIF-1α unhydroxylated. Thus, HIF-1α is not marked for degradation by the proteasome, and intranuclear levels of HIF-1α increase, leading to an upregulation of various genes in tissues facing hypoxia. A set of genes is involved in angiogenesis: VEGF, PDGF and FGF [36, 49].
The broad effects at gene expression level make PHIs such as ciclopirox olamine (CPX) attractive compounds in promoting local angiogenesis by HIF-1α stabilization [50]. Under normoxic conditions CPX, a lipophilic bidentate iron chelator, stabilizes HIF-1α [50, 51]. Thereby, CPX prevents the degradation of HIF-1α imitating an artificial hypoxia state, which results in an increased gene expression and an upregulation of angiogenic factors such as VEGF, PDGF and FGF which have been shown to have synergistic effects on sprouting [52]. Lim et al. (2016) showed that CPX in combination with the lysophospholipid sphingosine-1-phosphate promoted diabetic wound closure by an increase of functional vessels, accelerated granulation tissue formation and an increase in collagen fibers [51]. In that study, CPX and sphingosine-1-phosphate were applied subcutaneously to rats by implanted sponges [51]. These findings correlate with those of Ko et al. (2011) who reported significantly accelerated wound closure, increased angiogenesis, and increased dermal cellularity by CPX [53].

1.3.2.2. Vascularization strategies

The complex process of angiogenesis and its master regulator hypoxia are important for the revascularization of tissue engineered constructs [31]. A vascular network provides oxygen supply, nutrients, drugs, and the removal of carbon dioxide and waste products. For engineering vascularized tissues, vascularization can be induced by cells or scaffolds: cells such as ECs form vessels through neoangiogenesis and vascularized scaffolds provide tubulus or vessel-like structures [34].

Vascularization induced by cells

Vascularization induced by cells is divided by Novosel et al. (2011) in five groups: in vitro prevascularization, in vivo prevascularization, stimulation of neoangiogenesis by growth factors, immobilization of adhesion peptides or co-culture of different cell types [34].
For in vitro prevascularization, ECs combined with other cell types such as muscle cells are seeded on scaffolds to form a 3D prevascular network. After implantation, this prevascular

network ideally anastomoses with the in-growing vasculature of the host [33]. Tremblay et al. (2005) built in vitro an endothelialized skin construct with a vascular network in the dermis, by combining ECs, fibroblasts and keratinocytes in a collagen sponge [54]. On day 4 after implantation into mice, the inosculation of the in vitro tissue engineered capillaries with the host vasculature was shown [54].

Second, in vivo prevascularization uses a tissue engineered, non-vascularized construct which is implanted into a host body for de novo vascularization of the construct [34]. Sekine et al. (2008) showed the in vivo prevascularization of 3D cardiac tissue produced by layering cardiac cell sheets after implantation in rat hearts [55]. These cell sheets were produced by harvesting confluent cell monolayers from temperature-responsive cell culture dishes after temperature reduction [55].

Third, neoangiogenesis can be stimulated by growth factors such as VEGF, basic FGF (bFGF) and hepatocytes growth factor (HGF), or indirect angiogenic factors such as PDGF, transforming growth factor β (TGFβ) and angiopoietin [34]. The delivery of angiogenic factors is achieved directly by systemic application with the risk of uncontrollable blood vessel development or indirectly by incorporation into a biomaterial or indirect stimulation strategies [56]. As example for a simple scaffold-loading approach, matrigel plugs containing a combination of VEGF, PDGF and FGF were subcutaneously implanted into mice and showed high blood vessel formation [52]. Scaffolds are modified to provide binding sites for growth factors to enable a controllable release. One study showed the successful immobilization of VEGF in a collagen scaffold and demonstrated the increased penetration and proliferation of ECs within the collagen scaffold [57]. An indirect stimulation approach for angiogenic factor delivery uses PHIs such as CPX which has been shown to promote angiogenesis by HIF-1α stabilization (figure 1.4) [50]. Lim et al. (2013) showed an increased sprouting response of human umbilical vein endothelial cells (HUVECs) to CPX in a microfluidic system in the presence of fibroblasts. An additional approach towards neoangiogenesis by growth factors are transfected cells overexpressing angiogenic factors [34]. VEGF producing bone marrow-derived MSCs (BM-MSCs) have been shown to enhance vascularization in a study aiming at producing tissue engineered bone [58]. For clinical application, approaches enabling a controllable release of growth factors are of interest [56].

Fourth, the immobilization of adhesion peptides is another strategy to induce neoangiogenesis [34]. Conconi et al. (2010) studied the angiogenesis effect of four small peptides containing adhesion sequences originally developed to enhance cell adhesion on scaffolds [59]. They found out that less cell adhesion properties correlated with anti-angiogenic effects [59]. Hamada et al. (2003) reported the angiogenic effect of a synthetic osteopontin-derived peptide by effecting the adhesion and migration activity of ECs [60].

The adequate co-culture of different cell types with ECs demonstrates the fifth group to enhance neoangiogenesis according to Novosel et al. (2011) [34]. ECs of divergent origins such as dermal microvascular endothelial cells (d-mvECs), HUVECs, aortic ECs, capillary ECs or EPCs are applicable. It has been shown that ECs of divergent origin behaved different regarding responsiveness, but similar in the pattern of responsiveness to a receptor-dependent stimulation [61]. Co-culture of ECs with other cell types mediates communication inducing growth factor production, paracrine effects or cell-cell interactions [34]. Preferred cell types of co-culture strategies with ECs are mostly fibroblasts or MSCs. Fibroblasts have been shown to modulate the migration and network formation of ECs [62]. In addition, they are able to secrete angiogenic factors such as VEGF for example caused by hypoxia [51]. Lim et al. (2016) showed increased VEGF secretion of fibroblasts caused by a pharmacologically induced hypoxia with CPX leading to a pro-angiogenic response of HUVECs [51]. Chen et al. (2010) developed a 3D engineered vascular network by in vitro co-culture of ECs with fibroblasts loaded onto a fibrin gel [63]. The vascular network of this construct formed anastomoses with the host vasculature after implantation into immune compromised mice [63]. The success of forming anastomoses was increased in this study by increasing the density of fibroblasts and using EPCs instead of HUVECs [63]. Beyond fibroblasts, MSCs support the formation of microvascular networks [39]. MSCs are known to secrete angiogenic factors and modulate angiogenesis [40, 41]. In a co-culture study of MSCs with EPCs, angiogenesis was induced without the addition of exogenous growth factors suggesting cross-talk through a paracrine mechanism or direct cell-cell contact [64]. Loibl et al. (2014) showed differentiation of MSCs towards a pericyte-like phenotype by direct cell-cell contact in an in vitro co-culture of MSCs and EPCs [45].

Vascularization induced by scaffolds

Vascularized scaffolds have high potential to form a vascular tree [34]. This paragraph focuses on scaffolds providing a natural or synthetically rebuilt vascular architecture.
Naturally vascularized scaffolds reuse biological structures of tissues after decellularization providing the advantage of biocompatibility and relevant dimensions of a vascular network [34]. The small intestinal submucosa (SIS) is a tissue-derived scaffold after decellularization of an intestine segment, in most cases, porcine. Walles et al. (2005) developed a SIS-derived scaffold with a preserved capillary structure after decellularization of a porcine small bowl segment [65]. The preserved capillary structure is reseedable with ECs providing an artificial vascular network which can be perfused via a feeding artery, draining vein and a capillary bed utilizing a bioreactor system [65, 66]. This vascularized scaffold, so called the biological vascularized scaffold-TERM® (BioVaSc-TERM®), was used to build

vascularized skin [67], liver [66] or bone models (data not published, Christoph Rücker). Furthermore, it was used as a wrapping structure for a meniscus collagen scaffold (figure 1.5 A) [68]. Another vascularized scaffold is the engineered bioartificial heart of Ott et al. (2008) [69]. A cadaveric decellularized rat heart was completely reseeded with cardiac cells or ECs and cultured in a bioreactor system with simulated cardiac physiology (figure 1.5 B) [69]. Remarkably, they observed macroscopic contraction on day 4 and pump function of the bioartificial heart on day 8 of dynamic culture [69]. However, natural scaffolds have limitations in standardization and reproducibility, as most of them are animal-derived and hence are subject to interindividual variations.

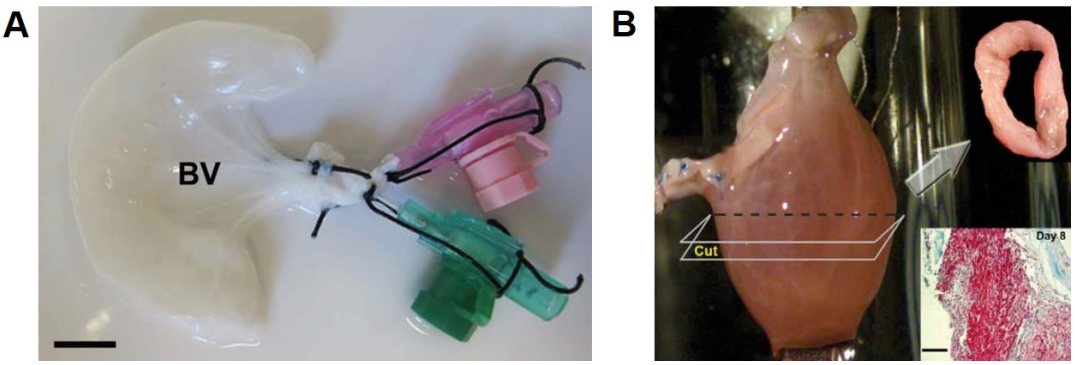

Figure 1.5.: Naturally vascularized scaffolds. A Photograph of a meniscus model composed of a collagen-based scaffold placed in the BioVaSc-TERM® (BV). Scale bar, 1 cm. Adapted from [68] with kind permission. **B** A bioartificial heart was engineered by recellularizing of a whole decellularized rat heart: bioartificial heart on day 4 of perfusion culture in a working heart bioreactor (left), cross-sectional ring of the bioartificial heart on day 8 (upper right) and Masson's trichrome staining of a ring-shaped section (lower right). Scale bar, 100 mm. Adapted from [69] with kind permission.

As alternative, synthetically manufactured vascularized scaffolds are of interest. The biodegradability, porosity, biocompatibility and interconnectivity between pores are important properties of synthetically manufactured vascularized scaffolds [33, 34]. A challenge lies in the manufacturing of porous structure of approx. 7μm, corresponding to the average width of capillaries in vivo [70]. Bertassoni et al. (2014) used a 3D micromolding technique to build microchannel networks within a hydrogel construct [71]. His group showed the successful formation of a HUVEC monolayer inside the microchannel [71]. They claimed being able to manufacture microchannels with a diameter from approx. 1000 down to 150 μm [71]. Organ printing by rapid prototyping or additive layer-by-layer biomanufacturing aims at printing a vascular tree directly into a bioprinted tissue construct [72]. McGuigan et al. (2006) engineered vascularized tissue constructs by modular assembly [73, 74]. The vascularized tissue constructs were then densely packed and placed in a

tubular mold resulting in perfusion tubes [73, 74]. However, organ printing still faces a lot of challenges in the human organ computer-aided design, the bioprinter device, the bioink and again proper vascularization [72].
In summary, vascularization remains a challenge for tissue engineering and most likely, a combination of multiple strategies is required to establish adequately vascularized and functional tissue implants.

1.3.3. Meniscus tissue engineering

Coming to meniscus tissue engineering, vascularization is not the only challenge. Selecting an optimal cell source, a suitable biochemical and biomechanical environment, and an appropriate type of scaffold are challenges building a meniscus implant [3]. Further, appropriate compressive and tensile material properties, surface characteristics to reduce chondral damage of femur and tibia, and a fixation technique to reduce extrusion of the implant have to be evaluated [22]. This chapter gives an overview of meniscus tissue engineering and its important components.

1.3.3.1. Cell sources

For meniscus tissue engineering, different cell sources are used: autologous and allogeneic or xenogeneic cells [3]. Autologous cells directly isolated from the patient are used to generate personalized patient-specific 3D tissue, whereas allogeneic cells derived from a genetically different individual of the same species, or xenogeneic cells derived from a different species, therefore genetically and immunologically incompatible, carry the risk of rejection. Different cell types have been studied to generate a tissue engineered meniscus model: MCs, stem cells such as MSCs derived from the bone marrow (BM-MSCs), adipose tissue (ASCs), synovial membrane (SMSCs) or co-cultures of these cell types [18].
MCs isolated from meniscus biopsies demonstrate a heterogeneous cell source as described in section 1.1. Therefore, different MCs are gained by isolation from meniscus biopsies: fusiform cells, fibroblast-like elongated cells and round/oval fibrochondrocytes [3]. Many studies still focus on MCs. Müller et al. (1999) seeded MCs into matrices composed of Col I, Col II and GAG in vitro and showed an increase in GAG synthesis and cell number [75]. They claim to have been first to publish results on MCs seeded in a collagen matrix [75]. However, using MCs requires two surgeries with the risk of tissue scarcity, donor site morbidity and joint infection: first, taking a biopsy to isolate autologous MCs and

second, to implant the tissue engineered meniscus implant [3]. Moreover, the number of healthy MCs to be obtained from a meniscus biopsy is limited [18]. Additionally, passaging during cell expansion can cause dedifferentiation of MCs leading to a changed cellular phenotype and changed gene expression profile as Col II decrease [76]. Different strategies such as adding FGF to the cell culture medium or hypoxic conditions for cell culture have shown to inhibit dedifferentiation processes [18]. However, the limited availability of healthy autologous MCs particularly after meniscal injury or degeneration remain problems building meniscus implants [3].

Thus, the use of stem cells has high potential. Many studies focus on MSCs from different sources such as bone marrow, adipose tissue or synovial membrane. According to the definition of the International Society for Cellular Therapy (ISCT), MSCs adhere to plastic surfaces, have specific cluster of differentiation (CD) surface markers such as CD73, CD90 and CD105 and have multi-lineage differentiation potential: adipogenic, osteogenic and chondrogenic potential [77]. From literature we know that MSCs secrete trophic factors important for musculoskeletal therapies [78]. Furthermore, it was reported that hypoxic conditions increase MSC secretion of trophic factors important for chondrogenesis such as HGF, TGFβ or Col II [78]. Taken together, two main abilities of MSCs are important for meniscus tissue engineering: first, their potential to differentiate to a meniscal/fibrocartilaginous phenotype and second, the secretion of trophic factors contributing to the intrinsic healing process [3].

Different strategies to use MSCs for meniscus tissue engineering have been studied. SMSCs were intraarticularly injected in pigs to treat a massive meniscus defect and showed promotion of meniscus regeneration [79]. However, the direct intraarticular and also the intravascular injection of MSCs via vascular access channels or vascular tunnels bare the risk of side effects in the knee joint or other areas [3]. Zellner et al. (2013) applied MSCs locally after suturing menisci to support meniscus regeneration [80]. They showed in rabbits with a longitudinal meniscal tear in the avascular zone that the augmentation of a meniscal suture with BM-MSCs in combination with a hyaluronan-collagen composite scaffold led to meniscus repair by a meniscus-like differentiated tissue [80]. To repair bigger defects or to restore the meniscus after partial meniscectomy, there are two cell-free meniscus implants on the market. The application of MSCs together with cell-free scaffolds to generate a personalized functional meniscus implant ex vivo has high potential to treat critical size meniscus defect. Pabbruwe et al. (2010) seeded human BM-MSCs into a collagen scaffold leading to enhanced mechanical properties such as tensile strength and suggested it as potential repair method for meniscal tears in the avascular zone [81].

In addition to monocultures, co-culture systems of different cell types were investigated. Co-cultures can be performed in a mixed cell culture with direct cell-cell contact or in a

separated cell culture with indirect transfer of growth factors [18]. As MSCs are known to secrete factors important for musculoskeletal therapies [78], they are a preferred cell type for co-culture studies of meniscus tissue engineering [18]. Direct co-culture of MCs with MSCs led to an increased ECM formation by upregulation of aggrecan, Col I and Col II mRNA expression and an increase of GAG [82]. Cui et al. (2012) suggested that hypertrophy may be prevented by co-culturing MCs with MSCs [83]. Taken together, MSCs and co-culture studies with MSCs have high potential for meniscus tissue engineering.

1.3.3.2. Biochemical stimulation

After selecting appropriate cell sources, these cells have to be subjected to biochemical stimuli leading to the generation of meniscal tissue. Different biochemical stimuli have been studied in context of meniscus tissue engineering.
The TGFβ family is regarded as one of the most important factors of cartilage tissue engineering and the chondrogenic differentiation of MSCs [3, 84]. The positive effect of TGFβ in meniscus tissue engineering has been reported in several studies as well [3]. TGFβ has been shown to increase cell division of MCs and production of proteoglycans [85]. Gunja et al. (2009) reported increased compressive properties, collagen and GAG deposition of constructs seeded with MCs after stimulation with TGFβ and hydrostatic pressure [86]. Further studies compared the effect of TGFβ-1, PDGF-AB, IGF-1 and bFGF on matrix synthesis of MCs cultured in monolayers and 3D culture in polyglycolic acid (PGA) scaffolds [87, 88]. They found that TGFβ-1 led to the highest response regarding collagen and proteoglycan production [87]. Ionescu et al. (2012) studied the effect of bFGF and TGFβ-3 on meniscus repair and the integration of an electrospun scaffold [89]. They showed enhanced meniscus repair and the integration of the scaffold [89].
Overall, important to know for meniscus tissue engineering is the ability of growth factors to modulate matrix contraction: increased matrix contraction may lead to a compacter matrix or adaption of mechanical properties, whereas the geometry may be negatively affected [3]. TGFβ, FGF, PDGF and IGF have been reported to induce matrix contraction by MCs, fibroblasts or articular chondrocytes [3].
In contrast to direct stimulation with growth factors, indirect biochemical stimulation can be achieved for instance through hypoxic conditions. Henrionnet et al. (2017) found out that hypoxic conditions led to an increased TGFβ induced chondrogenesis of MSC-laden alginate beads, even preventing in vitro hypertrophic differentiation [90].
Another technique to increase matrix synthesis in vitro is macromolecular crowding (MMC) (figure 1.6). Standard cell culture medium only has a low concentration of proteins (1 to

10 g/L or lower) [91]. In contrast, physiologic environments have a higher concentration of proteins: blood (80 g/L), interstitial fluids (30 to 70 g/L) or the cell interior (200 to 350 g/L) [91]. In standard cell culture, cells produce procollagen and the necessary proteinases for conversion to collagen [92]. These products are highly diluted in the standard cell culture (figure 1.6 A), whereas in a MMC environment inert polydisperse macromolecules are added to the medium to create effect volume occupany providing physiologically relevant conditions (figure 1.6 B) [92]. This highly crowded environment increases the relative density of procollagen and proteinases facilitating the conversion of procollagen to collagen and in general matrix synthesis [92].

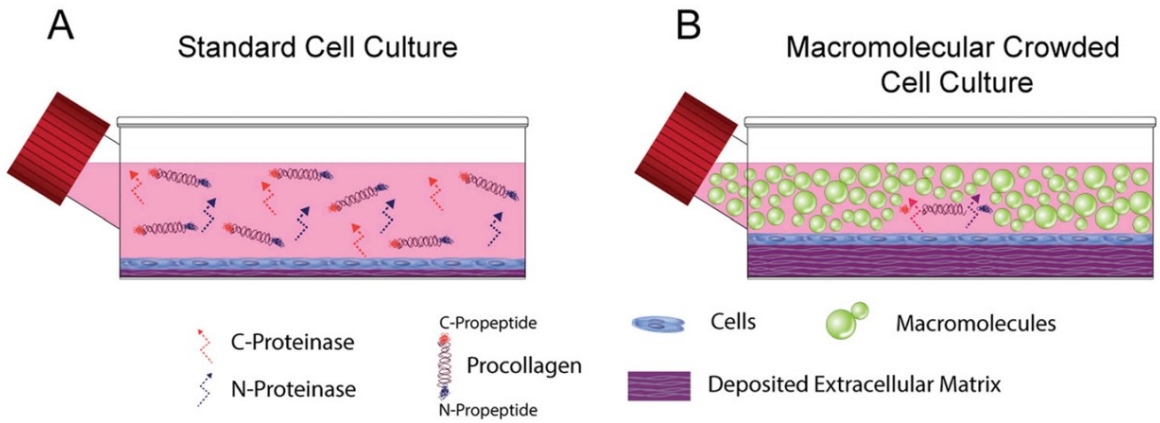

Figure 1.6.: The principle of MMC. A In standard cell culture, cells produce procollagen and specific N- and C-proteinases. In the very dilute in vitro microenvironment of a standard cell culture, collagen synthesis will be slow caused by deactivation of proteinases or dissolving of procollagen before conversion to collagen. **B** MMC is used to imitate the in vivo dense extracellular space by the addition of inert polydisperse macromolecules. These macromolecules create effective volume occupancy and increase the relative density of procollagen and proteinases facilitating conversion of procollagen to collagen and matrix synthesis. Adapted from [92] with kind permission.

Zeiger et al. (2012) showed that MMC directed ECM organization by increased collagen alignment leading to a reorganized cytoskeleton, increased secretion of matrix proteins, increased proliferation and decreased motility of MSCs [91]. So far, the application of MMC for 3D culture of meniscus models has not been studied. However, crowding of 3D collagen hydrogels showed increased collagen nucleation and fiber growth, higher stiffness, increased resistance to mechanical stress and an increased proliferation of MSCs cultured on MMC tuned collagen hydrogels [93]. Thus, MMC might also increase meniscus matrix synthesis and should be considered as further biochemical stimulus for meniscus tissue engineering.

1.3.3.3. Scaffolds

For 3D culture of cells, an appropriate scaffold has to be established. An ideal scaffold for meniscus tissue engineering should be biocompatible and biodegradable, allow free nutrient diffusion, permit cell adhesion, in-growth of cells and tissue, have a biochemical composition similar to meniscal tissue regarding Col I, Col II and proteoglycan content, and provide mechanical integrity with respect to load bearing and transformation [94]. Scaffolds to generate a meniscus model are divided in four categories: tissue-derived scaffolds, extracellular matrix (ECM) component scaffolds, synthetic polymer scaffolds and hydrogel scaffolds [3].

Tissue-derived scaffolds

Tissue-derived scaffolds comprise periosteal tissue, perichondral tissue and decellularized tissue such as SIS or decellularized meniscus [95]. These scaffolds provide a natural environment for cell seeding, migration, matrix deposition and have as further advantages a high biocompatibility and geometric fidelity [96]. However, the supply is limited as most of them are animal-derived; furthermore, standardization, reproducibility and inferior mechanical properties are current hurdles [96].
Tissue-derived scaffolds to generate meniscal tissue are mainly limited to decellularized tissue. By decellularizing a tissue or organ, all cellular and nuclear material are removed by the combination of mechanical force using agitation, sonifaction or snap freezing, enzymes such as trypsin, endonucleases or exonucleases, and chemical treatment using ionic solutions such as sodium dodecyl sulfate (SDS) or detergents [97]. Generally, the components of the ECM are similar among species and thus, xenogeneic recipients for decellularized scaffolds are possible [97]. The SIS was used as tissue-derived meniscus implant to treat large posterior vascular meniscus defects in a dog model [98]. Dogs treated with the SIS implant developed a meniscus-like repair tissue and showed less articular cartilage damage compared to dogs who underwent meniscectomy alone [98]. Fixation of the SIS implant and the direct access to the blood supply were concluded to be crucial [98]. The direct decellularization of the meniscus was studied as well. Stapleton et al. (2008) generated an acellular xenogeneic scaffold by decellularizing a porcine meniscus: biocompatibility, histoarchitecture and biomechanical properties were maintained, however, a loss of almost 60 % GAG was detected [99]. Nevertheless, the challenges of availability, standardization and mechanical integrity remain for decellularized tissue-derived scaffolds [3].

Extracellular matrix (ECM) component scaffolds

ECM component scaffolds are another group of natural scaffolds made of matrix components such as collagen, proteogylcans or elastin molecules [96]. Examples are collagen implants, hyaluronan scaffolds or combinations of these [3]. Stuckensen et al. (2018) introduced a meniscus collagen scaffold which provided an inner and outer zone like the native meniscus and enabled in-growth of human MSCs [68]. Zellner et al. (2013) suggested the use of an autologous MSC-loaded hyaluronan/collagen composite scaffold which they claimed to produce stable meniscus-like tissue after the repair of avascular meniscal tears in rabbits [80]. The MSC-loaded construct precultured for 2 weeks in chondrogenic medium comprising TGFβ-1 showed the most promising regeneration [80]. Another example for an ECM component scaffold is the commercially available CMI® implant [3]. This cell-free implant is a mesh of bovine Col I shaped as lateral or medial meniscus [3]. However, it has a small field of indication as implants to be applied after partial meniscectomy [3, 22]. Generally, ECM component scaffolds can be tailored in an optimal and natural 3D architecture providing mechanical strength, but most of them still have inherent disadvantages of shrinkage, shape deformation or scaffold degradation [3, 96].

Synthetic polymer scaffolds

Synthetic polymer scaffolds in meniscus tissue engineering such as PU, polycarbonate urethane (PCU), polycaprolactone (PCL), polylactic acid (PLA), PGA, PLGA etc. are mostly produced from polyester and are degraded by gradual hydrolysis [3]. They offer several advantages such as adjustable degradation, easy shaping with variable pore size, porosity and fiber size leading to a good scaffold geometry and satisfying mechanical properties [96]. Weaknesses are their hydrophobic properties, inferior integration with neighboring host tissue, immune responses or side effects from degradation products such as toxic diisocyanate from PU degradation [94, 96].
The PU-based Actifit® scaffold is commercially available as cell-free meniscus implant, but is indicated only for a very few patients as the CMI® implant [94]. The NUsurface® Meniscus Implant is another cell-free PCU-based implant with promising short-term clinical results [96]. However, it is still awaiting US Food and Drug Administration (FDA) approval, as the FDA requested to confirm that the NUsurface® Meniscus Implant prevents chondral degradation and OA [96]. Taken together, synthetic polymer scaffolds have some potential for meniscus tissue engineering. However, they are mainly applied as cell-free meniscus implants, lack inherent biological support, and provide minimal biomimicry [3].

Hydrogel scaffolds

Hydrogels can be synthesized by cross-linking of natural or synthetic polymer chains to a network [3]. The water content, mostly more than 90 %, determines the physical properties of hydrogels [3]. Advantages of the hydrogel scaffolds are their versatility, viscoelasticity and easy shaping ability [96]. However, low mechanical properties, shrinkage and shape deformation were not yet overcome [3]. For meniscus tissue engineering, cell-laden Col I gels represent a good starting point [94]. High-density Col I gels loaded with bovine MCs were prepared by injection molding as whole meniscus scaffold and directly compared with molded alginate menisci [100]. This study showed the preservation of meniscus shape, increased GAG concentrations, and a significant improvement of the mechanical properties for the high-density MC-laden Col I gels [100]. However on the downside, MCs, a limited cell source, were used as cells to be seeded [100]. The Col I gels shrunk and GAG content, collagen concentration and equilibrium modulus did not reach the numbers measured for native menisci [100]. Nevertheless, less contraction of MC-laden Col I gels was observed by increasing the collagen concentration [100].
A method to increase collagen concentration and even to enhance mechanical properties of hydrogels is compression, for instance plastic compression. Mechanically stable skin substitutes were generated by plastic compression featuring superior mechanical stability compared with uncompressed gels [101]. To our knowledge, there are no studies using plastic compression to build a meniscus model being part of the results of this thesis. In addition to increasing the collagen concentration resulting in less contraction [100], plastic compression of cell-laden gels may lead to a heterogeneous cellular distribution and biochemical composition.
Another important feature which should be implemented to hydrogel scaffolds in meniscus tissue engineering is the zonal organization. A possibility to generate a more zonally organized meniscus model is a hybrid material combining a hydrogel with another type of scaffold. The sandwich combination of a MC-laden ECM hydrogel composed of Col II, chondroitin sulfate and hyaluronan between two electrospun PLA layers offered a novel approach for partial meniscus replacement by supporting meniscus-like tissue formation with high tensile mechanical properties of the aligned electrospun PLA scaffolds [102]. To our knowledge, the combination of a cell-laden Col I gel with a decellularized scaffold has not been studied by other groups working on meniscus tissue engineering and is part of the results of this thesis [103].

1.3.3.4. Biomechanical stimulation

The mechanical environment is crucial for the development and maintenance of load bearing tissues such as the meniscus [104]. In this regard, biomechanical stimuli are interesting for meniscus tissue engineering. Generally, biomechanical stimulation is very popular for tissue engineered articular cartilage, however biomechanical stimulation for meniscus tissue engineering is still scarce [104]. Biomechanical stimulation approaches for tissue engineering articular cartilage or meniscal tissue are divided into four stimulation categories: compression, tension, shear and hydrostatic pressure (figure 1.7) [104, 105].

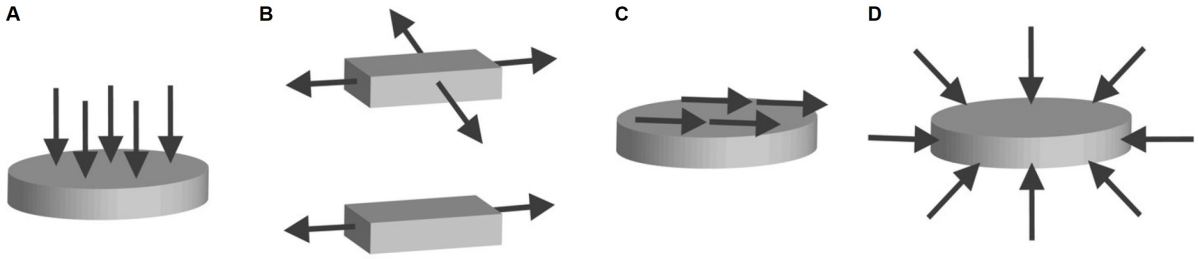

Figure 1.7.: Categories of biomechanical stimulation. **A** Direct compression, **B** biaxial tension (top) and uniaxial tension (bottom), **C** shear, and **D** hydrostatic pressure. Adapted from [105] with kind permission.

Compressive loading (figure 1.7 A) is known to facilitate the transport of nutrients and waste products in the meniscal tissue, and to influence the biochemical and biomechanical properties of the meniscus [104]. For the meniscus, a compressive strain of approx. 10 % is regarded as physiologic loading resulting in anabolic activity, whereas higher loading may cause catabolic activity [104]. Alginate-based meniscus constructs laden with MCs were dynamically compressed with a strain of 15 % three times a week for 1, 2 or 4 weeks followed by subsequent static culture for 4 weeks [106]. The results of this study showed that increased loading durations led to enhanced ECM formation, collagen accumulation and mechanical properties [106].
Tensile loading (figure 1.7 B) is a typical characteristic of the physiologic mechanical environment of the meniscus [3]. Connelly et al. (2010) showed that the combination of chondrogenic stimuli TGFβ-1 and tensile loading of 10 % tensile strain at 1 Hz enhanced the fibrochondrogenic differentiation of bovine BM-MSCs demonstrating promising potential for tissue engineering of fibrocartilage constructs [107]. Huey et al. (2011) applied mechanical stimulation by simultaneous tension and compression of 10 % strain at 1 Hz on meniscus constructs resulting in significantly increased compressive, tensile and biochemical properties of the constructs [108]. Furthermore, this mechanical stimulation was performed

with additional chemical stimulation by chondroitinase ABC and TGFβ-1, leading to additive increase of mechanical and biochemical properties [108].
In addition to compression and tension, the meniscus needs to withstand shear [3]. Shear stimulation (figure 1.7 C) can be induced by fluid flow provided in a bioreactor [105]. To our knowledge of literature, there are no research approaches studying the influence of merely shear stimulation on tissue engineered meniscus constructs. Petri et al. (2012) studied the effect of perfusion with 10 mL/min and cyclic compression of 10 % strain at 0.5 Hz for 8 hours on a collagen meniscus implant seeded with human BM-MSCs [109]. The combination of perfusion inducing shear stress, and compression stimulation enhanced the proliferation and differentiation of BM-MSCs [109].
Another approach for biomechanical stimulation is based on hydrostatic pressure providing uniform compression of all surfaces (figure 1.7 D) [105]. In the physiologic environment of the knee joint, the meniscus is hydrostatically pressurized by compressive loading because of its high water content and low permeability [110]. It was shown that dynamic hydrostatic pressure enhanced chondrogenic differentation of MCs from the axial and abaxial zone [111]. In an other study, a combined stimulation of TGFβ-1 and hydrostatic pressure was applied on PLLA constructs seeded with MCs leading to synergistic and additive effects on the biochemical and compressive properties of these constructs [86].

1.3.3.5. Gradual vascularization

Another important feature of the meniscus is its vascularization decreasing from the abaxial to the axial aspect (figure 1.1 D) [3]. Meniscal lesions located in the vascular abaxial aspect may heal well because of the adequate blood supply, whereas the healing of injuries located in the axial two-thirds is critical [112]. Hence, the induction of angiogenesis has been suggested to enhance the healing capacity [112] and also tissue engineered meniscus implants should provide a vascularized part. In this section, some exemplary studies of angiogenesis induction and vascularization approaches are explained.
For the induction of angiogenesis in meniscus tissue engineering, different growth factors were studied. VEGF was suggested to rather act as biomarker of meniscus healing than as potential therapeutic agent to enhance the healing capacity of meniscal lesions [112]. Factors such as HGF, endothelin-1 or CTGF may be better stimuli for angiogenesis induction [112]. HGF, a paracrine growth factor often secreted by a mesenchymal partner, was reported to induce vessel in-growth in tissue engineered meniscus implants [113]. In this study, PGA-based meniscus implants were seeded with genetically engineered MCs expressing HGF [113]. After subcutaneous implantation into nude mice, the seeded MCs

showed HGF expression leading to the formation of vascularized meniscus-like tissue [113]. Yuan et al. (2015) suggested endothelin-1 as angiogenic factor stimulating the migration and proliferation of MCs through culture in conditioned medium from HUVECs [114]. CTGF was shown to increase Col I, Col II and VEGF expression of rabbit MCs in vitro and to enhance meniscus repair in the avascular zone [115]. Lee et al. (2014) implanted a PCL-based meniscus implant spatially releasing CTGF and TGFβ-3 demonstrating that CTGF led to increased VEGF levels and enhanced healing of avascular meniscal lesions [116]. These studies revealed that VEGF may be a significant but not exclusive factor enhancing the healing of avascular meniscal lesions. Further investigations are needed to fully understand the effect of these growth factors.
Furthermore, cell sheets composed of MSCs and HUVECs as endothelial part were suggested to engineer prevascularized tissues [117]. However, the use of mvECs is recommended as they naturally reside as endothelial cell type in the meniscus [95]. Looking at all the drawbacks of vascularized scaffolds (part 1.3.2.2), BioVaSc-TERM® could provide a sustainable vascular network in meniscus tissue engineering [65, 68].

1.3.4. Matrix remodeling

After implantation, a tissue engineered implant should allow or even promote in-growth of host tissue. Thus, matrix remodeling to replace a cell-laden scaffold after implantation represents an essential and challenging process in tissue engineering. Generally, matrix remodeling describes the timely degradation and replacement of ECM, and is a major physiologic process of development, morphogenesis and tissue repair [118]. Controlled regulation of matrix remodeling is very important, as deregulated remodeling may cause diseases such as arthritis, OA, cancer, fibrosis, and acute or chronic cardiovascular disorders [118].
Matrix metalloproteinases (MMPs) regulate matrix remodeling and are endogenously inhibited by tissue inhibitors of metalloproteinases (TIMPs) [118]. MMPs are synthesized as pre-proenzymes and after removal of the signal peptide during translation, the proenzymes (proMMPs) are generated. ProMMPs are then activated by cleavage of its propeptide domain from the catalytic domain [119]. In humans, 23 different forms of MMPs classified in six subclasses are known: gelatinases (MMP-2 and -9), collagenases (MMP-1, -8 and -13), stromelysins (MMP-3, -10 and -11), matrilysins (MMP-7 and -26), membrane-type MMPs (MMP-14, -15, -16, -17, -24 and -25) and a heterogeneous subgroup with different substrate specifities (MMP-12, -19, -20, -21, -23, -27 and -28) [120, 119]. For example, the gelatinases MMP-2 and -9 digest elastin, Col IV and several other ECM molecules

with enhanced collagen affinity: MMP-2 cleaves chondroitinsulphate proteoglycan, decorin, Col I, Col II and Col III; the bioavailability of TGFβ is provided by MMP-9 cleaving a precursor of TGFβ [118].
Methods to detect MMPs are zymographic techniques based on the degradation of their preferential substrate and their molecular weight [120]. Gel zymography is based on protein separation by electrophoresis under SDS protein denaturation reversibly inhibiting the MMP activity in a gel containing a MMP substrate, for example gelatin to detect MMP-2 and -9 [120]. After incubation in appropriate buffers for activation of MMPs and subsequent Coomassie blue staining, the MMPs are detected as clear white bands against a blue background [120]. Due to different molecular weights, proMMPs and active MMPs can be distinguished [120]. Reverse zymography to study TIMPs in their ability to inhibit MMPs can be performed by adding TIMPs to the samples [120].
Taken together, zymographic techniques are important methods to analyze matrix remodeling processes of new diagnostic techniques and therapies [120]. As increased MMP expression has been identified in repair and remodeling processes, and a balance between MMPs and TIMPs is essential for physiologic tissue remodeling [120], matrix remodeling demonstrates an important component to be studied for tissue engineering. Furthermore, it was found out that MSC function is controlled by MMP activity which can be regulated by mechanical stimulation, an important part of meniscus tissue engineering [121].

1.4. Aim of the study

There is no optimal treatment for meniscal lesions. Replacing torn menisci by a tissue engineered meniscus model is a promising strategy. The aim of this study was to develop a vascularized meniscus implant (figure 1.8).

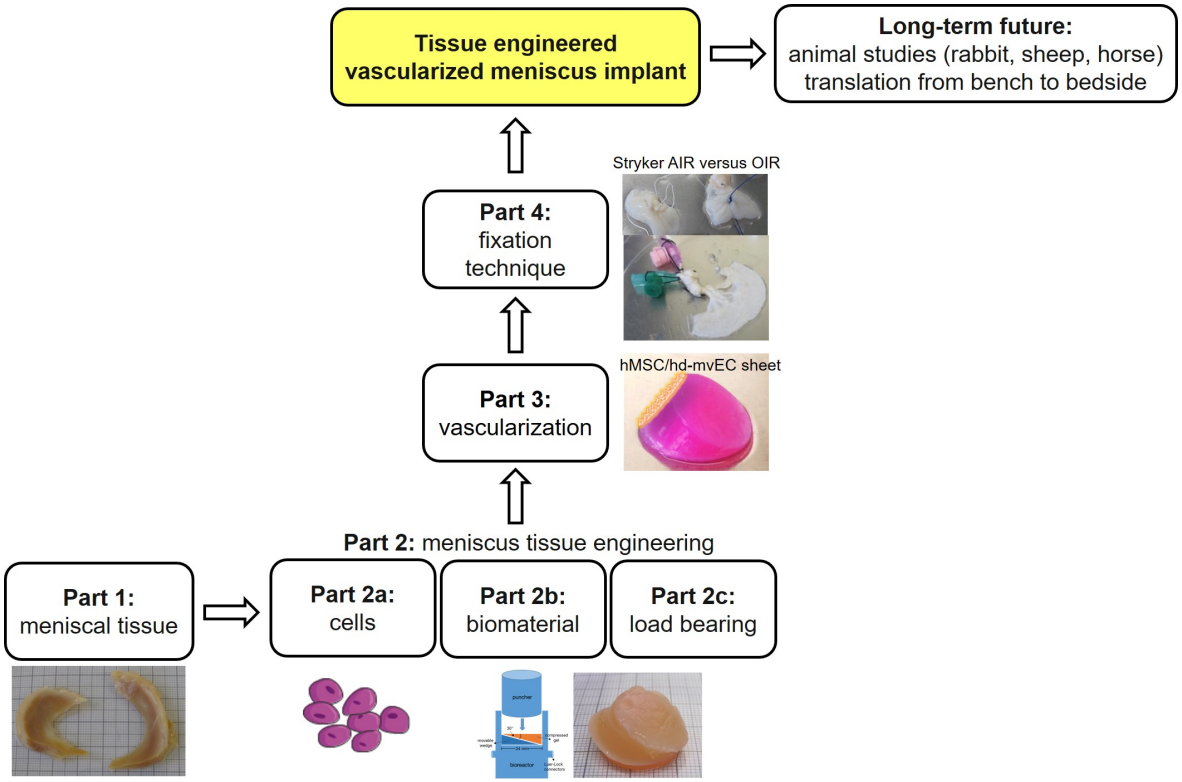

Figure 1.8.: Structure of this doctoral thesis. After characterization of the meniscal tissue (part 1), meniscus tissue engineering (part 2) was divided into three subparts: cells, biomaterial, load bearing. In part 3, different vascularization strategies were investigated to be applied for the tissue engineered meniscus implant. In part 4, different fixation techniques were evaluated for future application in meniscus implant surgeries. As a long-term goal, the tissue engineered vascularized meniscus implant will be applied in animal studies for the translation from bench to bedside.

After characterization of the heterogeneous meniscus as target tissue, the components of meniscus tissue engineering were determined to build a wedge-shaped meniscus model. As the meniscus is partly vascularized, different vascularization approaches were studied. For the future meniscus implant surgery, suture techniques were compared. The combination of all these parts is aiming at a vascularized meniscus implant with high potential for animal studies.

Chapter 2

Material

In the following chapter, biological material, biomaterial, chemicals, cell culture media and supplements, buffers, solutions, antibodies, primer pairs, commercially available kits as well as laboratory material, equipment, devices and software which were used to perform the methods of chapter 3 are listed.

2.1. Biological material

For isolating human (h) primary cells, human tissue biopsies including spongiosa, meniscus and foreskin were kindly provided by the University Hospital Würzburg and the Orthopedic Clinic König-Ludwig-Haus Würzburg, Germany (local ethics approval: 182/10, 25.11.2015). The human medial and lateral meniscus of patient 70 was a formalin fixed tissue kindly donated from the Institute of Anatomy and Cell Biology, University Hospital Würzburg, Germany.
For isolating equine (eq) primary cells, equine tissue biopsies were kindly provided from the University Equine Hospital, University of Veterinary Medicine Vienna, Austria. Tissue collection to obtain these cells had been performed according to the Good Scientific Practice and Ethics in Science and Research regulation implemented at the University of Veterinary Medicine Vienna. The animal owner's consent to collect and analyze the samples and to publish resulting data was obtained according to the standard procedure and approved by the ethics and animal welfare committee of the University of Veterinary Medicine Vienna. The warm blood horses, whose age was between 6 to 19 years, were euthanized for reasons unrelated to this study or musculoskeletal disease. All samples were obtained immediately post mortem using aseptic technique and were processed within 14 h after collection.
The donor data for primary cell isolation or histological studies are shown in table 2.1.

Table 2.1.: List of biological material.

Species	Coding	Sex	Age	Tissue type	Use
Human	30	female	50 years	spongiosa	hMSCs
Human	41	male	35 years	spongiosa	hMSCs
Human	42	male	76 years	spongiosa	hMSCs
Human	57	male	53 years	medial meniscus	hMCs
Human	58	female	50 years	medial meniscus	hMCs
Human	59	female	54 years	medial meniscus	hMCs
Human	60	female	61 years	medial meniscus	hMCs
Human	67	female	33 years	medial meniscus	histology
Human	68	male	33 years	medial meniscus	histology
Human	69	male	22 years	medial meniscus	histology
Human	70	female	70 years	medial meniscus, lateral meniscus	histology
Human	16.013	male	4 years	foreskin	hd-mvECs
Human	16.017	male	6 years	foreskin	hd-mvECs
Human	16.025	male	3 years	foreskin	hd-mvECs
Human	16.026	male	5 years	foreskin	hd-mvECs
Human	17.003	male	4 years	foreskin	hd-mvECs
Human	17.017	male	4 years	foreskin	hDF
Equine	1	male	11 years 2 months	meniscus, spongiosa	eqMCs, eqMSCs
Equine	2	female	19 years 10 months	meniscus, spongiosa	eqMCs, eqMSCs
Equine	3	male	16 years 8 months	meniscus, spongiosa	eqMCs, eqMSCs
Equine	4	male	14 years 0 months	meniscus, spongiosa	eqMCs, eqMSCs

2.2. Biomaterial

The biomaterial used for this study is listed in table 2.2. For Col I isolation, rat tails from male rats with an age of 8 to 10 weeks were purchased from Charles River.

For the preparation of the porcine (po) small intestinal submucosa with mucosa (SIS-muc-TERM®) and BioVaSc-TERM®, jejunum segments were dissected twice a month from male pigs with an age of 6 to 8 weeks and a weight of 14 to 18 kg (animal experimental project no. 55.2 2532-2-256). The jejunum segments were obtained immediately post mortem. My tasks included the dissection and preparation of jejunum segments for generating the BioVaSc-TERM®, the SIS-muc-TERM® and the small intestinal submucosa without mucosal layer (SIS-ser-TERM®) by the attendance of 36 pig surgeries during 3 years.

Table 2.2.: List of biomaterial.

Biomaterial	**Supplier**	**Catalog no.**
BioVaSc-TERM®	TERM	TERM
Col I solution	TERM	TERM
Col R solution 0.4 %	Serva	4256.01
Col I/II/Elastin sponge	Geistlich Biomaterials	Geistlich R&D
PARASORB® Fleece HD (Col I sponge)	Resorba®	DK8001
SIS-muc-TERM®	TERM	TERM

2.3. Chemicals

Chemicals and solutions are shown in table 2.3.

Table 2.3.: Chemicals and solutions.

Chemical/solution	**Supplier**	**Catalog no.**
Acetic acid, 100 %	Carl Roth	6755.2
Acetic acid (glacial), 100 %	Merck	13700
Acetone, $\geq$ 99.5 %	Carl Roth	5025.5
Agarose, qPCR	AppliChem	A2114\CA50
Agarose, low temperature gelling	Sigma-Aldrich	A9539-10G
Albumin fraction V (BSA)	Carl Roth	T844.2
Alcian blue 8GX	Sigma-Aldrich	A3157-10G
Alizarin Red S	Sigma-Aldrich	A5533-25G
Ammonia, 25 %	Carl Roth	5460.1
Antibody diluent	Dako	S302283
Aquatex	Merck	1.08562.0050
BSA (bovine serum albumine V)	Sigma-Aldrich	A3059-10G
Brillant Blue R 250	Carl Roth	3862.2

Chemical/solution	**Supplier**	**Catalog no.**
Calcium chloride ($CaCl_2$)	VWR	1.02391.1000
Chloral hydrate	Merck	102425
Citric acid monohydrate	Sigma-Aldrich	C1909-500G
Collagenase	Roche	11213865001
CPX (ciclopirox olamine)	Sigma-Aldrich	C0415-5G
DAPI (4',6-diamidino-2-phenylindole)	Thermo Fisher Scientific	62247
DAPI Fluoromount-G	Invitrogen	00-4959-52
Deionized water	TERM	TERM
Dexamethasone	Sigma-Aldrich	D4902-100MG
DMSO (dimethyl sulfoxide)	Sigma-Aldrich	D2438-50ML
DiI ($DiIC_{18}(3)$)	Promocell	PK-CA707-60010
Dinatriumhydrogenphosphate	Merck	1065801000
Dispase II powder	Invitrogen	17105-041
Donkey serum	Sigma-Aldrich	D9663-10ML
DMEM (Dulbecco's modified eagle medium) HG (high glucose, 4.5 g/L), powdered medium with L-glutamine	PAA	G001,3010
DMEM HG, GlutaMAX™	Gibco	61965-026
DMEM LG (low glucose), GlutaMAX™	Gibco	21885-025
Entellan®	Merck	1.079.600.500
Eosin	Morphisto	10177
EtOH (ethanol), absolute	Carl Roth	9065.2
EtOH, denaturated, 96 %	Carl Roth	T171.2
EDTA (ethylenediaminetetraacetic acid)	Sigma-Aldrich	E5134-1KG
FBS (fetal bovine serum)	PAN Biotech	P30-3306
FCS (fetal calf serum) for MSC culture	Bio & Sell GmbH	FCS.ADD.0500 Lot BS210601.5
Ficoll PM 70 kDa	Sigma-Aldrich	GE17-0310-10
Ficoll PM 400 kDa	Sigma-Aldrich	GE17-0300-10
Ficoll-paque premium	VWR	17-5442-03
FITC (fluorescein isothiocyanate)-Lectin	Sigma-Aldrich	L9006-2MG
Gentamycin	PAA	P11-004

Chemical/solution	**Supplier**	**Catalog no.**
β-glycerophosphate	Sigma-Aldrich	G5882-50ML
H_2O_2 (hydrogen peroxidase), 30 %	Carl Roth	8070.2
hbFGF (human basic fibroblast growth factor)	R&D Systems	233-GMP
HCl (hydrochloric acid), 1 N	Carl Roth	K025.1
HCl (hydrochloric acid), 5 M	Merck	HC73097511
Hematoxylin (Mayer)	Morphisto	10231
Hematoxylin (Weigert)	Morphisto	10225
HEPES (4-(2-hydroxyethyl)-1-piperazineethanesulfonic acid)	Sigma-Aldrich	H4034
Hyaluronidase	Sigma-Aldrich	H4272
Indomethacin	Sigma-Aldrich	I8280-5G
Insulin	Sigma-Aldrich	I9278-5ML
ITS (insulin-transferrin-sodium selenite) Premix Universal Culture Supplement	Corning	354350
IBMX (3-isobutyl-1-methylxanthine)	AppliChem	A0695.0001
Kernechtrot (nuclear fast red)	Morphisto	10264
L-ascorbic acid phosphate Mg salt	Wako	013-12061
L-cystein-hydrochloride	Carl Roth	3468.1
L-proline	Sigma-Aldrich	P5607-25G
Magnesium chlorite hexahydrate ($MgCl_2$ x 6 H_2O)	Lonza	HN03.3
Medium 199	Sigma-Aldrich	M0650
Methanol	Sigma-Aldrich	32213-1L
Methylcellulose	Sigma-Aldrich	M0512-1009
Monopotassium phosphate (KH_2PO_4)	Merck	1048731000
Mowiol	Carl Roth	0713
MSCGM-CD™	Lonza	00190632
MTT (3-(4,5-dimethyl-2-thiazolyl)-2,5-diphenyl-2H-tetrazolium bromide)	Serva	20395
Na_2EDTA salt x 2 H_2O	Sigma-Aldrich	E5134-1KG
Oil Red O	Merck	1.05230.0025
Papain	Sigma-Aldrich	P4762
Paraffin	Carl Roth	6642.6

Chemical/solution	**Supplier**	**Catalog no.**
PBS^+ (phosphate buffered saline, with calcium chloride and magnesium chloride)	Sigma-Aldrich	D8662
PBS^- (phosphate buffered saline, without divalent ions)	Sigma-Aldrich	D8537
PBS tablets	Invitrogen	A3813,1000
PenStrep (10,000 U/mL penicillin/ 10 mg/mL streptomycin)	PAA	P11-010
PFA (paraformaldehyde)	AppliChem	A3813,1000
Phalloidin-iFluor 488 Conjugate	Abcam	ab176753
Picrosirius Red	Morphisto	13422
PLA (polylactic acid; Proto-Pasta - High Temperature PLA - Iridescent Ice)	Filamentworld	PP175X500ICE
Potassium chloride (KCl)	Merck	1049361000
2-propanol	Carl Roth	9866.6
Reagent diluent, 10x (ELISA)	R&D Systems	DY995
Roti®-Histofix	Carl Roth	P087.2
Sodium acetate	Carl Roth	6773
Sodium chloride (NaCl)	Carl Roth	HN00.3
Sodium deoxycholate	Carl Roth	3484
Sodium deoxycholate	Sigma-Aldrich	D6750-25G
Sodium hydroxide (NaOH), 1N	Carl Roth	KK71.1
Sodium pyruvate, 100 mM	Invitrogen	11360-039
SsoFast™EvaGreen® Supermix	BioRad Laboratories	172-5201
Stop Solution (ELISA)	R&D Systems	DY994
Substrate Solution Color Reagent A & Color Reagent B (ELISA)	R&D Systems	DY999
Sucrose (D(+)-saccharose)	Carl Roth	9097.2
TGFβ-3 (transforming growth factor β-3)	R&D system	243-B3.002
TISSEEL 2 mL	Baxter	0739884
Tris	Carl Roth	4855.1
Triton-X 100	Carl Roth	3051.2
Trypan blue, 0.4 %	Sigma-Aldrich	T8154-100ML
Tween-20	VWR	8.22184.0500
Ultrapure water	Millipore	

Chemical/solution	Supplier	Catalog no.
VascuLife® (VEGF endothelial cell culture medium®)	CellSystems GmbH	LL-0005
VEGF (vascular endothelial growth factor)	Cell Signaling Technology	8065LC
Versene solution	Gibco	15040-033
WST-1 cell proliferation reagent	Roche	11644807001
Xylol	Carl Roth	9713.3

2.4. Media and solutions for cell culture and decellularization

Media and solutions used for cell culture and decellularization are listed in table 2.4.

Table 2.4.: Media and solutions for cell culture and decellularization.

Medium/solution	Composition	
Adipogenic differentiation medium (adipogenic DM)	1 μM	dexamethasone
	500 μM	IBMX
	1 μg/mL	insulin
	100 μM	indomethacin
	10 % (v/v)	FCS
		in DMEM HG
Chondrogenic DM	50 μg/mL	l-ascorbic acid phosphate Mg salt
	100 nM	dexamethasone
	100 μM	sodium pyruvate
	40 μg/mL	l-proline
	1 % (v/v)	ITS
	10 ng/mL	TGFβ-3
		in DMEM HG
Collagenase working solution	500 U/mL	collagenase
		in DMEM HG
Decellularization solution (DS)	33 mg/mL	sodium deoxycholate
		in ultrapure water

Medium/solution	**Composition**	
DF medium	10 % (v/v)	FCS in DMEM HG
DiI solution	0.93 mg/mL	DiI in EtOH, absolute
Dispase solution	1-4 U/mL	dispase II, powder in PBS^-
1x DMEM	13.38 g/L 3.7 g/L	DMEM HG, powder $NaHCO_2$ in ultrapure water
Gel neutralizing solution (GNL)	3.75 % (v/v) 40 % (v/v)	HEPES, 3M FCS in 4.7x DMEM HG
ITS	0.625 mg/mL 0.625 mg/mL 0.625 mg/mL 125 mg/mL 0.535 mg/mL	insulin transferrin selenious acid BSA linoleic acid
Live/Dead solution (viability staining)	2 μM 4 μM	calcein ethidium homodimer-1 in PBS^-
Low FCS MSC medium, from April 2017	2 % (v/v) 50 μg/mL 100 μM	FCS for MSC culture l-ascorbic acid phosphate Mg salt sodium pyruvate in DMEM LG
MC medium	10 % (v/v)	FCS in DMEM HG
Methylcellulose solution (sprouting assay)	6 g	methylcellulose (autoclaved) adding of 250 mL 60 °C pre-warmed VascuLife® basal medium, stirring at room temperature (RT) for 20 min, adding of 250 mL RT VascuLife® basal medium, stirring at 4 °C overnight (o/n), centrifugation at 2,500 g and collection of supernatant
MSC medium	2 % (v/v)	FCS

Medium/solution	**Composition**	
(MSCGM, Lonza),	1 % (v/v)	MSCGM-CD™SingleQuot™
until March 2017		in MSCBM-CD™
MSC medium,	10 % (v/v)	FCS for MSC culture
from April 2017	50 μg/mL	l-ascorbic acid phosphate Mg salt
	5 ng/mL	hbFGF
	100 μM	sodium pyruvate
		in DMEM HG
MTT reagent (metabolic	1 mg/mL	MTT
activity staining)		in cell culture medium
Osteogenic DM	50 μg/mL	l-ascorbic acid phosphate Mg salt
	100 nM	dexamethasone
	10 mM	β-glycerophosphate
	10 % (v/v)	FCS
		in DMEM HG
PBS^-/EDTA solution	0.1 % (v/v)	EDTA, 0.54 M
		in PBS^-
PenStrep 1x	10 U/mL	penicillin
working solution	100 μg/mL	streptomycin
Tris buffer, pH 8	6 mg/mL	Tris
	0.2 mg/mL	$MgCl_2$ x 6 H_2O
		in ultrapure water
Trypsin/EDTA	0.05 % (v/v)	Trypsin-EDTA, 0.5 %
working solution		in PBS^-/EDTA solution
VascuLife®	5 ng/mL	rhVEGF LifeFactor
	5 ng/mL	rhFGF basic LifeFactor
	15 ng/mL	rhIGF-1 LifeFactor
	5 ng/mL	rhEGF LifeFactor
	50 ng/mL	ascorbic acid LifeFactor
	1 μg/ml	hydrocortisone hemisuccinate
		LifeFactor
	10 mM	l-glutamine LifeFactor
	0.75 U/mL	heparin sulfate LifeFactor
	2 % (v/v)	FCS
		in VascuLife® basal medium

2.5. Solutions for biochemical analysis, histology, immunohistochemistry and immunofluorescence

Composition of solutions for biochemical analysis, histology, immunohistochemistry (IHC) and immunofluorescence (IF) are shown in table 2.5.

Table 2.5.: Solutions for biochemical analysis, histology, IHC and IF.

Solution	**Composition**	
Acetic acid, 3 %	3 % (v/v)	acetic acid, 100 % in deionized water
Acetic acid, 1 %	1 % (v/v)	acetic acid, 100 % in deionized water
Alcaline alcohol	10 % (v/v)	ammonium hydroxide in deionized water
Alcian blue	10 mg/mL	Alcian Blue 8GX in deionized water
Alizarin Red S, stock solution	10 mg/mL	Alizarin Red S in deionized water
Alizarin Red S, working solution	0.25 % (v/v)	ammonia, 25 % in Alizarin Red S, stock solution (prepared immediately before use)
Citrate buffer, pH 6	42 mg/mL	citric acid monohydrate in deionized water
Coomassie blue stain solution	45 % (v/v) 10 % (v/v) 2.5 g/L	methanol acetic acid, 100 % Brilliant Blue R 250 in ultrapure water (filtered)
Coomassie destain solution	10 % (v/v) 10 % (v/v)	2-propanol acetic acid, 100 % in ultrapure water
DAPI solution	1 μg/mL	DAPI in ultrapure water
ELISA wash buffer	0.05 % (v/v)	Tween-20 in PBS$^-$

Solution	**Composition**	
EtOH/Acetone	50 % (v/v) 50 % (v/v)	ethanol, denaturated acetone, $\geq$ 99.5 %
H_2O_2	3 % (v/v)	H_2O_2, 30 % in deionized water
Hyaluronidase	2 mg/mL	hyaluronidase in PBS^-
Oil Red O, stock solution	5 mg/mL	Oil Red O in 99 % (v/v) 2-propanol
Oil Red O, working solution	60 % (v/v)	Oil Red O, stock solution in deionized water (prepared 24 h before use and is filtered immediately before use)
Papain digestion buffer, pH 6	8.2 mg/mL 1.13 mg/mL 13.3 mg/mL	sodium acetate l-cystein-hydrochloride EDTA-Na_2xH_2O in deionized water
PBST	0.5 % (v/v)	Tween-20 in 1x PBS, pH 7.4
Pepsin	4 mg/mL	pepsin in 0.01 N HCl
Pronase	1 mg/mL	pronase in PBS^-
Reagent diluent (ELISA)	10 % (v/v)	reagent diluent, 10x in PBS^-
Tris buffered solution (TBS) 0.5 M (10x)	78.87 g/L 87.66 g/L	Trizma hydrochloride NaCl in ultrapure water
Triton-X permeabilizing solution	0.02 % (v/v)	Triton-X 100 in 0.05 M TBS buffer

2.6. Material for gel zymography

Material, chemicals and solutions for gel zymography are listed in table 2.6.

Table 2.6.: Material, chemicals and solutions for gel zymography.

Material/chemical/solution	Supplier	Catalog no.
Collagenase F	Sigma-Aldrich	C7926
MMP-2, active, human, recombinant, mouse cells	Calbiochem	PF023
MMP-2, proenzyme, human, recombinant, mouse cells	Calbiochem	PF037
MMP-9, active, human, recombinant (67 kDa)	Calbiochem	PF140
MMP-9, active, human, recombinant (83 kDa)	Calbiochem	PF024
Novex™ Tris-Glycine SDS Running Buffer (10X)	Invitrogen	LC2675
Novex™ Tris-Glycine SDS Sample Buffer (2X)	Invitrogen	LC2676
Novex™ Zymogram Developing Buffer (10X)	Invitrogen	LC2671
Novex™ 10 % Zymogram Plus (Gelatin) Protein Gels, 1.0 mm, 12-well	Invitrogen	ZY00102BOX
Novex™ Zymogram Renaturing Buffer (10X)	Invitrogen	LC2670
ProSieve QuadColor Protein Marker	Biozym	00193837

2.7. Antibodies

The antibodies used for flow cytometry (FCM) are listed in table 2.7, for IHC in table 2.8, and for IF in table 2.9. Isotype (IT) controls of antibodies for IHC and IF are listed in table 2.10.

Table 2.7.: List of antibodies for FCM.

Antibody	Clone	Host (IT)	Final concentration	Fluorescent dye	Supplier/ catalog no.
CD11b	ICRF44	mouse (IgG1)	0.125 mg/mL	APC-eFluor780	Thermo Fisher Scientific/ 47-0118–41

Antibody	Clone	Host (IT)	Final concentration	Fluorescent dye	Supplier/ catalog no.
CD19	HIB19	mouse (IgG1)	0.125 mg/mL	APC-eFluor780	Thermo Fisher Scientific/ 47-0199-41
CD31	WM59	mouse (IgG1)	0.03 mg/mL	PE-Cyanine7	Thermo Fisher Scientific/ 25-0349-41
CD34	4H11	mouse (IgG1)	0.25 mg/mL	FITC	Thermo Fisher Scientific/ 11-0349-41
CD44	IM7	rat (IgG2b)	0.125 mg/mL	eFluor450	Thermo Fisher Scientific/ 48-0441-80
CD45	HI30	mouse (IgG1)	0.25 mg/mL	eFluor506	Thermo Fisher Scientific/ 69-0459-41
CD73	AD2	mouse (IgG1)	0.03 mg/mL	PerCP-eFluor710	Thermo Fisher Scientific/ 46-0739-41
CD90	5E10	mouse (IgG1)	0.5 mg/mL	FITC	Thermo Fisher Scientific/ 11-0909–41
CD105	SN6	mouse (IgG1)	0.125 mg/mL	APC	Thermo Fisher Scientific/ 17-1057-41

Table 2.8.: List of antibodies for IHC detected by Super-Vision 2 HRP-Polymer-Kit.

Antibody	Clone	Host (IT)	Final concentration (DAB duration)	Demasking procedure	Supplier/ catalog no.
Aggrecan	1R11 14A6	mouse (IgG1)	1.25 μg/mL (DAB 30 s)	enzymatic (pronase)	Invitrogen/ AHP0012

Antibody	Clone	Host (IT)	Final concentration (DAB duration)	Demasking procedure	Supplier/ catalog no.
CD31	JC70A	mouse (IgG1)	0.41 μg/mL (DAB 7 min)	enzymatic (pronase)	DAKO/ M0823
Col I	EPR7785	rabbit (IgG)	0.875 μg/mL (DAB 2 min)	enzymatic (hyaluronidase + pepsin 30 min)	Abcam/ ab138492
Col II	II-4C11	mouse (IgG1)	0.67 μg/mL (DAB 30 s)	enzymatic (hyaluronidase)	Acris/ AF5710
Col X	X53	mouse (IgG1)	1 μg/mL (paraffin) 10 μg/mL (cryo) (DAB 4 min)	enzymatic (pronase)	Invitrogen/ 14-9771-80
VE-cadherin	poly-clonal	rabbit	0.01 mg/mL (DAB 5 min)	heat-induced (pH 6)	Sigma-Aldrich/ V1514
vWF	F8/86	mouse (IgG1)	0.12 μg/mL (DAB 7 min)	enzymatic (pronase)	DAKO/ M0616

Table 2.9.: List of primary and secondary antibodies for IF.

Antibody	Clone	Host (IT)	Final concentration	Demasking procedure	Supplier/ catalog no.
CD31	JC70A	mouse (IgG1)	0.41 μg/mL	heat-induced (pH 6)	DAKO/ M0823
CD44	EPR10 13Y	rabbit (IgG)	0.004 mg/mL	heat-induced (pH 6)	Abcam/ ab51037
Donkey anti-mouse, Alexa Fluor 555		donkey (IgG)	0.005 mg/mL	(secondary antibody)	Invitrogen/ A-31570
Donkey anti-mouse, Alexa Fluor 647		donkey (IgG)	0.005 mg/mL	(secondary antibody)	Invitrogen/ A-31571

Antibody	Clone	Host (IT)	Final concentration	Demasking procedure	Supplier/ catalog no.
Donkey anti-rabbit, Alexa Fluor 647		donkey (IgG)	0.005 mg/mL	(secondary antibody)	Invitrogen/ A-31573

Table 2.10.: List of IT controls.

IT control	Clone	Host	Final concentration/ demasking procedure	Supplier/ catalog no.
IgG1	DAK-GO2	mouse	same as for corresponding antibody	DAKO/ X0931
IgG	EPR25A	rabbit	same as for corresponding antibody	Abcam/ ab172730

2.8. Primers for gene expression analysis

Primer pairs for housekeeping genes (hGAPDH, hEF1α, hHPR3) and target genes (hVEGF, hHIF-1α) used for quantitative real-time polymerase chain reaction (qRT-PCR) are listed in table 2.11. Annealing temperature of 60 °C was determined for all listed primers by gradient PCR with melting curve.

Table 2.11.: Primer pairs for gene expression analysis via qRT-PCR (ss: sense, as: anti-sense).

Gene	Sequence	Supplier
hEF1α	ss AGGTGATTATCCTGAACCATCC as AAAGGTGGATAGTCTGAGAAGC	Eurofins
hGAPDH	ss TGACGCTGGGGCTGGCATTG as GCTCTTGCTGGGGCTGGTGG	Eurofins
hHIF-1α	ss GCAGTAGCTGCGCTGATAGA as GCGCGAACGACAAGAAAAAGA	Eurofins

Gene	Sequence	Supplier
hHPR3	ss TGACCTTGATTTATTTTGCATACC as CGAGCAAGACGTTCAGTCCT	Eurofins
hVEGF	ss CTTGCCTTGCTGCTCTACCT as GCAGTAGCTGCGCTGATA	Eurofins

2.9. Kits

The kits for molecular assays, histology and IHC are listed in table 2.12.

Table 2.12.: List of commercially kits used for molecular analysis, histology and IHC.

Kit	Description	Manufacturer/catalog no.
Cedex Bio Activator Bio Control A Level 2 Bio Control A Level 3 Bio Deproteinizer Bio Glucose Bio GLC2B Lactate Bio LAC2B	quantification of metabolites in medium supernatants	Roche Diagnostic /07766700001 /06682227001 /0682545001 /06440517001 /06343732001 /06343759001
DC™ Protein Assay Kit	determination of protein concentration	Bio-Rad Laboratories Inc./ 5000112
Glycosaminoglycans (GAG) Assay Blyscan™	quantification of sGAG content	Biocolor/B100
Human Pro-Collagen I alpha 1 DuoSet ELISA	quantification of human pro-collagen I alpha 1 (hCOLIA1)	R&D Systems/DY6220-05
Human VEGF Duo Set ELISA	quantification of hVEGF	R&D Systems/DY293B-05
iScript™ cDNA Synthesis Kit	cDNA synthesis	Bio-Rad Laboratories Inc./ 170-8891

Kit	Description	Manufacturer/catalog no.
Live/Dead Viability/ Cytotoxicity Kit (for mammalian cells)	Live/Dead staining for cell survival	Molecular Probes™/MP03224
Proteome Profiler™ Human Angiogenesis Array Kit	determination of relative levels of angiogenesis-related proteins	R&D Systems/ARY007
RNeasy Micro Kit	purification of RNA from cell and tissue samples	Qiagen/74004
Quant-iT™ PicoGreen® dsDNA assay	quantification of dsDNA content	Invitrogen/P7589
Super-Vision 2 HRP-Polymer-Kit	IHC	DCS Innovative Diagnostik-Systeme/PD000KIT

2.10. Laboratory disposable material

The disposable material is shown in table 2.13.

Table 2.13.: List of disposable material.

Disposable material	Supplier
Aluminium foil	Carl Roth
Bioreactor tubing	ESSKA.de GmbH
Bioreactor connectors	MedNet GmbH
Bottle top filter: 250 mL, 500 mL	VWR
Cell culture flasks: 25 cm^2, 75 cm^2, 150 cm^2	TPP
Cell culture multiwell plates: 6 well, 12 well, 24 well, 96 well	TPP
Centrifuge tubes: 15 mL, 50 mL	Greiner Bio-One
Combitips plus: 0.5 mL, 1 mL, 2.5 mL, 5 mL	Eppendorf
Cover slips for object slides	Menzel-Gläser
Cryo tubes: 1.5 mL	Nunc
Disposable bags	Hartenstein

Disposable material	**Supplier**
Disposable microtome blades: S22	pfm medical
Dome, sterile	Memscap AS
Easyflex^{+} 50 mL empty bags, sterile	Macopharma
Embedding cassettes	VWR
Embedding filter paper	Labonord
Glass pasteur pipettes	Brand
Glass slips	Menzel-Gläser
Microplate: 96 well, black	Greiner Bio-One
Nunc membrane: Nunc UpCell Multidish 6-Well (174914)	Thermo Fisher Scientific
Object slides	
Uncoated (26 x 76 x 1 mm)	Menzel-Gläser
Super-Frost®	R. Langenbrinck
Super-Frost® Plus	R. Langenbrinck
Parafilm®	Carl Roth
PCR tubes	Biozym Scientific
PDS® II (polydioxanone) Suture (OIR, outside-in-refixation technique)	Ethicon
Petri dishes	Greiner Bio-One
Pipette tips: 0.5-10/10-100/100-1000 μL	Eppendorf
Plate sealers (ELISA)	R&D systems
Reaction tubes: 1.5 mL, 2.0 mL	Sarstedt
Scalpel blades, rounded	Bayha
Serological pipettes: 5 mL, 10 mL, 25 mL, 50 mL	Greiner Bio-One
Sterile filter: diameter 50 mm, pore size 0.2 μm	Sartorius
Stryker AIR (All-Inside-Repair)	Stryker
Thincert plate: 6 deep well	Greiner Bio-One
TissueTek® O.C.T. Compound and Cryomolds®	Sakura Finetek Europe
96 U-bottom well plates (sprouting assay)	Greiner Bio-One

2.11. Laboratory equipment and devices

Laboratory equipment and devices are listed in table 2.14.

Table 2.14.: List of laboratory equipment and devices.

Equipment/device	**Supplier**
Aspiration device: VacuBoy	Integra Biosciences
Autoclave:	
Tecnoclav	Biomedis
Table-top Autoclave	Systec
Varioklav	H+P
Biopsy punch	pfm medical
Bioreactor components	TERM
Cameras:	
Digital camera DS126191	Canon
AxioCam MRc digital camera	Zeiss
Cedex Bio Analyzer	Roche Diagnostics
Cell crowns	TERM
Cell incubator: 37 °C, 5 % CO_2	Heraeus
Centrifuges:	
Centrifuge 5417R	Eppendorf
Centrifuge 5424	Eppendorf
Multifuge X3R	Thermo Fisher Scientific
Clean Bench Safety cabinet Safe 2020 1.8	Thermo Fisher Scientific
Cold protection gloves	VWR
Compression device	TERM
Confocal microscope: LSCM TCS SP8	Leica
Cryostat CN1859 UV cryostat	Leica
Cold-storage room, 4 °C	Genheimer
Cytofunnel	Thermo Fisher Scientific
Cytospin cytoclips	Thermo Fisher Scientific
DAKO Pen	Dako
Drying Oven TDO66	Medize
EVOS XL	Life Technologies
Flow Cytometry: BD LSR-2	BD Biosciences

Equipment/device	**Supplier**
FluorChem™ Q developing machine	Biozym Scientific
Fluorescence Microscope Keyence BZ-9000	Keyence Deutschland GmbH
Freeze dryer: Lyophilizator Alpha 1-2 LDplus	Christ
Freezer	
-20 °C	Liebherr
-80 °C	Kendo
Fume hood	Prutscher Laboratory Systems
Gel zymography: XCell SureLock™ Mini-Cell EI0001	Invitrogen
Glassware	Schott
Glass cuvette with lid: 110 x 90 x 80 mm	Mercateo
Hand counter	neoLab
Hot air sterilizer	Memmert
Humidity chamber	TERM
Hydrostatic pressure device with 6 deep well plate	TERM
Ice machine: AF-80	Scotsman
Immersion thermostat for water bath	LAUDA
Liquid nitrogen storage tank: MVE815P-190 (-180 °C)	German-cryo
Magnetic stirring bar	Hartenstein
Microplate reader	
NanoQuant Plate™	Tecan
Tecan Infinite M200	Tecan
Microsurgical instruments	Fine Science Tools
Mr. Frosty™	VWR
Multipipette plus	Eppendorf
Multistep pipette	Eppendorf
Neubauer improved cell counting chamber	Hartenstein
Object slide racks: glass, stainless steel	Mercateo
Paraffin embedding center EG1150	Leica
Paraffin embedding center TES Valida	Medite
Paraffinized tissue floating bath: type 1052	Medax
pH meter	Mettler Toledo
Pipetting aid	Brand

Equipment/device	**Supplier**
Pipettes: 0.5-10/10-100/100-1000 μL	Eppendorf
Polarized light microscope: Leica DM4000 B LED	Leica
Power supply EV243 (gel zymography)	peqLab
Pressure sensor	HJK Sensoren + Systeme GmbH & Co. KG
Pump	Ismatec
Pump tubing cassette	Ismatec
qPCR cyler C1000/CFX96	Bio-Rad Laboratories Inc.
Roller mixer	Hartenstein
Sealing rings	Arcus GmbH
Scanning electron microscope: AURIGA 60	Zeiss
Spatula	VWR
Spoon spatula	Hartenstein
Sliding microtome	
Leica SM 2010R	Leica
Leica CM 1850UV	Leica
Tweezers	Assistent
Ultrapure water system	Millipore
Vortexter	Carl Roth
Water bath	Julabo Labortechnik
Weighing machines:	
Analytical balance	Kern
Cubis Micro Balance®	Sartorius
Precision balance	Kern
XEED 3D Printer	Leapfrog 3D Printers
Zwick Z010	ZwickRoell GmbH & Co. KG

2.12. Software

Software used for data recording and analysis is listed in table 2.15.

Table 2.15.: List of software for data recording and analysis.

Software	**Version**	**Company**
Bio-Rad CFX Manager	3.1	Bio-Rad Laboratories Inc.
Bioreactor pressure control		TERM
GraphPad Prism	5	GraphPad Software Inc.
FlowJo	V10	FlowJo LLC
FluorChem™Q	3.2.2.0	ProteinSimple
ImageJ	1.51	National Institute of Health
Keyence BZ-II Viewer Keyence BZ-II Analyzer	BZ-9000	Keyence Deutschland GmbH
Microsoft Office (Word, Excel, PowerPoint)	Office 365	Microsoft Deutschland GmbH
IBM SPSS	23.0	IBM Corporation
Tecan-i-control™ Tecan XFluor™	1.11 (2014)	Tecan Austria GmbH

Chapter 3

Methods

If not indicated otherwise, PBS^- (PBS without calcium chloride and magnesium chloride) was used and the cell culture medium was supplemented with 1 % (v/v) PenStrep.

3.1. Cell culture

Cell culture was performed under sterile conditions using a laminar airflow safety cabinet class two providing product, personnel and environment protection. All used material for cell culture was sterile. Reusable material was autoclaved before use. Self-made buffers, media or solutions were sterile-filtered or autoclaved prior to use. Before cell culture use, all solutions were pre-warmed to 37 °C. Cells were cultured in cell culture flasks in a humidified atmosphere at 37 °C and 5 % CO_2. Daily microscopic observation was performed to monitor cell growth, cell density and characteristic cell morphology.

3.1.1. Cell isolation procedures

The sterility of culture medium or PBS used for transporting the tissue was confirmed by taking a control sample followed by overnight (o/n) incubation at 37 °C and 5 % CO_2 to exclude any contamination of the biopsies. In this study, meniscal cells (MCs), mesenchymal stem cells (MSCs) and dermal microvascular endothelial cells (d-mvECs) were isolated. Human dermal fibroblasts (hDFs) were kindly provided by Lisa Kiesewetter and cultured in DF medium until P5.

3.1.1.1. Meniscal cells (MCs)

Meniscus biopsies were used to isolate MCs (figure 4.7 A, B). Fat and other tissue remnants were removed from the meniscus biopsies. After washing twice with PBS, the meniscal tissue was cut into small pieces (figure 4.7 C), which were transferred into a 50 ml centrifuge tube. 5 mL 500 U/ml collagenase solution were added per 1.5 g meniscal tissue to partially digest the ECM of the meniscal tissue (figure 4.7 D). After o/n incubation at 37 °C and centrifugation at 1,200 rpm for 5 min, the supernatant was aspirated and the remaining meniscal tissue pieces were washed with MC medium. After centrifugation at 1,200 rpm for 5 min, the tissue pieces were suspended in 2 mL MC medium und transferred to a T75 culture flask. After one day, 6 mL MC medium were added. During the incubation period in the humidified atmosphere at 37 °C and 5 % CO_2, MCs grew out. After four days, tissue remnants were removed. MCs were cultured until passage 3 (P3).

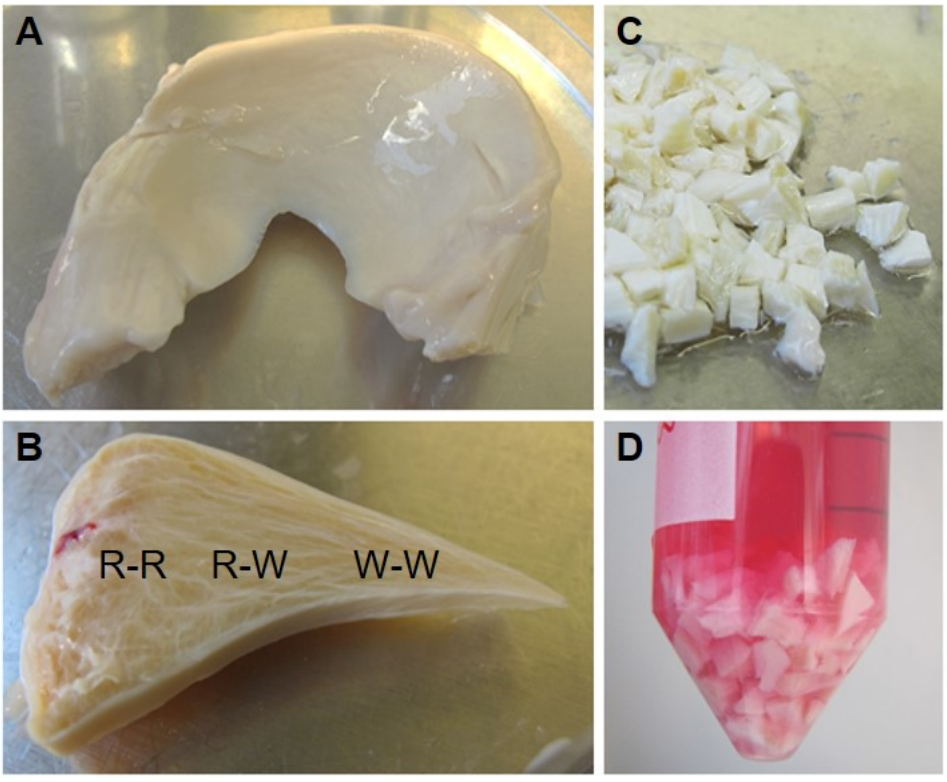

Figure 3.1.: Isolation of MCs from meniscus biopsies. **A** Equine meniscus. **B** Transverse meniscus section with the vascular R-R, the R-W and the avascular W-W zone. **C** The meniscal tissue was cut into small pieces. **D** The meniscal tissue pieces were incubated o/n with collagenase solution at 37 °C and 5 % CO_2.

3.1.1.2. Mesenchymal stem cells (MSCs)

MSCs were isolated from bone marrow. The bone marrow was transferred into a 50 mL centrifuge tube and diluted with PBS^+. 20 mL of the bone marrow solution were carefully loaded onto 15 mL Ficoll-paque premium solution in a new 50 mL centrifuge tube followed by gradient centrifugation at 800 g for 10 min. The buffy coat as middle phase contained the mononuclear cells which were carefully transferred into a new centrifuge tube. The addition of 35 mL PBS^+ and the centrifugation were repeated twice to remove the Ficoll-paque premium solution. After discarding the supernatant, the cell pellet was resuspended in MSC medium and the cell number was determined as described in section 3.1.2. One day after seeding MSCs into the T75 flasks, the cell layer was washed with PBS to remove erythrocytes. MSCs were cultured until P5. For the meniscus model, hMSCs of three hMSC donors were pooled (table 2.1).

3.1.1.3. Dermal microvascular endothelial cells (d-mvECs)

Foreskin biopsies were used to isolate d-mvECs. After washing three times with PBS, fat and other tissue remains were removed followed by three PBS washing steps. Then, the foreskin biopsies were cut into 2 to 3 mm wide strips followed by another three PBS washing steps. Afterwards, the foreskin strips were covered with 5 to 10 mL dispase solution per 6 cm^2 and incubated o/n at 4 °C for 16 to 18 h. After o/n incubation, the dispase solution was replaced by PBS. Next, the dermis and the epidermis were separated using two forceps to strip the dermis from the epidermis. For isolating d-mvECs, the dermis pieces were washed with PBS/EDTA solution followed by incubation in trypsin/EDTA working solution for 40 min at 37 °C and 5 % CO_2. Afterwards, the trypsin/EDTA reaction was stopped by adding 1 % (v/v) FCS. Then, the dermis pieces were transferred into pre-warmed VascuLife® medium. Each dermis piece was scraped carefully with a scalpel blade at least eight times. To detach d-mvECs, the obtained cell suspension was filtered through a cell strainer followed by three washing steps with VascuLife®. After centrifugation at 1,200 rpm for 5 min, the cell pellet was resuspended in VascuLife® and the cell number was calculated as described in section 3.1.2. In early passages, fibroblasts (DFs) were removed by PBS/EDTA treatment for 6 to 10 min at 37 °C depending on the DF amount and donor differences. DFs and d-mvECs were easily separated by their morphological differences. DFs have elongated shapes, whereas d-mvECs are smaller and build cobblestone-like colonies. D-mvECs were cultured until P3. For the vascularized meniscus model, a hd-mvEC pool by combining cells derived from 5 hd-mvEC donors was used (table 2.1).

3.1.2. Cell counting

After reaching a confluence of approx. 90 %, cells were detached by incubation with trypsin/EDTA working solution for 5 min at 37 °C and 5 % CO_2. D-mvECs were preincubated with PBS/EDTA for 10 min at 37 °C to facilitate the detaching process by EDTA as chelating agent. The trypsin reaction was stopped by adding 1 ml FCS and the cell suspension was transferred into a centrifuge tube. After washing with PBS/EDTA to obtain all detached cells and centrifugation at 1,200 rpm for 5 min, the resulting cell pellet was resuspended in cell type specific medium. The cell suspension and trypan blue were mixed 1:1 (dilution factor 2) and added to the interspace of the Neubauer counting chamber. Dead cells were stained blue as trypan blue penetrates damaged cell membranes. By light microscopy, the number of viable (white) and dead (blue) cells were counted manually in all four quadrants. The total number of viable and dead cells was calculated by the arithmetic average of one quadrant multiplied by 10,000 (Neubauer chamber volume factor), the dilution factor 2 and the volume in which the cells have been resuspended (3.1). The cell viability was calculated dividing the number of viable cells by the total number of cells (viable + dead cells) (3.2).

$$number\,of\,viable\,cells = \left(\frac{viable\,cells_{\,4\,\mathrm{quadrants}}}{4}\right) \times 10,000 \times 2 \times volume_{\,\mathrm{cell\,suspension}} \quad (3.1)$$

$$cell\,viability = \frac{number\,of\,viable\,cells}{total\,number\,of\,cells} \quad (3.2)$$

3.1.3. Freezing and thawing of cells

To preserve cell stocks of isolated primary cells, cells were cryo-preserved at a cell concentration of 1 million cells per mL in cell type specific medium supplemented with 10 % (v/v) FCS and 10 % (v/v) DMSO. Because of the hypertonic environment and possible cell damage by DMSO at room temperature (RT), 1 mL of the cell suspension was added to each cryo tube and the cryo tubes were immediately placed into a Mr. Frosty freezing container. This freezing container assured a slow freezing process of 1 °C per min to avoid ice crystal formations. Short-term storage of cells was performed at -80 °C and long-term storage in a liquid nitrogen storage tank.
To thaw cells, the cryo tubes were placed in a water bath at 37 °C until a small piece of ice was left. Subsequently, the thawed cell suspension was transferred to pre-warmed 9 mL

cell type specific medium. After centrifugation at 1,200 rpm for 5 min to remove DMSO, the cell pellet was resuspended in fresh cell type specific medium and seeded in a cell culture flask with a seeding density as listed in table 3.1.

Table 3.1.: Culture conditions and seeding density of cells.

Cell type	**Medium**	**Passage limitation**	**Seeding density**
DFs	DF medium	5	3.33 x 10^3/cm^2
MCs	MC medium	3	3.33 x 10^3/cm^2
MSCs	MSC medium	5	2.67 x 10^3/cm^2
d-mvECs	VascuLife®	3	3.33 x 10^3/cm^2

3.1.4. Cell labeling

For cell labeling, DiI (orange, x_{ex} = 549 nm, x_{em} = 565 nm) was used which labels the cell membrane by inserting its two long hydrocarbon chains into the lipid bilayers. Cell proliferation is inversely proportional to fluorescence intensity as it is halved with each cell division.
After cell detachment, the cell pellet was resuspended in serum-free medium with a concentration of 10^6 cells per mL. 5 μL of 0.93 mg/mL DiI solution were added per 1 mL cell suspension. After incubation at 37 °and 5 % CO_2 for 20 min, the cells were centrifuged at 1,200 rpm for 5 min followed by washing twice with at least 10 mL cell type specific medium. Then, the cell pellet was resuspended in cell type specific medium and was ready for cell seeding (table 3.1). As fluorescence dyes are light sensitive, the cell labeling procedure was performed under light protection.

3.2. Differentiation of MSCs

As defined by the ISCT, three criteria must be achieved for MSCs: plastic adherence, the expression of MSC surface markers and the multi-lineage differentiation potential towards adipocytes, osteoblasts and chondroblasts [77]. To study the differentiation capacity MSCs were cultured in respective differentiation medium (DM).

3.2.1. Adipogenic and osteogenic differentiation

For adipogenic or osteogenic differentiation, 5 x 10^5 MSCs suspended in MSC medium were seeded per well of a 24 well plate on glass slips. After reaching 70 % confluence, the MSC medium was changed to adipogenic or osteogenic DM. During differentiation, medium was changed three times a week. To visualize adipogenic differentiation, Oil Red O staining was performed on day 14 to detect lipid droplets. To confirm osteogenic differentiation, Alizarin Red S staining was performed on day 28 to detect the produced extracellular calcium by osteogenically differentiated hMSCs.

3.2.2. Chondrogenic differentiation

The chondrogenic differentiation was performed in pellet culture. 2.5 x 10^5 MSCs were suspended in MSC medium and centrifuged at 1,200 rpm for 5 min. The supernatant was replaced by chondrogenic DM supplemented with 10 ng/mL TGFβ-3. Medium was changed twice a week. On day 21, the pellets were fixed with 4 % PFA followed by paraffin embedding. Alcian blue staining and IHC for Col II were performed to confirm the chondrogenic differentiation.

3.3. Flow cytometry (FCM)

Surface markers of MSCs were confirmed by FCM. The procedure of FCM staining was performed under light protection and all centrifugation steps were carried out at 1,800 rpm for 6 min. 5 x 10^5 cells per tube were washed once with PBS and then with PBS supplemented with 1 % (v/v) FCS. The cells were resuspended in 50 μL antibody mixture and incubated for 30 min at 4 °C. Then, 1 ml PBS supplemented with 1 % (v/v) FCS was added followed by centrifugation and resuspension in 200 μL PBS supplemented with 1 % (v/v) FCS. The prepared cell suspension was stored at 4 °C under light protection until FCM analysis. Fluorescent measurement was performed with BD LSR-2 and unstained cells were used for the FCM setting. Analysis was performed with the FlowJo software.

3.4. Biomaterial

A meniscus model needs an appropriate biomaterial for 3D cell culture. The organic material of the meniscus mainly consists of collagen, especially Col I. Different Col I scaffolds were analyzed in this study for meniscus tissue engineering.

3.4.1. Commercially available Col I scaffolds

Col I scaffolds were kindly provided by Resorba® (Col I sponge) and Geistlich Biomaterials (Col I/II/Elastin sponge). Punched samples with a diameter of 8 mm were taken from each biomaterial and seeded with 0.5 x 10^6 cells in cell type specific medium. The Resorba® Col I sponge was seeded from the top. The Geistlich Col I/II/Elastin sponge was seeded by soaking from the top with 0.25 x 10^6 cells and from the bottom with 0.25 x 10^6 cells. On day 7, the cell-seeded scaffolds were analyzed for cell distribution by DiI cell labeling and hematoxylin and eosin (HE) staining, metabolic activity by MTT staining and viability by Live/Dead staining to evaluate their potential for meniscus tissue engineering.

3.4.2. Col I gel

Col I was isolated from rat tails. After thawing in PBS, the rat tails were incubated in 70 % (v/v) EtOH for 2 min. Subsequently, the skin of the rat tails was stripped by cutting two-thirds followed by PBS washing. Then, the tendons were removed with forceps and collected in a petri dish with PBS. For disinfection, the tendons were washed twice 10 min with 70 % (v/v) EtOH and three times with PBS to remove EtOH residues. After wet weight measuring, the tendons were incubated in 0.1 % (v/v) acetic acid in a spinner flask under constant agitation at 4 °C for 2 to 3 weeks until the collagen completely dissolved. Next, the collagen solution was centrifuged at 17,700 rpm for 1 h at 4 °C to remove solid residues of tendon tissue. Then, the collagen solution was mixed for 20 min. Finally, the collagen concentration was determined by drying 2 to 3 ml collagen solution at least 48 h at 60 °C. By measuring the dry weight, the collagen concentration was determined. The final concentration of 6 mg/mL was adjusted by adding 0.1 % (v/v) acetic acid. The Col I solution was stored in aliquots at -20 °C.
For Col I gel preparation, Col I solution was diluted 1:4 with gel neutralizing solution (GNL). If not indicated otherwise, 0.5 x 10^6 cells were suspended in ice-cold GNL. Ice-cold

Col I solution was added and suspended carefully with the GNL. This resulted in a neutral pH and the gels were incubated at 37 °C for at least 30 min for solidification.

3.4.3. Decellularized scaffolds

The decellularization procedure of the SIS-muc-TERM® and the BioVaSc-TERM® was performed in a pressure-controlled bioreactor system [65]. If not indicated otherwise, PBS was supplemented with 1 % (v/v) PenStrep. After successful decellularization and gamma sterilization with 25 kGγ, decellularized scaffolds were stored at 4 °C.

3.4.3.1. SIS-muc-TERM®

The SIS-muc-TERM® was produced by decellularization of a porcine jejunum segment including the ECM of the mucosal area. The jejunum segment was excised after inserting an arterial inlet. After rinsing with PBS through the capillary system by the arterial inlet and through the lumen to remove faeces and blood residues, the jejunum segment was filled with PBS and incubated o/n at 4 °C under constant agitation. After o/n incubation, PBS was removed and new PBS was pumped through the capillary system with a controlled pressure of 80 to 100 mmHg to remove air bubbles. Subsequently, 500 mL DS were pumped through the capillary system with a speed between 3 and 10 rpm. Then, the lumen was filled with DS and the capillary system with 2 mL DS. After o/n incubation at 4 °C, the scaffold was washed by pumping PBS through the lumen and the capillary system to remove any DS remnants with a pumping speed between 10 and 40 rpm. Next, the capillary system was removed and the matrix was cut into 6 to 8 cm long pieces. After removing the thin serosal layer, the matrix was washed three times with PBS. To remove DNA, the matrix pieces were incubated in 0.33 mg/mL DNase at 4 °C. After o/n incubation and three PBS washings, the SIS-muc-TERM® was stored in PBS until gamma sterilization by BBF Sterilisationsservice (Kernen-Rommelshausen, Germany).
For static 3D culture, custom-made cell crowns consisting of two concentric metal rings with a 1 cm^2 growth area (figure 3.2 A) were used to stabilize the SIS-muc-TERM® with the mucosal side facing up for cell seeding. 0.5 x 10^6 cells were seeded in 100 μL medium onto the SIS-muc-TERM® followed by 3 h incubation at 37 °C and 5 % CO_2 to allow cell attachment. For the biomaterial combination of SIS-muc-TERM® and Col I gel, 1 mL cell-laden Col I gel with 0.5 x 10^6 cells per cell crown was loaded onto the mucosal side of the SIS-muc-TERM® in the cell crown (figure 3.2 B, C).

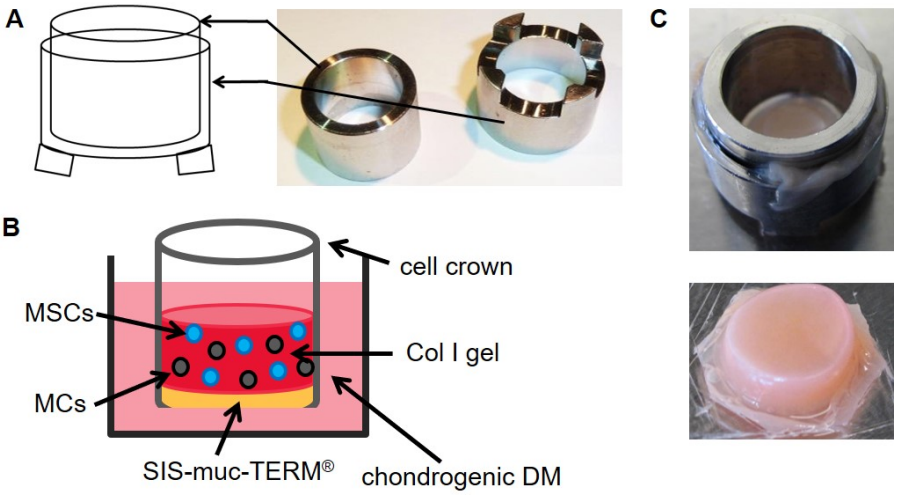

Figure 3.2.: SIS-muc-TERM® as decellularized scaffold to build 3D models. A Cell crowns to fix the SIS-muc-TERM®. **B** Schematic illustration for co-culturing MCs and MSCs in a Col I gel on SIS-muc-TERM® fixed in the cell crown. **C** Photos of 3D models composed of cell-laden Col I gel on SIS-muc-TERM® after 21 days of static culture.

3.4.3.2. BioVaSc-TERM®

The BioVaSc-TERM® (figure 3.3 D) was generated by decellularization of a porcine jejunum segment providing a maintained vascular network within the collagen matrix. The jejunum segment was excised after inserting an arterial inlet and a venous outlet (figure 3.3 A). After flushing PBS through the capillary system by the arterial inlet and through the lumen to remove faeces and blood residues (figure 3.3 B), 500 mL DS were pumped through the capillary system and 250 mL DS through the lumen interrupted by massaging the segment (figure 3.3 C). Subsequently, the capillary system was flushed with 1 L PBS and the lumen with 250 mL PBS followed by filling with DS. After o/n incubation at 4 °C under constant agitation, the capillary system was checked by phenol red injection in the arterial inlet (Figure 3.3 E). After washing the capillary system with 2 L PBS and the lumen with 250 mL PBS, the lumen was filled with DNase and the matrix was placed in a plastic beaker filled with DNase solution. After incubation at 37 °C for 2 h under constant agitation, the DNase solution was replaced by PBS. After o/n incubation at 4 °C, the BioVaSc-TERM® was washed with PBS three times and stored in PBS until gamma sterilization by BBF Sterilisationsservice (Kernen-Rommelshausen, Germany).
For cell seeding, 6 to 10 x 10^6 d-mvECs were seeded into the BioVaSc-TERM® through the arterial inlet and the venous outlet followed by a static cell attachment time of at least 3 h to 1 day. Subsequently, 3D dynamic culture by applying pulsatile pressure was started.

The bioreactor system used for 3D dynamic culture is described in section 3.6.3.

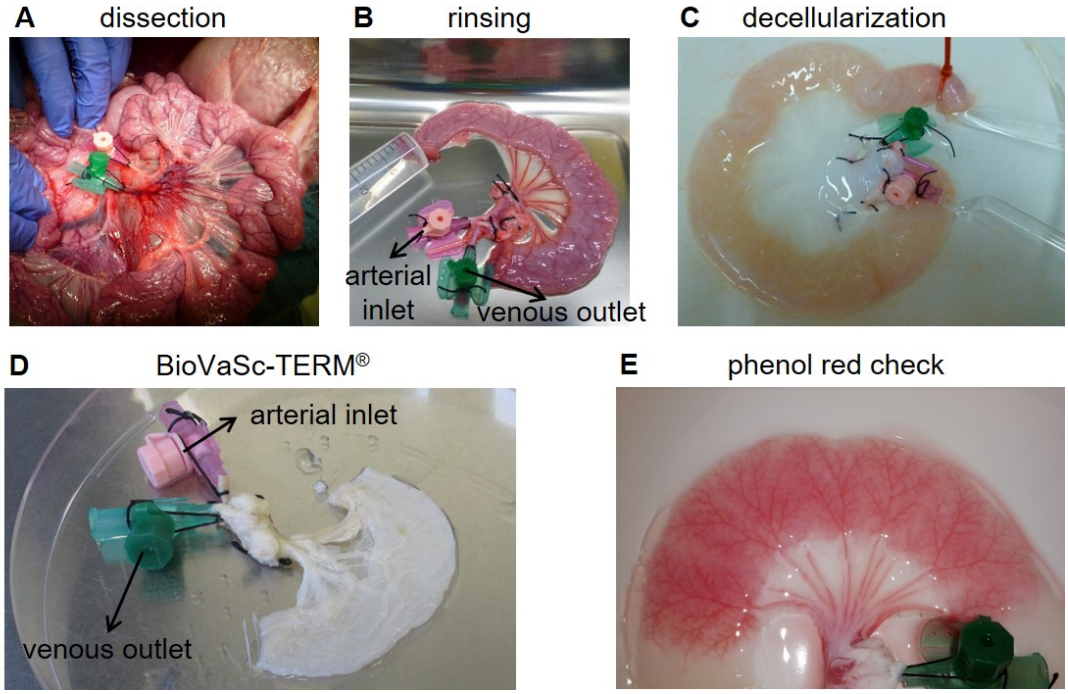

Figure 3.3.: Decellularization procedure to obtain the BioVaSc-TERM®. A A porcine jejunum segment was excised after inserting an arterial inlet and a venous outlet followed by rinsing (**B**) and decellularizing (**C**) the capillary system and the lumen. **D** BioVaSc-TERM® after the decellularization procedure with the arterial inlet and the venous outlet. **E** Phenol red injection to check the maintained vessel system.

3.5. Wedge-shape compression of Col I gels

3.5.1. Procedure of the wedge-shape compression

The wedge-shape compression of Col I gels was established to build a wedge-shaped meniscus model. A customized polysulfone-made bioreactor system for wedge-shape compression with a movable wedge was developed (figure 3.4 A). The bioreactor bottom consisted of a cylindric hollow interior which was open to the top with an inner diameter of 24 mm. Four Luer-Lock connectors were installed on the outside of the round bioreactor bottom with an offset of 90 ° to each other. During compression, the lower located pair was opened to let liquid produced by compression draining from the bioreactor. The top of the bioreactor body was a hollow cylinder (inner diameter 24 mm, length 3 cm) which was tightened using an O-ring sealing and used to increase the height and to guide the

puncher. The movable wedge was placed inside of the bioreactor bottom. The wedge (height 14.5 mm, angle 30 °) had a pore size of 1 mm to let the produced liquid produced by compression draining to the bottom. Filter paper was placed on top of the wedge to prevent leaking of collagen gel solution before gelation. To keep the inner part of the bioreactor sterile during gelation at 37 °C and 5 % CO_2, a lid was fixed at the bioreactor top. All parts of the bioreactor system including the movable wedge were autoclaved before use.

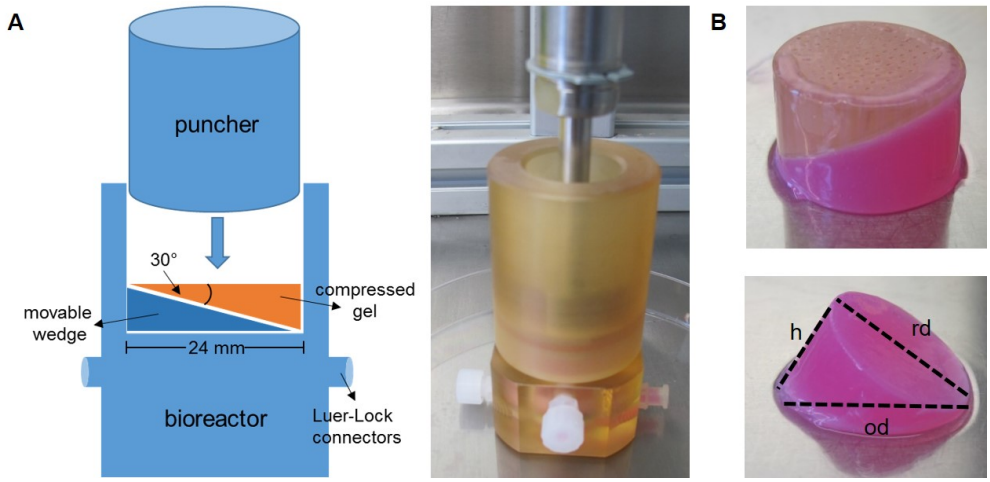

Figure 3.4.: Wedge-shape compression of Col I gels. A Customized compression system for wedge-shape compression consisted of a puncher from the top and the bioreactor system composed of the bioreactor bottom with a hollow cylinder and a movable wedge inside. A schematic illustration of the compression system is shown on the left and a photo on the right. **B** After compression, the cylinder was removed from the reactor, the bioreactor bottom was turned and the wedge-shaped Col I gel fell out together with the wedge (top). The size of the wedge-shaped Col I gels was measured by the round diameter (rd), the oval diameter (od) and the height (h).

For wedge-shape compression, the bioreactor system was assembled and the prepared MSC-laden Col I - GNL solution was pipetted carefully on top of the wedge (figure 3.4 A). After gelation for at least 30 min at 37 °C and 5 % CO_2, a filter paper was placed on top of the gel. Subsequently, the bioreactor was compressed by a stainless steel puncher installed in a self-made compression device of TERM. The MSC-laden Col I gel was compressed with a speed of 0.78 mm/min to a final volume of 4.18 mL and a final cell concentration of 0.5 x 10^6 MSCs per mL if not indicated otherwise. The compression factor (CF) was determined by division of the original volume upon filling and the calculated final volume. Different CFs were analyzed to determine the optimal CF: 1.6 (= 6.5 mL/4.18 mL) and 3.3 (= 14 mL/4.18 mL). After compression, the cylinder was removed from the reactor, the bioreactor bottom was turned and the wedge-shaped MSC-laden Col I gel fell out together

with the wedge (figure 3.4 B). The reusable wedge and the filter papers were removed. Then, the wedge-shaped MSC-laden Col I gel was ready for culture.

3.5.2. Static culture of wedge-shaped Col I gels

With the optimized CF of 3.3 resulting in a final Col I concentration of 13.3 mg/mL on day 0, wedge-shape compression of Col I gels was performed without (w/o) and with hMSCs, reaching a final concentration of 0.5 x 10^6 hMSCs per mL as described. The wedge-shaped constructs were cultured in chondrogenic DM supplemented w/o or with 10 ng/mL TGFβ-3 or additionally with MMC (macromolecular crowding) by adding 37.5 mg/mL Ficoll PM 70 kDa and 25 mg/mL Ficoll PM 400 kDa to the medium.

1. w/o cells with chondrogenic DM w/o TGFβ-3
2. hMSCs with chondrogenic DM w/o TGFβ-3
3. hMSCs with chondrogenic DM with TGFβ-3
4. hMSCs with chondrogenic DM with TGFβ-3 + MMC

The three weeks of static 3D culture were performed in 6 deep well plates. Medium change of 7.5 mL per gel in one well was performed twice a week. At each time point of medium change, medium was collected and stored at -80 °C until analysis by Cedex, ColIA1 ELISA and gel zymography. Moreover, wet weight was measured and photos were taken for size measurement. For size measurement, the round diameter (rd), the oval diameter (od) and the height (h) were measured (figure 3.4 B). For shrinkage evaluation by size measurement, the reduction of each parameter (rd, od and h) from day 21 compared with day 0 was calculated in %. The arithmetic average and the standard deviation of the determined shrinkage value in % of rd, od and h was calculated. On day 21, the culture was stopped and the wedge-shaped models were analyzed for the metabolic activity by MTT staining, the expression of meniscal markers by IHC, the quantification of GAG and DNA, and the biomechanical properties (section 3.5.3).

3.5.3. Biomechanical analysis of wedge-shaped Col I gel models

The biomechanical analysis of wedge-shaped Col I gel models was performed on day 21 in cooperation with Dr. Andreas Martin Seitz and Prof. Dr. Lutz Dürselen at the Institute

of Orthopaedic Research and Biomechanics, Ulm University, Germany. For biomechanical measurements, a 6 mm round sample was punched from the middle of the wedge-shaped models followed by dissecting in a top and a bottom piece (figure 3.5 A). These pieces were separately measured using the Zwick Z010, a standard material testing machine (figure 3.5 B, C). Compression testing was performed using a physiologic compressive strain of up to 12 % [122]. The linear modulus of the first strain $E_{lin}(1)$ and the last strain $E_{lin}(10)$ was determined. All tests were conducted using a previously described method [123, 124]. For following statistical analyses, the test results of the identical top and bottom pieces were summarized.

In addition to the biomechanical measurements, wet weight, size, water content, GAG and DNA content of the wedge-shaped models; and ColIA1 by ELISA, glucose and lactate via Cedex, MMP-2 and -9 by gel zymography of medium supernatants were analyzed. The water content was calculated as follows (3.3).

$$water\,content = \frac{(wet\,weight - dry\,weight)}{wet\,weight} \tag{3.3}$$

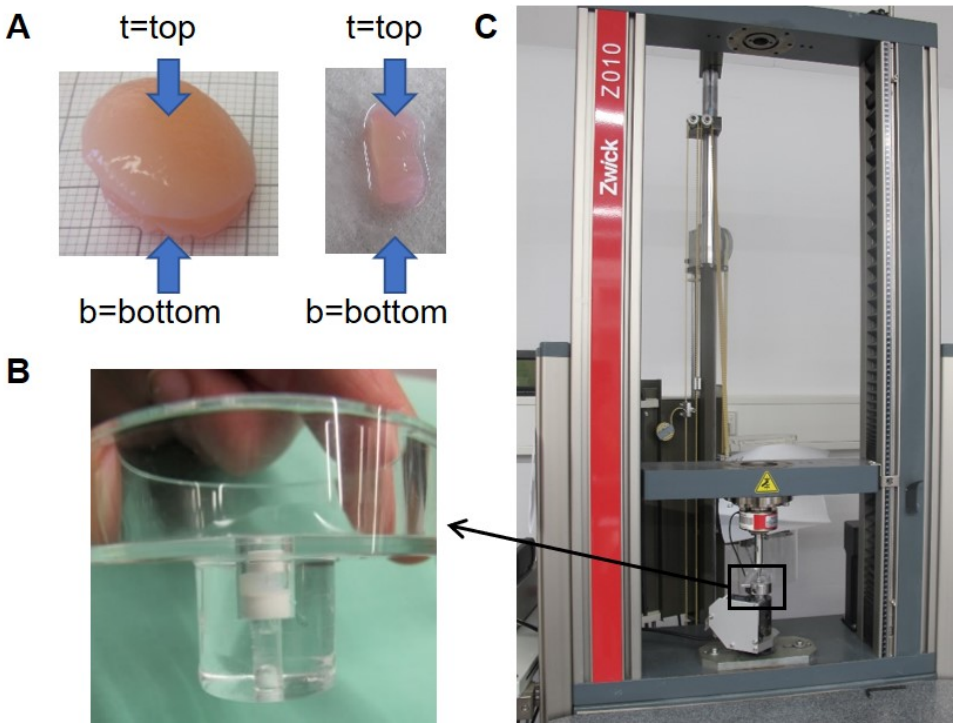

Figure 3.5.: Biomechanical measurements of wedge-shaped Col I gel models on day 21. **A** Punching of a 6 mm round sample out of the wedge-shaped models followed by dissecting in a top and a bottom piece. **B, C** Separate biomechanical measurement of the top and the bottom piece by the Zwick Z010 at the Institute of Orthopaedic Research and Biomechanics, Ulm University, Germany.

3.6. Vascularization strategies

3.6.1. Artificial hypoxia state via CPX

As PHIs such as CPX are promising compounds to induce vascularization by stabilizing HIF-1α, a master switch of angiogenesis [49], this vascularization strategy was studied.

3.6.1.1. Preparation of CPX

10 mM CPX stock solution was prepared in DMSO and stored at -20 °C. The CPX stock solution was diluted to achieve a 10 μM working solution in appropriate cell culture medium immediately before use.

3.6.1.2. MSC-conditioned medium

For the production of MSC-conditioned medium (MSC-CM), hMSCs of the characterized hMSC pool were grown in P3 in MSC medium until reaching 80 % confluence in six T150 flasks. Then, the medium was changed to low FCS MSC medium supplemented with 2 % (v/v) FCS. The low FCS MSC medium of three T150 flasks was supplemented with 10 μM CPX for the production of MSC-CM after CPX stimulation (MSC-CM CPX). As control, the remaining three T150 flasks were used to produce MSC-CM without stimulation (MSC-CM). After 24 h incubation at 37 °C and 5 % CO_2, the medium of the corresponding flasks was pooled and filtrated (0.2 μm filter) to remove cell debris. To exclude negative influence of CPX, the hMSCs were investigated microscopically. Furthermore, the cell number was determined and 5 x 10^5 cells were frozen for gene expression analysis. The produced MSC-CM was analyzed via hVEGF ELISA and Proteome Profiler™ Human Angiogenesis Array Kit. To study the pro-angiogenic effect of hMSCs on hd-mvECs, the MSC-CM was applied in the sprouting assay of hd-mvEC spheroids.

3.6.1.3. Sprouting assay

The method of sprouting assay was applied to study the influence of pro-angiogenic substances on hd-mvEC spheroids.

Hd-mvECs spheroids were prepared by adding of 3 x 10^5 hd-mvECs in a reagent reservoir followed by adding a solution of 12 mL methylcellulose solution and 48 mL VascuLife® resulting in 5,000 cells per mL. Subsequently, 100 μL of this cell suspension were pipetted per well of six non-adherent round bottom 96 well plates. After incubation for 18 to 24 h at 37 °C and 5 % CO_2, a spheroid composed of approx. 500 hd-mvECs formed per well. These hd-mvEC spheroids were harvested. After centrifugation at 1,200 rpm for 5 min, the supernatant was removed and the spheroids were resuspended in a volume of 5 mL with methylcellulose solution. Next, the spheroids were embedded in a Col I gel. For that, the collagen solution was prepared on ice by mixing 4 mL 0.4 % Col I R solution (Serva) with 2 mL 0.1 % (v/v) acetic acid, 600 μL medium 199 and an appropriate amount of 0.2 N NaOH to neutralize the Col I mixture. After carefully mixing with the harvested spheroids, 1 mL of the spheroid-containing Col I gel solution (50 spheroids per mL) was pipetted per well of a pre-warmed 24 well plate.
After polymerization for 30 min at 37 °C and 5 % CO_2, the stimulation of the spheroids was performed with a volume of 200 μL with the following experimental groups: VascuLife® basal medium (1) w/o stimulation agent, (2) with 25 ng/mL hVEGF as positive control, and (3) with 10 μM CPX; (4) MSC-CM and (5) MSC-CM CPX. After 24 h incubation at 37 °C and 5 % CO_2, the sprouting of spheroids was studied by taking pictures of ten randomly selected spheroids per group with the EVOS XL microscope. Digital quantification of the number of sprouts (NOS) and the cumulative sprouting length (CSL) was performed with ImageJ software.

3.6.2. Cell sheet engineering

As further vascularization strategy, cell sheet engineering of a co-culture of hMSCs and hd-mvECs was optimized in cooperation with Dr. Anke Hoppensack belonging to the Dr. Marie Weinhart group of the Freie Universität Berlin, Germany. These cell sheets were applied to the 3D meniscus model to mediate an oriented vascularization approach from the location of the RR zone (section 3.7).
Polyglycidylether (PGE) coated petri dishes for temperature triggered cell sheet fabrication were kindly provided by Dr. Anke Hoppensack. As PGE is a thermo-responsive polymer, these dishes allow for a mild and temperature triggered detachment of intact cell sheets with their ECM [125]. First, the PGE coated petri dishes were sterilized by incubation with 70 % (v/v) sterile EtOH for 15 min at RT followed by washing three times with PBS^+. Subsequently, 1.44 x 10^6 hMSCs in DMEM LG containing 10 % (v/v) FCS and 5 ng/mL hbFGF were seeded per well. After incubation for 4 h at 37 °C and 5 % CO_2, the medium

was carefully removed and 0.58 x 10^6 hd-mvECs resuspended in 50 % (v/v) DMEM LG with 10 % (v/v) FCS and 5 ng/mL hbFGF, and 50 % (v/v) VascuLife® were seeded onto the petri dish. After 24 h incubation at 37 °C and 5 % CO_2, the medium was replaced by RT pre-warmed PBS and incubated for 10 min at RT under microscopic observation. Next, the PBS was changed to 37 °C pre-warmed PBS and incubated for 5 min at 37 °C and 5 % CO_2. Afterwards, the cell sheet detachment process was observed at RT and approx. after 15 to 30 min resulted in a free-floating sheet. For characterization, the sheet was fixed with 4 % PFA for 30 min at RT followed by washing twice with PBS. The cell sheet was stored in PBS at 4 °C until immunofluorescent staining. The optimized procedure for the cell sheet transfer onto the RR zone of the meniscus models is described in section 3.7.1.

3.6.3. BioVaSc-TERM® bioreactor

All bioreactor components were autoclaved and assembled under sterile conditions (figure 3.6 A). Before hd-mvEC seeding, the assembled bioreactor system comprising the reactor, the medium-reservoir bottle and the pressure-compensation bottle (figure 3.6 A, B) was filled with culture medium and connected to the pump by pump tubes integrated into the bioreactor board to remove any air bubbles (figure 3.6 C).

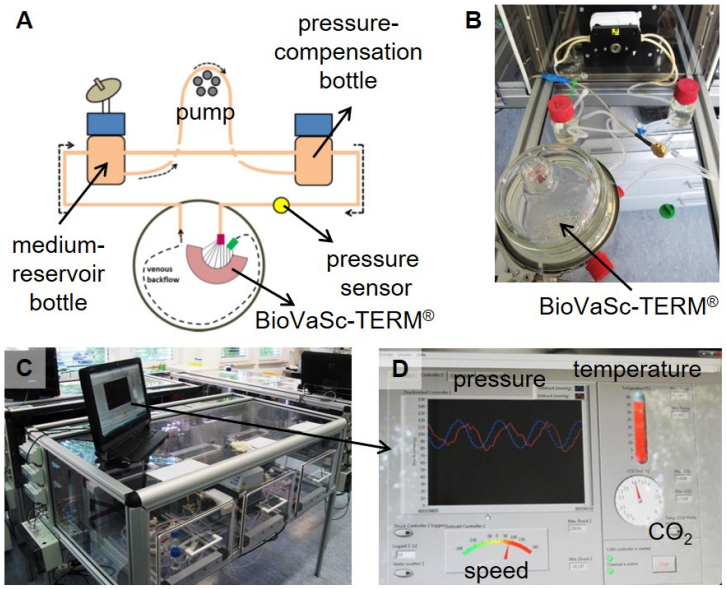

Figure 3.6.: Bioreactor of the BioVaSc-TERM®. **A** Schematic illustration of the bioreactor setup for 3D dynamic culture. **B** Experimental setup of the bioreactor with the reseeded BioVaSc-TERM® for 3D dynamic culture. **C** Bioreactor board. **D** Monitoring system coupled to the bioreactor system for controlling the pressure: reference value in blue and just value in red.

After o/n incubation in Vasculife®, the BioVaSc-TERM® was seeded with hd-mvECs under sterile conditions as described in section 3.4.3.2. After static incubation for at least 3 h to 1 day at 37 °C and 5 % CO_2, the arterial inlet of the BioVaSc-TERM® was connected to the bioreactor system containing no air bubbles and the bioreactor was placed into the bioreactor board providing cell culture conditions: 37 °C and 5 % CO_2. The peristaltic pump pumped the culture medium through the vessels with a constant flow rate of 10 rpm. The culture medium circulated from the medium-reservoir bottle into the arterial inlet (red) of the BioVaSc-TERM® perfusing the reseeded capillary network. An intermediate pressure sensor measured the applied pressure. After 24 h, the flow rate was changed to a pulsatile flow mimicking the blood pressure. An adjustable screw between the pressure-compensation bottle and the medium-reservoir bottle was used for adjusting the just value of the pressure to the reference value: the mean pressure of 100 mmHg with an amplitude of 20 mmHg (figure 3.6 D). The 3D culture of hd-mvECs within the BioVaSc-TERM® was performed under pulsatile pressure at least for 14 days. Medium change was performed once a week.

3.7. Establishment of a vascularized meniscus model

To establish a vascularized meniscus model, hd-mvECs were integrated into the wedge-shaped meniscus model. Two vascularization strategies were applied. First, the RR region of the wedge-shaped model was covered with the hMSC/hd-mvEC sheet (figure 3.7). For simplifying, the hMSC/hd-mvEC sheet is named as cell sheet in the following.

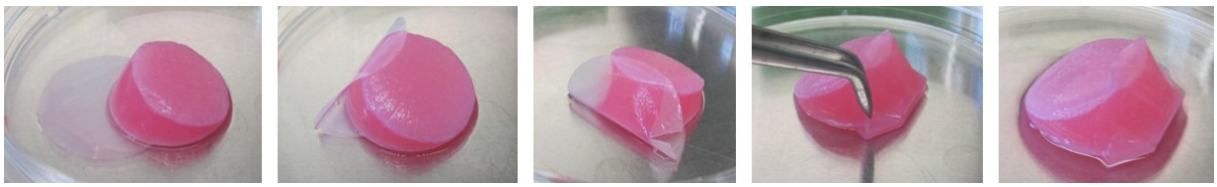

Figure 3.7.: Transfer of the cell sheet onto the RR zone of the wedge-shaped Col I gel using a Nunc membrane. The cell sheet was attached to the Nunc membrane and the Nunc membrane was wrapped around the RR region of the wedge-shaped Col I gel on day 1.

Second, a small gap of standardized size was cut into the RR region to inject a cell suspension of hMSCs and hd-mvECs in a cell concentration as used for the cell sheet (figure 3.8). These two strategies are described in the next two subchapters.
As medium, 50 % (v/v) chondrogenic DM and 50 % (v/v) VascuLife® supplemented with

10 ng/mL TGFβ-3 was used for the culture duration of 21 days. Medium was changed twice a week. As negative control, wedge-shaped hMSC-laden Col I gels w/o hd-mvECs were cultured in the same medium. At each time point, size and wet weight was measured. Furthermore, medium was collected and stored at -80 °C for later analysis by Cedex and gel zymography. On day 21, the models were stopped for analysis of metabolic activity by MTT staining, water content, expression of meniscal markers by IHC, and quantification of GAG and DNA content.

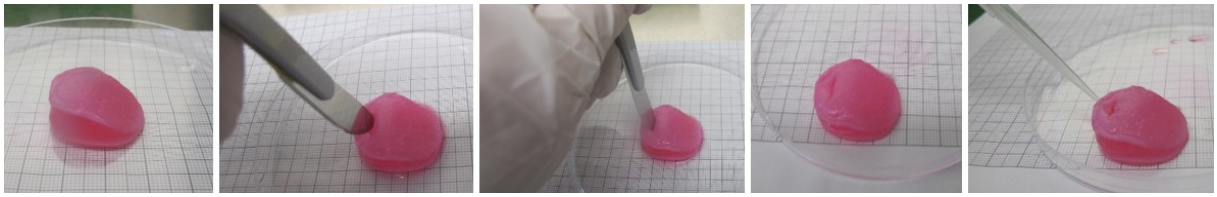

Figure 3.8.: Preparation of the gap into the wedge-shaped Col I gel. The gap (5 mm deep, 5 mm wide, 5 mm distance from RR edge) was cut with a scalpel into the wedge-shaped Col I gel on day 1 for the injection of the cell suspension.

3.7.1. Transfer of the cell sheet onto the wedge-shaped hMSC-laden Col I gel

On day 0, the wedge-shape compression of the hMSC-laden Col I gel was performed with the optimized CF of 3.3 as section 3.5 described. Moreover, the cell sheet was produced as explained in section 4.5.2. After 24 h, the RR side of the wedge-shaped hMSC-laden gel was covered with the cell sheet. For that, the sheet transfer onto the RR zone of the wedge-shaped Col I gel was successfully established as follows.
After the 24 h incubation at 37 °C and 5 % CO_2, the medium of the cell seeded PGE coated petri dish was replaced by RT pre-warmed PBS and incubated for 10 min at RT under microscopic observation. Afterwards, the PBS was carefully removed and a sterile Nunc membrane was placed onto the cell layer growing on the PGE coated petri dish without allowing any air bubbles. Subsequently, 200 μL PBS was added to the membrane surface. Then, the petri dish was incubated for 5 min at 37 °C and 5 % CO_2. Afterwards, the incubation was continued at RT and observed macroscopically and microscopically. After 15 min at RT, the cell sheet edges were carefully detached if needed and placed around the Nunc membrane with a 1 mL pipet tip. Then, the membrane was carefully lifted making sure that most of the cell sheet was attached to the Nunc membrane. The Nunc membrane with the transferred sheet was wrapped around the RR zone of the wedge-shaped Col I gels (figure 3.7). After adding 500 μL appropriate culture medium onto the top of the

membrane coated gel, they were incubated for 30 min at 37 °C and 5 % CO_2. Subsequently, 500 μL appropriate culture medium was pipetted onto the top of the membrane coated gel again and the membrane was carefully removed, provided that the sheet was fixed to the gel. After successful transfer, the constructs were covered by medium and cultured for 21 days. For the establishment of the here described procedure of the cell sheet transfer onto the Col I gel, metabolic activity test by MTT staining was used to confirm a successful transfer onto a wedge-shaped Col I gel w/o cells.

3.7.2. Injection of the cell suspension into the wedge-shaped hMSC-laden Col I gel

On day 0, the wedge-shape compression of the hMSC-laden Col I gel was performed as previously described (section 3.5). After 24 h, a gap (5 mm deep, 5 mm wide, 5 mm distance from the RR edge) was carefully cut with a scalpel into the wedge-shaped Col I gel (figure 3.8). Then, 1.44 x 10^6 hMSCs and 0.58 x 10^6 hd-mECs suspended in a volume of 20 μL were injected into the gap. The gap was closed by filling with the fibrin glue TISSEEL. After incubation for 30 min at 37 °C and 5 % CO_2, the constructs were covered by medium and cultured for 21 days. For establishment of the here described procedure, metabolic activity test by MTT staining was used to confirm a successful injection in a Col I gel w/o cells.

3.8. Tensile testing of meniscal sutures in the BioVaSc-TERM®

A meniscus implant has to be fixed properly in the knee joint as there are high mechanical forces. The BioVaSc-TERM® is planned to be a wrapping outer structure for the established wedge-shaped meniscus model. For the fixation within the knee joint, an appropriate meniscal suture is needed. To choose an appropriate fixation technique, the OIR with a resorbable PDS 2.0 suture and the Stryker AIR were compared by suturing into the BioVaSc-TERM® followed by tensile testing. The meniscal sutures OIR and Stryker AIR were sutured into the BioVaSc-TERM® by Dr. Kai Fehske who is a sport orthopedic surgeon (figure 3.9). Afterwards, the BioVaSc-TERM® scaffolds (n=4) containing the sutures (n_{OIR}=8, $n_{Stryker\ AIR}$=5) were cut into single pieces each containing one suture.

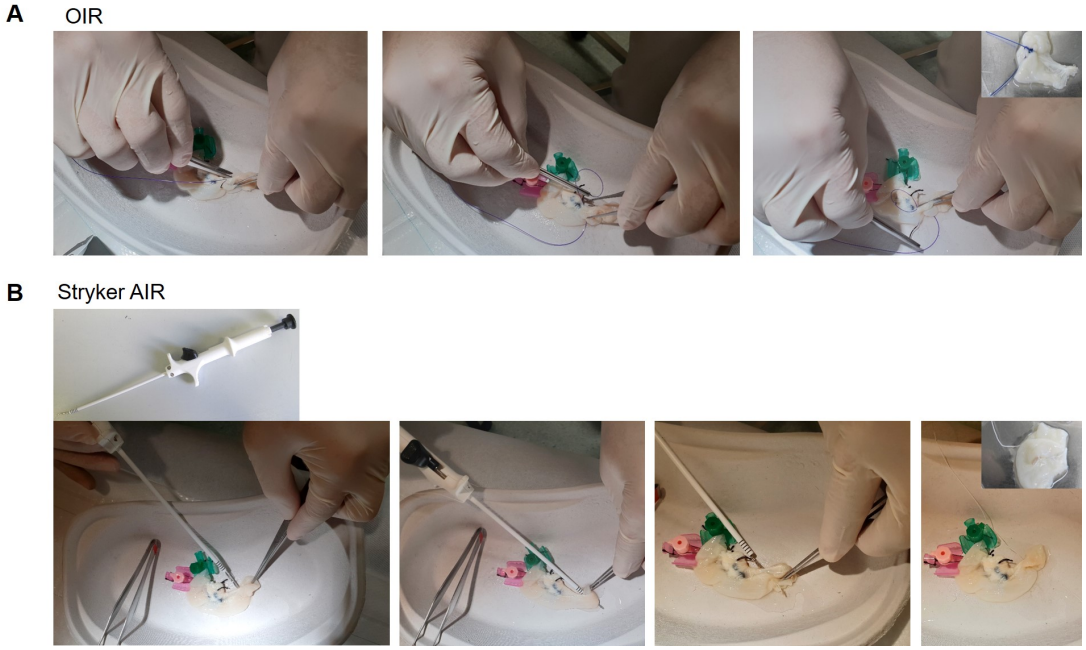

Figure 3.9.: Meniscal sutures in the BioVaSc-TERM®. The OIR with the PDS 2.0 suture (**A**) and the Stryker AIR (**B**) were sutured into the BioVaSc-TERM® by Dr. Kai Fehske.

The tensile testing of the meniscal sutures in the BioVaSc-TERM® was performed at the Institute of Orthopaedic Research and Biomechanics, Ulm University, Germany by Dr. Andreas Martin Seitz with the Zwick Z010 machine connected with a 20 N load cell (KAP-Z, AST). Each specimen was fixed at the overhanging BioVaSc-TERM® scaffold without influencing the meniscal suture. For tensile testing, the suture end (1 to 2 mm from the exit point) was pulled out with a load speed of 10 mm/second. The load speed of 10 mm/second mimicked the real loading conditions of a meniscal suture damage.

3.9. Metabolic activity and viability staining

3.9.1. Metabolic activity by MTT staining

The metabolic activity was assessed macroscopically by MTT staining. The assay is based on the reduction of the yellow tetrazolium dye MTT to blue insoluble formazan by cellular enzymes of metabolically active cells [126]. The samples were incubated with 1 mg/mL MTT solution for 90 min at 37 °C, washed with PBS and documented photographically.

3.9.2. Viability by Live/Dead staining

The viability was analyzed by the Live/Dead Viability/Cytotoxicity Kit for mammalian cells by fluorescence microscopy. The samples were incubated in Live/Dead solution (4 μM calcein, 2 μM ethidium homodimer-1) for 1 min at RT, washed with PBS and visualized microscopically. Calcein is retained within live cells and is stained in green (x_{ex} = 494 nm, x_{em} = 517 nm). Ethidium homodimer-1 penetrates cells with damaged membranes and intercalates into the DNA staining dead cells in red (x_{ex} = 528 nm, x_{em} = 617 nm).

3.10. Biochemical characterization

The GAG and DNA content of papain digested samples were measured. Medium supernatants were frozen at -80 °C until analysis for metabolites such as glucose and lactate by Cedex measurement, human VEGF (hVEGF) and human pro-collagen I α1 (hCOLIA1) by enzyme-linked immunosorbent assay (ELISA).

3.10.1. Papain digestion

For biochemical characterization of the GAG and DNA content, samples were wet weighed, frozen o/n at -80 °C, freeze dried with the Lyophilizator Alpha 1-2 LDplus, dry weighed and digested in papain digestion buffer containing 140 μg/mL papain enzyme o/n at 60 °C. The papain digested samples were stored at -20 °C until biochemical characterization. After thawing, the papain digested samples were vortexed and centrifuged at 4,700 rpm for 1 min before sample preparation for the DNA and GAG quantification.

3.10.2. DNA quantification

The DNA content of the papain digested samples was analyzed with the Quant-iT™ PicoGreen® dsDNA assay according to the manufacturer's instruction. In preparation, 20x TE buffer was diluted with ultrapure water. As standard curve, Lambda DNA stock solution of 100 μg/mL was diluted with 1x TE buffer (0, 1, 10, 100, 200, 300, 400, 500, 600, 800 and 1,000 ng/mL). Standards and samples/sample dilutions were pipetted in

duplicates in a black 96 well plate (100 μL per well) followed by the addition of 100 μL Quant-iT™ PicoGreen® dsDNA reagent diluted 1:200 in 1x TE buffer. After mixing and incubation for 2 min under light protection, the fluorescence was measured using the microplate reader Tecan Infinite M200 with an excitation wavelength of 480 nm and an emission wavelength of 525 nm. DNA content in samples was calculated based on the standard curve and the used dilution if applicable.

3.10.3. GAG quantification

The GAG content of the papain digested samples was analyzed with the GAG Blyscan™ assay according to the manufacturer's instructions. As standard curve, the GAG reference standard of 100 μg/mL was prepared in ultrapure water (0, 1, 2, 3, 4 and 5 μg). A volume of 100 μL per standard and samples/sample dilutions was incubated with 1 mL dye reagent for 30 min at RT on a mechanical shaker resulting in the formation of a GAG-dye complex. After centrifugation at 12,000 rpm for 10 min and discarding of the supernatant, 500 μL dissociation reagent were added followed by mixing. The GAG-bound dye was released within 10 min and 200 μL of each sample were pipetted in duplicates in a transparent 96 well plate per well. The optical density (OD) was measured at a wavelength of 620 nm with a reference wavelength of 405 nm using the microplate reader Tecan Infinite M200. GAG content in samples was calculated based on the standard curve and the used dilution if applicable.

3.10.4. Metabolit measurement by Cedex

Medium supernatants were analyzed for the metabolites glucose (GLC2B) and lactate (LAC2B) by Cedex measurement. The Cedex Bio Analyzer was prepared following the instructions of the manufacturer's manual. As controls for each measurement cycle, Control A Level 2 Bio and Control A Level 3 Bio were controlled.

3.10.5. Gel zymography

Gel zymography is a qualitative method to detect MMPs which are responsible for matrix remodeling. It was established as method at TERM. Gel zymography of medium

supernatants collected during 3D culture was performed. To detect MMP-2 and -9 by degradation of their substrate gelatin, 10 % Zymogram Plus (Gelatin) Protein Gels were loaded with 10 μL prepared sample solution (5 μL medium supernatant mixed with 5 μL Tris-Glycine SDS (TGS) Sample Buffer 2x). As protein marker, 5 μL ProSieve QuadColor Protein Marker were loaded. As positive control, 1 ng Collagenase F, or 1, 2 or 5 ng MMPs (proMMP-2, MMP-2 or MMP-9) were loaded. As running conditions in 1x TGS Running Buffer, an electric tension of 125 V was applied for 105 min. Afterwards, the proteins were renaturated by incubation in Zymogram Renaturing Buffer for 30 min at RT. Then, the gels were incubated in Zymogram Developing Buffer for 30 min at RT. After discarding the Zymogram Developing Buffer, new Zymogram Developing Buffer was added followed by o/n incubation at 37 °C. After o/n incubation, the gels were stained with Coomassie blue stain solution for 90 min. After destaining by three 40 min destaining steps with Coomassie destain solution, white bands on the blue background appeared indicating MMPs by degradation of the blue stained substrate gelatin. The pictures of the gels were taken with the FluorChem™ Q developing machine using the FluorChem™ Q software. Total MMP expression profiles by the pixel intensity of total MMPs were analyzed by intensity quantification (densitometry) using the ImageJ software. Total MMP expression profiles were analyzed due to overlapping molecular weights of MMPs such as MMP-2 with 62 kDa and MMP-9 with 67 kDa, and to get a general statement about matrix remodeling by changings of the pixel intensity of total MMPs. If indicated in the figure, different biochemical conditions for the culture of hMSC-laden Col I gels were visualized by MMP fold change as calculated by the division of the quantified pixel intensity of total MMPs of the two to be compared biochemical conditions.

3.10.6. ELISA

Medium supernatants were analyzed for hVEGF and hCOLIA1 by ELISA. An ELISA is based on the streptavidin-biotin interaction. The antigen of interest binds to a capture antibody of a coated plate and is detected by a biotinylated detection antibody. After adding a streptavidin coupled horse radish peroxidase (HRP) and the chromogen tetramethylbenzidine, the color of the solution will change corresponding to the amount of the antigen of interest.

The hVEGF and hCOLIA1 ELISA were performed according to the manufacturer's instructions. A 96 well plate was coated with 100 μL capture antibody per well by o/n incubation at RT. The next day, the plate was washed three times with ELISA wash buffer and blocked with reagent diluent for 1 h at RT. As standard curve, standard samples (0,

31.3, 62.5, 125, 250, 500, 1000 and 2000 pg/mL hVEGF or hCOLIA1) were prepared by serial dilution with reagent diluent. After blocking, the plate was washed three times. Then, 100 μL of standard samples and medium supernatants/medium supernatant dilutions were pipetted per well in duplicates and incubated for 2 h followed by three washing steps. Next, 100 μL detection antibody were added per well and incubated for 2 h at RT. After washing three times, the following procedure was conducted under light protection. 100 μL of the streptavidin-HRP working solution were added per well and incubated for 20 min at RT followed by three washing steps. Subsequently, 100 μL substrate solution were added and after incubation for 20 min at RT, 50 μL stop solution were added per well. The OD was measured immediately at a wavelength of 450 nm with a reference wavelength of 570 nm using the microplate reader Tecan Infinite M200. HVEGF and hCOLIA1 content in medium supernatants were calculated as described in the manual based on a four parameter logistic curve-fit as standard curve and the used dilution if applicable.

3.10.7. Proteome Profiler™ Human Angiogenesis Array Kit

Medium supernatants were analyzed for the expression profiles of angiogenesis-related proteins by the Proteome Profiler™ Human Angiogenesis Array Kit. The array is based on capture antibodies which are spotted in duplicates on nitrocellulose membranes. After incubation with the samples and biotinylated detection antibodies, any protein-detection antibody complex is bound by its capture antibody on the membrane and detectable after sequential adding of streptavidin HRP and chemiluminescent detection reagents. The produced light at each spot is proportional to the amount of bound analyte.
First, 2 mL of array buffer 7 (blocking buffer) were added per well of a 4 well dish. Each membrane was placed in one well. After incubation for 1 h at RT on a rocking platform shaker, prepared samples of 1 mL sample with 0.5 mL array buffer 4 and 15 μl reconstituted detection antibody cocktail, were pipetted into the wells. After incubation o/n at 4 °C, each membrane was washed three times with wash buffer for 10 min in an individual plastic container. Then, the membranes were returned to the 4 well dish containing 2 mL streptavidin HRP diluted in array buffer 5 followed by incubation for 30 min at RT under light protection. After three washing steps as described before, the membranes were covered with chemi reagent mix and incubated for 1 min at RT. Pictures of the membranes were taken by the FluorChem™ Q developing machine with an exposure time of 10 min. The expression profiles were analyzed by intensity quantification (densitometry) using the ImageJ software. For normalization, the determined expression profiles were divided by the measured total protein concentration.

3.10.8. Protein quantification

For normalization of hVEGF amounts (ELISA) and the expression profiles of angiogenesis-related proteins (Proteome Profiler™ Human Angiogenesis Array Kit) measured for the MSC-CM, the total protein concentration of MSC-CM was measured by the DC Protein Assay Kit. As standard curve, BSA dilutions were prepared (0, 100, 200, 400, 600, 800 and 1000 μg/mL). Standards and samples/sample dilutions were pipetted in duplicates in a 96 well plate (5 μL per well). Then, 25 μL alkaline copper solution prepared by mixing reagent S and A 1:50, and 200 μL Folin solution (reagent B) were added per well. After incubation for 15 min at RT under light protection, the OD was measured at a wavelength of 750 nm, a bandwidth of 9 nm and 25 flashes with the microplate reader Tecan Infinite M200. The protein concentration was calculated based on the standard curve and the used dilution if applicable.

3.11. Histological, immunohistological and immunofluorescent staining

The structure, the cellular and the matrix components were investigated by histological, immunohistological and immunofluorescent stained sections. Histological stainings are based on electrostatic interactions between dye and tissue components: the binding of cationic or anionic dyes to negatively or positively charged proteins of tissue sections or cell components. The principle of IHC or IF is the identification and histological localization of an antigen by antigen-antibody reaction. The primary antibody corresponds to the antigen of interest. The secondary antibody from a different species binds to the primary antibody and is labeled with a dye, either the HRP for IHC by DAB brown staining or a fluorescent dye for IF [70].

Cells seeded on glass slips were fixed with 1:1 EtOH/acetone for 10 min at RT and stored at -20 °C until staining. Cell pellets, native tissue or 3D models were fixed with 4 % PFA and embedded as described in section 3.11.1.

If not indicated otherwise after staining, the stained sections on object slides were dehydrated by 1 min 70 % (v/v) EtOH, 2 min 96 % (v/v) EtOH, 2x 5 min 2-propanol and 2x 5 min xylol, mounted in Entellan® and covered by glass slips.

3.11.1. Sample preparation and embedding

For microscopy, thin translucent sections are needed. To create sliceable structures, samples were embedded either in paraffin or TissueTek® compound (cryo embedding).
For paraffin embedding, cell pellets of the chondrogenic differentiation or tissue samples were fixed in 4 % PFA. After washing at least for 2 h in tap water, automatic paraffin embedding was performed: 1 h tap water, 1 h 50 % (v/v) EtOH, 1 h 70 % (v/v) EtOH, 1 h 80 % (v/v) EtOH, 1 h 96 % (v/v) EtOH, 2x 1 h 2-propanol, 1 h 2-propanol/xylol (1:1), 2x 1 h xylol and 2x 1.5 h paraffin. Afterwards, samples were embedded in paraffin in a stainless steel casting mold. Samples were cut with the Leica SM 2010R sliding microtome to 4 μm thin sections, mounted on glass slides and dried o/n at 37 °C. Prior to histological staining, IHC or IF, paraffin sections were incubated at 60 °C for 30 to 60 min to melt the paraffin. Then, they were deparaffinized and rehydrated in an ascending alcohol row: 2x 10 min xylol, 2x 1 min 96 % (v/v) EtOH, 1 min 70 % (v/v) EtOH, 1 min 50 % (v/v) EtOH and 5 min deionized water.
As hydrogels contain a high amount of water, a special freezing procedure was established for cryo embedding tissue and hydrogel samples. After o/n fixation in 4 % PFA at 4 °C, the samples were washed with PBS for 2 h. Then, the samples were incubated in 30 % (m/v) sucrose o/n at RT. Sucrose is a cryoprotective solution preventing ice crystal formation. The samples were completely soaked with sucrose by sinking to the bottom of the falcon. Subsequently, the samples were placed in cryomolds and embedded in TissueTek® compound. Cryoblocks were stored at -80 °C. At -20 °C, cryosections of 12 μm were generated with the Leica CM 1850UV sliding microtome and placed on Super-Frost® object slides. These object slides were stored at -20 °C until staining.

3.11.2. Alcian blue staining

Alcian blue staining was performed to visualize proteoglycans (table 3.2). Alcian blue is a cationic dye and stains in blue selectively for negatively charged proteoglycans at a pH of 2.5 provided by the prior incubation with 3 % (v/v) acetic acid. Cell nuclei were counterstained in red by nuclear fast red.

Table 3.2.: Alcian blue staining protocol.

Solution	Time [min]	Process
3 % (v/v) acetic acid	3	

Solution	Time [min]	Process
1 % (m/v) Alcian blue	30	staining of proteoglycans
Deionized water	until solution is clear	rinsing off Alcian blue
Nuclear fast red	5	staining of cell nuclei
Deionized water	until solution is clear	rinsing off nuclear fast red

3.11.3. Alizarin Red S staining

The osteogenic differentiation of MSCs on glass slips was detected by Alizarin Red S staining of the produced calcium phosphate (table 3.3). Before staining, samples were fixed 10 min with ice-cold methanol. Directly after the staining procedure, the glass slips were mounted in Aquatex onto object slides.

Table 3.3.: Alizarin Red S staining protocol.

Solution	Time [min]	Process
Deionized water	1	rinsing
Alizarin Red S, working solution	2	staining of calcium phosphate
Deionized water	3x 1	rinsing

3.11.4. Hematoxylin and eosin (HE) staining

HE staining was performed to get an overview of the cell and tissue morphology (table 3.4). Cell nuclei were stained in blue as hematoxylin binds to basophilic structures. Eosin binds to acidophilic structures such as cytoplasmic structures (red).

Table 3.4.: HE staining protocol.

Solution	Time [min]	Process
Hematoxylin (Mayer)	6	staining of basophilic structures
Deionized water	until solution is clear	rinsing of hematoxylin
Tap water	6	blueing
Eosin	6	staining of acidophilic structures

Solution	Time [min]	Process
Deionized water	1	rinsing

3.11.5. Oil Red O staining

The adipogenic differentiation of MSCs on glass slips was visualized by Oil Red O staining of the produced lipid droplets (table 3.5). Before staining, samples were fixed 10 min with 4 % PFA. Directly after the staining procedure, the glass slips were mounted in Aquatex onto object slides.

Table 3.5.: Oil Red O staining protocol.

Solution	Time [min]	Process
Deionized water	1	rinsing
60 % (v/v) 2-propanol	5	
Oil Red O, working solution	10	staining of lipid droplets
60 % (v/v) 2-propanol	1	
Deionized water	1	rinsing
Hematoxylin (Mayer)	0.5	staining of cell nuclei
Tap water	1	blueing
Deionized water	1	rinsing

3.11.6. Picrosirius Red staining

Picrosirius Red staining was performed to visualize collagen networks (table 3.6). Collagen was stained in red. Cell nuclei were counterstained in black by hematoxylin (Weigert). Under polarized light, collagen bundles appeared in green, red or yellow and offered an impression of the collagen structure.

Table 3.6.: Picrosirius Red staining protocol.

Solution	Time [min]	Process
Deionized water	4	rinsing

Solution	Time [min]	Process
Hematoxylin (Weigert)	8	staining of cell nuclei
Deionized water	1	rinsing
Tap water	10	blueing
Deionized water	1	rinsing
Picrosirius Red	60	staining of collagen
30 % (v/v) acetic acid	1	rinsing
30 % (v/v) acetic acid	1	rinsing

3.11.7. Immunohistological staining

For immunohistological staining of sections, antigens were enzymatically retrieved depending on the antibody (table 2.8) as 4 % PFA fixation results in protein cross-linking. If not indicated otherwise, enzymatic pretreatment was performed for 12 min at RT and heat-induced pretreatment with citrate buffer for 15 min at 90 to 100 °C. After washing once with PBST, the sections were blocked with 3 % (v/v) H_2O_2 for 10 min followed by another PBST washing. EtOH/acetone fixed cells did not need a pretreatment. Then, sections were blocked with 5 % (m/v) BSA for 30 min and incubated with the primary antibody diluted in antibody diluent o/n at 4 °C. After washing three times with PBST to remove not bound primary antibody, the Super-Vision 2 HRP-Polymer-Kit consisting of the DCS polymer enhancer (10 min), DCS HRP polymer reagent (20 min) and DAB was used to detect the specific antibody reaction. Each incubation time was followed by three PBST washings. HRP binding is indicated by brown staining after incubation with DAB. The duration for DAB incubation ranging from 30 s to 7 min was optimized for each antibody to get a specific and reliable signal (table 2.8). Cell nuclei were counterstained with hematoxylin (Mayer) for 6 min followed by blueing 10 min in warm tap water. For IHC, positive controls of native tissue and IT controls of all samples were performed and checked.

3.11.8. Immunofluorescent staining

For immunofluorescent staining of sections, antigens were enzymatically retrieved according to the used antibody (table 2.9) as described for IHC. In contrast, cells seeded on glass

slips received a pretreatment with 0.02 % (v/v) Triton X permeabilizing solution for 5 min to increase the permeability of the cell membrane. After pretreatment, the samples were washed once with PBST. After blocking with 5 % (m/v) BSA for 60 min and then with 5 % (v/v) donkey serum for 20 min at RT, the sections were incubated with the primary antibody diluted in antibody diluent o/n at 4 °C. After washing three times with PBST to remove not bound primary antibody, the sections were incubated with the fluorescent labeled secondary antibody in antibody diluent for 60 min at RT. Object slides were mounted with DAPI Fluoromount-G to stain cell nuclei.
In contrast, cell sheets were washed with PBS for 5 min after the IF staining procedure. Subsequently, a sufficient volume of DAPI solution completely covering the sheets was added. After incubation for 5 min, the sheets were washed with PBS for 5 min before being ready for microscopic analysis by confocal microscope. For IF, negative controls by staining without primary antibody were performed and checked.

3.11.9. Phalloidin staining

With a fluorescent phalloidin conjugate, actin filaments of cryosections were stained. Phalloidin working solution was prepared by diluting 1 μL Phalloidin-iFluor 488 Conjugate in 1 mL PBS supplemented with 1 % BSA (m/v).
First, the cryosections were washed three times with PBS. For increasing the permeability, the sections were incubated in 0.5 % (v/v) Triton-X 100 in PBS for 5 min followed by three PBS washings. Subsequently, the sections were incubated with phalloidin working solution for 90 min under light protection. Afterwards, the sections were washed three times with PBS to remove excess phalloidin conjugate. The sections were mounted in DAPI Fluoromount-G and analyzed by Keyence BZ-9000 microscopy (phallodin: x_{ex} = 493 nm, x_{em} = 517 nm).

3.11.10. Microscopic observation

If not indicated otherwise, histological, immunohistological and immunofluorescent stainings were analyzed by Keyence BZ-9000 microscope. For detailed visualization of the immunofluorescent staining of cell sheets, the confocal microscope LSCM TCS SP8 was used with the respective excitation wavelength corresponding to the fluorescent dye. Polarized light analysis was performed with the Leica DM4000 B LED.

3.12. Scanning electron microscopy (SEM)

SEM was performed as a microscopical analytical method to visualize the structure of the meniscal tissue and the models in fine details at moderate and higher magnifications. The coating procedure and the SEM analysis were performed at the Fraunhofer Institute for Silicate Research (ISC) in Würzburg. 30 μm thick cryosections of the samples were prepared on glass slips and stored at -20 °C until sputter coating. Sputtering relies on the striking out of metal atoms by activated argon plasma under high vacuum resulting in a homogeneous distribution on the sample surface. With this process, a thin layer of metal atoms is build which provides conductivity and contrast enhancement. For the sputtering, the glass slips with cryosections were fixed on sample holders and the adjacent platinum/carbon sputter coating was performed using the Med 010 instrument. At first, an approx. 5 nm thin and electrical carbon layer was produced by evaporation of a doubled thin carbon thread. Secondly, an approx. 2 nm thin platinum layer was sputtered. The second coating with material of a higher atomic number and density was performed mainly for signal enhancement purposes in SEM [127]. The SEM analytical data in form of images were acquired with the field emission scanning electron microscope AURIGA 60.

3.13. Gene expression analysis

In order to analyze cellular function on mRNA level, gene expression studies for proteins involved in vascularization such as hHIF-1α or hVEGF via qRT-PCR were carried out. To prevent degradation, all steps were performed on ice.

3.13.1. RNA isolation

Pellets of 5 x 10^5 cells, tissue or 3D models were snap-frozen in liquid nitrogen and stored at -80 °C until RNA isolation by the RNeasy Micro Kit. After adding RLT lysis buffer, cell pellets were disrupted by vortexing. Tissue or 3D samples were cut into small pieces on dry ice and transferred to a tube. After adding RLT lysis buffer and small iron balls, disruption was performed by using the TissueLyser for 3 min at 50 Hz. All following steps of the RNA isolation were carried out as described in the manufacturer's instructions. RNA concentration and quality was spectrophotometrically measured at 260 nm and 280 nm by

the Tecan Infinite M200. The ratio $OD_{260\ nm}/OD_{280\ nm}$ of high quality RNA is between 1.9 and 2.1. RNA was stored at -80 °C until cDNA synthesis.

3.13.2. cDNA synthesis

As next step, cDNA (complementary DNA) was synthesized which is the product of reverse transcription. The iScript™ cDNA Synthesis Kit was used according to the manual. A total amount of 500 ng mRNA in 15 µL RNase free water was mixed with 5 µL master mix composed of 4 µL 5x iScript Reaction Mix and 1 µL iScript Reverse Transcriptase. The transcription of mRNA was performed in a thermo cycler: 5 min at 25 °C for accumulation and annealing of primers, 30 min at 42 °C for elongation of cDNA, 5 min at 85 °C for separation of cDNA double strands, subsequent cooling at 4 °C. The cDNA samples with a concentration of 25 ng/µL were stored at -20 °C.

3.13.3. Qualitative real-time polymerase chain reaction

For qRT-PCR, samples were analyzed in duplicates each containing 15 ng cDNA in a volume of 2 µL. The PCR mastermix was composed of 10 µL SsoFast™EvaGreen® Supermix, 2 µL forward primer, 2 µL reverse primer and 4 µL RNase free water. In each well of the PCR 96 well plate, 18 µL PCR mastermix and 2 µL cDNA were added. The plate was sealed with a transparent Microseal®-adhesive foil to prevent evaporation of samples during qRT-PCR. The qRT-PCR was performed with the qPCR cycler (table 3.7).

Table 3.7.: Protocol for qRT-PCR with the qPCR cycler.

Step	**Temperature [°C]**	**Time [s]**	**Function**
1	95	30	initial denaturation
2	95	5	denaturation
3	60	5	primer annealing
4			plate reading
			repetition of steps 2-4 for 39 times
5	95	10	
6	65-95	5	melt curve by increasing temperature in 0.5 increments

For analysis, the melt curve as last step of the qRT-PCR protocol was checked for primer specificity. Subsequently, data acquisition was performed with the Bio-Rad CFX Manager. The expression levels of the different genes were calculated by the cycle threshold values (c_t-values). The c_t-value identifies the first cycle of higher fluorescence of the sample compared with the background signal. The expression of the genes of interest was normalized to three reference genes: hEF1α, hGAPDH and hHRP3. 100 % efficiency of the primer pairs was assumed for calculation. Analysis by Pfaffl method was performed with the Bio-Rad CFX Manager.

3.14. Statistics and data analysis

Quantitative data is presented as mean ± standard deviation. As not indicated otherwise, statistical data analysis was performed by nonparametric Mann-Whitney U test (2 samples) or Kruskal-Wallis test (more than 2 samples) using IBM SPSS software to detect significant differences between models regarding GAG/DNA, DNA/dry weight, cell metabolites, ColIA1, shrinkage or water content. Differences were considered as statistically significant for p-values < 0.05. Follow-up analysis by homogeneous subsets using IBM SPSS software was performed to confirm significant differences.

Chapter 4

Results

4.1. Characterization of the meniscal tissue

In the first part of this thesis, the meniscal tissue was characterized regarding its tissue structure and composition as reference for the tissue engineered meniscus model.

4.1.1. Anatomy and collagen structure of the human meniscal tissue

The lateral and medial meniscus of a 70 years old woman are shown in figure 4.1 A: the macroscopic image displays their semilunar shape. The three parts of each meniscus are labeled: the anterior horn (AH), the pars intermedia (PI) and the posterior horn (PH).

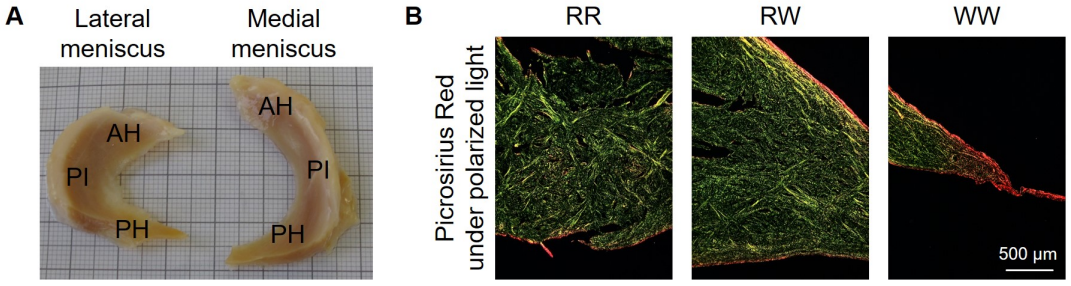

Figure 4.1.: Morphologic structure of the human menisci. A Macroscopic image of the lateral and medial meniscus of the left knee joint (hMen70: female, 70 years). The meniscus has a semilunar shape and is composed of the AH, the PI and the PH. **B** Picrosirius Red staining of the human medial meniscus (hMen67: female, 33 years, PH/PI) was visualized in its collagen structure by polarized light for the RR, RW and WW zone. The meniscus had a heterogeneous collagen structure with circumferentially oriented collagen fibril bundles in the central main portion, visible in RW. Scale bar as depicted, same magnification for all micrographs.

For the following analysis, transverse cryosections of the medial meniscus were prepared to analyze the collagen structure and its histological composition for meniscal and vascularization markers. Meniscus transverse sections show the wedge-shape of the meniscus. From literature we know that the meniscus has a heterogeneous collagen structure [16]. Here, the collagen structure of the medial meniscus was visualized by polarized light after Picrosirius Red staining (figure 4.1 B) and by SEM (figure 4.2). The microscopic images by polarized light showed the heterogeneous collagen structure with circumferentially oriented collagen fibril bundles in the central main layer (figure 4.1 B). Images taken by SEM confirmed the reported collagen structure. Figure 4.2 illustrates the wedge-shaped transverse section of the human medial meniscus with the three zones of the meniscus: the red-red (RR), the red-white (RW) and the white-white (WW) zone. The central main layer with the circumferential orientation of collagen fibers makes the main portion of the meniscus as depicted in the RW region of figure 4.2 B. The SEM images of the RR and the WW region show the superficial network with a meshwork of thin collagen fibrils and the lamellar layer with collagen fibrils in a radial direction or at various angles (figure 4.2 B).

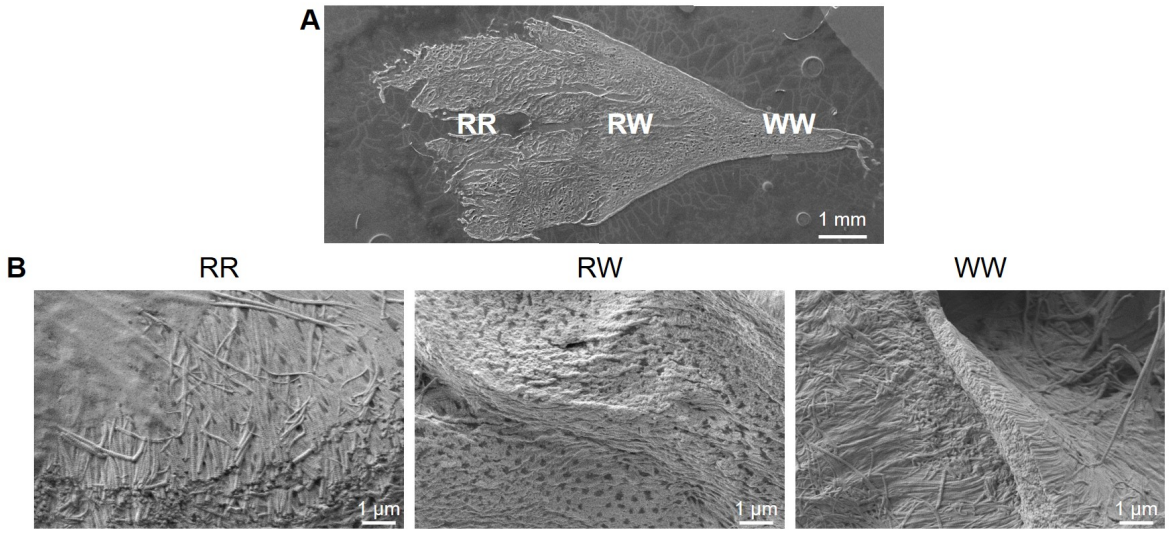

Figure 4.2.: SEM images of the human medial meniscus. The structure of the human medial meniscus (hMen67: female, 33 years, PH/PI) was visualized by SEM pictures taken of a meniscus cross sectional overview (**A**, merge of 2 images) and magnified images of the RR, RW and WW zone (**B**). The meniscus showed a heterogeneous structure with circumferentially oriented collagen fibril bundles in the central main portion, visible in the RW zone. The superficial network on the surface and the lamellar layer with randomly oriented collagen fibers is shown by the magnified images of the RR and WW zone. All scale bars as depicted.

4.1.2. Histological and immunohistochemical characterization of the human meniscal tissue

Markers specific for meniscal tissue and its vascularization were used for immunohistochemical stainings with appropriate IT controls. IT controls were performed for all immunohistochemical stainings and showed no DAB positive staining (figure A.1). Cell nuclei were counterstained with hematoxylin for immunohistochemical stainings. As meniscal markers, the immunohistochemical stainings for aggrecan as the most prominent proteoglycan of the meniscus, and the two collagen types Col I and Col II were optimized. Figure 4.3 displays the histological and immunohistochemical characterization of the human medial meniscus of a 33 years young woman for meniscal markers.

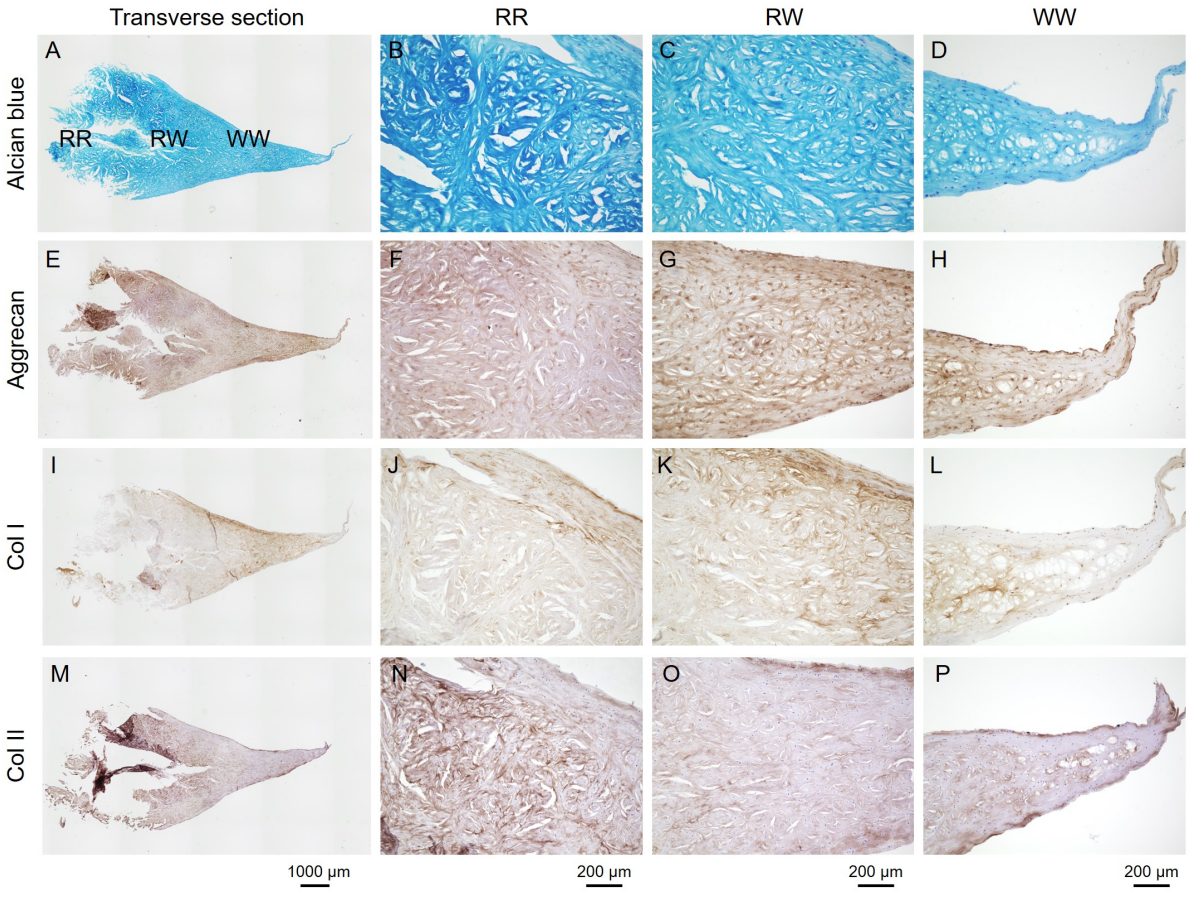

Figure 4.3.: Histological and immunohistochemical analysis of the human medial meniscus for meniscal markers. Alcian blue staining (**A-D**), immunohistochemical stainings for aggrecan (**E-H**), Col I (**I-L**) and Col II (**M-P**) visualized the heterogeneous zones of the human medial meniscus (hMen67: female, 33 years, PH/PI) by a transverse section with magnified images of the RR, the RW and the WW zone. All scale bars as depicted.

The stained transverse sections showed the wedge-shape of the meniscus (figure 4.3 A, E, I, M) and magnified images visualized a detailed view of the RR, RW and WW region (figure 4.3 B-D, F-H, J-L, N-P). The Alcian blue dye stained negatively charged proteoglycans in blue, whereas the cell nuclei were counterstained in red by nuclear fast red (figure 4.3 A-D). Aggrecan content was high in the RW and WW region as shown by pronounced staining in these regions (figure 4.3 E-H). Col I content was high in all three zones by similar staining throughout the meniscus (figure 4.3 I-L). Col II content was high in the WW region by pronounced staining (figure 4.3 M-P). Interestingly, the RR region of the young meniscus biopsy (hMen67) was positive for Col II as well (figure 4.3 N).
A medial meniscus donation from a 70 years old woman (figure 4.4) offered the possibility to compare an aged medial meniscus with the young medial meniscus of figure 4.3. The

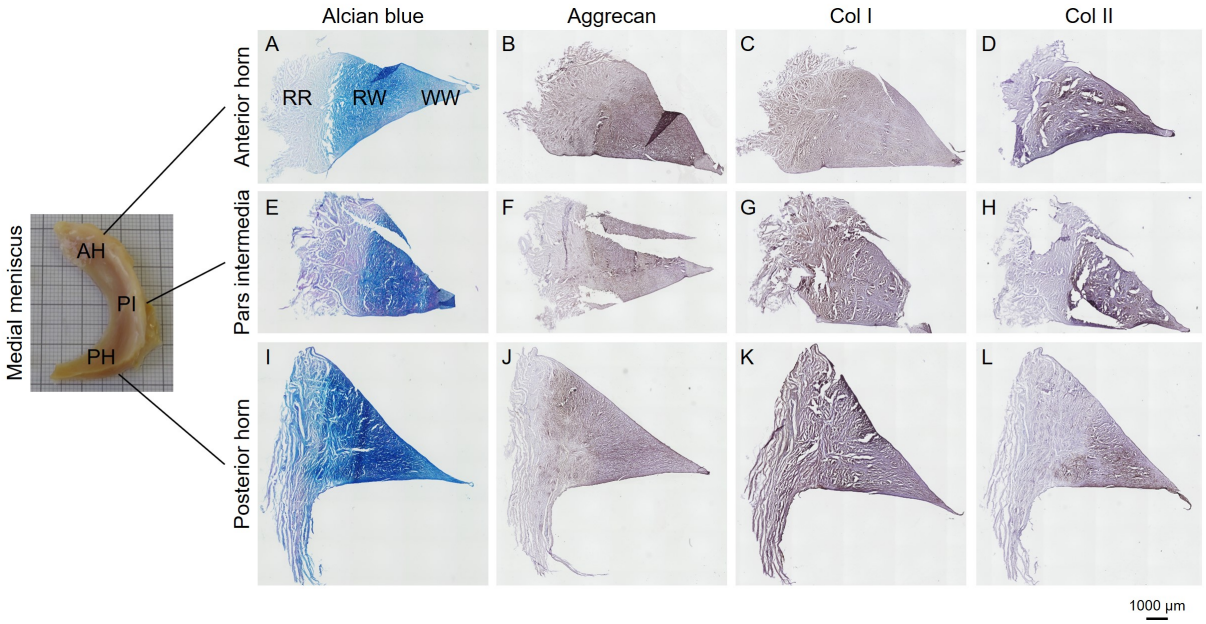

Figure 4.4.: Histological and immunohistochemical overview stainings of an aged human medial meniscus (AH, PI and PH) for meniscal markers. Transverse sections of the AH (**A-D**), the PI (**E-H**) and the PH (**I-L**) of an aged human medial meniscus (hMen70: female, 70 years) were stained with Alcian blue for proteoglycans and immunohistochemically for aggrecan, Col I and Col II. The stainings showed small differences in meniscal marker distribution and different morphological shapes of AH, PI and PH revealing the heterogeneity of the meniscal tissue. Scale bars as depicted, same magnification for all micrographs.

different parts AH (figure 4.4 A-D), PI (figure 4.4 E-H) and PH (figure 4.4 I-L) of the medial meniscus were stained by Alcian blue and immunohistochemically for aggrecan, Col I and Col II. The cross sections of the AH, the PI and the PH showed differences in their wedge-shapes and small differences in the distribution of meniscal markers. The PH

showed a homogeneous Alcian blue staining throughout the whole section (figure 4.4 I). The AH and the PI showed pronounced Alcian blue staining in the RW and WW zone (figure 4.4 A, E). Aggrecan was mainly found in the RW and WW region (figure 4.4 B, F, J). Col I content was equally distributed similar for the AH, the PI and the PH (figure 4.4 C, G, K) confirming the main collagen type of the meniscus. Col II was mainly detected in the RW and WW zone (figure 4.4 D, H, L) indicating the part with articular cartilage properties. The AH showed a more pronounced staining for Col II reaching parts of the RR zone in contrast to the PI and the PH. Compared with the young medial meniscus in figure 4.3, the positive staining for the meniscal markers in the aged medial meniscus seemed to be less pronounced.

Another important feature of the meniscus is its vascularization. In an aged meniscus, the vascularization is present in 10 to 25 % of the meniscus: the RR zone is highly vascularized, whereas the RW zone is partially vascularized [3]. Two endothelial markers were used to characterize the vascularization of the meniscal tissue. CD31 is physiologically expressed on the surface of ECs. The blood protein van Willebrand factor (vWF) is physiologically synthesized by ECs. The gradual decrease in vascularization from the RR to the RW zone of the meniscus was confirmed by immunohistochemical stainings for CD31 and vWF in the transverse section of the aged human medial meniscus (figure 4.5).

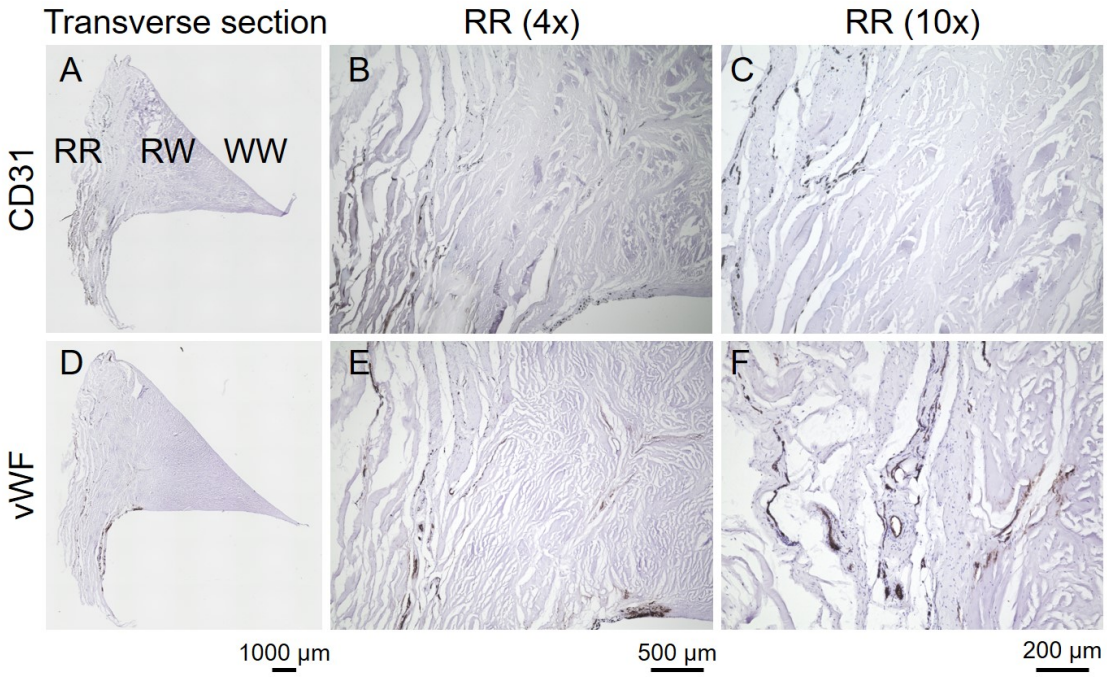

Figure 4.5.: Immunohistochemical analysis of the aged human medial meniscus for vascularization markers. Immunohistochemical stainings for CD31 (**A-C**) and vWF (**D-F**) visualized the vascularization in the RR zone of the aged human medial meniscus (hMen70: female, 70 years, PH). All scale bars as depicted.

4.1.3. Characterization of the equine meniscal tissue

For the translation of a meniscus model from bench to bedside, large animal models are necessary. As humans, horses are suffering from naturally occurring meniscal injuries as well. Although horses lack the full knee extension seen in humans, their gait is considered to best resemble the human besides sheep [128]. The semilunar shape and the different parts AH, PI and PH of the equine meniscus are shown in figure 4.6 A, B. The cross sectional areas confirmed the wedge-shape of the meniscus. Aggrecan (figure 4.6 C) and Col I (figure 4.6 D) were detected throughout the whole equine meniscus, whereas Col II (figure 4.6 E) positive staining was typically rare within the meniscus fibrocartilaginous tissue. Only the RW and the WW zone contained Col II positive staining similar to the immunohistochemical staining of the human meniscus (figure 4.4).

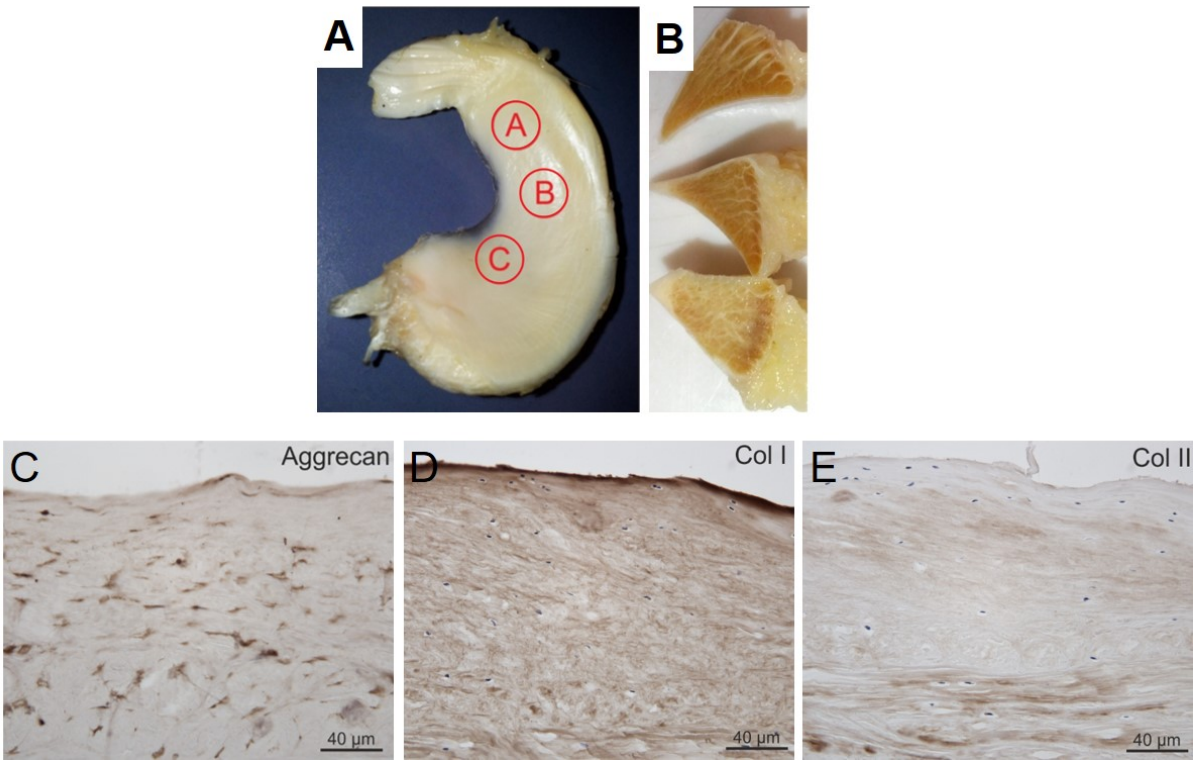

Figure 4.6.: Morphological structure and immunohistochemical analysis of the equine meniscus. Equine meniscus with labeled anatomic areas A: AH, B: PI and C: PH (**A**), and respective cross sectional areas (**B**). Immunohistochemical stainings for aggrecan (**C**), Col I (**D**) and Col II (**E**) of the equine meniscus. Scale bars as depicted, same magnification for all micrographs. Adapted from [103] with kind permission.

4.2. Cells in meniscus tissue engineering

Primary cells isolated from tissue biopsies are one main component of tissue engineering. MCs, MSCs and d-mvECs were successfully isolated for two species, humans and horses. Successfully characterized hMSCs and hd-mvECs were used to engineer the partly vascularized meniscus model.

4.2.1. Meniscal cells (MCs)

MCs represent the main type of the meniscus and have a stretched fibroblast-like morphology [103]. From May 2016 to May 2017, 20 MC isolations were performed with a success rate of 90 %. Between 7 and 14 days after isolation, 0.5 to 2 x 10^6 MCs were harvested from 1 g medial meniscal tissue. Isolated MCs had an average cell viability of 91.9 ± 5.3 %. EqMCs stained positive for aggrecan and Col I, but not for Col II (figure 4.7).

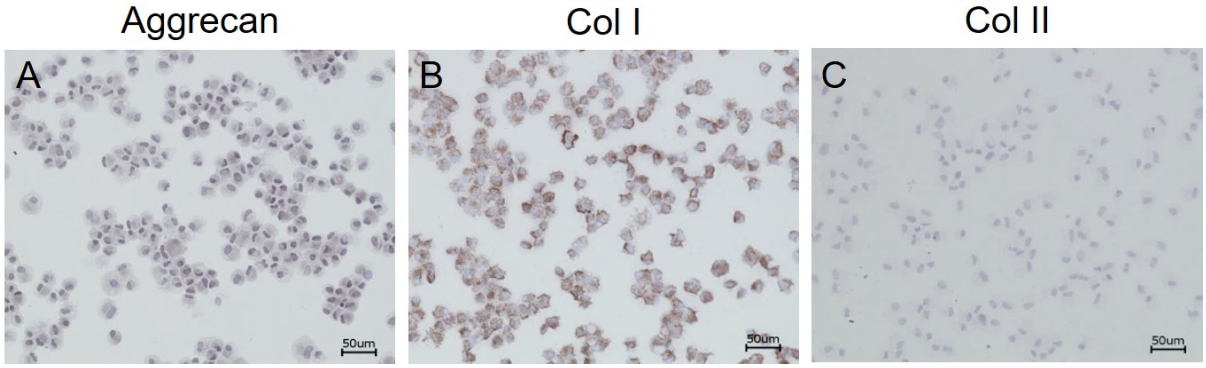

Figure 4.7.: Characterization of eqMCs by immunocytochemistry. EqMCs were prepared as cytospots and stained positive for the meniscal markers aggrecan (**A**) and Col I (**B**), and negative for Col II (**C**) by immunocytochemistry. Scale bars as depicted, same magnification for all micrographs. Adapted from [103] with kind permission.

4.2.2. Mesenchymal stem cells (MSCs)

As MCs are a limited cell source and have the disadvantage of dedifferentiation indicated by negative expression of Col II (figure 4.7 C), MSCs isolated from the bone marrow have high potential for meniscus tissue engineering. MSCs used in this thesis were taken from the established MSC bank of TERM.

A hMSC pool combining cells of three donors was used to engineer the human meniscus model. HMSCs were characterized according to the ISCT criteria [77]. First, the ability to adhere to plastic was confirmed by brightfield microscopy showing the characteristic large and flattened spindle-shaped morphology of primary hMSCs (figure 4.8 A). Second, a strong expression (>98 %) of MSC surface markers CD44, CD73, CD90 and CD105 was confirmed by FCM (figure A.2 A), whereas CD11b, CD19, CD31, CD34 and CD45 were not detectable (figure A.2 B). As last criterion, trilineage differentiation potential of hMSCs was confirmed. On day 14, the lipid droplets produced by adipogenically differentiated hMSCs were stained by Oil Red O confirming the adipogenic potential (figure 4.8 B). On day 28, the synthesized calcium phosphate of osteogenically differentiated hMSCs was stained by Alizarin Red S confirming the osteogenic potential (figure 4.8 C). On day 21, hMSC pellets cultured in chondrogenic DM showed chondrogenic differentiation confirmed by strong Alcian blue staining for negatively charged sulfated proteoglycans (figure 4.8 D) and by immunohistochemical staining for Col II (figure 4.8 E).

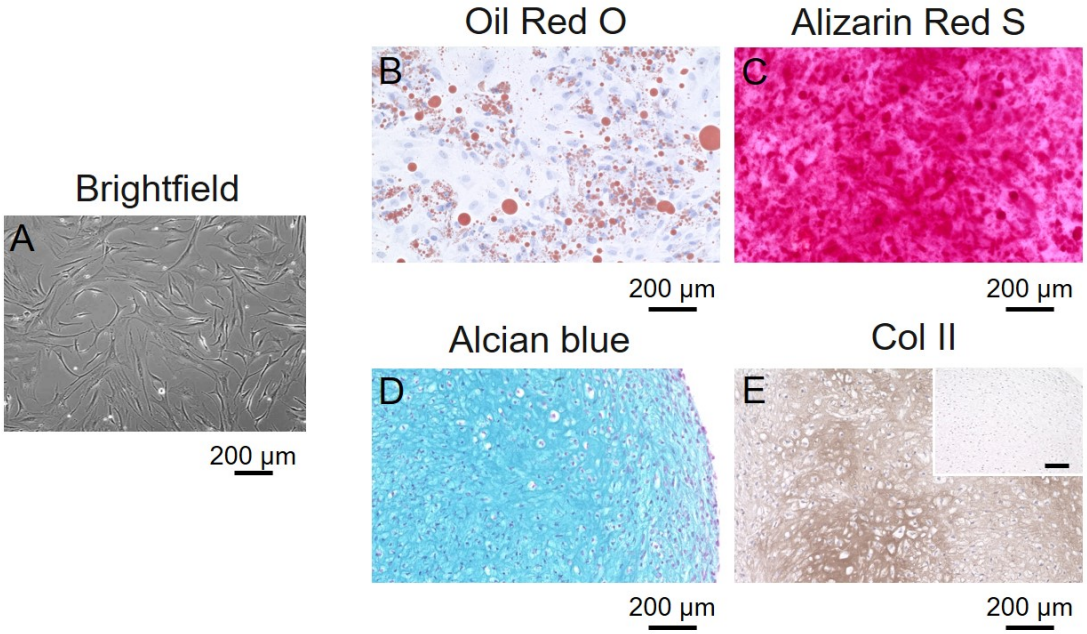

Figure 4.8.: Characterization of the hMSC pool. The hMSC pool was characterized by brightfield microscopy to prove cell attachment on plastic surfaces (**A**) and the multi-lineage differentiation potential (**B-E**). **B** The adipogenic differentiation of hMSCs was stopped on day 14 confirmed by Oil Red O staining of the lipid droplets produced by adipogenically differentiated hMSCs. **C** The osteogenic differentiation of hMSCs was stopped on day 28 confirmed by Alizarin Red S staining of produced calcium phosphate. **D, E** The chondrogenic differentiation of hMSC pellets was stopped on day 21 followed by Alcian blue staining for GAG and immunohistochemical staining for Col II. IT control is located in the upper right corner. All scale bars, 200 μm. Adapted from [48] with kind permission.

4.2.3. Dermal microvascular endothelial cells (d-mvECs)

From July 2016 to June 2017, 9 from 10 d-mvEC isolations from foreskin biopsies were successful. On day 1, a number of 0.4 to 0.8 x 10^6 d-mvECs per 5 cm^2 foreskin surface was isolated with an average cell viability of 76.9 ± 7.1 %.
A hd-mvEC pool from five donors was used to engineer the human partly vascularized meniscus model. The endothelial cell phenotype of the hd-mvEC pool was confirmed by immunocytochemistry. Hd-mvECs stained positively for vWF (figure 4.9 A), VE-cadherin (vascular endothelial cadherin) (figure 4.9 B) and CD31 (figure 4.9 C).

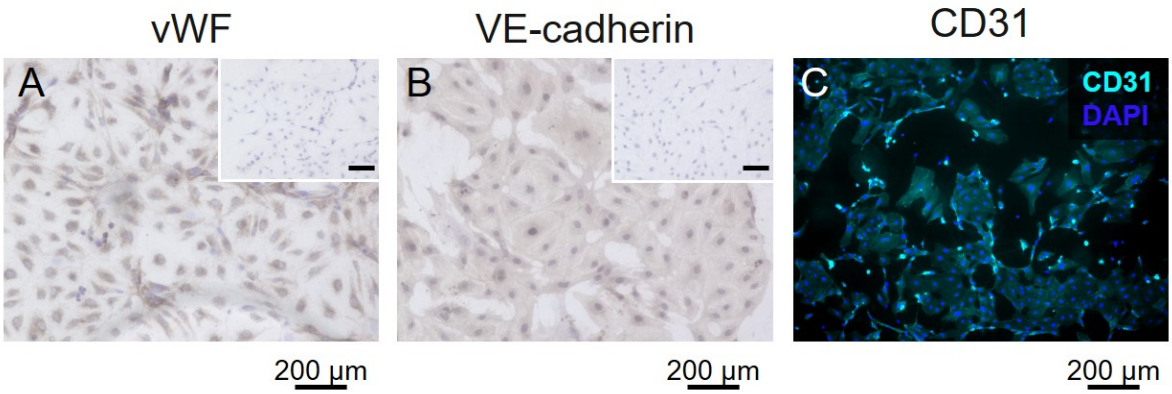

Figure 4.9.: Characterization of the hd-mvEC pool. The hd-mvEC pool was characterized by immunocytochemistry for endothelial surface markers vWF (**A**), VE-cadherin (**B**) and CD31 (**C**). IT controls for IHC is located in the upper right corner. All scale bars, 200 μm. Adapted from [48] with kind permission.

4.3. Biomaterial in meniscus tissue engineering

For meniscus tissue engineering, the primary cells were cultured in a 3D environment. Different scaffolds were characterized to test for criteria crucial for meniscus tissue engineering. All scaffolds tested in this thesis were based on Col I, as the main collagen type of the meniscus is Col I [3]. As crucial criteria, the biomaterial to engineer a meniscus model should possess high viability of cells, a good cellular distribution over the whole scaffold and a voluminous matrix structure with less porosity.

4.3.1. Commercially available Col I scaffolds

First, two commercially available Col I scaffolds were analyzed: the Resorba® Col I sponge (figure 4.10 A) and the Geistlich Col I/II/Elastin sponge (figure 4.11 A). Sterile samples were kindly provided by both companies.
The Resorba® Col I sponge showed seeded hMCs or hMSCs on the cell seeding surface as shown by MTT and Live/Dead staining on day 7 (figure 4.10 B, C). No infiltration of cells to the scaffolds was observed by fluorescence microscopy using DiI-labeled cells (figure 4.10 D). The DiI-labeled cells were only growing on the surface of the Col I sponge. This was confirmed by HE staining (figure 4.10 E): the hMSCs were growing on the surface, whereas the porous structure deeper in the Resorba® Col I sponge was not infiltrated.

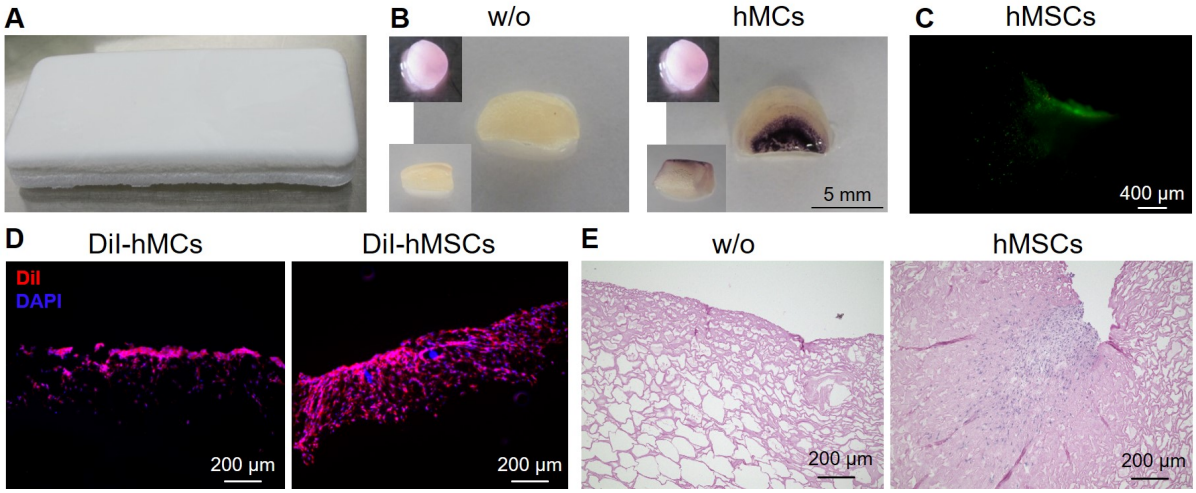

Figure 4.10.: Analysis of the Resorba® Col I sponge. A Macroscopic image of the dry Col I sponge. **B** On day 7, Col I sponges w/o and with hMCs were stained with MTT. The upper left image shows the seeded Col I sponge before MTT test. The large image shows the MTT stained sample and the bottom left corner a cross sectional image of the MTT stained sample. **C** Live/Dead staining of Col I sponge with hMSCs on day 7 (cross section). **D** Col I sponges seeded with DiI-labeled hMCs and hMSCs on day 7 were visualized by fluorescence microscopy with DAPI counterstaining of the cell nuclei (cross section). **E** HE staining of Col I sponges w/o and with hMSCs on day 7 (cross section). On day 7, cells were only growing on the surface and did not invade the Col I sponge. All scale bars as depicted.

The Geistlich Col I/II/Elastin sponge showed seeded hMSCs distributed over the whole scaffold as illustrated by MTT and Live/Dead staining on day 7 (figure 4.11 B, C). The cells infiltrated the whole sponge as visualized by DiI-labeled hMSCs using fluorescence microscopy (figure 4.11 D). However, the Geistlich Col I/II/Elastin sponge seeded with

hMSCs had a high porous and brittle structure difficult for embedding as identified in the HE staining (figure 4.11 E).
Taken together, the cell growth on the Resorba® Col I sponge and the Geistlich Col I/II/Elastin sponge was confirmed. However, both scaffolds did not fulfil the criteria for an appropriate biomaterial for meniscus tissue engineering, as the cells did not infiltrate the Resorba® Col I sponge and the Geistlich Col I/II/Elastin sponge was too porous.

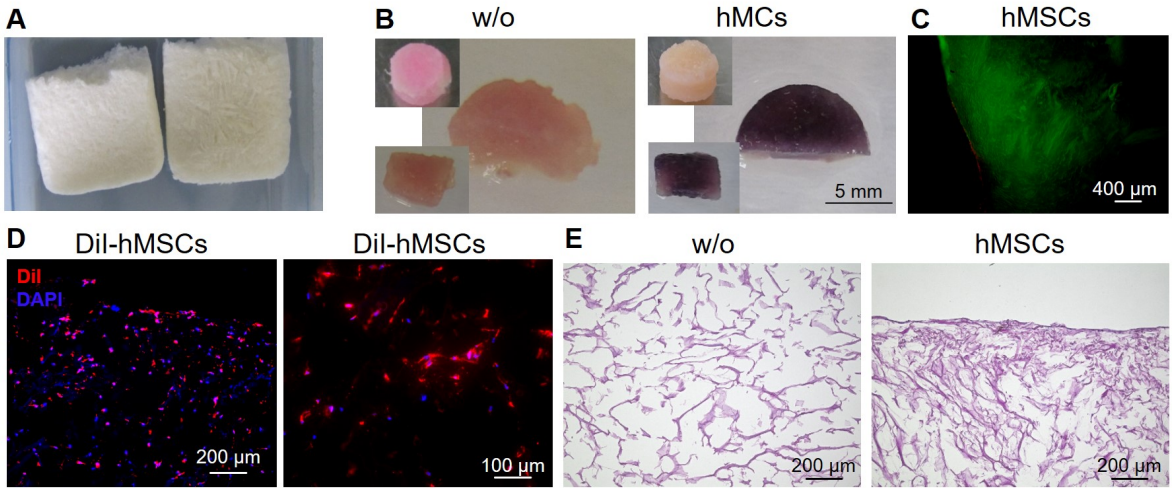

Figure 4.11.: Analysis of the Geistlich Col I/II/Elastin sponge. A Macroscopic image of the dry Col I/II/Elastin sponge. **B** On day 7, Col I/II/Elastin sponges w/o and with hMCs were stained with MTT. The upper left image shows the seeded Col I sponge before MTT test. The large image shows the MTT stained sample and the bottom left corner a cross sectional image of the MTT stained sample. **C** Live/Dead staining of Col I/II/Elastin sponge seeded with hMSCs on day 7 (cross section). **D** Col I/II/Elastin sponge seeded with DiI-labeled hMSCs on day 7 was visualized by fluorescence microscopy with DAPI counterstaining of the cell nuclei (cross section). **E** HE staining of Col I/II/Elastin sponges w/o and with hMSCs on day 7 (cross section). On day 7, cells were growing within the Col I/II/Elastin sponge and not only on the cell seeding surface. However, the Col I/II/Elastin sponge revealed a porous biomaterial. All scale bars as depicted.

4.3.2. Col I gel and SIS-muc-TERM®

A biomaterial to build a 3D meniscus model has to provide a fibrocartilaginous and voluminous matrix which is based on Col I. Col I gel and SIS-muc-TERM® were studied as scaffolds in meniscus tissue engineering. 3D static constructs based on a Col I gel stabilized with the SIS-muc-TERM® at the bottom were built up. Here, a co-culture ratio of 50 % MCs and 50 % MSCs was cultured in the 3D static constructs in chondrogenic

DM supplemented with TGFβ-3. As hMCs were limited, equine primary cells eqMCs and eqMSCs were used and the constructs directly compared to native equine meniscal tissue. The generated matrix of the 3D in vitro constructs was stained immunohistochemically for Col I, Col II and aggrecan on day 21 (figure 4.12).

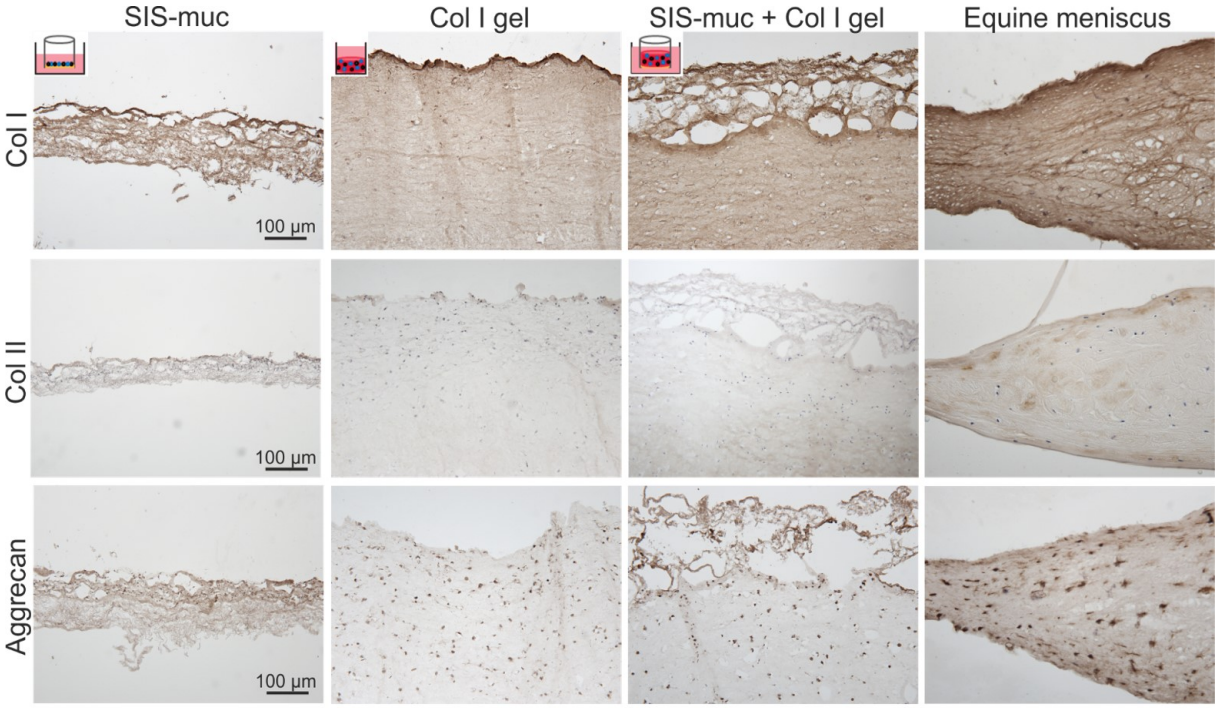

Figure 4.12.: Immunohistochemical analysis of 3D constructs based on the Col I gel and the SIS-muc-TERM® (n=3). Immunohistochemical stainings for Col I, Col Il and aggrecan on day 21. Upper left corner with schematic illustration of the 3D constructs: co-culture of eqMCs and eqMSCs directly on the SIS-muc-TERM® (SIS-muc), resuspended in a Col I gel (Col I gel) or embedded in a Col I gel on SIS-muc-TERM® (SIS-muc + Col I gel). The three left columns show the 3D constructs loaded with 50 % eqMCs and 50 % eqMSCs based on SIS-muc, Col I gel and SIS-muc + Col I gel, in comparison with native equine meniscal tissue in the right column. The Col I gel proved to be a suitable biomaterial for building a meniscus model based on similar expression of meniscal markers as in the equine meniscus. Scale bars as depicted, same magnification for all micrographs. Adapted from [103] with kind permission.

Structured matrix formation with pronounced staining for Col I and aggrecan was achieved for SIS-muc-TERM® models on day 21 (figure 4.12 left column). 3D constructs merely based on the cell-laden Col I gel or the combination of the cell-laden Col I gel with the SIS-muc-TERM® at the bottom showed positive and homogeneous distribution of Col I, Col II and aggrecan (figure 4.12 middle columns). Similar to native equine meniscal tissue (figure 4.12 right column), Col I as predominant meniscal collagen was highly expressed

in contrast to a lower Col II expression observed. However, shrinkage of the merely Col I gel-based constructs was observed (data not shown). Less shrinkage was observed by combining the two biological scaffolds. Moreover, the SIS-muc-TERM® was firmly attached to the cell-laden Col I gel.

4.3.3. Wedge-shape compression of hMSC-laden Col I gels

The characterization of the meniscal tissue revealed its heterogeneity in the collagen structure, meniscal markers and its vascularization as described in section 4.1. Moreover, a cross section of the meniscus visualized its wedge-shape, for example displayed in figure 4.2 A. For building a 3D meniscus model, the Col I gel was chosen as biomaterial and hMSCs as cell type to be embedded in the Col I gel. In contrast to the described 3D static constructs in part 4.3.2 showing a homogeneous expression of meniscal markers, the wedge-shape compression of a hMSC-laden Col I gel was established and optimized to build a wedge-shaped 3D meniscus model to achieve more heterogeneity as observed in native meniscal tissue.

4.3.3.1. Optimization of wedge-shape compression of hMSC-laden Col I gels

We developed a customized system for wedge-shape compression consisting of a bioreactor and a self-made compression device (figure 3.4).
First, the wedge-shape compression of hMSC-laden Col I gels was established and optimized. Different compression factors (CFs) were applied: a CF of 1.5 with a final Col I concentration of 6 mg/mL and a CF of 3.3 with a final Col I concentration of 13.3 mg/mL on day 0. The CF was determined by division of the original volume upon filling and the calculated final volume. After culture in chondrogenic DM until day 21, polarized light microscopic images of Picrosirius Red stained samples revealed a compact and dense collagen structure of hMSC-laden Col I gels compressed with a CF of 3.3 (figure 4.13 B). The collagen structure of the constructs compressed with a CF of 1.5 showed less staining and a thinner collagen structure. Additionally, the polarized light microscopic images of the hMSC-laden Col I gels compressed with a CF of 3.3 were morphological most similar in the collagen structure to human meniscal tissue (figure 4.13 A). Hence, the CF of 3.3 was chosen to build the 3D meniscus model by wedge-shape compression of a hMSC-laden Col I gel.

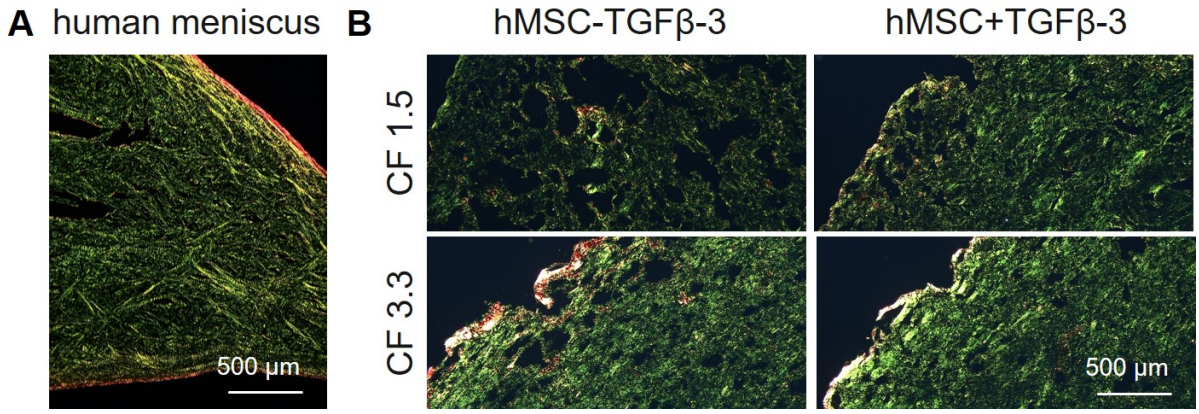

Figure 4.13.: Optimization of the CF for wedge-shape compression of hMSC-laden Col I gels (n=3). A Human medial meniscus (hMen67). **B** Wedge-shaped hMSC-laden Col I gels after wedge-shape compression with CF 1.5 (final Col I concentration of 6 mg/mL) or CF 3.3 (final Col I concentration of 13.3 mg/mL) were cultured without and with TGFβ-3 until day 21 and analyzed by polarized light after Picrosirius Red staining. Wedge-shaped hMSC-laden Col I gels on day 21 after wedge-shape compression with a CF of 3.3 showed a compact collagen structure and were consequently used to build the 3D meniscus model. Scale bars as depicted, same magnification for all micrographs.

4.3.3.2. 3D meniscus model by wedge-shape compression of a hMSC-laden Col I gel

Based on the optimization results of wedge-shape compression, 3D meniscus models were built by wedge-shape compression of hMSC-laden Col I gels with a CF of 3.3. These models were cultured in chondrogenic medium without or with 10 ng/mL TGFβ-3 for 21 days (n=3). As control, cell-free Col I gels were included for wedge-shape compression and the culture of 21 days. For the models cultured with TGFβ-3, a shrinkage of 37.3 $\pm$ 0.8 % was determined over the culture period of 21 days, whereas the models cultured without TGFβ-3 had a shrinkage of 12.2 $\pm$ 3.5 % (figure 4.14 A). The observed shrinkage reached a plateau on day 14 for both constructs (data not shown). All hMSC-laden models revealed high cell metabolic activity by blue formazan staining on day 21 in contrast to the cell-free control (figure 4.14 B). Moreover, the models cultured with TGFβ-3 showed a darker blue formazan staining on day 21 and a significant higher cell metabolism starting from day 7 compared with the ones cultured without TGFβ-3. This increased cell metabolism from day 7 was identified by a significant decrease of the remaining glucose amount ($p<0.001$) (figure 4.14 C) and a significant increase of produced lactate ($p<0.001$) (figure 4.14 D) in the medium supernatants starting from day 7 until day 21.

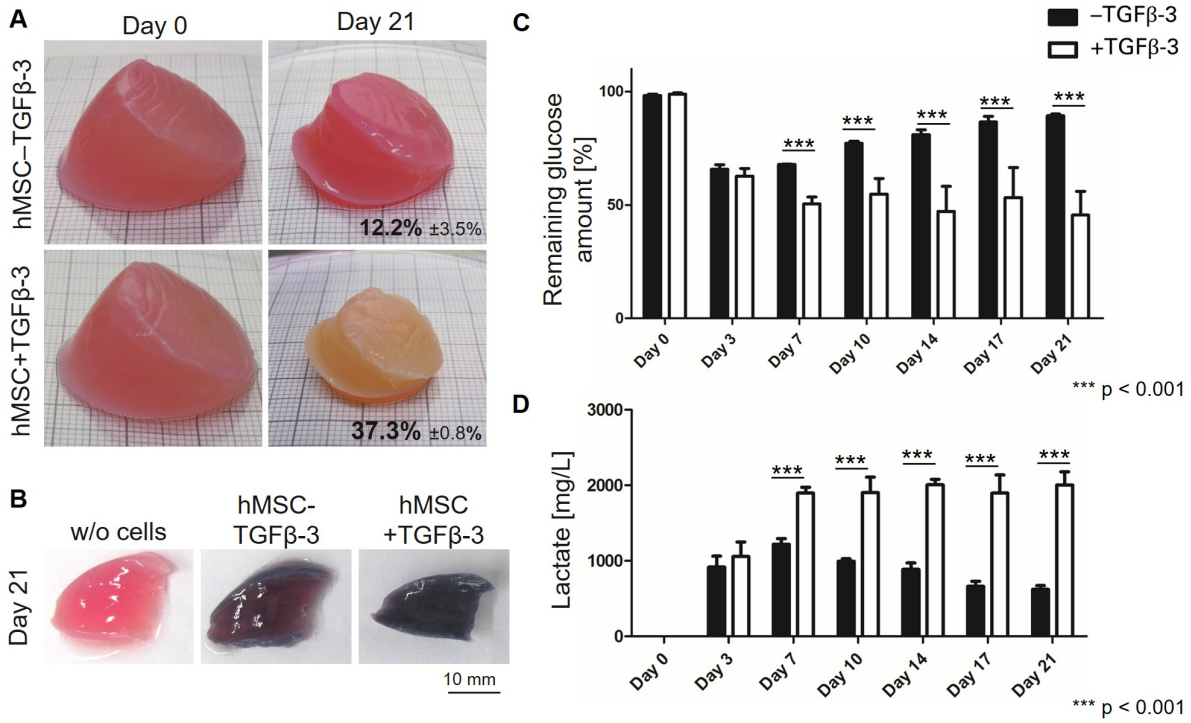

Figure 4.14.: Shrinkage and cell metabolism analysis of 3D meniscus models based on wedge-shape compression (CF 3.3) of a hMSC-laden Col I gel (n=3). A Macroscopic images taken on day 0 and 21 revealed a shrinkage of $12.2 \pm 3.5\,\%$ for wedge-shaped hMSC-laden Col I gels cultured without TGFβ-3 and of $37.3 \pm 0.8\,\%$ for cultures with TGFβ-3. Shrinkage reached a plateau on day 14 (data not shown). **B** On day 21, MTT test of wedge-shaped hMSC-laden Col I gels cultured without TGFβ-3 or with TGFβ-3 revealed active cell metabolism by blue formazan staining in contrast to the wedge-shaped Col I gel w/o cells. Scale bar as depicted. **C, D** Remaining glucose amount and lactate measured in medium supernatants from day 0 to 21 revealed significantly higher cell metabolism for the wedge-shaped hMSC-laden Col I gels cultured with TGFβ-3 in contrast to the culture without TGFβ-3: $^{***}p < 0.001$, n=3, error bars represent standard deviation (Mann-Whitney U test).

Figure 4.15 shows the models on day 21. The models cultured with TGFβ-3 contained more GAG than the models cultured without TGFβ-3, as shown by Alcian blue staining (figure 4.15 A, B). The overview section indicated a heterogeneous expression of meniscal markers. Thus, these models were divided in three parts comparable to the WW, RW and RR zone of the native meniscus. The content of GAG and DNA was quantified to detect differences between the three different zones, also defined as WW, RW and RR zone as in native meniscal tissue (figure 4.16). No significant difference in the WW, the RW and the RR zone of the models was detectable in the chondrogenic index GAG/DNA (p=0.990) (figure 4.16 A) and the DNA amount normalized by dry weight (p=0.743) (figure 4.16 B).

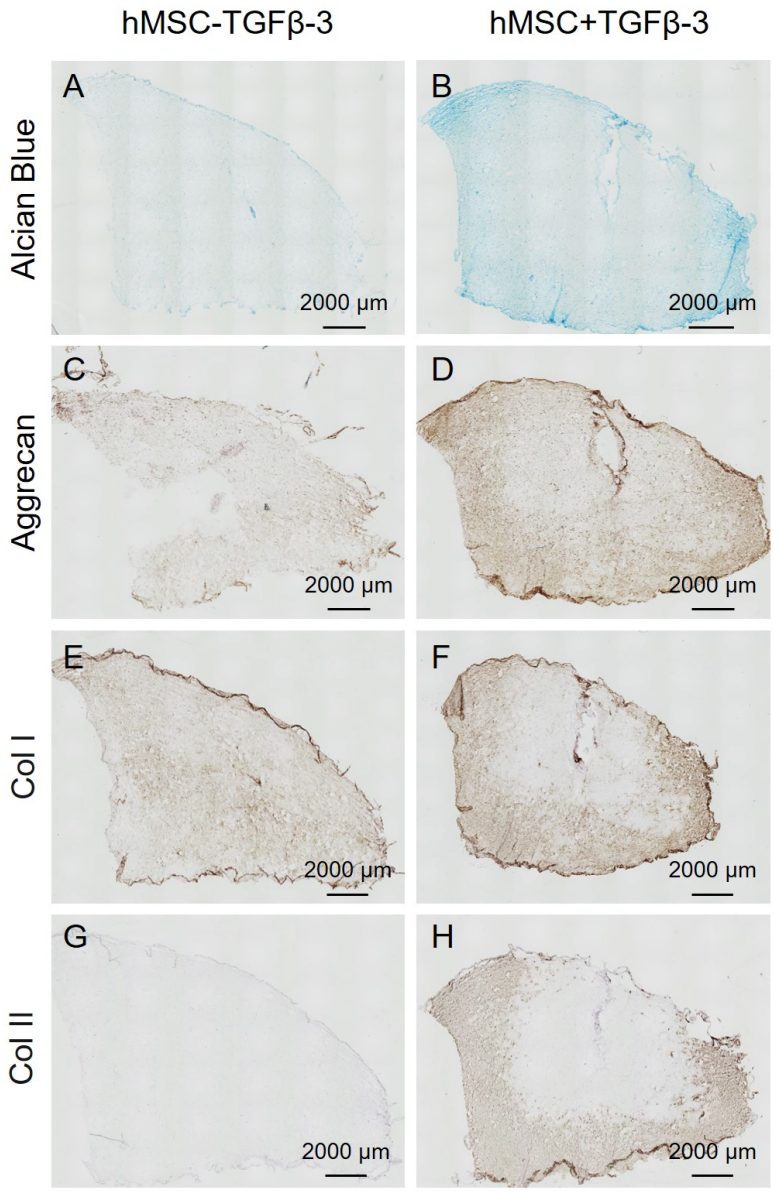

Figure 4.15.: Histological and immunohistochemical analysis of 3D meniscus models based on wedge-shape compression (CF 3.3) of a hMSC-laden Col I gel on day 21 (n=3). Alcian blue staining (**A-B**) and immunohistochemical staining for aggrecan (**C-D**), Col I (**E-F**) and Col II (**G-H**) for the wedge-shaped hMSC-laden Col I gels cultured without TGFβ-3 or with TGFβ-3 showed more pronounced staining of proteoglycans by Alcian blue, aggrecan and Col I for the models cultured with TGFβ-3. Col II was only detected for cultures with TGFβ-3. Scale bars as depicted, same magnification for all micrographs.

Immunohistochemical staining for aggrecan as the main proteoglycan of meniscal tissue showed pronounced aggrecan detection in models cultured with TGFβ-3 (figure 4.15 C, D). The immunohistochemical staining for human Col I illustrated newly synthesized Col

I in both constructs almost independent of TGFβ-3 supplementation (figure 4.15 E, F). The reactivity of the Col I antibody for human Col I was confirmed, as the Col I solution was isolated from rat tails and no positive staining was detectable for cell-free Col I gels (figure A.3). Col II was only expressed in the models cultured with TGFβ-3 (figure 4.15 G, H). In general, less expression of meniscal markers were detected in the inner part of the models especially for Col II.

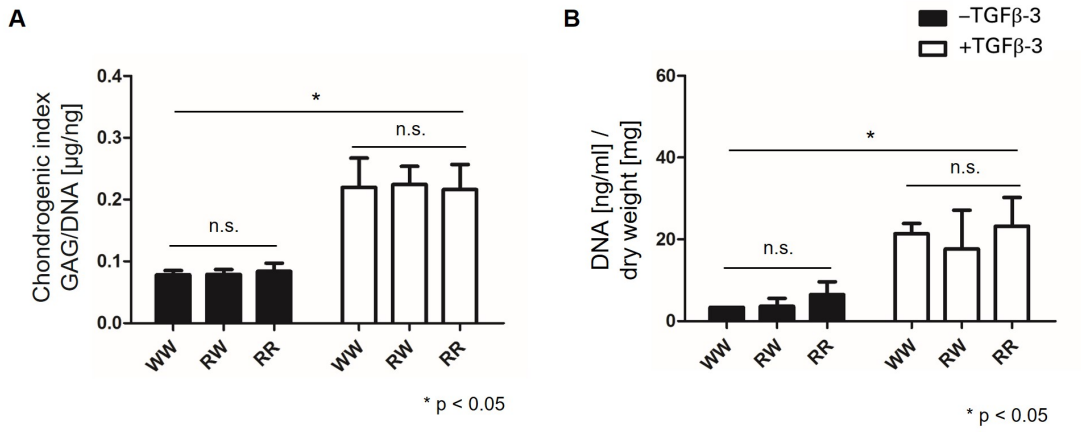

Figure 4.16.: Analysis of the chondrogenic index GAG/DNA and DNA amount of 3D meniscus models based on wedge-shape compression (CF 3.3) of a hMSC-laden Col I gel on day 21 (n=3). Chondrogenic index GAG/DNA (**A**) and DNA normalized by dry weight (**B**) of wedge-shaped hMSC-laden Col I gels cultured without TGFβ-3 or with TGFβ-3 for the WW, RW and the RR zone on day 21. No significant difference of the chondrogenic index GAG/DNA and the DNA amount was detectable between the different zones. A significant increase in GAG/DNA and DNA amount was observed for wedge-shaped hMSC-laden Col I gels cultured with TGFβ-3 compared with the culture without TGFβ-3: *p $<$ 0.05, n=3, error bars represent standard deviation (Kruskal-Wallis test).

For further detailed analysis of the meniscal markers, the RW zone in the models was evaluated based on microscopic images of the histological and immunohistochemical analysis (figure 4.17 A). As already shown for the overview sections, models cultured with TGFβ-3 contained more proteogylcans and aggrecan as illustrated by microscopic images of the RW zone. This observation correlated with the significantly increased chondrogenic index GAG/DNA found for the models cultured with TGFβ-3 in total (p=0.050) (figure 4.16 A, 4.17 B). Additionally, the total DNA amount of these models was significantly increased through culture with TGFβ-3 (p=0.050) (figure 4.16 B, 4.17 C). The meniscus models cultured with TGFβ-3 (figure 4.17 A middle column) showed more pronounced GAG staining and expression of the meniscal markers aggrecan, Col I and Col II comparable to native human meniscal tissue (figure 4.17 A right column).

Aggrecan and Col I were predominantly expressed, whereas Col II was less expressed. Col X was negative for the models and the native human meniscus. Thus, the chondrogenic differentiation was achieved by the static culture of the 3D wedge-shaped meniscus models with chondrogenic DM supplemented with 10 ng/mL TGFβ-3 for 21 days.

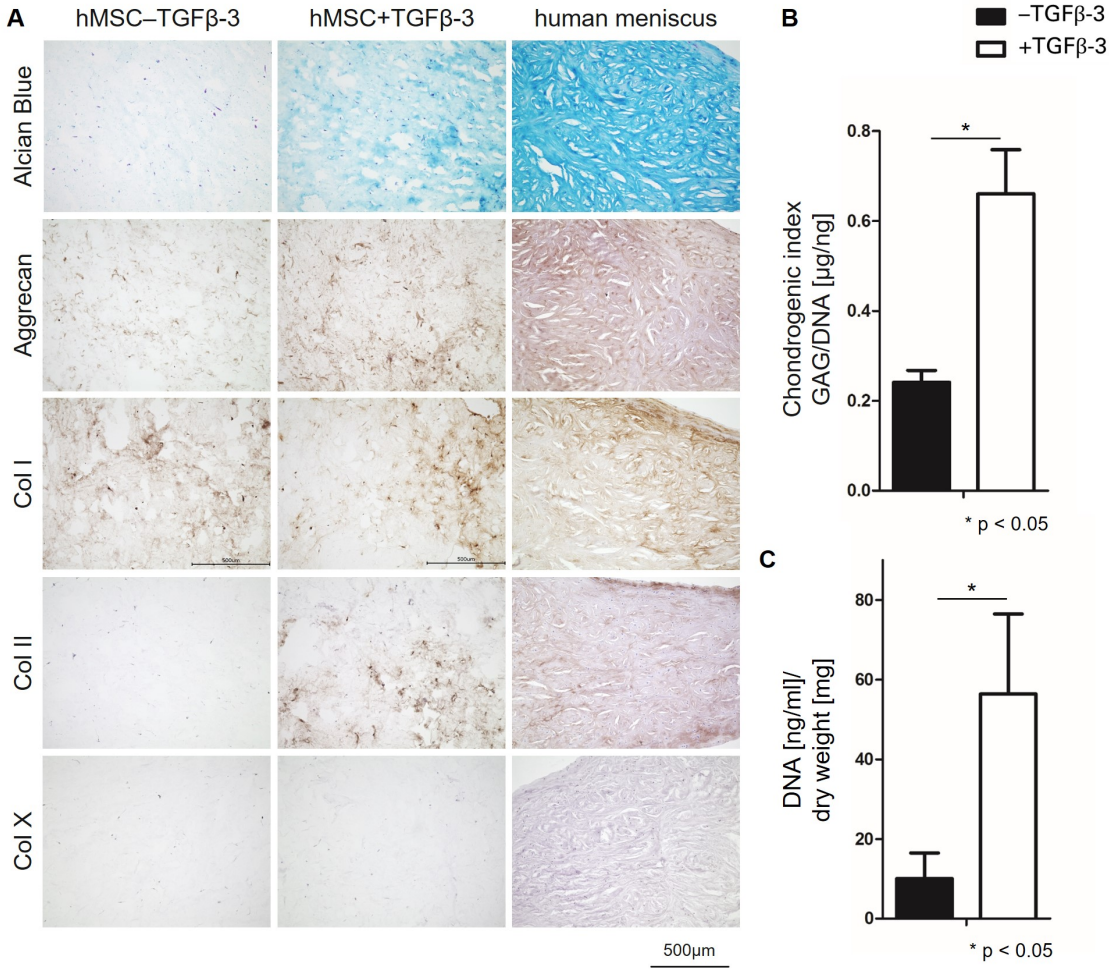

Figure 4.17.: Analysis of meniscal markers of 3D meniscus models based on wedge-shape compression (CF 3.3) of a hMSC-laden Col I gel on day 21 by histology and biochemical analysis (n=3). A Alcian blue staining and immunohistochemical staining for aggrecan, Col I, Col II and Col X for wedge-shaped hMSC-laden Col I gels cultured without TGFβ-3 or with TGFβ-3 on day 21 in comparison to a human medial meniscus (hMen67). Microscopic images of the RW zone are shown. Models cultured with TGFβ-3 showed staining for meniscal markers comparable to the native human meniscus: proteoglycans by Alcian blue, and aggrecan, Col I and Col II by IHC. Col X staining was negative for the models and the native human meniscus. Scale bar as depicted, same magnification for all micrographs. **B, C** Chondrogenic index GAG/DNA and DNA normalized by dry weight of wedge-shaped hMSC-laden Col I gels cultured without TGFβ-3 or with TGFβ-3 on day 21. A significant increase in GAG/DNA and DNA amount was detected for the models cultured with TGFβ-3: $^*p < 0.05$, n=3, error bars represent standard deviation (Kruskal-Wallis test).

4.3.3.3. The influence of macromolecular crowding (MMC) on the wedge-shaped meniscus models

As explained, MMC represents an addition of inert polydispersed macromolecules in the culture medium. We introduced MMC to the optimized conditions of chondrogenic DM supplemented with TGFβ-3 by adding 37.5 mg/mL Ficoll PM 70 kDa and 25 mg/mL Ficoll PM 400 kDa as polydispersed macromolecules. To detect an effect of MMC on meniscus matrix synthesis, the wedge-shaped meniscus models cultured with TGFβ-3 were compared with models cultured with TGFβ-3 + MMC. The models cultured using MMC showed an increase of shrinkage of approx. 10 % (figure 4.18 A). No difference was observed for cell metabolic activity by MTT staining and cell metabolism determined by remaining glucose amount (p=0.697) (figure 4.18 B) and lactate (p=0.597) (figure 4.18 C) between the models cultured with TGFβ-3 or with TGFβ-3 + MMC.

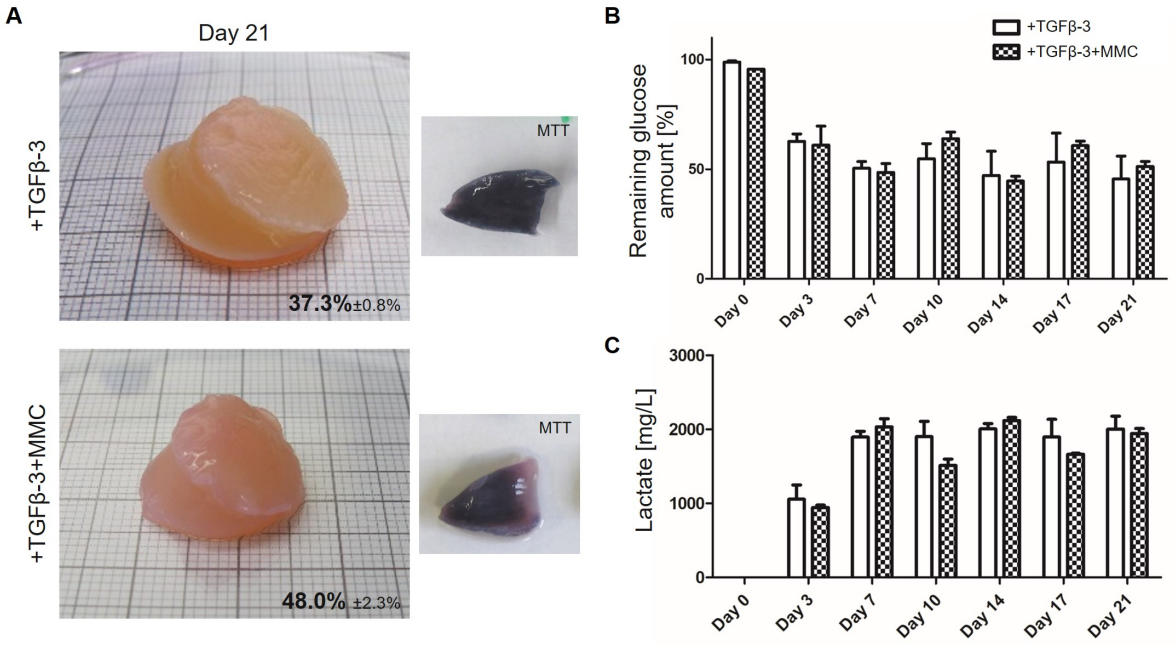

Figure 4.18.: Analysis of MMC on shrinkage and cell metabolism of the established 3D meniscus model based on wedge-shape compression (CF 3.3) of a hMSC-laden Col I gel cultured with TGFβ-3 (n=3). A Left: Macroscopic images taken on day 21 revealed a shrinkage of 37.3 ± 0.8 % for the models cultured with TGFβ-3 and of 48.0 ± 2.3 % for cultures with TGFβ-3 + MMC. Shrinkage reached a plateau on day 14 (data not shown). Right: MTT test of the models cultured with TGFβ-3 or with TGFβ-3 + MMC on day 21. **B, C** Remaining glucose amount and lactate measured in medium supernatants from day 0 to 21 of the models cultured with TGFβ-3 or with TGFβ-3 + MMC. No difference in MTT staining, remaining glucose amount or lactate by MMC was detectable: $p > 0.05$, n=3, error bars represent standard deviation (Mann-Whitney U test).

The Alcian blue staining for GAG and the immunohistochemical staining for aggrecan, Col I and Col II did not show a difference after introducing MMC (figure 4.19 A). The models cultured under MMC showed a more specific DAB signal for Col I and Col II around the embedded cells within the gel. The chondrogenic index GAG/DNA and the quantified DNA amount normalized by dry weight showed no difference between the models cultured with TGFβ-3 or with TGFβ-3 + MMC (p=0.827) (figure 4.19 B, C).

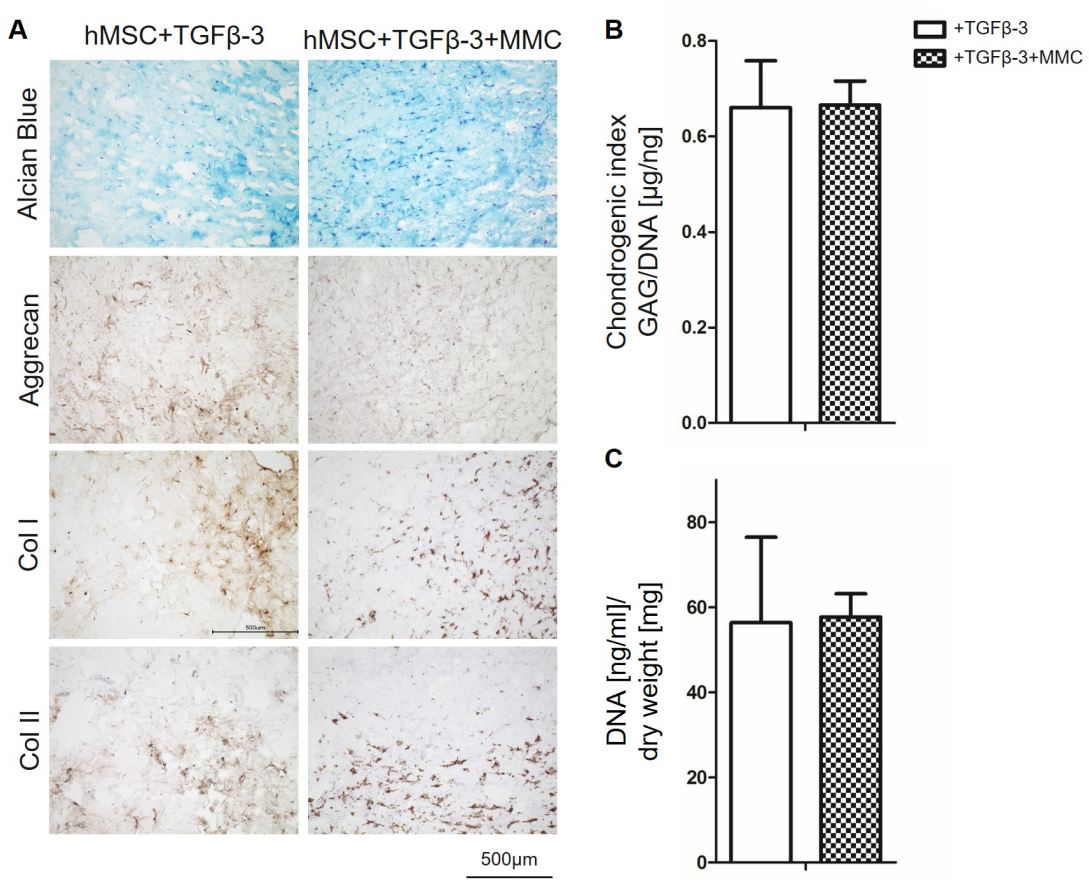

Figure 4.19.: Analysis of MMC on meniscal markers of the established 3D meniscus model based on wedge-shape compression (CF 3.3) of a hMSC-laden Col I gel cultured with TGFβ-3 (n=3). **A** Alcian blue staining and immunohistochemical staining for aggrecan, Col I and Col II of models cultured with TGFβ-3 or with TGFβ-3 + MMC. Microscopic images of the RW zone are shown. Scale bar as depicted, same magnification for all micrographs. **B, C** Chondrogenic index GAG/DNA and DNA normalized by dry weight of models cultured with TGFβ-3 or with TGFβ-3 + MMC on day 21. No significant difference in GAG/DNA and DNA amount by MMC was detectable: $p > 0.05$, n=3, error bars represent standard deviation (Kruskal-Wallis test).

To visualize the matrix of the models in detail, SEM was performed (figure 4.20 A). The structure was similar between the models. Furthermore, human pro-collagen I alpha 1

(COLIA1) was quantified in the medium supernatants (figure 4.20 B). MMC did not cause a difference of COLIA1 synthesis (p=0.478). In contrast, a decrease of COLIA1 by MMC was observed from day 14 for models cultured under MMC conditions.

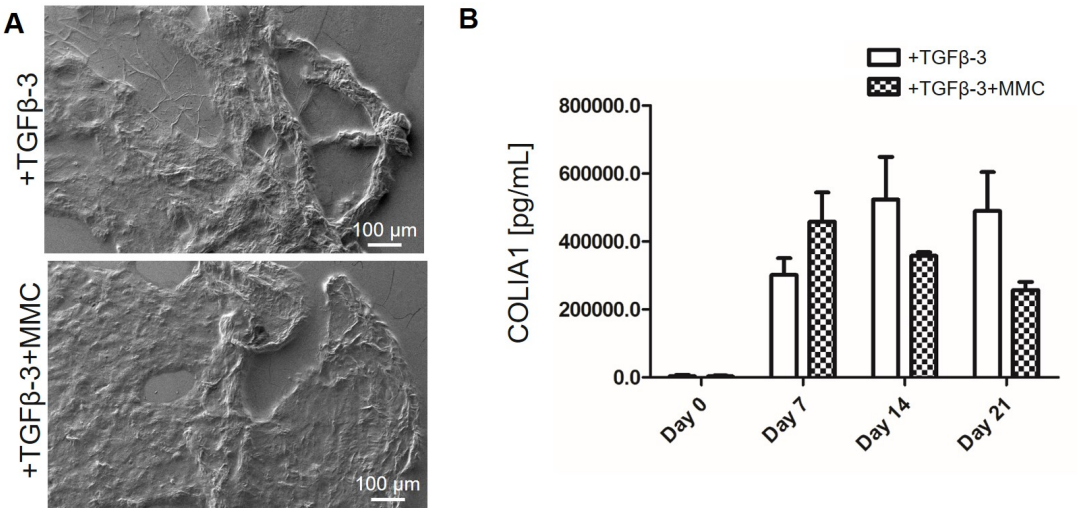

Figure 4.20.: Analysis of MMC influence on the established 3D meniscus model based on wedge-shape compression (CF 3.3) of a hMSC-laden Col I gel cultured with TGFβ-3 by SEM and COLIA1 ELISA of medium supernatants (n=3). **A** SEM images of models cultured with TGFβ-3 or with TGFβ-3 + MMC. Scale bars as depicted, same magnification for all micrographs. **B** COLIA1 measured in medium supernatants from day 0 to 21 of models cultured with TGFβ-3 or with TGFβ-3 + MMC. No difference in COLIA1 amounts of medium supernatants by introducing MMC was observed: $p > 0.05$, n=3, error bars represent standard deviation (Mann-Whitney U test).

To detect potential differences in matrix remodeling induced by MMC, gel zymography containing gelatin as substrate was performed. This method was optimized with gelatin-processing MMPs: proMMP-2 (72 kDa), active MMP-2 (62 kDa) and active MMP-9 (67 kDa and 83 kDa) were loaded on the gelatin containing gels (figure 4.21 A).
In the medium supernatants of the models cultured with TGFβ-3 and with TGFβ-3 + MMC, different MMPs were detected (figure 4.21 B). On day 7, a thick band for MMP-2 (62 kDa)/MMP-9 (67 kDa) and proMMP-2 (72 kDa), and a thin band for MMP-9 (83 kDa) were detected. From day 14 to 21, an increase of these MMPs and additionally MMP-2 (32 kDa) and proMMP-2 (43 kDa) were observed. The determined total MMP fold change of TGFβ-3 culture under MMC conditions divided by TGFβ-3 culture confirmed no difference by MMC from day 14 (figure 4.21 C). MMP fold change values higher than 1 indicated an increase, values lower than 1 indicated a decrease ot the total MMPs. From day 14, the MMP fold change remained at a value of 1 indicating no MMP increase under

MMC conditions. The standard deviation was not shown, as this is a qualitative way of quantification by densitometry and the observed effect was similar between the biological replicates (n=3). Thus, the addition of MMC components to the chondrogenic DM did not lead to an increase in MMPs and was similar to the MMP levels detected for models cultured without MMC.

Taken together, no increase in matrix synthesis, meniscal markers, matrix structure and MMPs was induced by the addition of MMC components to the culture medium. Hence, the culture conditions using chondrogenic DM supplemented with 10 ng/mL TGFβ-3 as optimized in section 4.3.3.2 were maintained for the established 3D meniscus model.

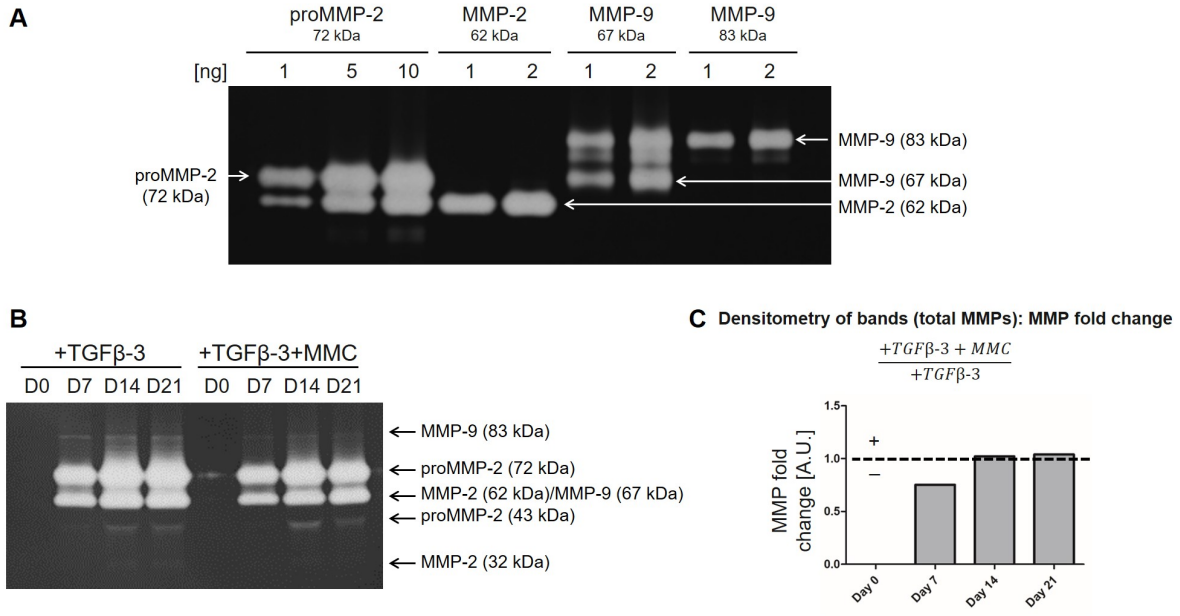

Figure 4.21.: Gel zymography as method to detect MMPs responsible for matrix remodeling and for the analysis of MMC influence on the established 3D meniscus model based on wedge-shape compression (CF 3.3) of a hMSC-laden Col I gel (n=3). **A** Establishment of the gel zymography with gelatin-processing MMPs as positive controls: proMMP-2 with a molecular weight of 72 kDa, active MMP-2 with 62 kDa, active MMP-9 with 67 kDa and active MMP-9 with 83 kDa. The purchased proMMP-2 with 72 kDa and MMP-9 with 67 kDa were not pure and additional bands were found. **B** Gel zymography of medium supernatants (day (d) 0, 7, 14, 21) of models cultured with TGFβ-3 or with TGFβ-3 + MMC. In the medium supernatants of the models, proMMP-2 (43 kDa and 72 kDa), active MMP-2 (32 kDa and 62 kDa) and active MMP-9 (67 kDa and 83 kDa) were detected from day 7 through day 21, independent of MMC. **C** The MMP fold change (+ TGFβ-3 + MMC divided by + TGFβ-3) was calculated after quantifying the pixel intensity of total MMPs by densitometry of (**B**). The MMP fold change remained 1 from day 14 and confirmed no influence of MMC on the total MMP amount.

4.4. Load bearing and biomechanical stimulation of the meniscus model

To build a meniscus model for implant purposes, the mechanical properties of the model regarding load bearing capabilities are important. The load bearing capability of the established 3D meniscus model after 21 days static culture with TGFβ-3 was studied. Additionally, two systems of biomechanical stimulation to imitate the physiologic loading of the knee joint were designed and are described in the following.

4.4.1. Load bearing of the meniscus model

On day 21, compression testing of the meniscus model compared to the controls cell-free Col I gel and hMSC-laden Col I gel without TGFβ-3 was performed. The linear modulus of the first strain $E_{lin}(1)$ and the last strain $E_{lin}(10)$ was determined (figure 4.22). $E_{lin}(1)$ of the meniscus model was significantly increased compared with the controls w/o and hMSC-TGFβ-3 (p=0.035). It was more than 10 fold higher as the two controls. For the last strain $E_{lin}(10)$, there was no significant difference between the meniscus model and the controls (p=0.390).

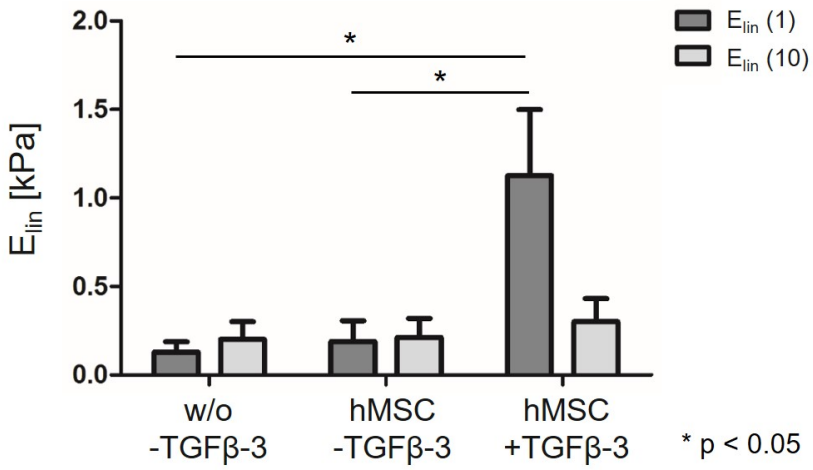

Figure 4.22.: Biomechanical characterization of the 3D meniscus model based on wedge-shape compression (CF 3.3) of a hMSC-laden Col I gel cultured with TGFβ-3 on day 21 (n=4). The linear modulus of the first strain $E_{lin}(1)$ and the last strain $E_{lin}(10)$ was determined. A significantly higher $E_{lin}(1)$ was calculated for the 3D meniscus model as compared to the controls w/o and hMSC-TGFβ-3: $^*p < 0.05$, n=4, error bars represent standard deviation (Kruskal-Wallis test).

In addition, the water content and the shrinkage were studied. The 3D meniscus model had the lowest water content of approx. 95 % (p=0.012) (figure 4.23 A), the highest shrinkage of approx. 40 % (p=0.012) (figure 4.23 C) and the highest reduction in wet weight of approx. 75 % (p=0.012) (figure 4.23 D). Furthermore, the COLIA1 amount in the medium supernatants of the meniscus model was significantly higher on day 7, 14 and 21 compared with the measured COLIA1 amount of the controls (p<0.05) (figure 4.23 B).

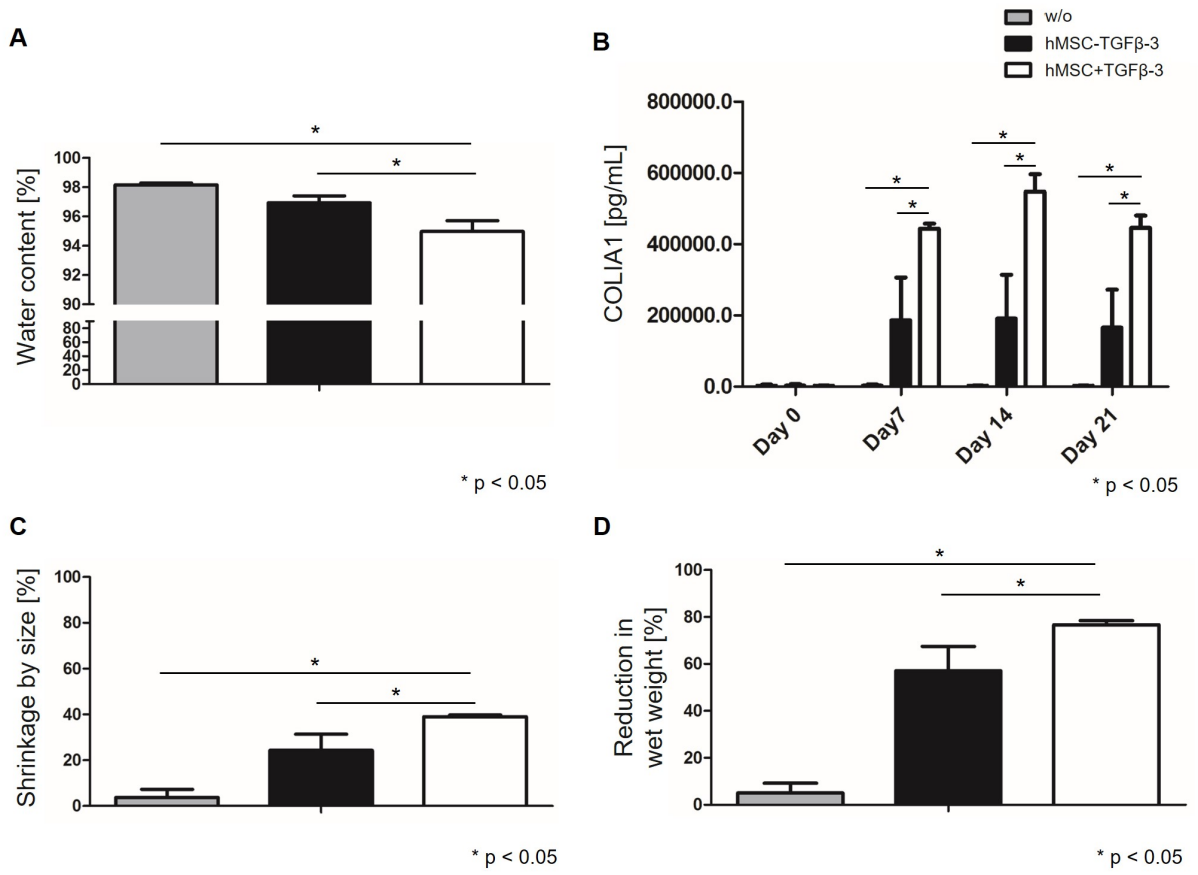

Figure 4.23.: Analysis of water content, shrinkage and ColIA1 of the 3D meniscus model based on wedge-shape compression (CF 3.3) of a hMSC-laden Col I gel cultured with TGFβ-3 built for biomechanical measurements (n=4). Water content on day 21 (**A**), COLIA1 measured in medium supernatants from day 0 to 21 (**B**), shrinkage by size on day 21 (**C**) and reduction in wet weight on day 21 (**D**) of the 3D meniscus model compared to the controls w/o and hMSC-TGFβ-3. A significant decrease of water content, a significant increase of COLIA1 of medium supernatants on day 7, 14 and 21, a significant increase of shrinkage by size and reduction in wet weight were found for the 3D meniscus model as compared to the controls: *p < 0.05, n=4, error bars represent standard deviation (Kruskal-Wallis test).

As previously detected (figure 4.17 B), the chondrogenic index GAG/DNA of the 3D

meniscus model reached approx. 0.7 and was significantly higher compared to the control of the wedge-shaped hMSC-laden Col I gel cultured without TGFβ-3 (p=0.009) (figure 4.24).

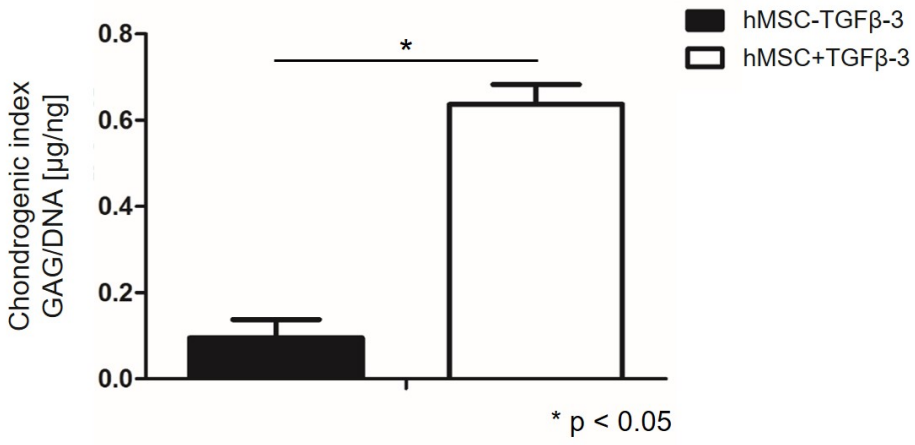

Figure 4.24.: Analysis of the chondrogenic index GAG/DNA of the 3D meniscus model based on wedge-shape compression (CF 3.3) of a hMSC-laden Col I gel cultured with TGFβ-3 built for biomechanical measurements (n=4). Chondrogenic index GAG/DNA of the 3D meniscus model compared to the controls w/o and hMSC-TGFβ-3 on day 21. A significant increase of the chondrogenic index GAG/DNA was found for the 3D meniscus model as compared to the controls: $^{*}p < 0.05$, n=4, error bars represent standard deviation (Kruskal-Wallis test).

Gel zymography of the medium supernatants of the established 3D meniscus model in comparison with the hMSC-laden Col I gel cultured without TGFβ-3 was performed to make a statement about matrix remodeling. From day 7 to 21, bands of proMMP-2 (43 kDa and 72 kDa), active MMP-2 (62 kDa) and active MMP-9 (67 kDa and 83 kDa) were detected for the meniscus model. In contrast, the control of the wedge-shaped hMSC-laden Col I gel cultured without TGFβ-3 showed only thin bands of proMMP-2 (72 kDa), active MMP-2 (62 kDa) and active MMP-9 (67 kDa) (figure 4.25 A). The calculated MMP fold change confirmed the observation of an increase of total MMPs for the culture with TGFβ-3 (figure 4.25 B). MMP fold change values higher than 1 indicated an increase for the culture with TGFβ-3 in contrast to the culture without TGFβ-3. On day 7 and 14, a value of 2 meant a doubled amount of total MMPs for the meniscus model cultured with TGFβ-3. On day 21, a 3 fold increased amount of total MMPs was detected. The standard deviation was not shown, as this is a qualitative quantification way by densitometry and the observed effect was similar between the biological replicates (n=4).

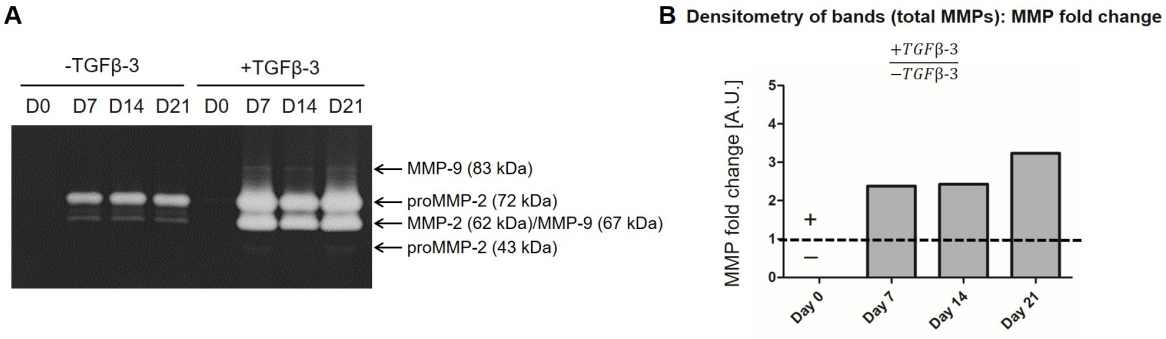

Figure 4.25.: Analysis of matrix modeling by gel zymography of the 3D meniscus model based on wedge-shape compression (CF 3.3) of a hMSC-laden Col I gel cultured with TGFβ-3 built for biomechanical measurements (n=4). **A** Gel zymography of medium supernatants (day (d) 0, 7, 14, 21) of the established 3D meniscus model compared to the hMSC-laden Col I gel cultured without TGFβ-3. Bands for proMMP-2 (43 kDa and 72 kDa), active MMP-2 (62 kDa) and active MMP-9 (67 kDa and 83 kDa) were detected for the 3D meniscus model. The control only showed thin bands of proMMP-2 (72 kDa), active MMP-2 (62 kDa) and active MMP-9 (67 kDa). **B** The calculated MMP fold change (+TGFβ-3 divided by -TGFβ-3) after densitometry of (**A**) showed by values greater than 1 an increase of total MMPs for the culture with TGFβ-3.

4.4.2. Biomechanical stimulation of the meniscus model

The meniscus is under constant mechanical pressure in the knee joint. Hence, a physiologic environment in meniscus tissue engineering should provide biomechanical stimulation [104]. Here, two methods for the biomechanical stimulation of the established wedge-shaped 3D meniscus model were designed: (1) compression, (2) hydrostatic pressure. The long-term aim of these biomechanical stimulation systems is the improvement of the load bearing properties as studied in the previous part 4.4.1.

4.4.2.1. Compression

The method for the biomechanical stimulation by compression was designed. Together with our engineers at TERM, we designed a 3D printable prototype which fitted in 6 deep well plates (figure 4.26 A). This prototype contained a wedge-shaped bottom with an angle of 30 ° for providing a flat surface after inserting the wedge-shaped meniscus model (figure 4.26 B). This PLA-based prototype was printed with the Xeed 3D Printer. After printing, small holes were drilled into the wedge-shaped bottom and 4 holes into the cylinder of

the prototype to allow medium perfusion during culture. The printed prototypes were autoclaved. In a pretest, the static culture of 21 days was successfully performed in the prototype under sterile conditions with wedge-shaped Col I gels w/o cells or with hMSCs cultured in chondrogenic medium without or with TGFβ-3 (figure 4.26 C). On day 21, the MTT test revealed metabolic activity of the hMSC-laden constructs by blue formazan staining (figure 4.26 C bottom).

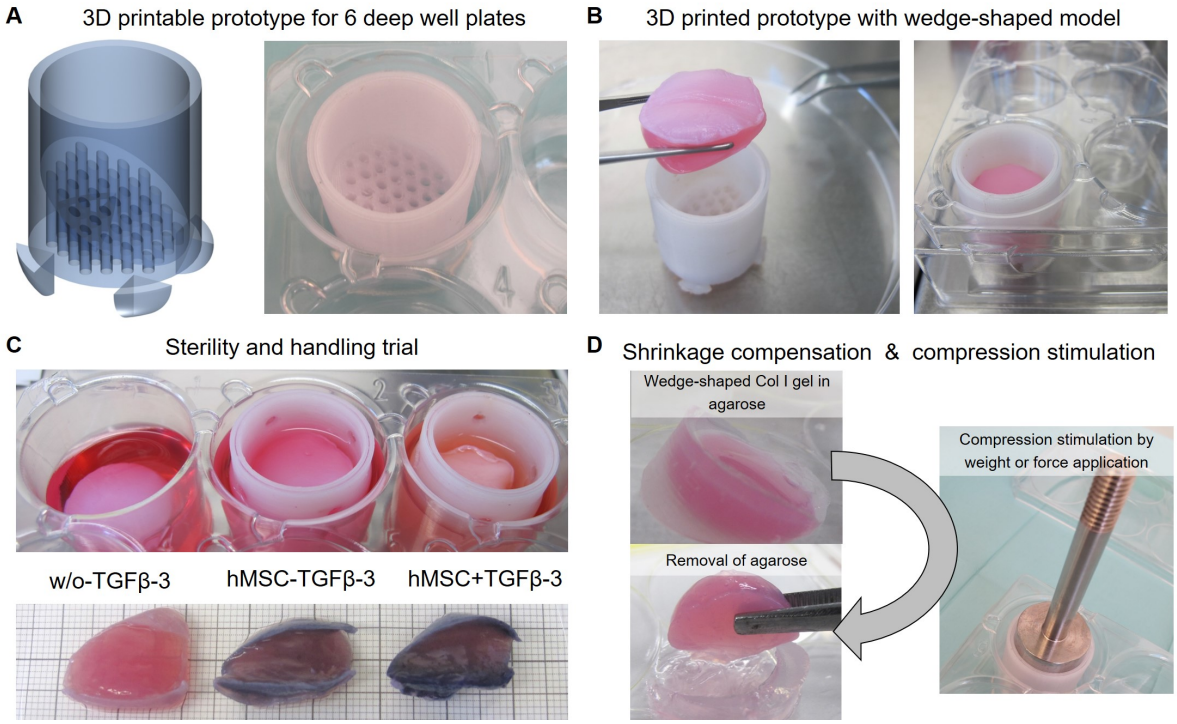

Figure 4.26.: Biomechanical stimulation method I by compression. **A** A 3D printable prototype with a wedge-shaped bottom (angle of 30 °) was designed (left) which could be placed in a 6 deep well plate (right). **B** The wedge-shaped meniscus model was placed in the prototype and the prototype was placed in the 6 deep well plate. **C** In a pilot test, the prototypes were used for the culture of wedge-shaped Col I gels w/o cells or with hMSC cultured without and with TGFβ-3 for 21 days (top). Medium perfusion was facilitated by holes in the bottom wedge and 4 holes in the cylinder of the prototype. On day 21, MTT test was performed to confirm metabolic activity of the hMSC-laden models (bottom). **D** For comparable biomechanical stimulation by compression, the shrinkage of the 3D meniscus model in the prototype could be compensated by a special agarose. This agarose clotted at 37 °C. The biomechanical stimulation by compression is planned to be performed with defined weight or force application. After compression stimulation, the agarose could be removed without influencing the meniscus model because of its higher stiffness.

As shown, the meniscus model cultured with TGFβ-3 showed a shrinkage by size of approx. 40 % (figure 4.23 C). This reduction of size has to be compensated for a comparable

compression stimulation by weight or force application. In favor, a shrinkage compensation using agarose gelling at 37 °C was established (figure 4.26 D). The method for sterile preparation of the low temperature gelling agarose was optimized as described in the following. The agarose was dissolved in sterile water with a concentration of 15 mg/mL. The solution was heated by boiling in the microwave. After boiling, the agarose solution was filled into a sterile pre-warmed 50 mL glass bottle under the hood. Subsequently, this bottle was placed into a 45 °C pre-warmed water bath. The temperature of the agarose was controlled under sterile conditions. After reaching approx. 45 °C, the liquid agarose solution was poured onto the shrinked models. As the gelling temperature of this agarose is 37 °C, the 45 °C warm agarose solution clotted after getting in touch with the models cultured at 37 °C. For biomechanical stimulation by compression, the shrinkage compensation with agarose should be performed for all models to ensure reproducibility. An advantage of this low temperature gelling agarose is its easy removal ability due to its higher stiffness as illustrated in figure 4.26 D. To achieve this stiffness, the used agarose concentration was optimized to 15 mg/mL.
For future planning, the compression stimulus is planned to be applied as defined weight (figure 4.26 D) or force application using a compression device. The detailed parameters for the compression stimulus have to be investigated in future studies.

4.4.2.2. Hydrostatic pressure

Second, a system for the biomechanical stimulation by hydrostatic pressure was designed. This system is based on a bag pump squeezing the medium out of an infusion bag (Easyflex$^+$ 50 mL empty bag) into a closed system resulting in a controllable hydrostatic pressure. This bag pump is air-driven using compressed air. Originally, the bag pump consisting of two infusion bags for providing a continuous medium circulation with pulsatile flow was developed by our engineers at TERM [129]. The infusion bags were stacked in the designed bag pump housing. One bag was connected to a pressure-controlled air system, the other bag was connected to the bioreactor system. In this original system, one bag was responsible for applying pressure, whereas the other bag provided passive cell culture medium supply for the fluid circuit. This original setup provided constant pressure and flow in addition to dynamic flow conditions.
For this study, the original system was modified to provide a constant hydrostatic pressure stimulus. The system was composed of one 50 mL infusion bag filled with medium which was connected to a 6 deep well plate including a pressure sensor (figure 4.27 A). The meniscus model was placed in the 6 deep well plate (figure 4.27 B). After closing the 6

deep well plate, the system was connected to the hydrostatic pressure device by clamping the filled infusion bag into the bag pump housing (figure 4.27 C). With the control panel (figure 4.27 D), the pressure was set at a constant value and the system was switched on. The pressure was increased by squeezing the medium out of the infusion bag into the closed system. As no air was able to leave the system, the squeezing volume led to an increased hydrostatic pressure in the medium which was recorded and controlled by the pressure sensor. A constant pressure starting from 50 mmHg was able to be maintained over a time period of more than 30 min.

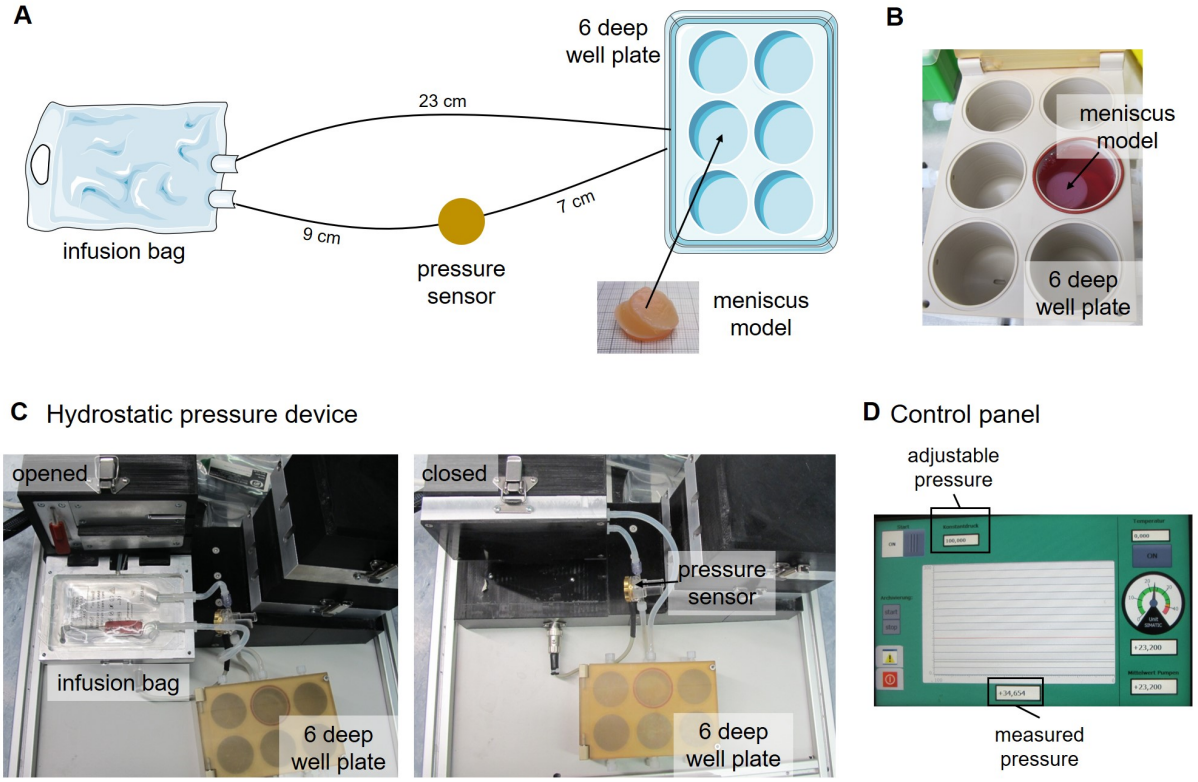

Figure 4.27.: Biomechanical stimulation method II by hydrostatic pressure. A The system for the biomechanical stimulation by hydrostatic pressure was composed of a 50 mL infusion bag connected to a 6 deep well plate in which the 3D meniscus model was placed in. A pressure sensor for measuring the hydrostatic pressure was included. **B** The meniscus model was placed in the 6 deep well plate. **C** The infusion bag filled with medium was placed in the hydrostatic pressure device and closed. The pressure sensor was connected and subsequently, the hydrostatic pressure was induced. **D** The control panel was used to adjust the pressure and to show the measured pressure.

As pilot test, disk-shaped cell-free Col I gels were stimulated by hydrostatic pressure of 50, 100 and 150 mmHg for 30 min at RT. The medium volume in the system was optimized to 88 mL. After 30 min of hydrostatic pressure stimulation, no deformation in size was

observed for the cell-free Col I gel disks (figure 4.28 A). Next, a hDF-laden Col I gel disk was stimulated with 100 mmHg for 30 min at RT and analyzed for metabolic activity. The MTT staining on day 0 showed no influence on the metabolic activity by the hydrostatic pressure stimulation of 100 mmHg for 30 min at RT in comparison with the not stimulated control (figure 4.28 B).

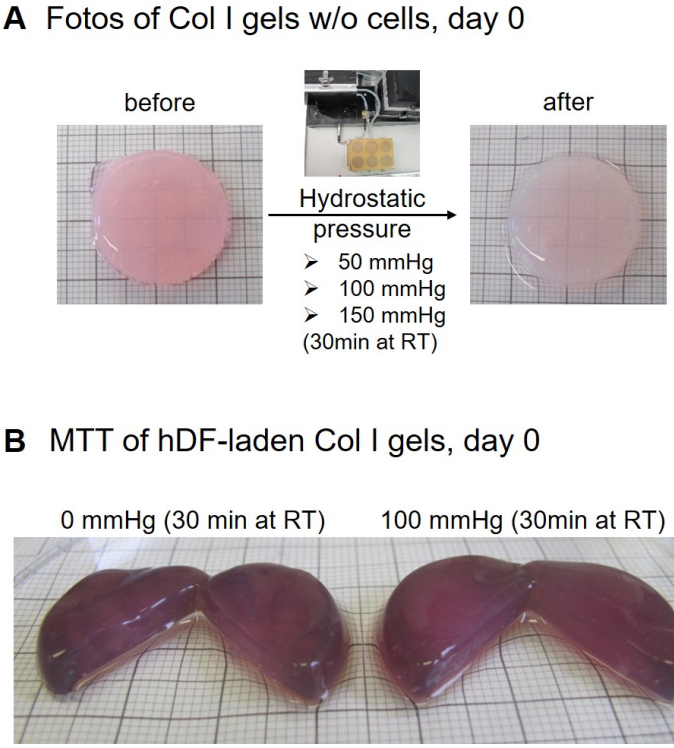

Figure 4.28.: Biomechanical stimulation method II by hydrostatic pressure: pilot test with cell-free and hDF-laden Col I gel disks (n=1). A Disk-shaped cell-free Col I gels were stimulated in the hydrostatic pressure device with 50, 100 and 150 mmHg for 30 min at RT. No deformation of the Col I gel disks was observed. **B** MTT test showed no difference comparing stimulated and not stimulated hDF-laden Col I gel disks.

With these results, a preliminary experiment using hDFs and hMSCs was performed to analyze the hydrostatic pressure stimulation of 100 mmHg and 150 mmHg for 30 min in comparison with no stimulation. On day 1 and 3 after hydrostatic pressure stimulation, the cell-laden Col I gels were analyzed for metabolism and matrix remodeling. No difference in MTT staining for cell metabolic activity was observed on day 1 and 3 with regard to cell type or applied hydrostatic pressure (figure 4.29 A, B). Furthermore, the remaining glucose amount (figure 4.29 C, D) and the produced lactate (figure 4.29 E, F) measured in the medium supernatants also showed no difference on day 1 and 3.

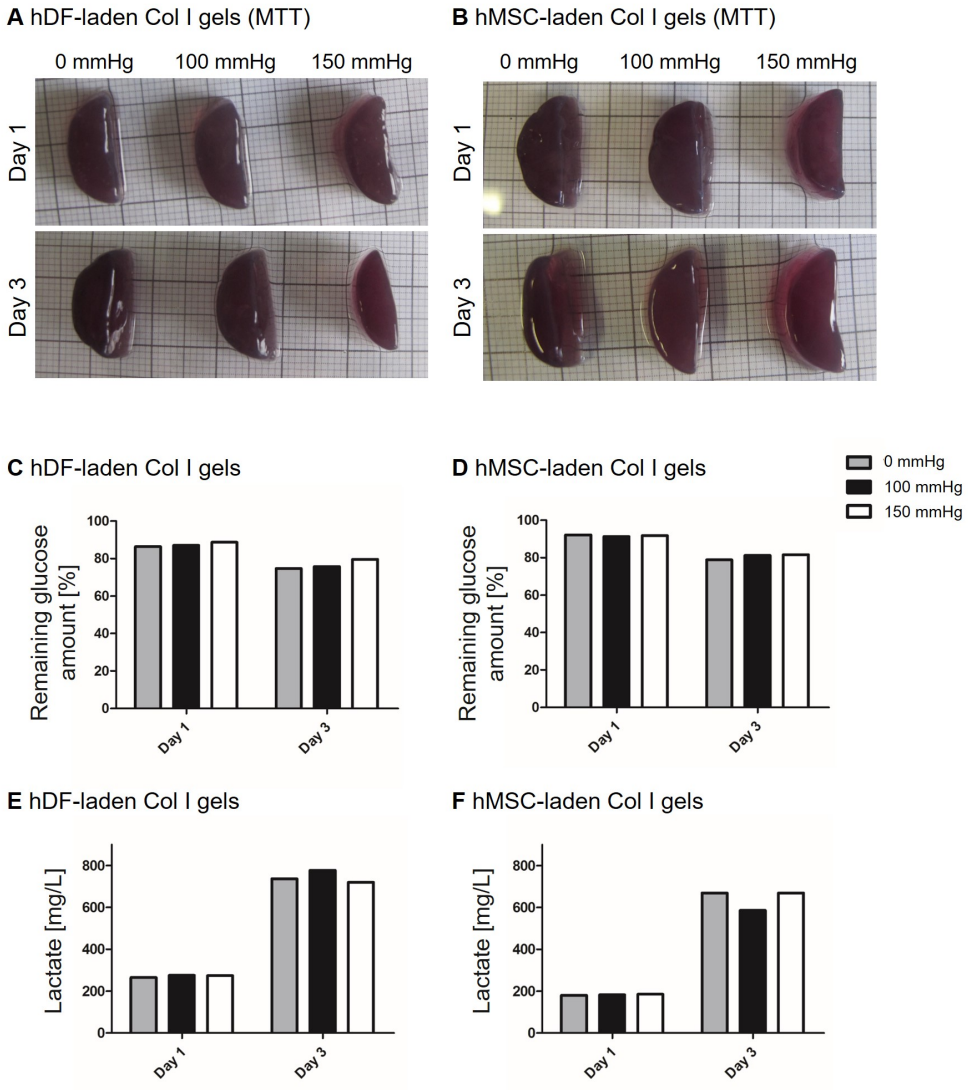

Figure 4.29.: Biomechanical stimulation method II by hydrostatic pressure: preliminary test with cell-laden Col I gel disks on metabolism (n=1). MTT test (**A-B**), remaining glucose amount (**C-D**) and lactate (**E-F**) in medium supernatants of cell-laden Col I gel disks on day 1 and 3. HDF-laden Col I gel disks (**A, C, E**) were compared with hMSC-laden Col I gel disks (**B, D, F**) on day 1 and 3 after hydrostatic pressure stimulation of 0, 100 and 150 mmHg for 30 min at RT. MTT test revealed metabolic activity of cell-laden Col I gel disks independent of cell type or applied hydrostatic pressure. From day 1 to 3, the remaining glucose amount decreased and the measured lactate amount increased similar between the different applied hydrostatic pressures confirming active cell metabolism.

Gel zymography was performed with the medium supernatants of hDF- and hMSC-laden Col I gel disks collected on day 0, 1 and 3 (figure 4.30 A, 4.31 A). From day 0 to 3, an increase of total MMPs was detected. On day 0, proMMP-2 (72 kDa) and MMP-9 (83 kDA) were detected as bands. On day 3, MMP-2 (62 kDa) and MMP-9 (67 kDa) were

additionally detected. From day 1 to 3, the detected bands of the MMPs became thicker indicating increased MMP production as confirmed by quantified pixel intensity of total MMPs (figure 4.30 B, 4.31 B). However, no difference in MMP detection was observed by the applied hydrostatic pressure.

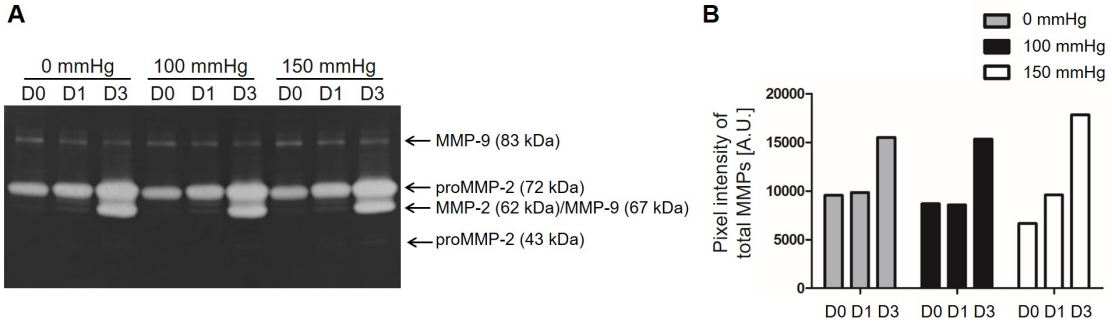

Figure 4.30.: Biomechanical stimulation method II by hydrostatic pressure: preliminary test with hDF-laden Col I gel disks analyzed by gel zymography (n=1). Gel zymography of medium supernatants on day (d) 0, 1 and 3 of hDF-laden Col I gel disks after hydrostatic pressure stimulation of 0, 100 and 150 mmHg for 30 min at RT (**A**) and quantified total amount of MMPs visualized by pixel intensity (**B**). Matrix remodeling by MMPs increased from day 0 to 3, as observed for proMMP-2 (43 kDa and 72 kDa), active MMP-2 (62 kDa) and active MMP-9 (67 kDa and 83 kDa) independent of the applied hydrostatic pressure.

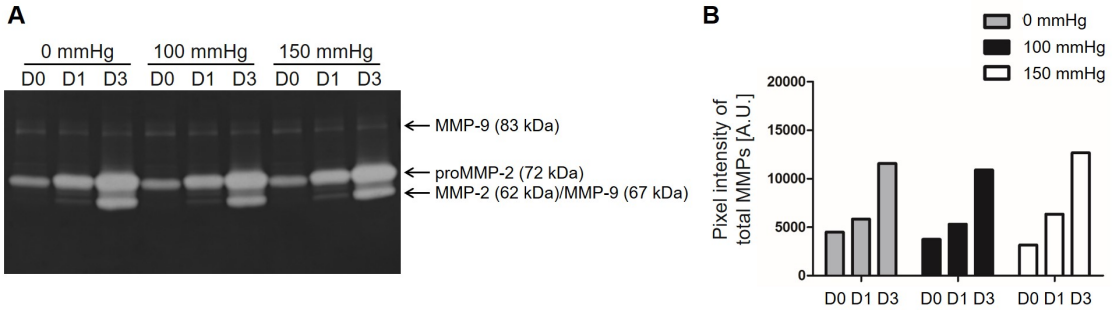

Figure 4.31.: Biomechanical stimulation method II by hydrostatic pressure: preliminary test with hMSC-laden Col I gel disks analyzed by gel zymography (n=1). Gel zymography of medium supernatants on day (d) 0, 1 and 3 of hMSC-laden Col I gel disks after hydrostatic pressure stimulation with 0, 100 and 150 mmHg for 30 min at RT (**A**) and quantified total amount of MMPs visualized by pixel intensity (**B**). Matrix remodeling by MMPs increased from day 0 to 3, as observed for proMMP-2 (72 kDa), active MMP-2 (62 kDa) and active MMP-9 (67 kDa and 83 kDa) independent of the applied hydrostatic pressure.

HE staining on day 1 and 3 revealed similar matrix stainings (figure 4.32). On day 3, the cell-laden Col I gel showed a compacter structure compared with day 1 indicated by a

more homogeneous HE staining. Additionally, the gels were stained with Phalloidin (figure 4.33). Phalloidin stains all variants of actin filaments and offers information on the activity level of the cytoskeleton. Phalloidin staining of the cell-laden Col I gel disks revealed no difference based on the applied hydrostatic pressure on day 1 and 3, and the used cell type. Taken together, the applied hydrostatic pressure did not influence metabolism, MMPs expression and the generated matrix of the cell-laden Col I gel disks.

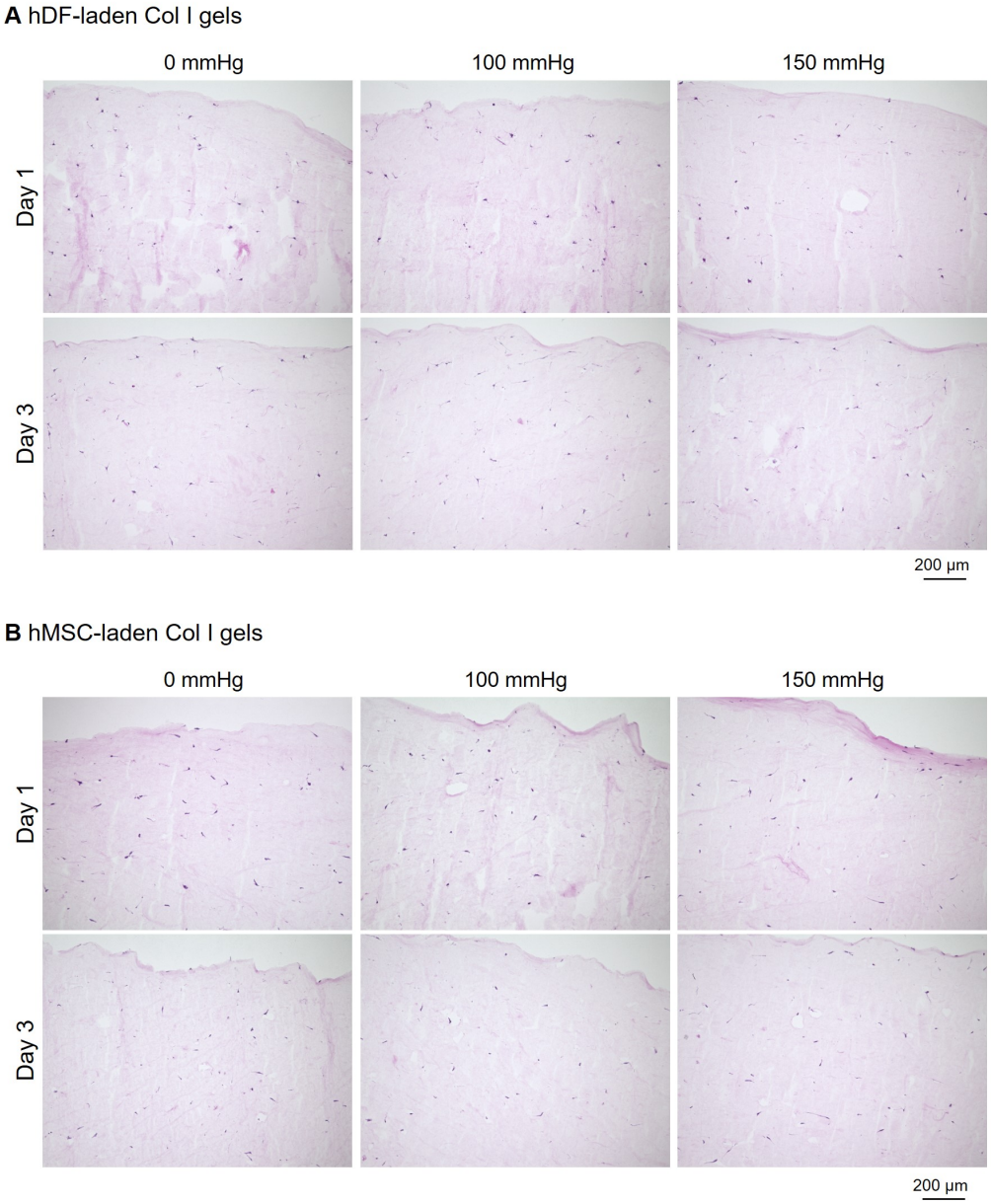

Figure 4.32.: Biomechanical stimulation method II by hydrostatic pressure: preliminary test with cell-laden Col I gel disks analyzed by HE staining (n=1). HE staining of hDF-laden Col I gel disks (**A**) and hMSC-laden Col I gel disks (**B**) on day 1 and 3 after hydrostatic pressure stimulation of 0, 100 and 150 mmHg for 30 min at RT. Scale bars as depicted, same magnification for all micrographs.

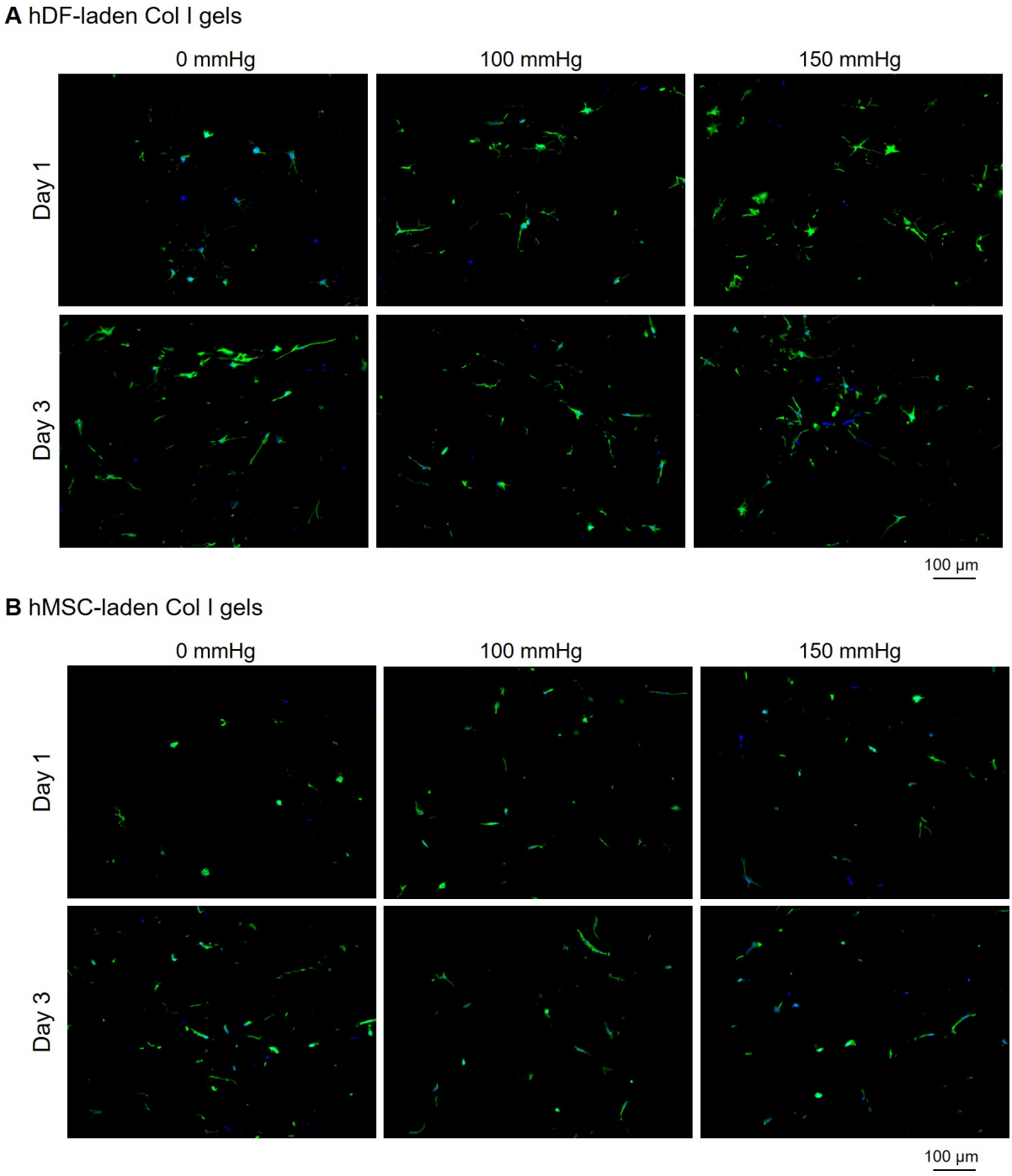

Figure 4.33.: Biomechanical stimulation method II by hydrostatic pressure: preliminary test with cell-laden Col I gel disks analyzed by Phalloidin staining (n=1). Phalloidin staining of hDF-laden Col I gel disks (**A**) and hMSC-laden Col I gel disks (**B**) on day 1 and 3 after hydrostatic pressure stimulation of 0, 100 and 150 mmHg for 30 min at RT. Scale bars as depicted, same magnification for all micrographs.

4.5. Vascularization strategies

In this part, three different vascularization strategies were investigated to establish a vascularization gradient necessary in meniscus tissue engineering: (1) artificial hypoxia state by CPX, (2) cell sheet engineering and (3) the BioVaSc-TERM® as vascularized scaffold.

4.5.1. Artificial hypoxia state by CPX

HMSCs were stimulated with CPX. Gene expression analysis of CPX stimulated hMSCs revealed a decrease of HIF-1α expression, whereas VEGF expression was upregulated compared with unstimulated hMSCs (figure 4.34 A). The medium of these cells was harvested as conditioned medium for analysis and application in sprouting assay. MSC-CM of 10 μM CPX stimulation (MSC-CM CPX) was analyzed in comparison with the control (MSC-CM of unstimulated hMSCs). MSC-CM CPX contained 1.5 fold more VEGF than the control (figure 4.34 B).

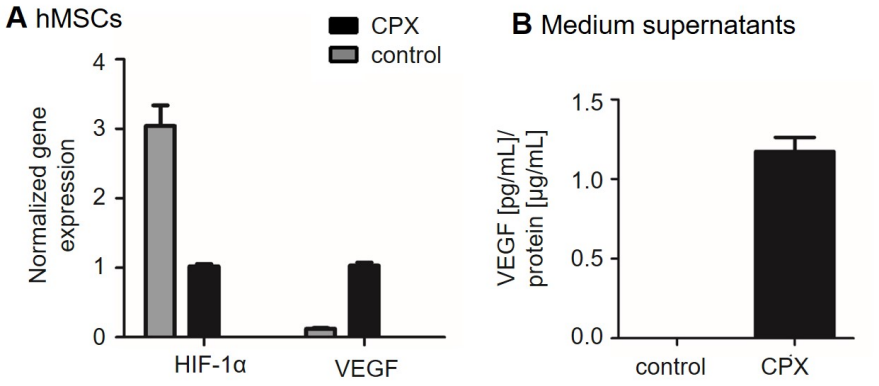

Figure 4.34.: Gene expression analysis of 10 μM CPX stimulated hMSCs and VEGF protein quantification of the MSC-CM CPX. A Gene expression of HIF-1α and VEGF of hMSCs under CPX stimulation (CPX) in comparison with unstimulated hMSCs (control). **B** VEGF quantification of MSC-CM CPX (CPX) in comparison with the MSC-CM (control) by ELISA. Adapted from [48] with kind permission.

Expression of angiogenic factors was analyzed (figure 4.35) and a number of pro-angiogenic factors were substantially increased in conditioned medium under CPX. Angiopoietin-2,

endothelin-1, IL-8, vasohibin and VEGF-C were just above the detection threshold under CPX but not detectable in the control (figure 4.35 left). MSC-CM CPX contained 2.5 fold more angiogenin and 12.5 fold more FGF-7 than the control. Decreased protein levels of IGFBP-1, IGFBP-2, IGFBP-3, MCP-1, MMP-8, MMP-9, pentraxin, PD-ECGF, PDFG-AA, persephin, serpin E1, serpin F1, TIMP-1, TIMP-4, thrombospondin-1, uPA were detected for the MSC-CM CPX compared with the control (figure 4.35 right). MMP-8, MMP-9, PD-ECGF, PDFG-AA, persephin, TIMP-4 were only detected for the control.

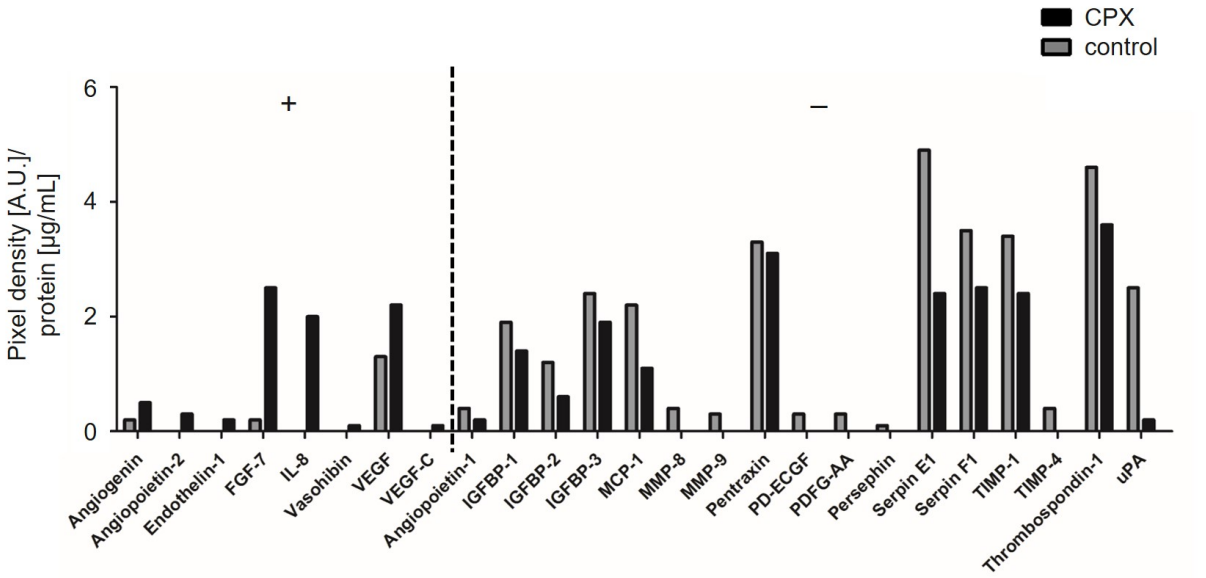

Figure 4.35.: Analysis of expression levels for angiogenic factors in the MSC-CM CPX by the Proteome Profiler™ Human Angiogenesis Array. Left: Increased expression (+) of factors in MSC-CM CPX (CPX), right: decreased expression (−) of factors in MSC-CM CPX in comparison with MSC-CM (control). Adapted from [48] with kind permission.

Next, CPX was used as a stimulation agent in sprouting assays of hd-mvEC spheroids through direct application and by MSC-CM CPX. After 24 h stimulation, spheroids stimulated with 25 ng/ml VEGF, 10 μM CPX and MSC-CM CPX showed pronounced sprouting, whereas the untreated control (w/o) showed no sprouting and the MSC-CM control less sprouting (figure 4.36 A). The number of sprouts (NOS) was significantly increased by stimulation with 25 ng/mL VEGF and 10 μM CPX compared with the untreated control (p=0.004) (figure 4.36 B). The NOS after 10 μM CPX stimulation was 2 fold higher than the control, whereas the stimulation with 25 ng/mL VEGF was only 1.6 fold increased. MSC-CM CPX showed a slight NOS increase compared with its control MSC-CM and the untreated control. The NOS of 10 μM CPX and 25 ng/ml VEGF was higher than the NOS of conditioned medium (MSC-CM and MSC-CM CPX) .

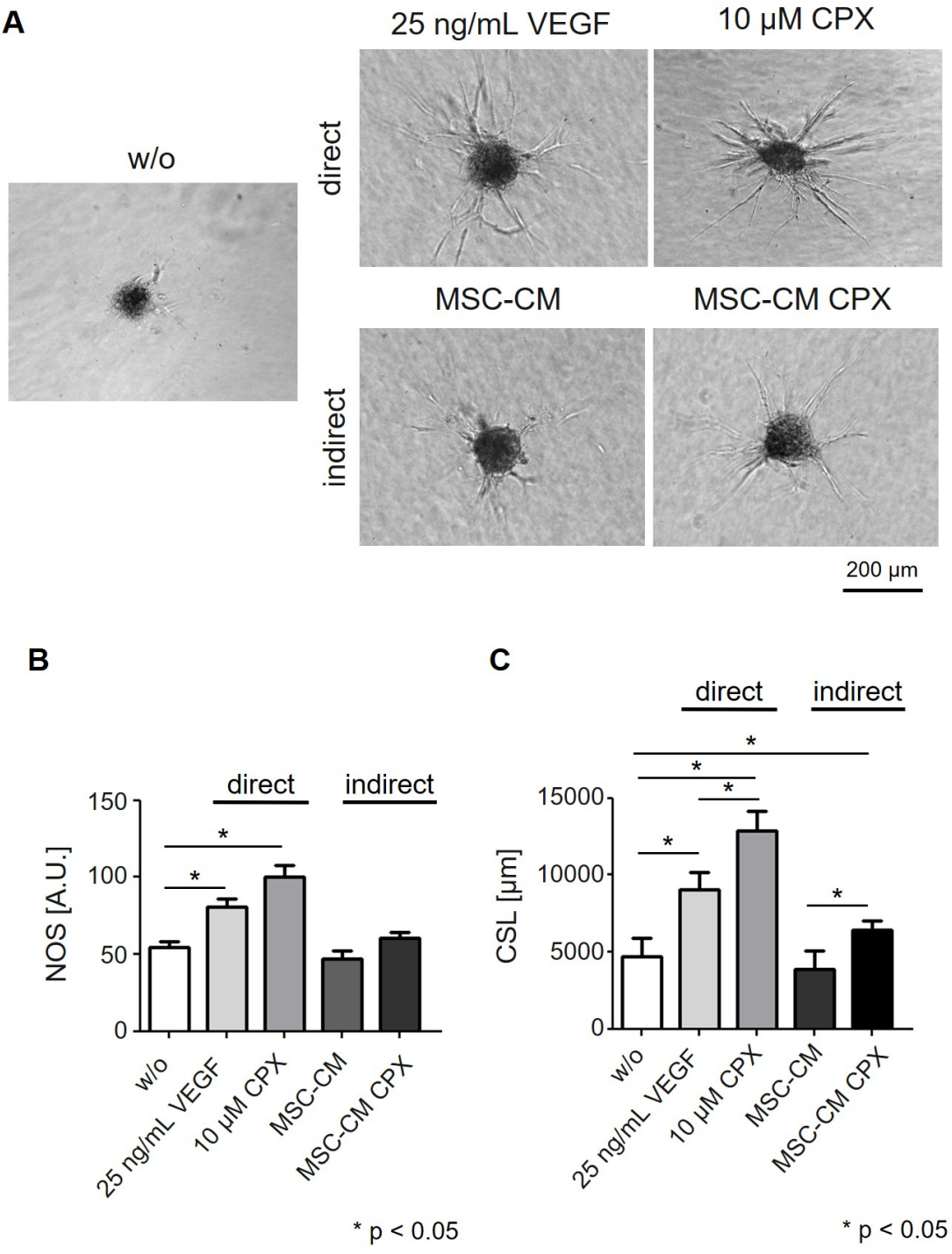

Figure 4.36.: Vascularization strategy I: CPX induced sprouting of hd-mvEC spheroids. **A** Morphology of the spheroids after 24 h of stimulation visualized by brightfield microscopy (scale bar as depicted, same magnification for all micrographs), **B, C** NOS and CSL after 24 h of stimulation. Direct stimulation with 25 ng/mL VEGF and 10 μM CPX versus indirect stimulation with MSC-CM (control) and MSC-CM CPX (CPX) are depicted: *p < 0.05, n $= 4$, error bars represent standard deviation (Kruskal-Wallis test). Adapted from [48] with kind permission.

The cumulative sprouting length (CSL) describes the sum of sprouting lengths of all measured sprouts of ten randomly selected spheroids per condition. The CSL after direct stimulation of hd-mvEC spheroids with 25 ng/mL VEGF and 10 μM CPX was significantly increased in contrast to the untreated control (p=0.001) (figure 4.36 C). Direct stimulation with 10 μM CPX even showed a significantly higher CSL increase which was 1.5 fold higher than the positive control of 25 ng/mL VEGF. Indirect stimulation with CPX by MSC-CM CPX led to a significant increase of CSL which was almost 1.5 fold higher than the control MSC-CM. Additionally, indirect stimulation with CPX (MSC-CM CPX) led to a significant CSL increase compared to the untreated control. In contrast, the CSL of directly stimulated spheroids with 25 ng/ml VEGF or 10 μM CPX was higher compared to the indirect stimulation with CPX (MSC-CM CPX).

4.5.2. Cell sheet engineering

As second vascularization strategy, engineering of a hMSC/hd-mvEC sheet, simplified in the following as cell sheet, was established by a temperature triggered cell sheet fabrication using PGE coated petri dishes. The sheet detaching protocol after 24 h was established obtaining a free-floating cell sheet (figure 4.37 A). As plate controls for the cell sheet engineering, the polystyrol (PS) plate did not allow cell attachment and the tissue culture polystyrol (TCPS) did not allow sheet detachment after 24 h (figure 4.37 B).

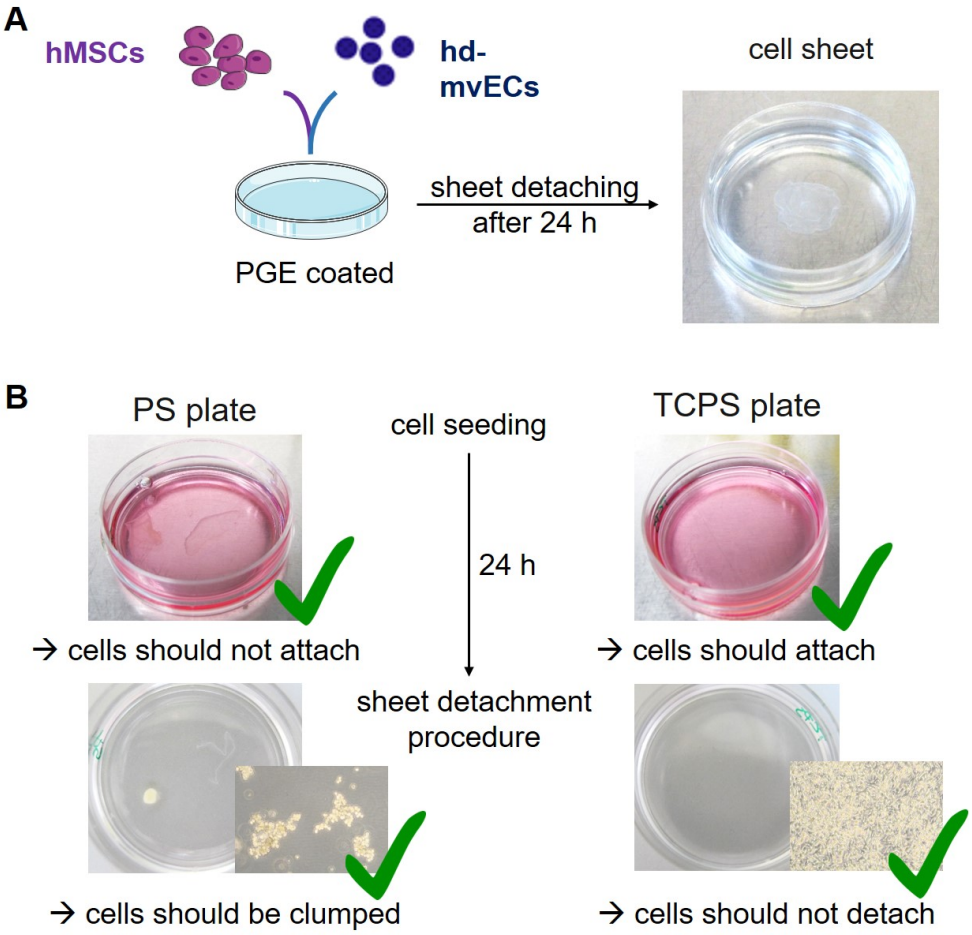

Figure 4.37.: Vascularization strategy II: engineering of a cell sheet with plate controls. A A cell sheet was built by seeding hMSCs and hd-mvECs on a temperature-responsive PGE coated petri dish. The intact and free-floating cell sheet was detached by a temperature triggered procedure after 24 h. **B** Plate controls for cell sheet engineering: the cell seeding of hMSCs and hd-mvECs, and the following sheet detachment procedure was performed on a PS plate and a TCPS plate. The cells did not attach to the PS plate, whereas the seeded cells did not detach from the TCPS plate by temperature triggered detachment procedure performed after 24 h.

The free-floating cell sheet was characterized by immunofluorescent staining (figure 4.38). CD31 positive staining was detected for the hd-mvECs, and CD44 stained for the hMSCs. Cell nuclei were counterstained with DAPI. These cell sheets were used to build a vascularized meniscus model with an oriented vascularization approach from the location of the RR zone as introduced in section 4.6.

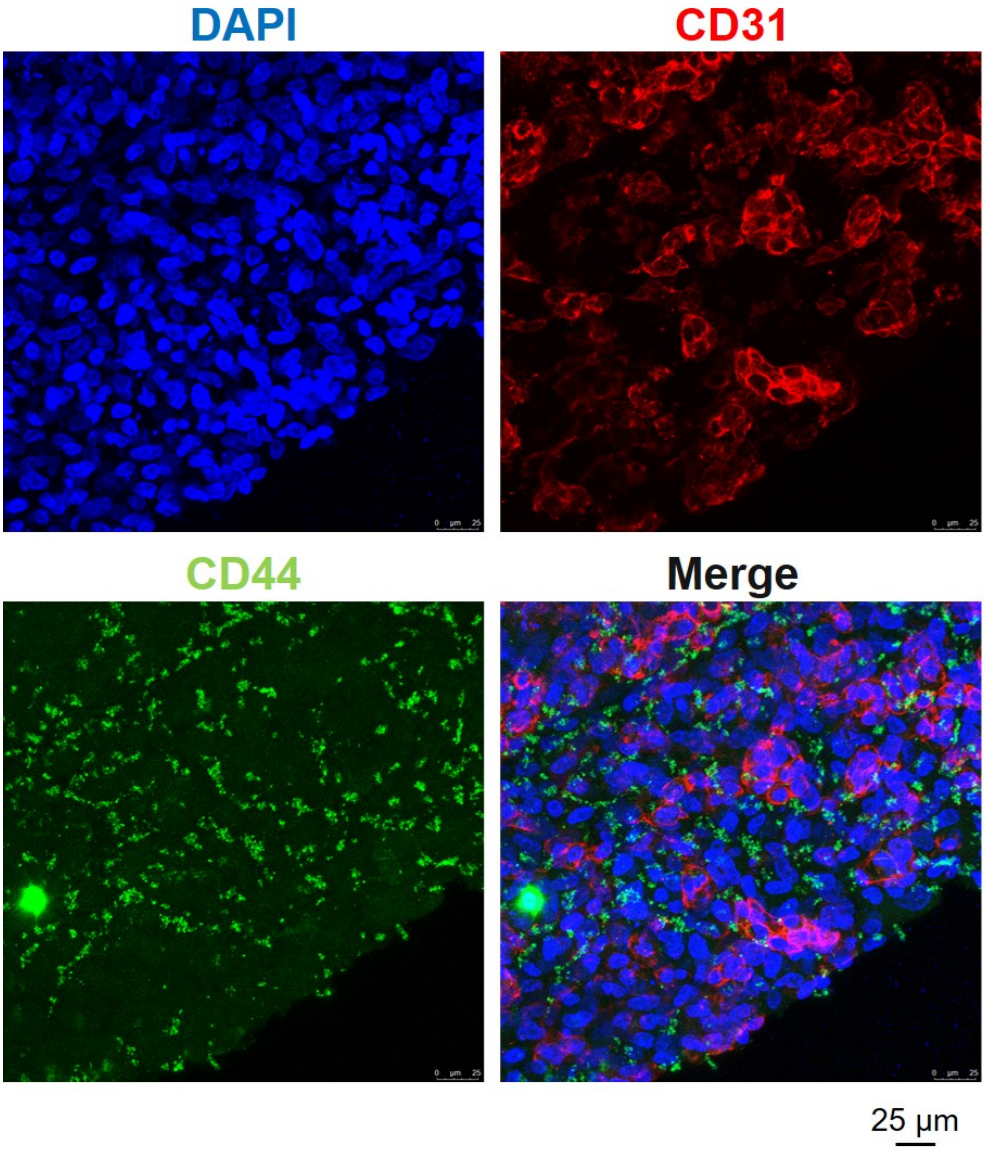

Figure 4.38.: Immunofluorescent analysis of the free-floating cell sheet. Immunofluorescent staining for CD31 (red) as hd-mvEC marker, CD44 (green) as hMSC marker and DAPI (blue) for cell nuclei. Scale bar as depicted, same magnification for all micrographs. Adapted from [130] with kind permission.

4.5.3. BioVaSc-TERM®

The vascularized scaffold BioVaSc-TERM® was studied as third vascularization strategy for wrapping the meniscus model. This scaffold contains a preserved capillary system which can be seeded with ECs such as hd-mvECs. MTT test confirmed metabolic activity of the seeded hd-mvECs in the re-endothelialized capillary system of the BioVaSc-TERM® (figure 4.39 A). Live/Dead staining confirmed the viability of the re-endothelialized vascular network of the reseeded BioVaSc-TERM® (figure 4.39 B). The immunohistochemical staining for vWF visualized the vascular network of the BioVaSc-TERM® by positive vWF detection of endothelial structures within the scaffold (figure 4.39 C).

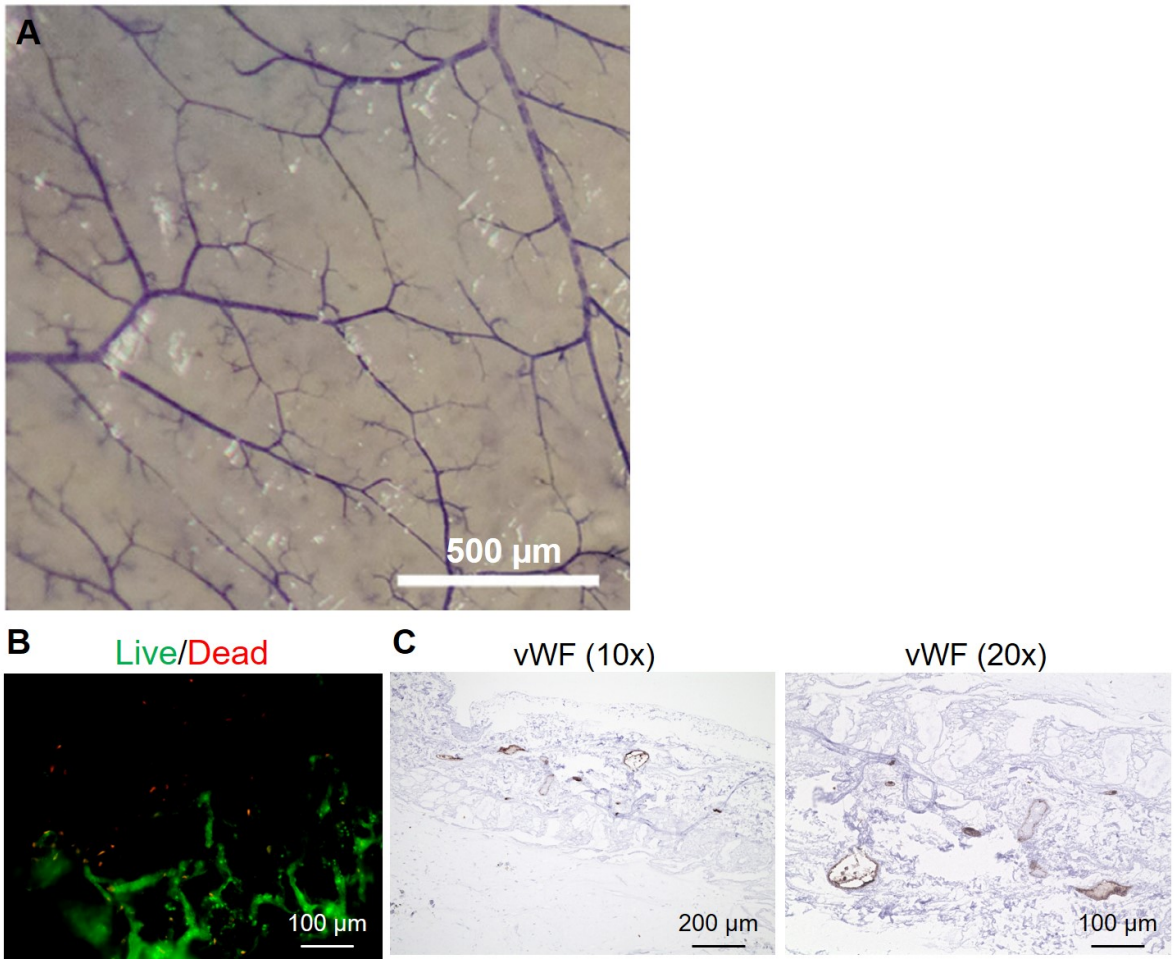

Figure 4.39.: Vascularization strategy III: BioVaSc-TERM® as vascularized scaffold. A MTT staining of the re-endothelialized vascular network of the BioVaSc-TERM® revealed cell metabolic activity by blue formazan staining. Scale bar as depicted. Adapted from [67] with kind permission. **B** Live/Dead staining and **C** immunohistochemical staining for vWF of BioVaSc-TERM® reseeded with hd-mvECs on day 21. Scale bars as depicted.

4.6. Vascularized meniscus model

The meniscus contains a gradual vascularization starting in the vascular RR zone and decreasing in the RW zone towards the avascular WW region (figure 4.40 A) [3]. In the following, the established 3D meniscus model based on wedge-shape compression of a hMSC-laden Col I gel was processed into a vascularized meniscus model. Two different approaches to build a vascularized meniscus model were studied.

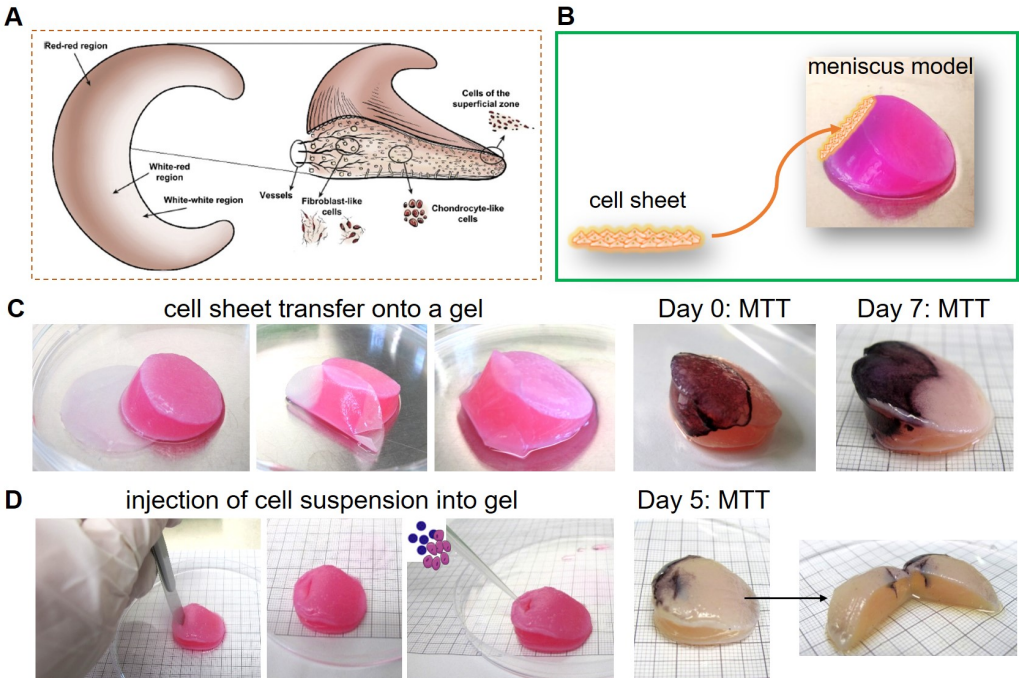

Figure 4.40.: Schemata and pretests to build a vascularized meniscus model. **A** The meniscus is partly vascularized, namely in the RR and the RW region. Reprinted from [3] with permission from Elsevier. **B** Schematic illustration of the cell sheet transfer onto the RR zone of the meniscus model. **C** Optimization of the sheet transfer protocol proven by a MTT test on day 0 and 7 after cell sheet transfer onto a wedge-shaped cell-free Col I gel. **D** Optimization of the injection of a cell suspension composed of hMSCs and hd-mvECs into a defined gap of the RR region of the wedge-shaped Col I gel. The procedure for the control was proven by a MTT test on day 5 after injection in a cell-free Col I gel.

First, the characterized cell sheet (section 4.5.2) was transferred onto the RR zone of the wedge-shaped Col I gel (figure 4.40 B). To achieve a complete sheet transfer, the protocol for the transfer onto the RR zone of the wedge-shaped gel was optimized using a membrane as explained in the method part 3.7.1. On day 0, a complete cell sheet transfer onto a wedge-shaped cell-free Col I gel was confirmed by MTT assay (figure 4.40 C). After

7 days of culture, the cell sheet was firmly attached to the cell-free Col I gel as confirmed by blue formazan staining (figure 4.40 C). As second approach, a cell suspension of hMSCs and hd-mvECs was injected into a defined gap of the RR region of the wedge-shaped cell-free Col I gel. After 5 days of culture, blue formazan staining confirmed metabolically active cells located in the gap, whereas the cell-free gel did not change its color (figure 4.40 D). With these two approaches, 3D vascularized meniscus models based on wedge-shape compression were built: (a) hMSC-laden Col I gel without hd-mvECs served as a control and was defined as gel, (b) hMSC-laden Col I gel with the transferred cell sheet onto the RR region was defined as gel+sheet and (c) hMSC-laden Col I gel with the injected cell suspension of hMSCs and hd-mvECs was defined as gel+cells (figure 4.41 A).

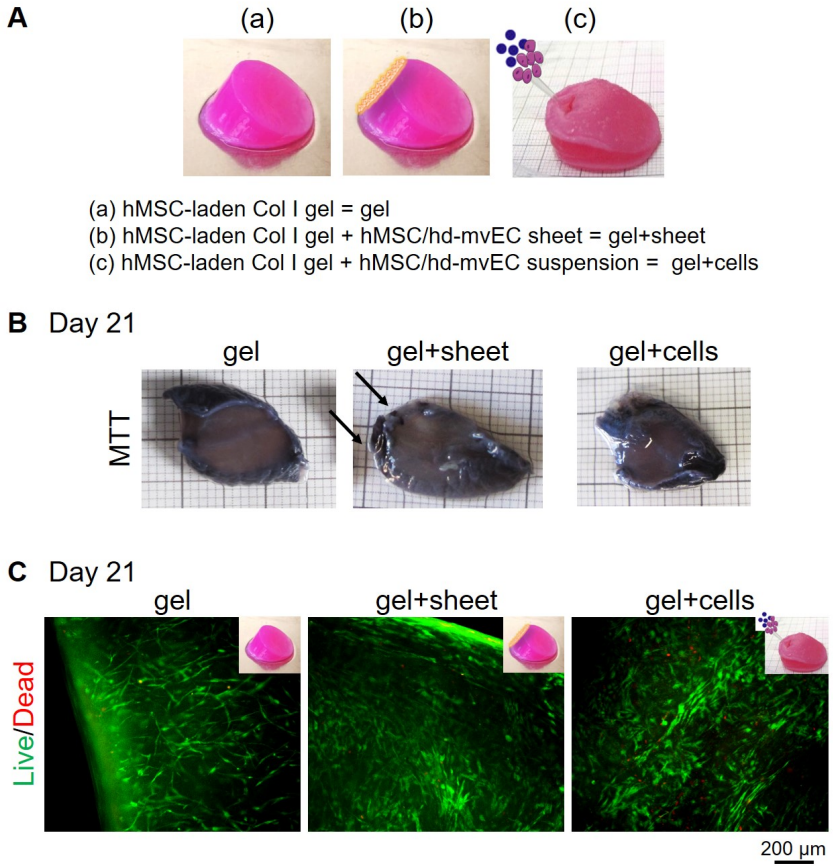

Figure 4.41.: 3D vascularized meniscus model: experimental setup and analysis of metabolic activity and viability (n=4). A The following models were prepared: (a) hMSC-laden Col I gel defined as gel, (b) hMSC-laden Col I gel with transferred cell sheet defined as gel+sheet and (c) hMSC-laden Col I gel with injected cell suspension of hMSCs and hd-mvECs defined as gel+cells. The models were cultured in 50 % VascuLife®, 50 % chondrogenic DM and 10 ng/mL TGFβ-3 until day 21. **B, C** MTT test and Live/Dead staining (scale bar as depicted, same magnification for all micrographs) on day 21 revealed similar metabolic activity and viability for gel, gel+sheet and gel+cells. The arrows in the MTT staining of gel+sheet indicate parts of the sheet.

These models were cultured for 21 days with 50 % VascuLife®, 50 % chondrogenic DM and 10 ng/mL TGF. On day 21, MTT test revealed metabolic activity of all three models by blue formazan staining (figure 4.41 B). Parts of the sheets stained darker blue indicated by arrows (figure 4.41 B). The Live/Dead staining confirmed the viability for all three approaches (figure 4.41 C). Viable cells within the models were stained in green, whereas only a small percentage of dead cells in red were detected. No difference in metabolic activity by MTT staining and viability by Live/Dead staining was noticed between gel, gel+sheet and gel+cells. Next, the remaining glucose amount (figure 4.42 A) and the produced lactate (figure 4.42 B) were quantified in medium supernatants from day 3 to 21. From day 3 to 7, the remaining glucose amount significantly decreased and lactate significantly increased ($p<0.05$) confirming active metabolism. At each time point (day 3, 7, 10, 14, 17 and 21) the medium was changed to fresh medium. The measured remaining glucose amount ($p=0.876$) and lactate ($p=0.259$) did not differ between the three different models.

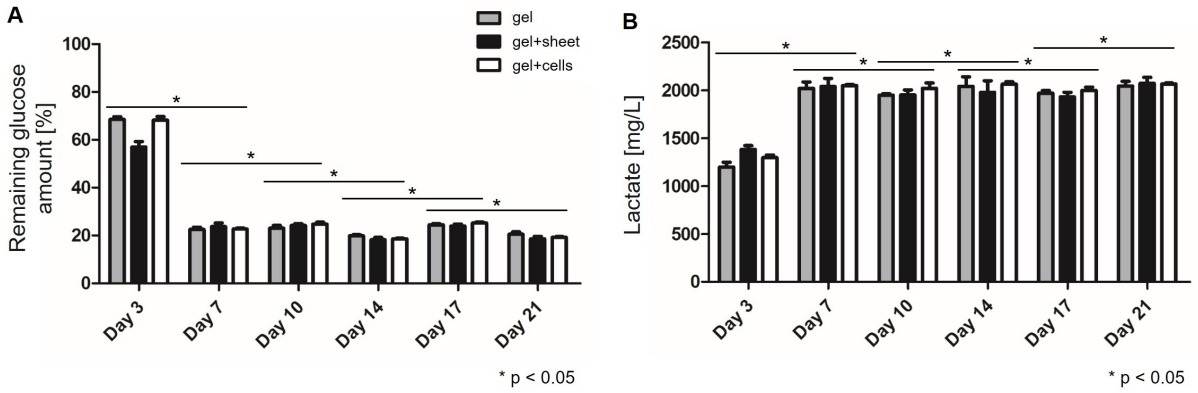

Figure 4.42.: 3D vascularized meniscus model: analysis of cell metabolism (n=4). Remaining glucose amount (**A**) and lactate (**B**) in medium supernatants of gel, gel+sheet and gel+cells was determined from day 3 to 21. No significant differences between gel, gel+sheet and gel+cells were found. From day 3 to day 7, the remaining glucose amount decreased significantly and the lactate amount increased significantly for all models: $^*p < 0.05$, n = 4, error bars represent standard deviation (Kruskal-Wallis test).

In addition, gel zymography was performed with medium supernatants of day 7, 14 and 21 to get an impression of the level of matrix remodeling (figure 4.43). On day 7, similar bands for proMMP-2 (72 kDa), active MMP-2 (62 kDa) and active MMP-9 (67 kDa and 83 kDa) were detected for all three models (figure 4.43 A). From day 7 to 21, the bands seemed to become thicker for all three models. The total MMP increase over time was confirmed by the quantified pixel intensity of total MMPs (figure 4.43 B). No difference

in MMP detection was observed between the three models. The standard deviation of the quantified pixel intensity was not shown, as this is a qualitative quantification by densitometry and the observed effect was similar between the biological replicates (n=4).

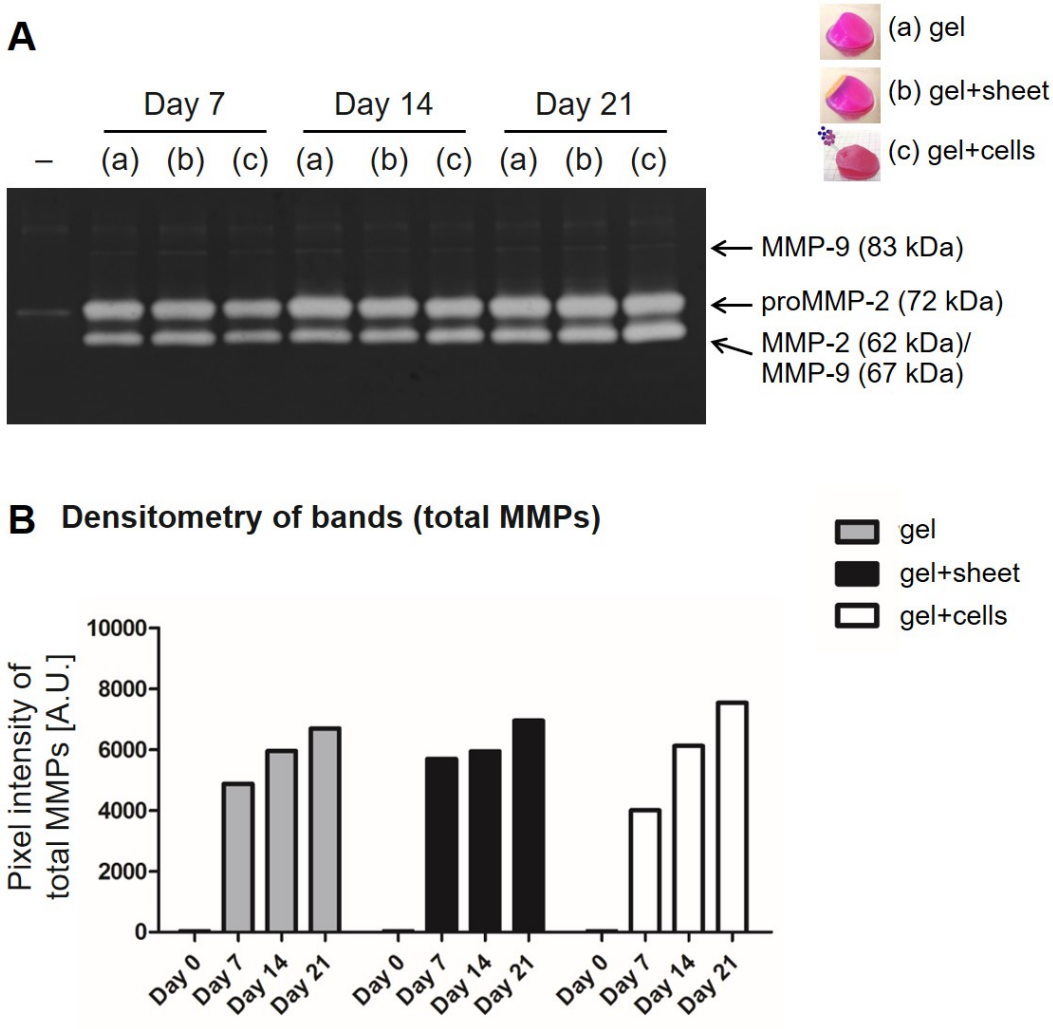

Figure 4.43.: 3D vascularized meniscus model: analysis of MMPs by gel zymography (n=4) Gel zymography of medium supernatants (day 7, 14 and 21) of the meniscus models gel, gel+sheet and gel+cells (**A**), and its densitometry quantifying the pixel intensity of total MMPs (**B**). ProMMP-2 (72 kDa), active MMP-2 (62 kDa) and active MMP-9 (67 kDa and 83 kDa) were detected. An increase of total MMPs from day 7 to day 21 was observed. No difference between the different setups was observed.

On day 21, the gel+sheet model had a water content of approx. 97 % which was significantly lower compared to gel or gel+cells (p=0.031) (figure 4.44 A). The shrinkage by size was approx. 40 % for all three models (p=0.155) (figure 4.44 B). However, the reduction in wet weight of the gel+sheet model with approx. 70 % was significantly higher than for gel or gel+cells (p=0.019) (figure 4.44 C).

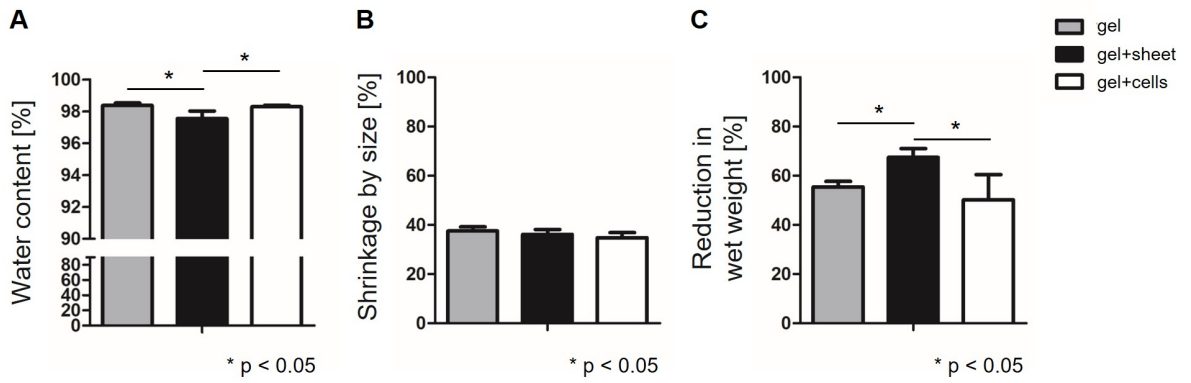

Figure 4.44.: 3D vascularized meniscus model: analysis of the water content and shrinkage (n=4). Water content (**A**), shrinkage by size (**B**) and reduction in wet weight (**C**) on day 21 of the models gel, gel+sheet and gel+cells. A significant decrease of water content and reduction in wet weight for gel+sheet in contrast to gel or gel+cells was found: $^{*}p < 0.05$, n=4, error bars represent standard deviation (Kruskal-Wallis test).

The hd-mvEC part of the models was studied by immunohistochemical analysis for the vascularization markers CD31 and vWF. Overview stainings are shown in figure 4.45.

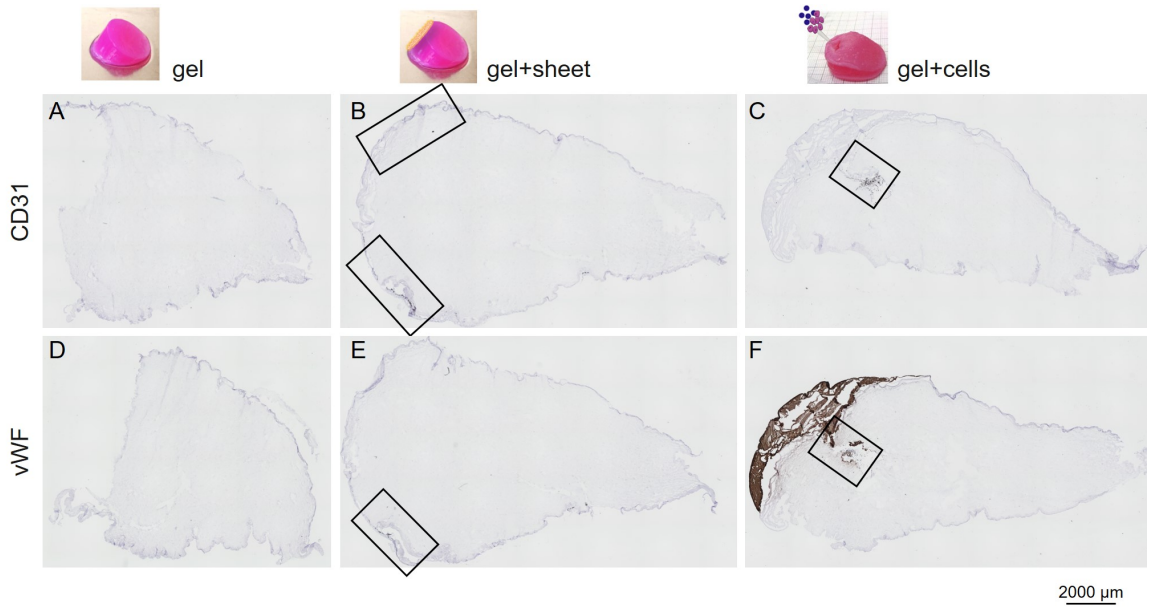

Figure 4.45.: 3D vascularized meniscus model: immunohistochemical analysis for vascularization markers (n=4). Immunohistochemical staining for CD31 (**A-C**) and vWF (**D-E**) of the models gel, gel+sheet and gel+cells. The model merely based on the gel was negative for CD31 and vWF. The model gel+sheet was CD31 and vWF positive in the sheet areas and the model gel+cells in the injection area. The used fibrin glue was positive for vWF. Positively stained areas are framed. Scale bar as depicted, same magnification for all micrographs.

The model gel without hd-mvEC part did not show positive immunohistochemical staining for CD31 and vWF (figure 4.45 A, D). The model gel+sheet stained positively for CD31 and vWF in the sheet areas as indicated by frames (figure 4.45 B, E). The third model gel+cells showed positive staining for CD31 in the framed injection area (figure 4.45 C). Positive staining for vWF was detected in the framed injection area and the fibrin glue which was used to close the gap after injection of the cell suspension (figure 4.45 F). The two approaches for establishing a vascularized meniscus model were studied in detail based on magnified micrographs of CD31 and vWF stained sections (figure 4.46). The transferred cell sheet onto the RR region of the hMSC-laden Col I gel (gel+sheet) showed positive staining for CD31 and vWF of a straight layer firmly attached to the gel (figure 4.46 A, D). In comparison, the RR zone of human native meniscus displayed layers of CD31 and vWF positive staining as well (figure 4.46 C, F). The model gel+cells showed positive staining for CD31 and vWF of single cells or cell clumps in the injection area (figure 4.46 B, E). No newly formed tissue was found in the injection area of the model gel+cells.

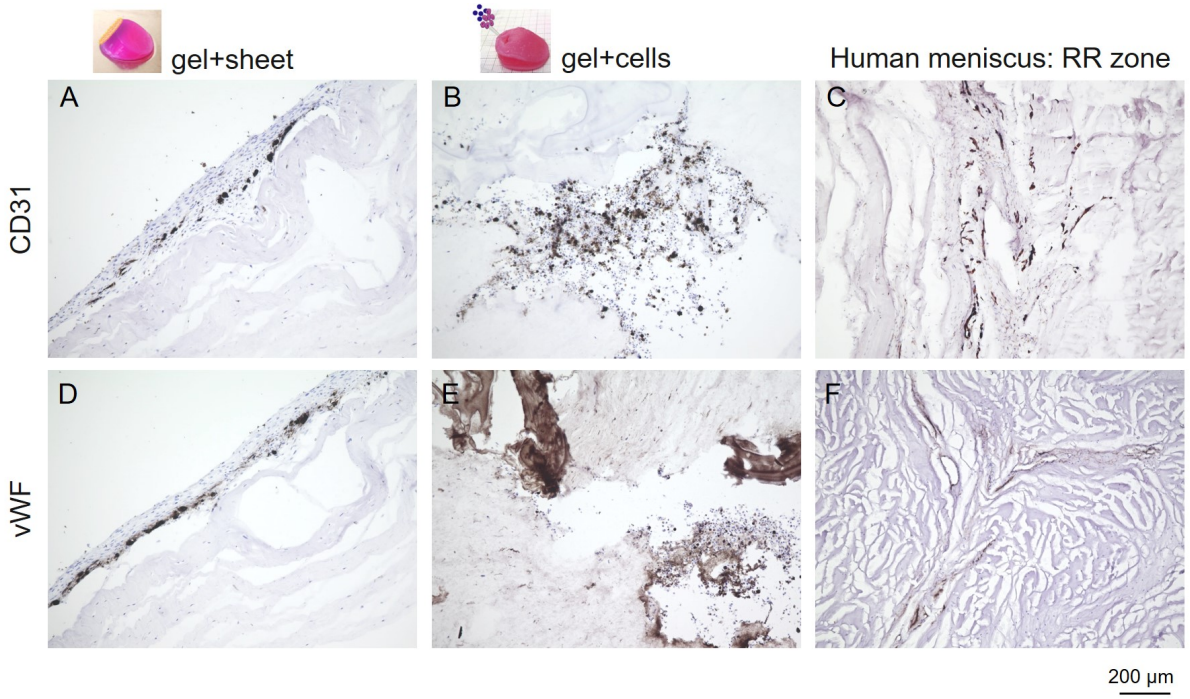

Figure 4.46.: 3D vascularized meniscus model: immunohistochemical analysis for vascularization markers (n=4). Immunohistochemical staining for CD31 (**A-C**) and vWF (**D-F**) of the models gel+sheet and gel+cells in comparison to human meniscal tissue of the RR zone (hMen70 PH). The model gel+sheet was CD31 and vWF positive in the sheet areas similar to the RR region of the human meniscus. Scale bar as depicted, same magnification for all micrographs.

After analysis for vascularization markers, the meniscal properties of the models were

checked. The three models were stained with Alican blue for proteoglycans and immunohistochemically for aggrecan, Col I and Col II, and directly compared with human meniscal tissue. Magnified micrographs of the location of the RW zone are depicted in figure 4.47.

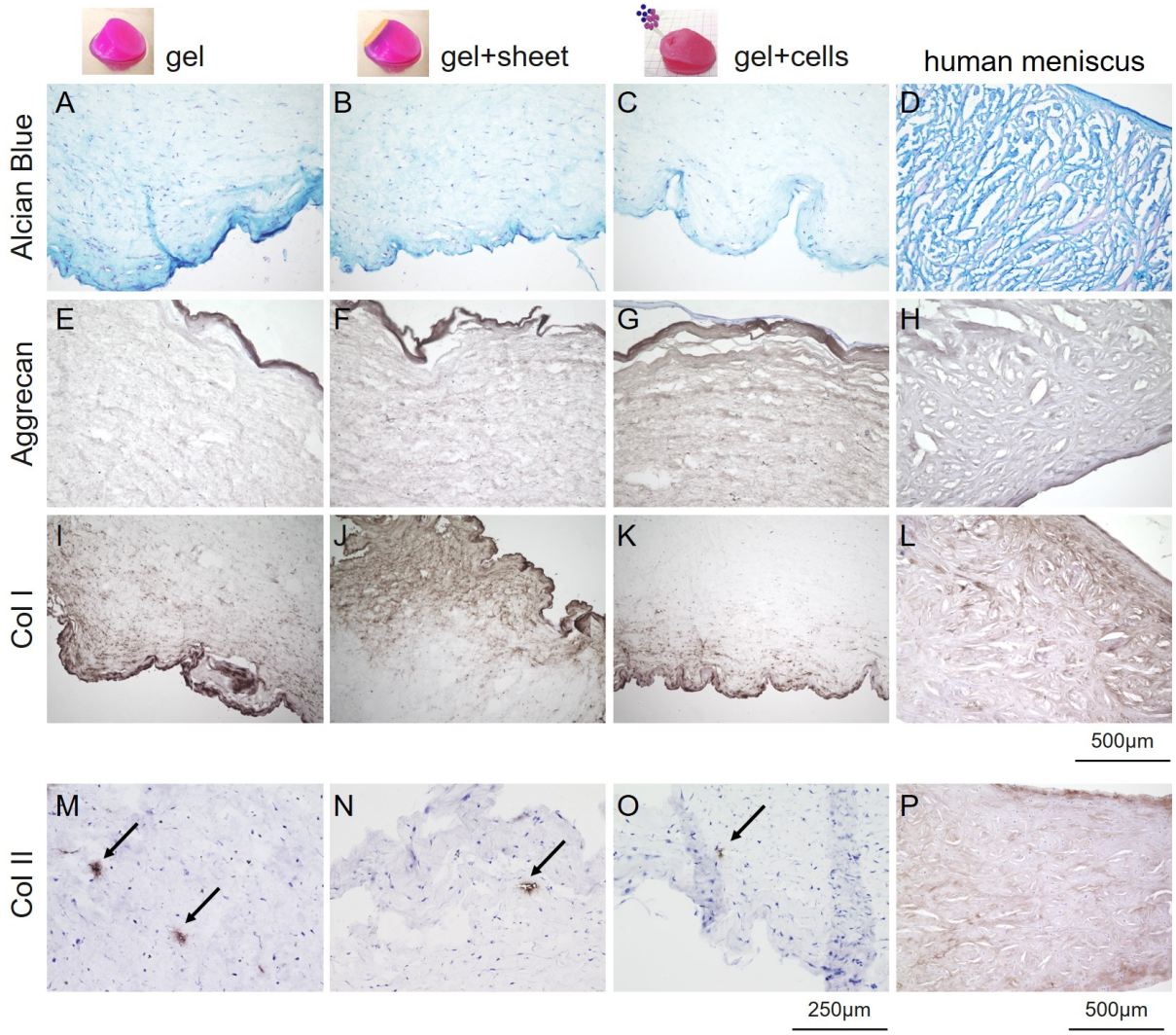

Figure 4.47.: 3D vascularized meniscus model: histological and immunohistochemical analysis for meniscal markers (n=4). Alcian blue staining for proteoglycans (**A-D**) and immunohistochemical staining for aggrecan (**E-H**), Col I (**I-L**) and Col II (**M-P**) of the models gel, gel+sheet and gel+cells in comparison to human meniscal tissue of the RW zone. The meniscal markers aggrecan and Col I stained positively for the three meniscus models. For Col II, only some Col II positive cells were detected in the models indicated by arrows. Scale bars, 500 μm for A-L and P. Scale bar, 250 μm for M-O.

Alcian blue staining revealed synthesized proteoglycans in the three models (figure 4.47 A-C). Aggrecan as main proteoglycan of the meniscus was found throughout all three

models similar to human meniscus (figure 4.47 E-H). The main collagen of the meniscus Col I was distributed throughout the models (figure 4.47 I-K). The model gel+sheet showed pronounced Col I staining at the borders similar to human meniscus (figure 4.47 J, L). However, only some Col II positive cells were detected in the models (figure 4.47 M-O), not imitating the native Col II distribution of human meniscal tissue (figure 4.47 P). For further analysis of meniscal markers, the GAG and DNA amount were quantified (figure 4.48). The chondrogenic index GAG/DNA was around 0.6 for gel+sheet and significantly increased for gel and gel+sheet in contrast to gel+cells (p=0.022) (figure 4.48 A). No significant difference was found in the DNA amount normalized by dry weight between the three models (p=0.584) (figure 4.48 B).

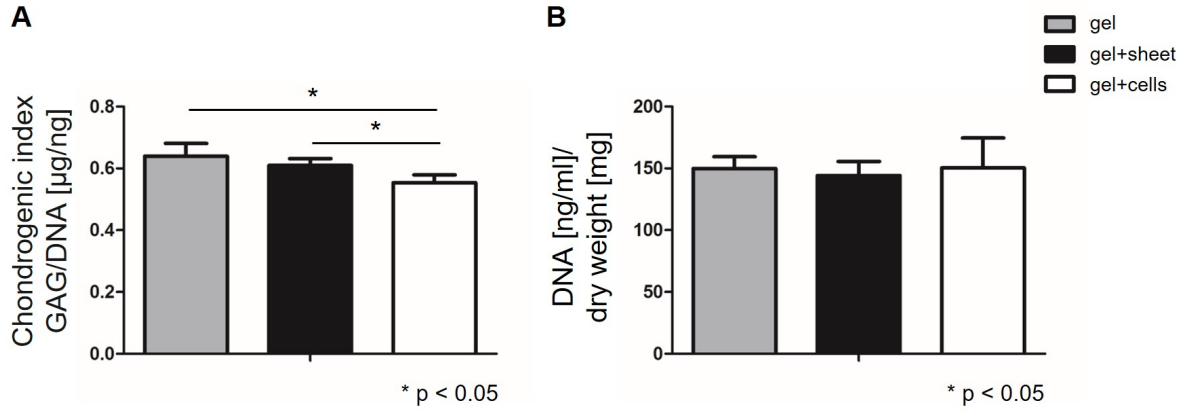

Figure 4.48.: 3D vascularized meniscus model: biochemical analysis by chondrogenic index GAG/DNA and DNA quantification (n=4). Chondrogenic index GAG/DNA (**A**) and DNA normalized by dry weight (**B**) for the models gel, gel+sheet and gel+cells. The chondrogenic index GAG/DNA was significantly increased for gel and gel+sheet in contrast to gel+cells. The DNA amount normalized by dry weight did not show a difference between the models: $^{*}p < 0.05$, n=4, error bars represent standard deviation (Kruskal-Wallis test).

Taken together, the model composed of the wedge-shaped hMSC-laden Col I gel with the transferred cell sheet represents a potential 3D vascularized meniscus model to be further improved in its endothelial and meniscal properties by applying the designed biomechanical stimulation systems of section 4.4.2.

4.7. Wrapping and fixation technique for the meniscus model

A meniscus model needs a proper fixation technique to be applied as an implant for meniscal surgeries in the future. The established 3D meniscus model was based on the wedge-shape compression of a hMSC-laden Col I gel which can be vascularized by a cell sheet (section 4.6). To fix this model in the knee joint, the following procedure is suggested and was preliminarily investigated (figure 4.49).

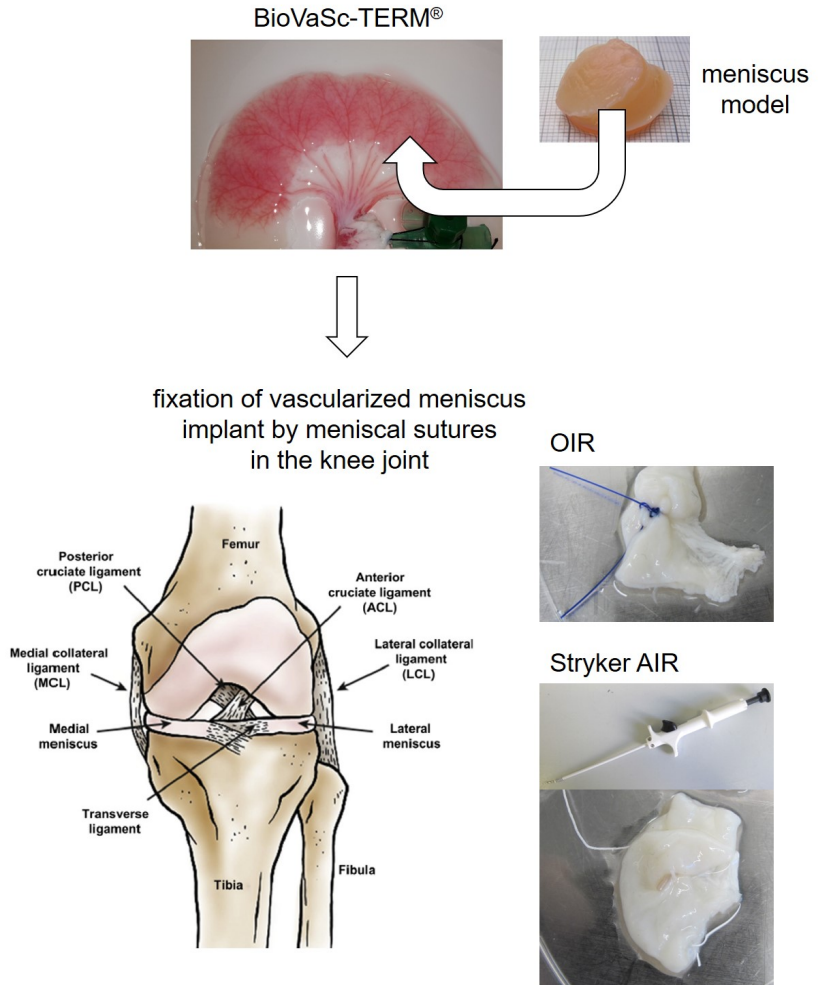

Figure 4.49.: Schematic illustration for the fixation techniques. The wedge-shaped meniscus model is placed in the lumen of the BioVaSc-TERM® as future meniscus implant model. Thus, the BioVaSc-TERM® provides a wrapping scaffold for fixation with a functional vascularized network after reseeding with ECs. For implantation into the knee joint (reprinted from [3] with permission from Elsevier), meniscal sutures are necessary. In the following part, two different suture techniques were studied: the OIR and the Stryker AIR.

The 3D meniscus model should be placed into the lumen of the re-endothelialized BioVaSc-TERM®. Thereby, the BioVaSc-TERM® provides the wrapping of the model, and also a vascularization approach as introduced in section 4.5.3. This future meniscus implant model composed of the meniscus model located in the lumen of the BioVaSc-TERM® has to be fixed in the knee joint by suture techniques.

We analyzed two different meniscal suture techniques to be applied: the outside-in-refixation technique (OIR) and the Stryker All-Inside-Repair (AIR). These two standard fixation techniques for meniscal surgeries were tested on the empty BioVaSc-TERM® scaffold by the experienced sport orthopedic surgeon Dr. Kai Fehske. Subsequently, we performed tensile testing of the meniscal sutures in the BioVaSc-TERM® to compare the mechanical properties of these two fixation techniques. Figure 4.50 illustrates macroscopic images of the tensile testing by pulling the meniscal sutures OIR and Stryker AIR with a velocity of 10 mm/second. This velocity mimicked the real loading conditions upon a meniscal suture defect.

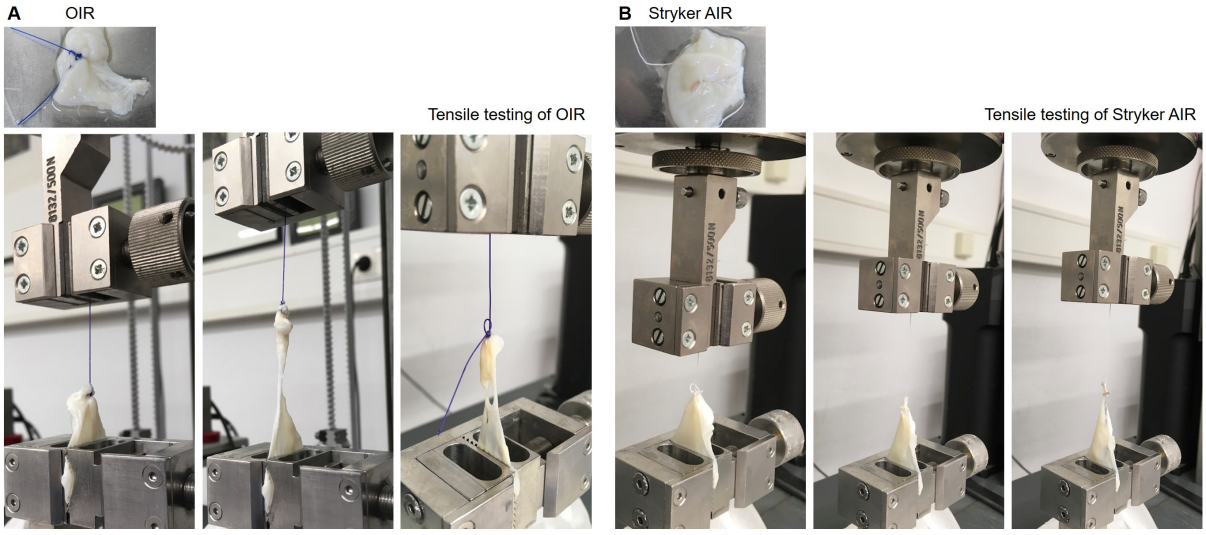

Figure 4.50.: Macroscopic images of the tensile testing of meniscal sutures in the BioVaSc-TERM®. A Macroscopic images of the OIR sutured in the BioVaSc-TERM® (top) and the tensile testing (bottom). **B** Macroscopic images of the Stryker AIR sutured in the BioVaSc-TERM® (top) and the tensile testing (bottom). The measurement was performed at the Institute of Orthopaedic Research and Biomechanics, Ulm University, Germany.

Figure 4.51 displays the results of the tensile testing. The maximal force to failure F_{max} was approx. 10 N and similar between the OIR and the Stryker AIR (p=0.622) (figure 4.51 A). However, the Stryker AIR had a significant higher deformation dL until F_{max} as compared to the OIR (p=0.019) (figure 4.51 B). This correlated with a bigger work until

reaching the maximal force to failure W until F_{max} observed for the Stryker AIR (figure 4.51 D). On the contrary, the OIR showed a significantly increased total stiffness F_{max}/dL (p=0.003) (figure 4.51 C).

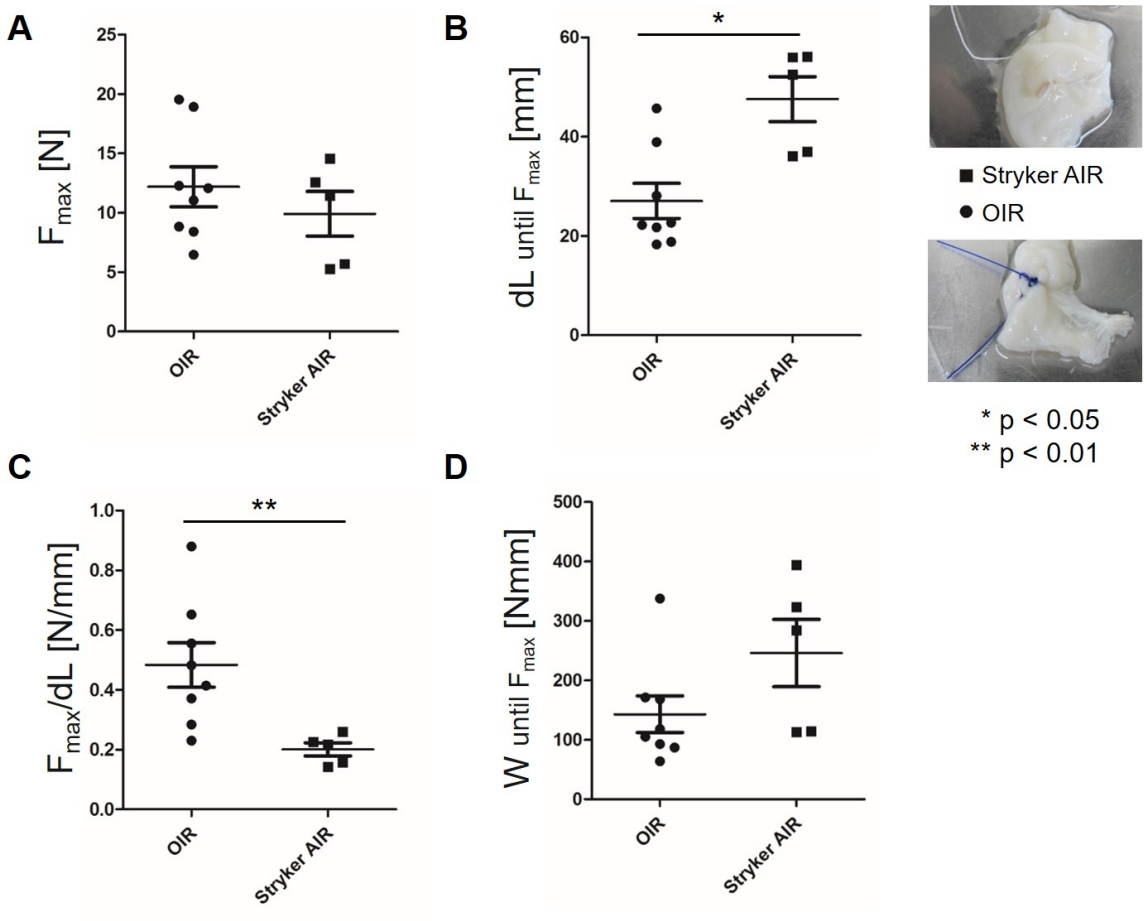

Figure 4.51.: Measurements of the tensile testing of meniscal sutures in the BioVaSc-TERM®. Tensile testing of the OIR (n=8) and the Stryker AIR (n=5) sutured in the BioVaSc-TERM® was performed with a velocity of 10 mm/second. The following parameters were determined: maximal force to failure F_{max} (**A**), deformation dL until F_{max} (**B**), total stiffness F_{max}/dL (**C**), and work until reaching the maximal force to failure by W until F_{max} (**D**). The OIR had a significantly higher total stiffness, whereas the Stryker AIR had a significantly higher deformability and bigger work until reaching the maximal force to failure: $^{*}p < 0.05$, $^{**}p < 0.01$, n_{OIR}=8, $n_{Stryker\ AIR}$=5, error bars represent standard deviation (Mann-Whitney U test).

Chapter 5

Discussion

Currently, there is no optimal treatment for meniscal injuries or degeneration. Especially lesions located in the avascular zone are a clinical challenge due to their poor healing potential [3]. So far, the gold standard of treatment is suturing or partial meniscectomy with the aim of preserving as much meniscal tissue as possible [5]. The current two implants on the market Actifit® and CMI® are cell-free and only indicated for limited cases after partial meniscectomy with maintained meniscal rim, intact AH and PH for proper fixation [22]. As current treatment regimes do not lead to sustainable outcome, replacing a torn meniscus by a tissue engineered cell-based meniscus implant offers a promising prospect for meniscus regeneration. Although research efforts are strong, no convincing meniscus implant has yet been established.
The development of a tissue engineered vascularized meniscus implant was the focus of this thesis. For that, the meniscus was characterized as target tissue to define the requirements of a meniscus implant which is discussed in section 5.1. Next, the developed meniscus implant by combining an appropriate cell type, biomaterial, biochemical conditions and biomechanical stimuli is evaluated in section 5.2. Then, the vascularization strategies and their implementation into the meniscus model are discussed in section 5.3. Finally, the suggested implantation method by wrapping and fixation is evaluated in section 5.4. An outlook and the future perspectives are addressed in part 5.5.

5.1. Characterization of the heterogeneous meniscus as target tissue

The human and equine meniscus was comprehensively characterized in this thesis. The meniscus is a wedge-shaped fibrocartilaginous tissue with a high water content [3]. The human medial meniscus was used as template in this thesis for characterization purposes

and as reference tissue for the tissue engineered meniscus model, as tears of the medial meniscus are more frequent compared to the lateral meniscus [15]. Depending on the anatomic location AH, PI or PH and its ligamentary fixation, the meniscus had different wedge-shapes (figure 4.4). The wedge-shape of the meniscus is an important requirement in meniscus tissue engineering, also causing the heterogeneous cellular and biochemical composition as introduced in figure 1.2 [18]. However, the biochemical composition of the different anatomic locations showed only very small differences which can be disregarded for tissue engineering of a meniscus model.

The main component of the meniscus matrix is collagen with Col I as most prominent collagen [3], confirmed in figure 4.3 I-L, 4.4 C, G, K, and 4.6 D. As Col I is the main collagen, scaffolds based on Col I represent potential scaffolds in meniscus tissue engineering which is discussed in section 5.2.2. Col X indicating hypertrophic or osteoarthritic cartilage [20] should be negative in the meniscus models as shown for meniscal tissue (figure 4.17). The axial part of the meniscus showed positive staining for Col II and aggrecan indicating articular cartilage-like properties of this part (figure 4.4). From a histological point of view the equine meniscus (figure 4.6) was similar to the human. For the immunohistological characterization of meniscus models, Col I, Col II and aggrecan as main proteoglycan of the meniscus were defined as main meniscal markers to illustrate the biochemical composition which is aimed to be heterogeneous in meniscus models.

The meniscus of a 33 years young patient showed also positive Col II staining in the RR zone (figure 4.3 M, N), whereas the meniscus section of a 70 years old patient was positively stained for Col II in the axial two-thirds as expected (figure 4.4 D, H, L) [3]. As the meniscus biopsy of the young patient was obtained during partial meniscectomy as treatment for a meniscal lesion, possible alterations of the meniscus due to the injury can not be excluded. Thus, the stainings of the aged meniscus are seen to be more reliable, as this tissue was donated as a complete meniscus and did not have a previous meniscal lesion history. These findings strengthen the assumption that it is important to build a personalized meniscus model respecting the conditions of each patient such as their medical history or age. This can be achieved by using primary cells directly isolated from the patient.

From literature we know that aging also leads to a decrease in vascularization, resulting in a gradual vascularization of approx. 10 to 25 % of the meniscus in adults [3]. This reduced vascularization by aging was confirmed by the meniscus section of the 70 years old patient only showing vascularization in the RR zone (figure 4.5). Reduced vascularization also correlates with a decreased regenerative potential of degenerated menisci [12]. Hence, implementing vascularization in a meniscus model is considered essential.

However, modeling of a wedge-shaped heterogeneous meniscus and implementation of

vascularization are not the only challenges in meniscus tissue engineering. The mechanical properties, surface characteristics and an appropriate fixation technique have to be further established [22]. The tissue engineered meniscus model described in this thesis is discussed in the next sections.

5.2. Tissue engineering of a wedge-shaped meniscus model

To generate a wedge-shaped meniscus model, the components of tissue engineering had to be optimized. In this chapter, the selection of the cell type and biomaterial are discussed followed by the evaluation of the developed wedge-shaped meniscus model and possible improvement strategies by biomechanical stimulation.

5.2.1. Bone marrow-derived MSCs are suitable cells for a tissue engineered meniscus model

As cellular components of meniscus tissue engineering, MCs and MSCs from human and equine tissues were successfully isolated and expanded in vitro. Being the main cell type of the meniscus [18], MCs seemed to be an appropriate initial cell source to build a meniscus model. Additionally, MCs are able to synthesize collagen and proteoglycans which are considered essential to increase healing [131]. In absence of TGFβ-3, immunocytochemical analysis revealed positive staining for aggrecan and Col I (figure 4.7 A, B). However, MCs were negative for Col II (figure 4.7 C) indicating fibrochondrocyte dedifferentiation. Dedifferentiation is the loss of phenotype and other characteristics of chondrocytes [132]. It is the major cause of cartilage degeneration and a disadvantage of using MCs to generate a meniscus model. Moreover, MCs are an autologous cell source with limited availability [3]. In this thesis, equine biopsies were big enough to isolate a sufficient number of MCs for cell type characterization and meniscus tissue engineering. However, the obtained human meniscus biopsies between 0.15 and 1.5 g were not big enough. Another disadvantage of using MCs are possible alterations of phenotype, morphology or gene expression levels due to potential meniscal injury or degeneration. There are several studies using MCs describing meniscus models with promising results regarding meniscus matrix production, though, most of them used animal-derived MCs isolated, for example, from calf, bovine

or rabbit menisci [18, 75]. For long-term future, a human cell source to build a meniscus model for the patient is needed.
From this perspective it is obvious to shift the focus of this thesis to adult stem cells, namely MSCs which were isolated from bone marrow. Characterization of MSCs was successfully performed according to the ISCT criteria [40]: plastic adherence, positive and negative MSC surface markers, and trilineage differentiation potential (figure 4.8 and A.2). In contrast to isolating SMSCs, the isolation of MSCs from bone marrow is simple, this cell source is easily accessible and isolated MSCs can be expanded in vitro. Using MSCs in meniscus tissue engineering offers several benefits: secretion of trophic factors supporting musculoskeletal therapies and mediating regenerative potential [78], self-renewal capacity, potential of differentiation to meniscus repair cells [133] or enhancement of meniscus matrix formation by co-culture with MCs [82]. Although bone marrow-derived MSCs are isolated from a bony tissue source suggesting an ideal cell type for bone tissue engineering, these cells are also an ideal cell source to generate meniscal tissue as shown by several studies resulting in effective fibrocartilage generation [3, 18, 133].

5.2.2. Cell-laden Col I gel is an appropriate biomaterial for a tissue engineered meniscus model

A variety of scaffolds extending from autologous tissue such as perichondrium or natural scaffold material such as collagen, hydrogels, polymer-hyaluronan to synthetic material such as nanomaterial, PCL or PU are being investigated for meniscus regeneration [96]. To choose the appropriate biomaterial to engineer the meniscus model of this thesis, different scaffolds based on the main meniscal matrix component Col I were studied.
Cells were able to grow on the two commercially available scaffolds Resorba® Col I sponge and Geistlich Col I/II/Elastin sponge as confirmed by MTT and Live/Dead staining. However, cells seeded on the Resorba® Col I sponge grew only on the surface and did not migrate into the material (figure 4.10) which is needed to generate voluminous tissue. Although the Geistlich Col I/II/Elastin sponge showed seeded cells throughout the scaffold, the structure was still very porous after 3D cell culture (figure 4.11). These results indicated that these two commercially available scaffolds were not ideal for meniscus tissue engineering due to limited cell infiltration and their too porous structure not allowing to generate the voluminous matrix of fibrocartilage. The observed porosity might also be due to the lyophilized character of the two sponges.
To achieve a more voluminous matrix, a hydrogel scaffold has high potential providing

versatility, viscoelasticity and easy shaping which is needed to generate meniscal tissue [96]. As Col I is the main collagen of the meniscus [3], we decided to use a Col I gel. Studies using cell-laden Col I gels to generate meniscal tissue showed promising results with respect to meniscus matrix production [96]. Our Col I gels loaded with 50 % MCs and 50 % MSCs showed generation of a homogeneous meniscal matrix by Col I, Col II and aggrecan staining on day 21 as illustrated in figure 4.12 [103]. The direct comparison of the static co-culture constructs to meniscal tissue revealed a good remodeling. As the number of hMCs was limited, eqMCs and eqMSCs were used for these static co-culture constructs.

Hydrogels have well-known weaknesses, namely low mechanical properties and matrix contraction also called shrinkage [96]. Remarkably, the contraction of the 3D co-culture constructs was altered by combining Col I gel with SIS-muc-TERM®. The overall width and length of the constructs was maintained and only the height of the construct was reduced. This one-dimensional shrinkage in height might lead to better collagen fiber alignment and is most likely attributed to the longitudinal tensile strength provided by SIS-muc-TERM®. This tissue-derived scaffold is biodegradable promoting cell proliferation and differentiation [134], which was also confirmed by the co-culture of MCs and MSCs on SIS-muc-TERM® (figure 4.12). Several researchers have already tested SIS alone to induce regeneration of meniscus defects or to provide an implant, however with contradictory results [98, 135, 136, 137]. Reasons for the diverging outcome may be the lack of appropriate shape and mechanical properties due to its unstable nature. In contrast, fibrocartilage is a tissue with a high ECM content [3, 22] which the SIS-muc-TERM® alone cannot offer. However, the combination of SIS-muc-TERM® and the cell-laden Col I gel provided a good matrix combination for meniscus tissue engineering. The discussed results encourage the combination of the meniscus model based on a wedge-shaped hMSC-laden Col I gel with a tissue-derived decellularized scaffold such as SIS-muc-TERM® or BioVaSc-TERM®.

5.2.3. A meniscus model was developed by wedge-shape compression of a hMSC-laden Col I gel in presence of TGFβ-3

In this thesis, a 3D meniscus model was developed by wedge-shape compression of a hMSC-laden Col I gel. In general, compression of Col I gels increases Col I concentration resulting in a high-density Col I gel leading to less contraction and enhanced mechanical properties [100, 138]. To our knowledge, there are no publications on plastic compression

to build a meniscus model. We established a specific technology of plastic compression, namely wedge-shape compression (figure 3.4). We chose a low cell seeding density of $0.5\,\mathrm{x}\,10^6$ hMSCs per mL after wedge-shape compression reflecting the hypocellular native meniscus [3, 18]. The optimized CF of 3.3 resulting in a final Col I concentration of approx. 13.3 mg per mL on day 0 led to a high-density and wedge-shaped hMSC-laden Col I gel with a compact collagen structure on day 21 similar to human meniscus (figure 4.13).
In addition to an increased Col I concentration with compact collagen structure, the wedge-shape compression aimed to produce a matrix with heterogeneous cellular and biochemical composition mimicking meniscal tissue [18]. The static culture in chondrogenic DM supplemented with TGFβ-3 for 21 days showed the best outcome regarding metabolic activity, stable shrinkage, deposition of the meniscal markers Col I, Col II and aggrecan, significantly increased chondrogenic index GAG/DNA and DNA amount as described in section 4.3.3.2. Furthermore, highest ColIA1 in the medium supernatants, lowest water content and highest compressive properties by $E_{lin}(1)$ were found for the meniscus model subjected to TGFβ-3 stimulus (section 4.4.1).
The positive effect of TGFβ on meniscus tissue engineering was already reported several times: enhancement of meniscal properties such as deposition of collagen and GAG, or compressive properties [3, 86]. Furthermore, it was shown that TGFβ might be beneficial for the regeneration of the most axial WW zone, which is naturally containing more Col II [139]. But also negative effects of TGFβ such as contraction or hypertrophic differentiation indicated by Col X expression were reported [3, 140].
For this study, TGFβ-3 was used as biochemical stimulus to induce chondrogenic differentiation of the wedge-shaped hMSC-laden Col I gel. The combination of a wedge-shaped high-density Col I gel, hMSCs derived from the bone marrow and the biochemical stimuli TGFβ-3 was chosen by purpose. Col I is the main collagen of the wedge-shaped meniscus, found throughout the meniscus with a higher content in the abaxial part [3]. That was the reason to select Col I gel as biomaterial and establish wedge-shape compression to increase Col I concentration, and to heterogeneously distribute Col I and hMSCs. The axial one-third of the meniscus contains more Col II providing hyaline cartilage-like properties [18]. In this meniscus model, Col II should be produced by hMSCs stimulated with TGFβ-3, as chondrogenic differentation of hMSC pellets was shown to be dependent on TGFβ-3 supplementation [130]. The TGFβ-3 stimulus led to Col II production in the meniscus model by direct stimulation of loaded hMSCs (figure 4.15 H). A pattern-like Col II production was observed with higher Col II deposition in the axial part and abaxial border areas of the meniscus model which might be due to limited medium diffusion in the middle part of the models or heterogeneously distributed hMSCs. A smaller size of the meniscus model or a dynamic culture providing constant medium perfusion may improve

diffusion and TGFβ-3 mediated chondrogenic differentiation. Additionally, the TGFβ-3 stimulus significantly increased the chondrogenic index GAG/DNA and DNA amount, and led to an enhanced deposition of aggrecan and Col I throughout the wedge-shaped meniscus model (figure 4.17) indicating meniscus matrix. However, no significant differences between the divided zones RR, RW and WW of the meniscus model were detectable in the chondrogenic index GAG/DNA and DNA amount (figure 4.16). Matrix remodeling of the wedge-shaped hMSC-laden Col I gel was analyzed by gel zymography of medium supernatants to detect MMPs, as matrix remodeling is regulated by MMPs [118]. Matrix remodeling was confirmed by a 3 fold increase of MMP fold change on day 21 subjected to TGFβ-3 stimulus (figure 4.25).

To further increase remodeling of the meniscus matrix, MMC (figure 1.6) was introduced to increase meniscal matrix synthesis by directly adding 37.5 mg/mL Ficoll PM 70 kDa and 25 mg/mL Ficoll PM 400 kDa as macromolecules to the medium. An increase in the matrix synthesis was expected under MMC conditions [92]. However, no difference was observed by introducing MMC: the metabolic activity by MTT staining, remaining glucose amount and lactate production, immunohistochemical staining for the meniscal markers Col I, Col II and aggrecan, chondrogenic index GAG/DNA and DNA amount showed no difference as described in section 4.3.3.3. The immunohistochemical staining for Col I and Col II of the MMC crowded meniscus model in figure 4.19 A seemed to show a more specific DAB signal around the embedded cells suggesting further analysis. Images taken by SEM did not show a difference in the collagen structure of the MMC crowded meniscus model (figure 4.20 A). Moreover, there was no difference in matrix remodeling (figure 4.21 B, C). These results indicated that MMC did not increase matrix synthesis of the meniscus model. In contrast to our results, a study by Dewavrin et al. (2014) showed enhanced collagen synthesis and proliferation of MSCs after seeding on MMC crowded Col I gels [93]. However, there were major differences compared to our study. Dewavrin et al. (2014) performed crowding of non-compressed Col I gels with a Col I concentration of 0.8 mg/mL by directly adding MMC components to the solutions prior to solidification of the gel [93]. After solidification, MSCs were seeded on top of the MMC crowded Col I gels [93]. In this thesis, MSCs were suspended homogeneously in the Col I gel and after wedge-shape compression, the MMC components were added to the culture medium of the meniscus model. Moreover, hMSC-laden Col I gels had a final concentration of approx. 13.3 mg/mL after wedge-shape compression, which was a much higher Col I concentration as used by Dewavrin et al. (2014) [93]. Wedge-shape compression might already lead to a self-crowding system by increasing Col I concentration in the meniscus model. Therefore, the additional introduction of MMC components might not induce the known effect of an enhanced matrix synthesis [92].

Based on these results, adding of further biochemical stimuli in addition to TGFβ-3 is questionable. TGFβ-3 is a well-established chondrogenesis inducer for MSCs resulting in proteoglycan and Col II production [141]. Further biochemical approaches are not part of this thesis, because the generated meniscus model subjected to TGFβ-3 stimulus represented an appropriate, satisfactory and reproducible model mimicking meniscal tissue. Reproducibility is an essential requirement for a tissue engineered model to be translated to clinic [3, 32]. For the biomechanical compressive testing, the meniscus models (section 4.3.3.2, n=3) were all generated by the same procedure (section 4.4.1, n=4) and showed similar values regarding shrinkage, chondrogenic index GAG/DNA and DNA. The generation of our meniscus model was reproducible and the procedure defined as follows: wedge-shape compression of hMSC-laden Col I gel with subsequent 21 days of static culture in chondrogenic DM with TGFβ-3.

5.2.4. Two biomechanical stimulation systems were designed for the meniscus model to provide a physiologic loading environment

The compression testing of the 21 days statically cultured meniscus model showed a significantly increased compressive modulus of the first strain $E_{lin}(1)$ compared with the controls (figure 4.22). This result correlated with a significantly reduced water content, shrinkage by size and reduction in wet weight in comparison with the controls (figure 4.23). The compressive modulus describes the resistance of a material or model against elastic deformation. According to Chia & Hull (2008), compression testing was performed with a 12 % strain level, an estimate of a physiologic strain experienced in the axial and radial directions [122]. However, the recorded $E_{lin}(1)$ of the meniscus model was low in contrast to native meniscus which reached values of more than 300 kPa measured for thawed meniscal tissue samples by Chia & Hull (2008) [122]. Therefore, the performed compression testing originally designed for meniscus samples [122] was maybe not appropriate to measure the mechanical properties of the tissue engineered meniscus model at such an early stage. Further matrix remodeling by continued culture might be needed to achieve higher mechanical properties.

A more promising approach to enhance this meniscus model and its mechanical properties is the modification of the culture system, as the meniscus model was cultured under static conditions for 21 days. In contrast, native menisci located in the knee joint are subjected to mechanical stress during daily activity [3]. Mechanical factors such as compression,

tension, shear and hydrostatic pressure play crucial roles in the development, maintenance, degeneration and repair of the meniscus [110]. Consequent loading with increasing weights and knee motion during life are supposed as reasons for the decrease of vascularization and the increase of mechanical properties [11, 15]. Thus, dynamic culture providing mechanical stresses by biomechanical stimulation would mimic the physiologic environment in the knee joint and even the development of a prenatal meniscus to a mature structure [104]. The research of biomechanical stimulation in meniscus tissue engineering is still in its infancy [104, 142]. In this thesis, two systems of biomechanical stimulation were designed for the meniscus model. One provides a compression stimulus, the other hydrostatic pressure. The application and effects of these two systems are discussed in the following.

5.2.4.1. Compression

The system based on direct compression was successfully designed for the wedge-shaped meniscus model as described in part 4.4.2.1. In the knee joint, the menisci are subjected to compressive load facilitating the exchange of nutrients and waste products [3]. It has been shown that biomechanical stimulation by direct compression enhances biomechanical and biochemical properties of tissue engineered meniscus models and cartilage [104, 105]. Our system is composed of a 3D printable prototype with a wedge-shaped bottom to provide a planar surface after placing in the wedge-shaped meniscus model. This prototype is usable for 3D cell culture and enables medium perfusion through drilled holes. The observed shrinkage of the meniscus models by approx. 40 % became stable from day 14 and can be compensated by a low gelling agarose during stimulation. The gelled agarose is completely removable after stimulation. To ensure a reproducible compression stimulus, the compensation of shrinkage with agarose have to be optimized for the meniscus model. Day 14 when a stable shrinkage of the meniscus model was reached seemed to be a good starting point for reproducible compression stimulation by shrinkage compensation with agarose.

There are two ways to perform compression stimulation with this system: passive direct compression by weight application or dynamic direct compression controlled by an engine. Stimulation by passive direct compression is simple to design. However, parameters such as the duration of loading and the extent of compressive strain have to be defined and adapted to the used cell type and scaffold [105]. Elder et al. (2008) studied the effect of passive direct compression on self-assembled articular cartilage constructs [143]. Passive axial compression was performed from day 10 to 14 by placing a steel cylinder, corresponding to 0.5 kPa of stress, on top of each articular cartilage construct [143]. The application of

passive compressive loading increased the tensile properties and even total collagen content of the self-assembled articular cartilage constructs [143]. Passive direct compression by a low compressive stress combined with a longer duration of loading demonstrates a potential approach to be applied for the meniscus model. However, disadvantages of passive direct compression are diffusion limitations [105]. A dynamic direct compression by an engine using a puncher for dynamic compressive loading can reduce such diffusion limitations facilitating nutrient-waste exchange [105]. Puetzer et al. (2012) applied dynamic direct compression on alginate-based meniscus constructs with a custom-made bioreactor containing a loading platen for stimulation [106]. Dynamic direct compression of 15 % compressive strain at 1 Hz was performed three times a weeks with two loading cycles per day, each lasting one hour with one hour rest in between, for 1, 2 and 4 weeks followed by 4 weeks static culture [106]. The loaded meniscus constructs showed matrix formation with increased collagen accumulation and enhanced mechanical properties [106]. In general, a frequency of 1 Hz and a compressive strain of approx. 10 % are regarded as physiologic for direct dynamic compression [104]. For biomechanical stimulation by compression of our wedge-shaped meniscus model a static preculture of at least 14 days to achieve stable shrinkage is recommended. The precise parameters of compression should be determined according to literature and specifically optimized for the wedge-shaped meniscus model. Starting with low parameters of compressive strain and low frequencies is recommended to slowly enhance the mechanical properties of the meniscus model avoiding destructive effects by too strong stimulation. After reaching higher compressive moduli as determined by the statically cultured meniscus model on day 21, an ascending regimen of compression stimulation should be applied. This proceeding will mimic increased loading by increased weight and knee motion during aging.

5.2.4.2. Hydrostatic pressure

The second system provided hydrostatic pressure, as the meniscus is hydrostatically pressurized in its physiologic environment of the knee joint by compressive loading due to its high water content and low permeability [110]. The advantage of hydrostatic pressure is the compression of all surfaces as illustrated in figure 1.7 D [105]. Most hydrostatic pressure systems use a fluid-filled chamber with a piston for inducing pressure which is subsequently translated to the construct [105].
Our system was established to provide passive hydrostatic pressure by a bag pump as explained in part 4.4.2.2. The required 6 deep well plate can be placed in an incubator to perform biomechanical stimulation during 3D cell culture in a humidified atmosphere

at 37 °C and 5 % CO_2. A preliminary test using simple cell-laden Col I gel disks showed that hydrostatic pressure up to 150 mmHg for 30 min did not have a negative influence, as there was no decrease of metabolic activity, MMPs and matrix synthesis compared to no stimulation. With these results, the hydrostatic pressure system was fully established to be applied for the wedge-shaped meniscus model.
So far, there are still much more studies using hydrostatic pressure to stimulate articular cartilage constructs than meniscus constructs. For an articular cartilage construct composed of a Col I scaffold seeded with chondrocytes, a hydrostatic pressure stimulation with 0.5 MPa at 0.5 Hz during the first 6 days of culture led to an increased GAG production [144]. The positive effect of hydrostatic pressure stimulation in context of meniscus tissue engineering was demonstrated by enhanced chondrogenic differentiation, and improved biochemical and compressive properties [86, 111]. For the hydrostatic pressure stimulation of our wedge-shaped meniscus model a static preculture of at least 14 days to achieve stable shrinkage and a stiffer matrix is recommended as mentioned for the compression stimulation. Then, parameters such as the magnitude of hydrostatic pressure, duration and frequency of stimulation have to be optimized and adapted for the meniscus model. A regimen starting with low pressures followed by a steady increase, as recommended for the compression stimulation, should be considered.

5.2.4.3. Long-term future of biomechanical stimulation

A combination of the two established systems is imaginable, as also in the physiologic environment of the knee joint different forces act on the menisci [3]. Compression stimulation might be performed during medium change, while hydrostatic pressure could be applied as passive stimulus at specific time points during long-term culture. However, the two systems should at first be individually optimized for the wedge-shaped meniscus model in order to detect and solve limitations of these systems prior to combining them.
MMP activity can be analyzed to get an impression of the effect of mechanical stimulation. MMP activity has been shown to be essential for the transfer of mechanical stimuli and resulting behavior of MSCs [121]. Kasper et al. (2007) found out that extracellular MMP-2, -3 and -13 were upregulated in MSCs responding to mechanical loading [121]. With the established method of gel zymography using gelatin as substrate for MMP-2 and -9 (figure 4.21 A) [120] the influence of mechanical stimulation on the meniscus model can be easily studied. However, further techniques should be considered to detect more types of MMPs. Instead of gelatin, gel zymography with collagen as substrate could be used to assess the collagenases MMP-1, -8 and -13 [145]. Further types of MMPs could be

specifically detected by immunohistochemical staining or biochemical quantification by ELISA if the required antibodies are available. Moreover, the balance between MMPs and their inhibitors TIMPs plays a crucial role in transferring mechanical signals [121]. The ability of TIMPs to inhibit MMPs is studied by reverse zymography adding TIMPs to the samples [120]. The mentioned techniques would help to further evaluate the effect of the mechanical stimulation.

5.3. Vascularization strategies for the wedge-shaped meniscus model

A particular characteristic of meniscal tissue is its decreasing vascularization from the abaxial to the axial part, termed as gradual vascularization (figure 1.1 D) [3]. The healing capacity of meniscal lesions is known to depend on the vascularization level, because vascularization provides regenerative potential leading to a better repair [12]. Therefore, a tissue engineered meniscus implant should contain a vascularized part to mimic physiologic meniscal tissue and to provide regenerative potential.
In general, vascularization is a big challenge in tissue engineering [31]. In this thesis, three vascularization approaches were studied with the long-term aim to be applied for meniscus tissue engineering. In the following, these approaches are discussed regarding their general potential for tissue engineering and the planned or performed application on the wedge-shaped meniscus model.

5.3.1. CPX promotes the angiogenic response of ECs and MSCs by an artificial hypoxia

PHIs are promising compounds to promote angiogenesis by stabilizing HIF-1α [50]. Increased HIF-1α presence induces expression of pro-angiogenic genes such as VEGF [36, 50]. In this study, the FDA-approved CPX was chosen as PHI. Compared with other PHIs, CPX has a higher lipophilicity, allowing better membrane penetration, and a higher affinity for iron, allowing lower concentrations for HIF-1α stabilization [50]. Originally, CPX was developed as an antifungal agent for the treatment for mycoses of the skin and nails [146, 147]. The pro-angiogenic effect of CPX through HIF-1α stabilization and VEGF expression was discovered as coincidence when a mouse skin wound model was treated

with commercially available CPX containing dermal cream [50].
In this thesis, we investigated the pharmacological induction of hypoxia via CPX. This was studied in sprouting assays of hd-mvEC spheroids directly and indirectly via activation of hMSCs. HUVEC spheroids are frequently used for angiogenesis sprouting assays [148]. HUVECs grow well in defined culture media and can be sourced easily [149]. Though, it was shown in sprouting assays that HUVECs are more sensitive to pro-angiogenic stimuli than ECs derived from adult blood vessels [150]. This might lead to an overestimation of the potential of angiogenesis strategies tested with HUVECs. We therefore chose to work with freshly isolated mvECs, as ECs from different tissues have been shown to respond differently [151]. Earlier work has shown that HUVEC monocultures do not appear to respond substantially to PHI [152]. Moreover, mvECs are naturally a present cell type in the meniscal tissue [95, 153].
We showed that in contrast to HUVECs [152], hd-mvECs react with a direct and strong sprouting response in 3D multi-cellular spheroids to CPX stimulation in the absence of VEGF or other pro-angiogenic agents in the basal medium. It became evident that 10 μM CPX in the basal medium showed an even stronger effect than 25 ng/mL VEGF (figure 4.36). This means that CPX stimulation can replace external VEGF supplementation because sufficient levels of VEGF and other pro-angiogenic factors are induced by the pharmacological hypoxia.
It was hitherto assumed that PHIs such as CPX work best via a mesenchymal partner to indirectly stimulate the pro-angiogenic response of ECs as bankshot approach; Lim et al. (2013) dissected the sprouting response of HUVECs to CPX in a microfluidic system in the presence of fibroblasts [154]. Sprouts only occurred in the presence of fibroblasts, which were the main source of VEGF in this system [154]. Earlier it had been shown, that in mixed cultures of fibroblasts and HUVECs, fibroblasts expressed HIF-1α much more strongly in the presence of a PHI [152]. Therefore, it was assumed that in a mixed cell population, for example in a wound, mesenchymal cells would be the true targets of PHIs to effect angiogenesis in ECs [50, 53]. The results obtained open the possibility that ECs may be direct targets for PHIs, as well, and that this may depend on the origin of the EC and their ability to get stimulated via autocrine action or inducing neighbors via paracrine mechanism.
In accordance with Lim et al. (2013) [154], exposure of hMSCs to CPX led also to an upregulation of pro-angiogenic factors in this study. Gene expression analysis revealed a drop of HIF-1α mRNA, while VEGF mRNA increased after 24 hours (figure 4.34 A). As HIF-1α transcription normally has a short half-life, stabilization with CPX might lead to a negative feedback and thus to downregulation of HIF-1α mRNA expression. On the protein level, VEGF production was increased by 1.5 fold (figure 4.34 B). In addition to

VEGF, other pro-angiogenic factors were found increased in CPX-treated MSC culture medium (MSC-CM CPX) (figure 4.35). HIF-1α directly facilitates transcription of VEGF, angiopoietin-2 and stem cell factor (SCF) genes [155]. Accordingly, increased levels of angiogenic factors angiogenin, chemokine IL-8, endothelin-1, angiopoietin-2 being important for neovascularization [156] and FGF being important for endothelial capillary initiation [156] were found in CPX-treated MSC culture medium. However, the CPX-treated MSC culture medium showed only a slight pro-angiogenic effect on sprouting. This might be attributed to dilution effects related to the application of conditioned media five-times diluted in sprouting assays. Thus, a much lower concentration of pro-angiogenic factors in CPX-treated MSC culture medium might cause the slight sprouting increase.
In general, VEGF is the master regulator of physiologic but also pathological angiogenesis and the most common target for therapeutic angiogenesis approaches [157]. However, as a single agent in supraphysiologic doses, VEGF leads to the formation of tortuous and leaky microvessels and tumor formation [158]. Local delivery and combination with other pro-angiogenic factors would be desirable and therefore using a PHI to locally induce a portfolio of angiogenic factors would be safer and more efficacious.
Taken together, the direct stimulation of ECs with CPX replaced external VEGF supplementation by HIF-1α stabilization through a pharmacological hypoxia resulting in sufficient levels of VEGF and other pro-angiogenic factors. Using ECs as direct target for a PHI such as CPX is an innovative vascularization approach independent of auxiliary cells by stimulating angiogenesis with growth factors. This strategy may have high potential for tissue engineering of vascularized models. For the implementation of this vascularization approach into the meniscus model, supplementation of the culture medium with CPX or a localized injection in the wedge-shaped hMSC-laden Col I gel might be considered. Beyond angiogenesis stimulation, hypoxia has been also shown to enhance TGFβ induced chondrogenesis of MSCs and to prevent calcification [90], offering further benefits for the wedge-shaped meniscus model which is generated from a hMSC-laden Col I gel.

5.3.2. Vascularized meniscus model by transfer of a cell sheet

A further strategy to enhance angiogenesis are co-cultures of different cell types with ECs [34]. Studies have found out that MSCs can promote the maturation of newly formed luminal structures and the formation of microvascular networks [41, 47]. Another study showed that interactions between MSCs and EPCs may induce differentiation towards a pericyte-like phenotype [45]. Thus, co-cultures of ECs and MSCs are of high interest building a vascularized model.

As MSCs are the main cell type of the meniscus model based on the hMSC-laden Col I gel and mvECs are a cell type present in the meniscus [95, 153], a co-culture of MSCs and mvECs was envisaged for this study. As vascularization strategy, cell sheet engineering was chosen to build a cell sheet composed of hMSCs and hd-mvECs. This cell sheet was successfully engineered by temperature triggered cell sheet fabrication. Such temperature triggered cell sheet fabrication is simply performed by temperature reduction leading to hydration of the polymer and detaching of an intact cell sheet [125]. This intact cell sheet is harvested with its secreted ECM, cell-cell junctions, all cell surface proteins and cellular polarization [125]. Temperature triggered cell sheet fabrication using thermoresponsive PGE coated plates was previously established for cell sheets of fibroblasts by Stoebener et al. (2017) [125] and optimized in this thesis to fabricate cell sheets composed of hMSCs and hd-mvECs. For cell seeding, hMSCs were seeded first and after 4 hours attachment time, hd-mvECs were seeded on top. Hd-mvECs and hMSCs were easily distinguishable by immunofluorescent staining of the cell-type specific markers CD31 for hd-mvECs and CD44 for hMSCs as illustrated in figure 4.38. According to the cell seeding order the endothelial part by hd-mvECs was visible as clusters above the monolayer of hMSCs. To our knowledge of literature, there are no publications on engineering a cell sheet composed of MSCs and primary ECs. There is only research generating cell sheets composed of MSCs and HUVECs [117, 159]. Therefore, engineering this cell sheet composed of hMSCs and hd-mvECs was an outstanding achievement.

This cell sheet was used to implement a gradual vascularization. For this, the cell sheet was transferred onto the RR zone of the wedge-shaped hMSC-laden Col I gel aimed to generate a vascularized part as in the mature meniscus (figure 4.40). The transfer of the complete sheet from the plate onto the gel was a challenge and successfully optimized using a membrane facilitating attachment and detachment of the sheet as described in methods part 3.7.1. Up to know, there is only very limited research on angiogenic approaches in the context of meniscus tissue engineering ongoing. Most studies focus on growth factors to stimulate angiogenesis [112]. Based on our knowledge, this was the first gradual vascularization approach in meniscus tissue engineering using a cell sheet composed of hMSCs and hd-mvECs.
The meniscus model composed of a wedge-shaped hMSC-laden Col I gel with transferred cell sheet on the RR zone (gel+sheet) is discussed in comparison to the two control models, hMSC-laden Col I gel without an endothelial part (gel) and hMSC-laden Col I gel with injected cell suspension of hMSCs and hd-mvECs (gel+cells) (section 4.6). High metabolic activity and high viability was confirmed on day 21 for all three models. Metabolic activity over time was confirmed by glucose consumption and lactate production. Matrix remodel-

ing was detected by an increase of total MMPs over time. As previously described, all models reached a stable size after shrinkage of approx. 40 % by day 14. These comparable results indicated that addition of hMSCs and hd-mvECs by sheet or injection did not lead to differences between gel, gel+sheet and gel+cells regarding metabolic activity, matrix remodeling and shrinkage. Therefore, the focus of our further evaluations was shifted to immunohistological analysis of vascularization markers and meniscal marker.

The endothelial parts of gel+sheet and gel+cells were nicely stained by immunohistochemical staining as shown in figure 4.46. However, the injected cells of the control model gel+cells (figure 4.46 B, E) showed a clumped structure which might indicate a modified phenotype of the injected cells. Furthermore, no newly generated ECM was detectable. This might correlate with the results of MMP detection, as no increase in comparison to gel and gel+sheet was observed (figure 4.43). In contrast, the model gel+sheet (figure 4.46 A, D) showed a firm attachment of the sheet to the RR zone of the wedge-shaped hMSC-laden Col I gel. The nicely layered endothelial structure on the RR zone was comparable to CD31 and vWF positive areas in the RR zone of native human meniscal tissue (figure 4.46 C, F). However, no in-growth of hd-mvECs from the sheet into the vascularized meniscus model was observed. Nevertheless, the induction of in-growth of hd-mvECs is a long-term aim for this vascularized meniscus model. This might be induced by local injection of growth factors such as VEGF, CTGF or HGF [112] into the hMSC-laden Col I gel directly after wedge-shape compression, or the pharmacological induction of hypoxia via CPX [50] might be applied as indirect approach: the injection of CPX into the wedge-shaped hMSC-laden Col I gel instead of using growth factors. As growth factors such as VEGF have the risk of inducing tumor formation [158], an indirect approach by CPX leading to the secretion of different pro-angiogenic factors together with VEGF may be safer. The immobilization of growth factors or CPX by incorporation into the biomaterial demonstrates another possibility to achieve a safe and even more efficacious delivery of pro-angiogenic factors [56].

Regarding the chondrogenic differentiation, the chondrogenic index GAG/DNA (figure 4.48) showed comparable results to the established meniscus model of section 4.3.3.2. Unfortunately, the meniscal markers analyzed by immunohistochemical staining in figure 4.47 did not confirm the convincing results of the established meniscus model (figure 4.17 A). Especially the staining for Col II only showed single Col II positive cells in all three models. After a deep literature research, it was concluded that the low chondrogenic differentiation shown for the models gel, gel+sheet and gel+cells might be caused by the medium change of original 100 % chondrogenic DM supplemented with 10 ng/mL TGFβ-3 to 50 % chondrogenic DM with 50 % VascuLife® medium supplemented with 10 ng/mL TGFβ-3. The original serum-free medium contained only pro-chondrogenic

factors together with TGFβ-3, the most important growth factor to induce chondrogenic differentiation [160]. Col II production by TGFβ-3 might be inhibited by factors contained in the VascuLife® medium.

VascuLife® medium is a low serum medium with 2 % FBS optimized for the culture of human ECs. According to the product description, VascuLife® medium contains the following growth factors: FGF, IGF-1, EGF and VEGF. FGF is a very controversially discussed factor in the context of chondrogenesis. It is known to potentially modulate proliferation of MSCs and to maintain MSCs in an immature state allowing expansion as chondro-osteo progenitor cells [161]. Therefore, FGF is one of the main components added to MSC expansion medium [160], also contained in our MSC medium. In the signaling cascade regulating cell proliferation of MSCs during expansion, FGF leads to the inhibition of TGFβ [160]. As 50 % VascuLife® medium was added to 50 % chondrogenic DM and 10 ng/mL TGFβ-3, the contained FGF in the VascuLife® medium might have inhibited the supplemented TGFβ-3. That could be one reason for the less pronounced chondrogenic differentation in the models gel, gel+sheet and gel+cells. Not only, FGF has anti-chondrogenic potential, also EGF and VEGF have been shown to negatively influence chondrogenesis [162, 163]. One study revealed the negative regulation of chondrogenesis by EGF [163]. Marsano et al. (2016) showed that blocking VEGF signaling led to spontaneous in vivo chondrogenesis of BM-MSCs [162]. Furthermore, it was described that high VEGF levels may counteract the influence of TGFβ [164]. Only IGF-1 is known to positively stimulate chondrogenic differentiation of MSCs [165]. Even, a synergistic effect of IGF-1 with TGFβ has been shown [166].

Taken together, three out of four growth factors contained in the VascuLife® medium had potential to adversely affect the chondrogenic differentiation. Therefore, the addition of VascuLife® medium containing potential anti-chondrogenic factors might be the reason for less chondrogenic differentiation. In conclusion, the medium used for our vascularized meniscus model has to be improved. A concentration optimization of such anti-chondrogenic but pro-angiogenic factors should be envisaged with the aim not to counteract the effect of TGFβ. Pro-chondrogenic factors with pro-angiogenic potential such as IGF-1 [165, 166] should be implemented. In the context of medium optimization for this complex co-culture, Col X as hypertrophic cartilage marker should be monitored, as vascularization, VEGF and serum, as 2 % FBS is contained in the VascuLife® medium, can accelerate the development of hypertrophic cartilage [164, 167]. It is known from the literature that vascular invasion into cartilage may lead to replacement of hypertrophic cartilage by bony tissue [164]. For meniscus tissue engineering a chondrogenic differentiation stage without the development of hypertrophic cartilage is of high importance to achieve proper meniscal tissue with a fibrocartilaginous abaxial zone and a hyaline cartilage-like

axial zone [3, 15].
Nevertheless, the vascularized meniscus model composed of gel+sheet is a promising model. After medium optimization, the above mentioned methods to induce in-growth of mvECs in the gel may lead to a meniscus model with proper gradual vascularization in the three distinct zones. However, one big challenge remains. There is still a lack of basic understanding of the meniscus and the role of its gradual vascularization [11]. A better understanding of this characteristic would facilitate the biomimetic construction of a partly vascularized meniscus implant.

5.3.3. BioVaSc-TERM®

In this thesis, a natural scaffold reusing biological structures, namely the BioVaSc-TERM®, was studied in part 4.5.3 as third vascularization strategy. Walles et al. (2005) developed this SIS-derived scaffold providing a preserved vascular tree after decellularization of a porcine small bowl segment [65]. After decellularization, the BioVaSc-TERM® scaffold is composed of an ECM with high content of elastin (14 %) and collagen fibers (16 %) [168]. The DNA amount of $26.4 \pm 1.4\,\mu$g/mg in native intestinal tissue is reduced to $0.5 \pm 0.01\,\mu$g/mg DNA in the decellularized scaffold [168]. The preservation of vascular structures is the key feature of the BioVaSc-TERM®. The vascular tree is reseedable with EC such as hd-mvECs as illustrated in figure 4.39 and previous studies [65, 66, 168]. Metabolic activity and viability of the seeded hd-mvECs located in the vascular network were confirmed (figure 4.39 A, B). Moreover, immunohistochemical staining for vWF revealed the successful re-endothelialization of the vascular structures (figure 4.39 C).
As vascularization remains a challenge in tissue engineering [31], this scaffold provides promising potential to build vascularized tissue models [65, 66]. Vascularized skin was already generated using BioVaSc-TERM® as biomaterial [67]. Furthermore, it has been shown that the re-endothelialized BioVaSc-TERM® can facilitate vascular anastomosis [168]. However, such animal tissue-derived scaffolds have limitations regarding standardization and reproducibility which synthetic scaffolds can easily overcome by a standardized manufacturing procedure [34]. Hence, researchers try to bioprint microchannels in hydrogels or to print vascular trees directly into a construct [71, 72]. However, the complexity to print small porous structures in the dimension of capillaries with an average width of $7\,\mu$m and to design the relevant 3D geometries [71, 72] hinder the synthesis of native-like structures as offered by natural tissue-derived scaffolds [34]. To overcome the mentioned limitations of tissue-derived scaffolds, the production of the BioVaSc-TERM® has been standardized at TERM as described in method part 3.4.3.2. Its production is in line with

current good manufacturing practice (GMP) guidelines and a manufacturing authorization for the scaffold as tracheal implant is currently reviewed by local authorities for the use in a clinical phase I study, emphasizing the high degree of standardization. However, ethical aspects concerning animal sources have to be kept in mind [34].
For meniscus tissue engineering, the BioVaSc-TERM® scaffold has already been used as a wrapping structure of a meniscus collagen scaffold [68]. Such a wrapping technique is planned for the developed meniscus model of this thesis as displayed in figure 4.49. Wrapping of the wedge-shaped meniscus model with the re-endothelialized BioVaSc-TERM® will provide several benefits. After wrapping the re-endothelialized BioVaSc-TERM® can be connected to the bioreactor system for dynamic culture providing pulsatile pressure (figure 3.6). Then, the vascular network of BioVaSc-TERM® will supply the model with nutrients. Furthermore, BioVaSc-TERM® may reduce contraction and facilitate mechanical stabilization of the meniscus model as discussed in section 5.2.2 for the combination of Col I gel with SIS-muc-TERM®. Combined with the vascularized meniscus model composed of the wedge-shaped hMSC-laden Col I gel with the transferred cell sheet as discussed in the prior part 5.3.2, a direct connection of the cell sheet to the reseeded BioVaSc-TERM® may improve the zonal composition with a gradual vascularization.
Last but not least, wrapping of the meniscus model with the re-endothelialized BioVaSc-TERM® is a crucial criteria for the translation from bench to bedside, as a meniscus model has to be fixed in the knee joint during implantation. The suggested implantation procedure by wrapping and fixation using the BioVaSc-TERM® scaffold for future meniscus surgery is discussed in the next section 5.4.

5.4. Suggested implantation procedure by wrapping and fixation

As illustrated in figure 4.49, the meniscus model is planned to be placed into the lumen of the BioVaSc-TERM® providing a re-endothelialized vascular network. Besides providing nutrition via the vascular network, the BioVaSc-TERM® might be used for fixation of the implant in the knee joint. There are different meniscal fixation techniques: inside-out, outside-in (OIR) and all-inside (AIR) methods [25]. For the current two implants on the market, different fixation techniques are recommended. For implantation of the CMI®, either an inside-out or an AIR technique is used [15]. AIR is a less time-consuming technique and it appears that fewer sutures are needed for implantation compared to

the inside-out technique [15]. The suturing technique for the PU-based Actifit® implant depends on the location of the defect. AIR is commonly used for defects of the posterior part, whereas for defects in the middle and anterior portion OIR or inside-out techniques are recommended [15]. However, the inside-out technique has a potential risk of causing friction with the articular surfaces due to the rigid cannulas [169].

After consultation with the experienced sport orthopedic surgeon Dr. Kai Fehkse, we decided to analyze OIR and AIR as suture techniques for the fixation of the meniscus implant. To suggest the best suturing technique to fix our meniscus implant in the future, these two techniques were tested in empty BioVaSc-TERM® scaffolds and compared under tensile stress (figure 4.50 and 4.51). There was no difference between OIR and Stryker AIR in the maximal force of failure, reaching approx. 10 N. Many studies often show maximal forces higher than 10 N [170, 171, 172]. However, comparison with such studies is difficult, as most of them used much lower velocities, for example 5 mm per minute [170, 171], not reflecting the real situation. We used a high velocity of 10 mm per second mimicking real loading conditions upon a meniscal suture defect.

Our tensile testing showed that the Stryker AIR had a significantly higher disposition to deformation. The high deformation propensity correlated with a bigger work loading. In contrast, the OIR implied a significantly higher total stiffness as compared to the Stryker AIR. For a good anchorage of the meniscus implant, a suture technique with a high deformation ability and work loading will lead to a stable fixation [15]. Therefore, Stryker AIR might be chosen as preferred suturing technique.

The AIR technique is particularly useful for sutures located at the PH of the meniscus [169]. However, access to the anterior part by AIR technique is limited [15]. The OIR suture is best suitable for the anterior and middle part of the meniscus by suturing through the superior and inferior surfaces of the meniscus [173]. Thus, the decision of the appropriate fixation technique should be based upon the location of the defect and the remaining meniscal tissue which may be used for suturing. Moreover, a combination of both suture techniques OIR and Stryker AIR seemed to be beneficial to achieve a proper and secure fixation of the meniscus implant in the knee joint. The interpretation of these results was discussed with meniscus experts and sport orthopedic surgeons.

A limitation of our tensile testing is the use of the empty BioVaSc-TERM® scaffold. However, the pull out study of meniscal sutures in the empty scaffold is still an important preliminary experiment. After successful development of the vascularized meniscus implant which will be composed of the vascularized meniscus model and the re-endothelialized BioVaSc-TERM®, the tensile testing of meniscal sutures in the vascularized meniscus implant has to be repeated to confirm the obtained results. By using the vascularized meniscus implant, even higher mechanical properties are expected.

5.5. Outlook and future perspectives

Taken together, all important components to build a vascularized meniscus implant have been successfully established in this thesis. The results open the opportunity to use the developed meniscus model for animal studies. For long-term future, the meniscus implant should be partly vascularized and biomechanically stable enough to be implanted using the suggested fixation techniques Stryker AIR and OIR. After implantation into the knee joint, the meniscus implant will be located in its physiologic environment. Steck et al. (2009) showed that in vivo signaling molecules and biomechanical stimuli provided an appropriate environment for MSC differentiation to Col X negative chondrocytes; hypertrophy, an undesirable side effect of in vitro chondrogenic differentiation of MSCs, was not observed in vivo [174]. A similar effect may be expected for the meniscus model after implantation. Thus, biochemical and biomechanical stimuli in the physiologic environment of the knee joint may enhance the fibrocartilage differentiation of MSCs and the meniscal properties of the implant.

When it comes to developing and translating new implants into clinical practice, one crucial point is the choice of appropriate animal models [175]. Small animal studies followed by large animal studies will prove the meniscus implant's stability and functionality. As small animal, the New Zealand White rabbit is a common model for meniscus repair [175]. As the University of Regensburg is experienced with New Zealand White rabbits as meniscus repair model [80], we have started a cooperation with them to plan small animal studies using the established meniscus model.

As large animal model for meniscus repair, sheep menisci closely resemble the dimensions of human menisci [176]. Besides sheep, the gait of horse is considered to best match the human, although horses lack the full knee extensions compared to humans [128]. Horses are a well-accepted, well-established and clinically relevant animal model particularly for studying joint disorders [128, 177]. As demonstrated in this thesis, the gross anatomic and histologic meniscus structure of horses is similar to humans, therefore, suggesting the horse as a potential animal model [103]. Moreover, horses do not only serve as animal model, but at the same time they are also patients suffering from naturally occurring meniscal injuries [178, 179]. In cooperation with the University of Veterinary Medicine in Vienna, we will be able to isolate all needed cells for meniscus tissue engineering and to directly transfer the human model of this thesis to sheep or horses.

After successful conclusion of animal studies, such a vascularized meniscus implant can be prepared for clinical translation from bench to bedside. In discussion with sport orthopedic surgeons, the most benefiting patient group for such a meniscus repair would be young

athletes with an age between 20 to 30 years. These patients should not smoke, suffer from adiposity or have ligament instability. Meeting those conditions, patients should have sufficient vascularization which may enable vessel in-growth into such an implant. Moreover, further cartilage defects may be prevented after implantation.
In conclusion, such a tissue engineered vascularized meniscus implant will have promising potential for a personalized meniscus repair in veterinary and human medicine.

Bibliography

[1] J. Bland-Sutton, "Ligaments: their nature and morphology," *JK Lewis*, vol. 2nd ed. London, 1897.

[2] D. J. Dandy and R. W. Jackson, "The diagnosis of problems after meniscectomy," *J Bone Joint Surg Br*, vol. 57, no. 3, pp. 349–52, 1975.

[3] E. A. Makris, P. Hadidi, and K. A. Athanasiou, "The knee meniscus: Structure, function, pathophysiology, current repair techniques, and prospects for regeneration," *Biomaterials*, vol. 32, no. 30, pp. 7411 – 7431, 2011.

[4] R. Koch-Institut, "Gesundheit in Deutschland. Gesundheitsberichterstattung des Bundes. Gemeinsam getragen von Robert Koch-Institut und Destatis," *Robert Koch-Institut, Berlin*, 2015.

[5] H. J. Jeong, S. H. Lee, and C. S. Ko, "Meniscectomy," *Knee Surg Relat Res*, vol. 24, no. 3, pp. 129–36, 2012.

[6] T. McMurray, "The semilunar cartilages," *Br J Surg*, vol. 29, pp. 407–14, 1942.

[7] J. Gillquist, P. Hamberg, and J. Lysholm, "Endoscopic partial and total meniscectomy. a comparative study with a short term follow up," *Acta Orthop Scand*, vol. 53, no. 6, pp. 975–9, 1982.

[8] A. Trillat, "Les lesions meniscales internes. Les lesions meniscales externes," *Chirurgie du genou. Journees Lyonnaises de Chirurgie du Genou*, 1971.

[9] K. A. Milachowski, K. Weismeier, and C. J. Wirth, "Homologous meniscus transplantation. experimental and clinical results," *Int Orthop*, vol. 13, no. 1, pp. 1–11, 1989.

[10] T. Kusayama, C. D. Harner, G. J. Carlin, J. W. Xerogeanes, and B. A. Smith, "Anatomical and biomechanical characteristics of human meniscofemoral ligaments," *Knee Surg Sports Traumatol Arthrosc*, vol. 2, no. 4, pp. 234–7, 1994.

[11] W. Petersen and B. Tillmann, "Age-related blood and lymph supply of the knee menisci. A cadaver study," *Acta Orthop Scand*, vol. 66, no. 4, pp. 308–12, 1995.

[12] S. P. Arnoczky and R. F. Warren, "Microvasculature of the human meniscus," *Am J Sports Med*, vol. 10, no. 2, pp. 90–5, 1982.

[13] J. Herwig, E. Egner, and E. Buddecke, "Chemical changes of human knee joint menisci in various stages of degeneration," *Ann Rheum Dis*, vol. 43, no. 4, pp. 635–40, 1984.

[14] C. S. Proctor, M. B. Schmidt, R. R. Whipple, M. A. Kelly, and V. C. Mow, "Material properties of the normal medial bovine meniscus," *J Orthop Res*, vol. 7, no. 6, pp. 771–82, 1989.

[15] P. Beaufils and R. Verdonk, "The Meniscus," *Springer-Verlag Berlin Heidelberg, ISBN: 978-3-6420-2450-4*, 2010.

[16] W. Petersen and B. Tillmann, "Collagenous fibril texture of the human knee joint menisci," *Anat Embryol (Berl)*, vol. 197, no. 4, pp. 317–24, 1998.

[17] M. Tissakht and A. M. Ahmed, "Tensile stress-strain characteristics of the human meniscal material," *J Biomech*, vol. 28, no. 4, pp. 411–22, 1995.

[18] W. Niu, W. Guo, S. Han, Y. Zhu, S. Liu, and Q. Guo, "Cell-based strategies for meniscus tissue engineering," *Stem Cells Int*, vol. 2016, p. 4717184, 2016.

[19] D. R. Eyre, "The collagens of articular cartilage," *Semin Arthritis Rheum*, vol. 21, no. 3 Suppl 2, pp. 2–11, 1991.

[20] K. von der Mark, T. Kirsch, A. Nerlich, A. Kuss, G. Weseloh, K. Gluckert, and H. Stoss, "Type X collagen synthesis in human osteoarthritic cartilage. Indication of chondrocyte hypertrophy," *Arthritis Rheum*, vol. 35, no. 7, pp. 806–11, 1992.

[21] P. G. Scott, T. Nakano, and C. M. Dodd, "Isolation and characterization of small proteoglycans from different zones of the porcine knee meniscus," *Biochim Biophys Acta*, vol. 1336, no. 2, pp. 254–62, 1997.

[22] A. J. Fox, F. Wanivenhaus, A. J. Burge, R. F. Warren, and S. A. Rodeo, "The human meniscus: a review of anatomy, function, injury, and advances in treatment,"

Clin Anat, vol. 28, no. 2, pp. 269–87, 2015.

[23] C. W. Hayes, M. K. Brigido, D. A. Jamadar, and T. Propeck, "Mechanism-based pattern approach to classification of complex injuries of the knee depicted at mr imaging," *Radiographics*, vol. 20 Spec No, pp. S121–34, 2000.

[24] K. M. Fischenich, J. Lewis, K. A. Kindsfater, T. S. Bailey, and T. L. Haut Donahue, "Effects of degeneration on the compressive and tensile properties of human meniscus," *J Biomech*, vol. 48, no. 8, pp. 1407–11, 2015.

[25] K. E. DeHaven, "Meniscus repair," *Am J Sports Med*, vol. 27, no. 2, pp. 242–50, 1999.

[26] F. R. Noyes and S. D. Barber-Westin, "Treatment of meniscus tears during anterior cruciate ligament reconstruction," *Arthroscopy*, vol. 28, no. 1, pp. 123–30, 2012.

[27] R. Verdonk, H. Madry, N. Shabshin, F. Dirisamer, G. M. Peretti, N. Pujol, T. Spalding, P. Verdonk, R. Seil, V. Condello, B. Di Matteo, J. Zellner, and P. Angele, "The role of meniscal tissue in joint protection in early osteoarthritis," *Knee Surg Sports Traumatol Arthrosc*, vol. 24, no. 6, pp. 1763–74, 2016.

[28] S. J. Spencer, A. Saithna, M. R. Carmont, M. S. Dhillon, P. Thompson, and T. Spalding, "Meniscal scaffolds: early experience and review of the literature," *Knee*, vol. 19, no. 6, pp. 760–5, 2012.

[29] J. C. Monllau, P. E. Gelber, F. Abat, X. Pelfort, R. Abad, P. Hinarejos, and M. Tey, "Outcome after partial medial meniscus substitution with the collagen meniscal implant at a minimum of 10 years' follow-up," *Arthroscopy*, vol. 27, no. 7, pp. 933–43, 2011.

[30] R. Langer and J. P. Vacanti, "Tissue engineering," *Science*, vol. 260, no. 5110, pp. 920–6, 1993.

[31] F. Berthiaume, T. J. Maguire, and M. L. Yarmush, "Tissue engineering and regenerative medicine: history, progress, and challenges," *Annu Rev Chem Biomol Eng*, vol. 2, pp. 403–30, 2011.

[32] N. Pallua and C. Suschek, "Tissue Engineering: From Lab to Clinic," *Springer-Verlag Berlin Heidelberg, ISBN: 978-3-6420-2824-3*, 2010.

[33] J. Rouwkema, N. C. Rivron, and C. A. van Blitterswijk, "Vascularization in tissue engineering," *Trends Biotechnol*, vol. 26, no. 8, pp. 434–41, 2008.

[34] E. C. Novosel, C. Kleinhans, and P. J. Kluger, "Vascularization is the key challenge in tissue engineering," *Adv Drug Deliv Rev*, vol. 63, no. 4-5, pp. 300–11, 2011.

[35] S. Patan, "Vasculogenesis and angiogenesis," *Cancer Treat Res*, vol. 117, pp. 3–32, 2004.

[36] T. D. Nauta, V. W. van Hinsbergh, and P. Koolwijk, "Hypoxic signaling during tissue repair and regenerative medicine," *Int J Mol Sci*, vol. 15, no. 11, pp. 19791–815, 2014.

[37] P. Carmeliet, "Angiogenesis in health and disease," *Nature Medicine*, vol. 9, no. 6, pp. 653–660, 2003.

[38] C. Y. Lee and V. L. Bautch, "Ups and downs of guided vessel sprouting: the role of polarity," *Physiology (Bethesda)*, vol. 26, no. 5, pp. 326–33, 2011.

[39] T. O. Pedersen, A. L. Blois, Y. Xue, Z. Xing, Y. Sun, A. Finne-Wistrand, J. B. Lorens, I. Fristad, K. N. Leknes, and K. Mustafa, "Mesenchymal stem cells induce endothelial cell quiescence and promote capillary formation," *Stem Cell Res Ther*, vol. 5, no. 1, p. 23, 2014.

[40] A. I. Caplan and J. E. Dennis, "Mesenchymal stem cells as trophic mediators," *J Cell Biochem*, vol. 98, no. 5, pp. 1076–84, 2006.

[41] S. Pacini and I. Petrini, "Are MSCs angiogenic cells? New insights on human nestin-positive bone marrow-derived multipotent cells," *Front Cell Dev Biol*, vol. 2, p. 20, 2014.

[42] J. Plumas, L. Chaperot, M. J. Richard, J. P. Molens, J. C. Bensa, and M. C. Favrot, "Mesenchymal stem cells induce apoptosis of activated T cells," *Leukemia*, vol. 19, no. 9, pp. 1597–604, 2005.

[43] D. G. Phinney and D. J. Prockop, "Concise review: mesenchymal stem/multipotent stromal cells: the state of transdifferentiation and modes of tissue repair–current views," *Stem Cells*, vol. 25, no. 11, pp. 2896–902, 2007.

[44] G. Chamberlain, J. Fox, B. Ashton, and J. Middleton, "Concise review: mesenchymal stem cells: their phenotype, differentiation capacity, immunological features, and potential for homing," *Stem Cells*, vol. 25, no. 11, pp. 2739–49, 2007.

[45] M. Loibl, A. Binder, M. Herrmann, F. Duttenhoefer, R. G. Richards, M. Nerlich, M. Alini, and S. Verrier, "Direct cell-cell contact between mesenchymal stem cells and endothelial progenitor cells induces a pericyte-like phenotype in vitro," *Biomed Res Int*, vol. 2014, p. 395781, 2014.

[46] A. Blocki, Y. Wang, M. Koch, P. Peh, S. Beyer, P. Law, J. Hui, and M. Raghunath, "Not all MSCs can act as pericytes: functional in vitro assays to distinguish pericytes from other mesenchymal stem cells in angiogenesis," *Stem Cells Dev*, vol. 22, no. 17, pp. 2347–55, 2013.

[47] M. Herrmann, A. Binder, U. Menzel, S. Zeiter, M. Alini, and S. Verrier, "CD34/CD133 enriched bone marrow progenitor cells promote neovascularization of tissue engineered constructs in vivo," *Stem Cell Res*, vol. 13, no. 3 Pt A, pp. 465–77, 2014.

[48] A. Kremer, M. Wussmann, M. Herrmann, M. Raghunath, and H. Walles, "Ciclopirox olamine promotes the angiogenic response of endothelial cells and mesenchymal stem cells," *Clin Hemorheol Microcirc*, vol. pre-press, no. pre-press, pp. 1–12, 2019.

[49] B. L. Krock, N. Skuli, and M. C. Simon, "Hypoxia-induced angiogenesis: good and evil," *Genes Cancer*, vol. 2, no. 12, pp. 1117–33, 2011.

[50] T. Linden, D. M. Katschinski, K. Eckhardt, A. Scheid, H. Pagel, and R. H. Wenger, "The antimycotic ciclopirox olamine induces HIF-1alpha stability, VEGF expression, and angiogenesis," *Faseb j*, vol. 17, no. 6, pp. 761–3, 2003.

[51] N. S. Lim, A. Sham, S. M. Chee, C. Chan, and M. Raghunath, "Combination of ciclopirox olamine and sphingosine-1-phosphate as granulation enhancer in diabetic wounds," *Wound Repair Regen*, vol. 24, no. 5, pp. 795–809, 2016.

[52] S. K. Kim, J. Lee, M. Song, M. Kim, S. J. Hwang, H. Jang, and Y. Park, "Combination of three angiogenic growth factors has synergistic effects on sprouting of endothelial cell/mesenchymal stem cell-based spheroids in a 3D matrix," *J*

Biomed Mater Res B Appl Biomater, vol. 104, no. 8, pp. 1535–1543, 2016.

[53] S. H. Ko, A. Nauta, S. D. Morrison, H. Zhou, A. Zimmermann, G. C. Gurtner, S. Ding, and M. T. Longaker, "Antimycotic ciclopirox olamine in the diabetic environment promotes angiogenesis and enhances wound healing," *PLoS One*, vol. 6, no. 11, p. e27844, 2011.

[54] P. L. Tremblay, V. Hudon, F. Berthod, L. Germain, and F. A. Auger, "Inosculation of tissue-engineered capillaries with the host's vasculature in a reconstructed skin transplanted on mice," *Am J Transplant*, vol. 5, no. 5, pp. 1002–10, 2005.

[55] H. Sekine, T. Shimizu, K. Hobo, S. Sekiya, J. Yang, M. Yamato, H. Kurosawa, E. Kobayashi, and T. Okano, "Endothelial cell coculture within tissue-engineered cardiomyocyte sheets enhances neovascularization and improves cardiac function of ischemic hearts," *Circulation*, vol. 118, no. 14 Suppl, pp. S145–52, 2008.

[56] M. W. Laschke, Y. Harder, M. Amon, I. Martin, J. Farhadi, A. Ring, N. Torio-Padron, R. Schramm, M. Rucker, D. Junker, J. M. Haufel, C. Carvalho, M. Heberer, G. Germann, B. Vollmar, and M. D. Menger, "Angiogenesis in tissue engineering: breathing life into constructed tissue substitutes," *Tissue Eng*, vol. 12, no. 8, pp. 2093–104, 2006.

[57] Y. H. Shen, M. S. Shoichet, and M. Radisic, "Vascular endothelial growth factor immobilized in collagen scaffold promotes penetration and proliferation of endothelial cells," *Acta Biomater*, vol. 4, no. 3, pp. 477–89, 2008.

[58] F. Geiger, H. Lorenz, W. Xu, K. Szalay, P. Kasten, L. Claes, P. Augat, and W. Richter, "VEGF producing bone marrow stromal cells (BMSC) enhance vascularization and resorption of a natural coral bone substitute," *Bone*, vol. 41, no. 4, pp. 516–22, 2007.

[59] M. T. Conconi, F. Ghezzo, M. Dettin, L. Urbani, C. Grandi, D. Guidolin, B. Nico, C. Di Bello, D. Ribatti, and P. P. Parnigotto, "Effects on in vitro and in vivo angiogenesis induced by small peptides carrying adhesion sequences," *J Pept Sci*, vol. 16, no. 7, pp. 349–57, 2010.

[60] Y. Hamada, K. Nokihara, M. Okazaki, W. Fujitani, T. Matsumoto, M. Matsuo, Y. Umakoshi, J. Takahashi, and N. Matsuura, "Angiogenic activity of osteopontin-

derived peptide SVVYGLR," *Biochem Biophys Res Commun*, vol. 310, no. 1, pp. 153–7, 2003.

[61] K. Harvey, Z. Welch, A. T. Kovala, J. G. Garcia, and D. English, "Comparative analysis of in vitro angiogenic activities of endothelial cells of heterogeneous origin," *Microvasc Res*, vol. 63, no. 3, pp. 316–26, 2002.

[62] L. A. Kunz-Schughart, J. A. Schroeder, M. Wondrak, F. van Rey, K. Lehle, F. Hofstaedter, and D. N. Wheatley, "Potential of fibroblasts to regulate the formation of three-dimensional vessel-like structures from endothelial cells in vitro," *Am J Physiol Cell Physiol*, vol. 290, no. 5, pp. C1385–98, 2006.

[63] X. Chen, A. S. Aledia, S. A. Popson, L. Him, C. C. Hughes, and S. C. George, "Rapid anastomosis of endothelial progenitor cell-derived vessels with host vasculature is promoted by a high density of cotransplanted fibroblasts," *Tissue Eng Part A*, vol. 16, no. 2, pp. 585–94, 2010.

[64] A. Aguirre, J. A. Planell, and E. Engel, "Dynamics of bone marrow-derived endothelial progenitor cell/mesenchymal stem cell interaction in co-culture and its implications in angiogenesis," *Biochem Biophys Res Commun*, vol. 400, no. 2, pp. 284–91, 2010.

[65] H. Mertsching, T. Walles, M. Hofmann, J. Schanz, and W. H. Knapp, "Engineering of a vascularized scaffold for artificial tissue and organ generation," *Biomaterials*, vol. 26, no. 33, pp. 6610–7, 2005.

[66] J. Schanz, J. Pusch, J. Hansmann, and H. Walles, "Vascularised human tissue models: a new approach for the refinement of biomedical research," *J Biotechnol*, vol. 148, no. 1, pp. 56–63, 2010.

[67] F. Groeber, L. Engelhardt, J. Lange, S. Kurdyn, F. F. Schmid, C. Rucker, S. Mielke, H. Walles, and J. Hansmann, "A first vascularized skin equivalent as an alternative to animal experimentation," *ALTEX*, vol. 33, no. 4, pp. 415–422, 2016.

[68] K. Stuckensen, A. Schwab, M. Knauer, E. Muinos-Lopez, F. Ehlicke, J. Reboredo, F. Granero-Molto, U. Gbureck, F. Prosper, H. Walles, and J. Groll, "Tissue mimicry in morphology and composition promotes hierarchical matrix remodeling of invading stem cells in osteochondral and meniscus scaffolds," *Adv Mater*, vol. 30,

no. 28, p. e1706754, 2018.

[69] H. C. Ott, T. S. Matthiesen, S. K. Goh, L. D. Black, S. M. Kren, T. I. Netoff, and D. A. Taylor, "Perfusion-decellularized matrix: using nature's platform to engineer a bioartificial heart," *Nat Med*, vol. 14, no. 2, pp. 213–21, 2008.

[70] R. Lüllmann-Rauch, "Taschenlehrbuch Histologie," *Georg Thieme Verlag KG, ISBN: 978-3-1316-8563-6*, 2011.

[71] L. E. Bertassoni, M. Cecconi, V. Manoharan, M. Nikkhah, J. Hjortnaes, A. L. Cristino, G. Barabaschi, D. Demarchi, M. R. Dokmeci, Y. Yang, and A. Khademhosseini, "Hydrogel bioprinted microchannel networks for vascularization of tissue engineering constructs," *Lab Chip*, vol. 14, no. 13, pp. 2202–11, 2014.

[72] V. Mironov, V. Kasyanov, C. Drake, and R. R. Markwald, "Organ printing: promises and challenges," *Regen Med*, vol. 3, no. 1, pp. 93–103, 2008.

[73] A. P. McGuigan and M. V. Sefton, "Vascularized organoid engineered by modular assembly enables blood perfusion," *Proc Natl Acad Sci U S A*, vol. 103, no. 31, pp. 11461–6, 2006.

[74] A. P. McGuigan and M. V. Sefton, "Design and fabrication of sub-mm-sized modules containing encapsulated cells for modular tissue engineering," *Tissue Eng*, vol. 13, no. 5, pp. 1069–78, 2007.

[75] S. M. Mueller, S. Shortkroff, T. O. Schneider, H. A. Breinan, I. V. Yannas, and M. Spector, "Meniscus cells seeded in type I and type II collagen-GAG matrices in vitro," *Biomaterials*, vol. 20, no. 8, pp. 701–9, 1999.

[76] N. J. Gunja and K. A. Athanasiou, "Passage and reversal effects on gene expression of bovine meniscal fibrochondrocytes," *Arthritis Res Ther*, vol. 9, no. 5, p. R93, 2007.

[77] M. Dominici, K. L. Blanc, I. Mueller, I. Slaper-Cortenbach, F. Marini, D. Krause, R. Deans, A. Keating, D. Prockop, and E. Horwitz, "Minimal criteria for defining multipotent mesenchymal stromal cells. The International Society for Cellular Therapy position statement," *Cytotherapy*, vol. 8, no. 4, pp. 315–317, 2006.

[78] H. R. Hofer and R. S. Tuan, "Secreted trophic factors of mesenchymal stem cells

support neurovascular and musculoskeletal therapies," *Stem Cell Res Ther*, vol. 7, no. 1, p. 131, 2016.

[79] D. Hatsushika, T. Muneta, T. Nakamura, M. Horie, H. Koga, Y. Nakagawa, K. Tsuji, S. Hishikawa, E. Kobayashi, and I. Sekiya, "Repetitive allogeneic intraarticular injections of synovial mesenchymal stem cells promote meniscus regeneration in a porcine massive meniscus defect model," *Osteoarthritis Cartilage*, vol. 22, no. 7, pp. 941–50, 2014.

[80] J. Zellner, K. Hierl, M. Mueller, C. Pfeifer, A. Berner, T. Dienstknecht, W. Krutsch, S. Geis, S. Gehmert, R. Kujat, S. Dendorfer, L. Prantl, M. Nerlich, and P. Angele, "Stem cell-based tissue-engineering for treatment of meniscal tears in the avascular zone," *J Biomed Mater Res B Appl Biomater*, vol. 101, no. 7, pp. 1133–42, 2013.

[81] M. B. Pabbruwe, W. Kafienah, J. F. Tarlton, S. Mistry, D. J. Fox, and A. P. Hollander, "Repair of meniscal cartilage white zone tears using a stem cell/collagen-scaffold implant," *Biomaterials*, vol. 31, no. 9, pp. 2583–91, 2010.

[82] N. F. Matthies, A. Mulet-Sierra, N. M. Jomha, and A. B. Adesida, "Matrix formation is enhanced in co-cultures of human meniscus cells with bone marrow stromal cells," *J Tissue Eng Regen Med*, vol. 7, no. 12, pp. 965–73, 2013.

[83] X. Cui, A. Hasegawa, M. Lotz, and D. D'Lima, "Structured three-dimensional co-culture of mesenchymal stem cells with meniscus cells promotes meniscal phenotype without hypertrophy," *Biotechnol Bioeng*, vol. 109, no. 9, pp. 2369–80, 2012.

[84] A. M. Mackay, S. C. Beck, J. M. Murphy, F. P. Barry, C. O. Chichester, and M. F. Pittenger, "Chondrogenic differentiation of cultured human mesenchymal stem cells from marrow," *Tissue Eng*, vol. 4, no. 4, pp. 415–28, 1998.

[85] S. Collier and P. Ghosh, "Effects of transforming growth factor beta on proteoglycan synthesis by cell and explant cultures derived from the knee joint meniscus," *Osteoarthritis Cartilage*, vol. 3, no. 2, pp. 127–38, 1995.

[86] N. J. Gunja, R. K. Uthamanthil, and K. A. Athanasiou, "Effects of TGF-beta1 and hydrostatic pressure on meniscus cell-seeded scaffolds," *Biomaterials*, vol. 30, no. 4, pp. 565–73, 2009.

[87] C. A. Pangborn and K. A. Athanasiou, "Effects of growth factors on meniscal fibrochondrocytes," *Tissue Eng*, vol. 11, no. 7-8, pp. 1141–8, 2005.

[88] C. A. Pangborn and K. A. Athanasiou, "Growth factors and fibrochondrocytes in scaffolds," *J Orthop Res*, vol. 23, no. 5, pp. 1184–90, 2005.

[89] L. C. Ionescu, G. C. Lee, K. L. Huang, and R. L. Mauck, "Growth factor supplementation improves native and engineered meniscus repair in vitro," *Acta Biomater*, vol. 8, no. 10, pp. 3687–94, 2012.

[90] C. Henrionnet, G. Liang, E. Roeder, M. Dossot, H. Wang, J. Magdalou, P. Gillet, and A. Pinzano, "Hypoxia for mesenchymal stem cell expansion and differentiation: the best way for enhancing TGFss-induced chondrogenesis and preventing calcifications in alginate beads," *Tissue Eng Part A*, vol. 23, no. 17-18, pp. 913–922, 2017.

[91] A. S. Zeiger, F. C. Loe, R. Li, M. Raghunath, and K. J. Van Vliet, "Macromolecular crowding directs extracellular matrix organization and mesenchymal stem cell behavior," *PLoS One*, vol. 7, no. 5, p. e37904, 2012.

[92] A. Satyam, P. Kumar, X. Fan, A. Gorelov, Y. Rochev, L. Joshi, H. Peinado, D. Lyden, B. Thomas, B. Rodriguez, M. Raghunath, A. Pandit, and D. Zeugolis, "Macromolecular crowding meets tissue engineering by self-assembly: a paradigm shift in regenerative medicine," *Adv Mater*, vol. 26, no. 19, pp. 3024–34, 2014.

[93] J. Y. Dewavrin, N. Hamzavi, V. P. Shim, and M. Raghunath, "Tuning the architecture of three-dimensional collagen hydrogels by physiological macromolecular crowding," *Acta Biomater*, vol. 10, no. 10, pp. 4351–9, 2014.

[94] C. A. Murphy, J. B. Costa, J. Silva-Correia, J. M. Oliveira, R. L. Reis, and M. N. Collins, "Biopolymers and polymers in the search of alternative treatments for meniscal regeneration: state of the art and future trends," *Applied Materials Today*, vol. 12, pp. 51 – 71, 2018.

[95] M. A. Sweigart and K. A. Athanasiou, "Toward tissue engineering of the knee meniscus," *Tissue Eng*, vol. 7, no. 2, pp. 111–29, 2001.

[96] J. Sun, S. Vijayavenkataraman, and H. Liu, "An overview of scaffold design and fabrication technology for engineered knee meniscus," *Materials (Basel)*, vol. 10,

no. 1, 2017.

[97] T. W. Gilbert, T. L. Sellaro, and S. F. Badylak, "Decellularization of tissues and organs," *Biomaterials*, vol. 27, no. 19, pp. 3675–83, 2006.

[98] J. L. Cook, D. B. Fox, P. Malaviya, J. L. Tomlinson, K. Kuroki, C. R. Cook, and S. Kladakis, "Long-term outcome for large meniscal defects treated with small intestinal submucosa in a dog model," *Am J Sports Med*, vol. 34, no. 1, pp. 32–42, 2006.

[99] T. W. Stapleton, J. Ingram, J. Katta, R. Knight, S. Korossis, J. Fisher, and E. Ingham, "Development and characterization of an acellular porcine medial meniscus for use in tissue engineering," *Tissue Eng Part A*, vol. 14, no. 4, pp. 505–18, 2008.

[100] J. L. Puetzer and L. J. Bonassar, "High density type I collagen gels for tissue engineering of whole menisci," *Acta Biomater*, vol. 9, no. 8, pp. 7787–95, 2013.

[101] E. Braziulis, M. Diezi, T. Biedermann, L. Pontiggia, M. Schmucki, F. Hartmann-Fritsch, J. Luginbuhl, C. Schiestl, M. Meuli, and E. Reichmann, "Modified plastic compression of collagen hydrogels provides an ideal matrix for clinically applicable skin substitutes," *Tissue Eng Part C Methods*, vol. 18, no. 6, pp. 464–74, 2012.

[102] J. Baek, X. Chen, S. Sovani, S. Jin, S. P. Grogan, and D. D. D'Lima, "Meniscus tissue engineering using a novel combination of electrospun scaffolds and human meniscus cells embedded within an extracellular matrix hydrogel," *J Orthop Res*, vol. 33, no. 4, pp. 572–83, 2015.

[103] A. Kremer, I. Ribitsch, J. Reboredo, J. Durr, M. Egerbacher, F. Jenner, and H. Walles, "Three-dimensional coculture of meniscal cells and mesenchymal stem cells in collagen type i hydrogel on a small intestinal matrix-a pilot study toward equine meniscus tissue engineering," *Tissue Eng Part A*, vol. 23, no. 9-10, pp. 390–402, 2017.

[104] M. Chen, W. Guo, S. Gao, C. Hao, S. Shen, Z. Zhang, Z. Wang, X. Li, X. Jing, X. Zhang, Z. Yuan, M. Wang, Y. Zhang, J. Peng, A. Wang, Y. Wang, X. Sui, S. Liu, and Q. Guo, "Biomechanical stimulus based strategies for meniscus tissue engineering and regeneration," *Tissue Eng Part B Rev*, vol. 24, no. 5, pp. 392–402,

2018.

[105] E. Y. Salinas, J. C. Hu, and K. Athanasiou, "A guide for using mechanical stimulation to enhance tissue-engineered articular cartilage properties," *Tissue Eng Part B Rev*, vol. 24, no. 5, pp. 345–358, 2018.

[106] J. L. Puetzer, J. J. Ballyns, and L. J. Bonassar, "The effect of the duration of mechanical stimulation and post-stimulation culture on the structure and properties of dynamically compressed tissue-engineered menisci," *Tissue Eng Part A*, vol. 18, no. 13-14, pp. 1365–75, 2012.

[107] J. T. Connelly, E. J. Vanderploeg, J. K. Mouw, C. G. Wilson, and M. E. Levenston, "Tensile loading modulates bone marrow stromal cell differentiation and the development of engineered fibrocartilage constructs," *Tissue Eng Part A*, vol. 16, no. 6, pp. 1913–23, 2010.

[108] D. J. Huey and K. A. Athanasiou, "Tension-compression loading with chemical stimulation results in additive increases to functional properties of anatomic meniscal constructs," *PLoS One*, vol. 6, no. 11, p. e27857, 2011.

[109] M. Petri, K. Ufer, I. Toma, C. Becher, E. Liodakis, S. Brand, P. Haas, C. Liu, B. Richter, C. Haasper, G. von Lewinski, and M. Jagodzinski, "Effects of perfusion and cyclic compression on in vitro tissue engineered meniscus implants," *Knee Surg Sports Traumatol Arthrosc*, vol. 20, no. 2, pp. 223–31, 2012.

[110] A. L. McNulty and F. Guilak, "Mechanobiology of the meniscus," *J Biomech*, vol. 48, no. 8, pp. 1469–78, 2015.

[111] J. Zellner, M. Mueller, Y. Xin, W. Krutsch, A. Brandl, R. Kujat, M. Nerlich, and P. Angele, "Dynamic hydrostatic pressure enhances differentially the chondrogenesis of meniscal cells from the inner and outer zone," *J Biomech*, vol. 48, no. 8, pp. 1479–84, 2015.

[112] L. B. Williams and A. B. Adesida, "Angiogenic approaches to meniscal healing," *Injury*, vol. 49, no. 3, pp. 467–472, 2018.

[113] C. Hidaka, C. Ibarra, J. A. Hannafin, P. A. Torzilli, M. Quitoriano, S. S. Jen, R. F. Warren, and R. G. Crystal, "Formation of vascularized meniscal tissue by combining gene therapy with tissue engineering," *Tissue Eng*, vol. 8, no. 1,

pp. 93–105, 2002.

[114] X. Yuan, G. M. Eng, D. E. Arkonac, P. H. Chao, and G. Vunjak-Novakovic, "Endothelial cells enhance the migration of bovine meniscus cells," *Arthritis Rheumatol*, vol. 67, no. 1, pp. 182–92, 2015.

[115] W. He, Y. J. Liu, Z. G. Wang, Z. K. Guo, M. X. Wang, and N. Wang, "Enhancement of meniscal repair in the avascular zone using connective tissue growth factor in a rabbit model," *Chin Med J (Engl)*, vol. 124, no. 23, pp. 3968–75, 2011.

[116] C. H. Lee, S. A. Rodeo, L. A. Fortier, C. Lu, C. Erisken, and J. J. Mao, "Protein-releasing polymeric scaffolds induce fibrochondrocytic differentiation of endogenous cells for knee meniscus regeneration in sheep," *Sci Transl Med*, vol. 6, no. 266, p. 266ra171, 2014.

[117] L. Ren, D. Ma, B. Liu, J. Li, J. Chen, D. Yang, and P. Gao, "Preparation of three-dimensional vascularized MSC cell sheet constructs for tissue regeneration," *Biomed Res Int*, vol. 2014, p. 301279, 2014.

[118] H. Nagase, R. Visse, and G. Murphy, "Structure and function of matrix metalloproteinases and TIMPs," *Cardiovasc Res*, vol. 69, no. 3, pp. 562–573, 2006.

[119] J. Woessner, J. F., "The family of matrix metalloproteinases," *Ann N Y Acad Sci*, vol. 732, pp. 11–21, 1994.

[120] P. A. Snoek-van Beurden and J. W. Von den Hoff, "Zymographic techniques for the analysis of matrix metalloproteinases and their inhibitors," *Biotechniques*, vol. 38, no. 1, pp. 73–83, 2005.

[121] G. Kasper, J. D. Glaeser, S. Geissler, A. Ode, J. Tuischer, G. Matziolis, C. Perka, and G. N. Duda, "Matrix metalloprotease activity is an essential link between mechanical stimulus and mesenchymal stem cell behavior," *Stem Cells*, vol. 25, no. 8, pp. 1985–1994, 2007.

[122] H. N. Chia and M. L. Hull, "Compressive moduli of the human medial meniscus in the axial and radial directions at equilibrium and at a physiological strain rate," *J Orthop Res*, vol. 26, no. 7, pp. 951–6, 2008.

[123] A. M. Seitz, U. Wolfram, C. Wiedenmann, A. Ignatius, and L. Durselen, "Impact

of measurement errors on the determination of the linear modulus of human meniscal attachments," *J Mech Behav Biomed Mater*, vol. 10, pp. 120–7, 2012.

[124] A. M. Seitz, F. Galbusera, C. Krais, A. Ignatius, and L. Durselen, "Stress-relaxation response of human menisci under confined compression conditions," *J Mech Behav Biomed Mater*, vol. 26, pp. 68–80, 2013.

[125] D. D. Stöbener, M. Uckert, J. L. Cuellar-Camacho, A. Hoppensack, and M. Weinhart, "Ultrathin poly(glycidyl ether) coatings on polystyrene for temperature-triggered human dermal fibroblast sheet fabrication," *ACS Biomaterials Science & Engineering*, vol. 3, no. 9, pp. 2155–2165, 2017.

[126] S. Schmitz, "Der Experimentator: Zellkultur," *Spektrum Akademischer Verlag Heidelberg, ISBN: 978-3-8274-2573-7*, 2011.

[127] P. Schmidt, "Praxis der Rasterelektronenmikroskopie und Mikrobereichsanalyse," *expert-Verlag GmbH, Fachverlag für Wirtschaft und Technik, ISBN: 978-3-8169-1597-3*, 2012.

[128] H. Madry, M. Ochi, M. Cucchiarini, D. Pape, and R. Seil, "Large animal models in experimental knee sports surgery: focus on clinical translation," *J Exp Orthop*, vol. 2, no. 1, p. 9, 2015.

[129] S. Schuerlein, T. Schwarz, S. Krziminski, S. Gatzner, A. Hoppensack, I. Schwedhelm, M. Schweinlin, H. Walles, and J. Hansmann, "A versatile modular bioreactor platform for tissue engineering," *Biotechnol J*, vol. 12, no. 2, 2017.

[130] M. Wußmann, "Characterization of a tissue engineered 3D vascularization model," *Master thesis, Julius-Maximilians-Universität Würzburg*, 2018.

[131] T. Tanaka, K. Fujii, and Y. Kumagae, "Comparison of biochemical characteristics of cultured fibrochondrocytes isolated from the inner and outer regions of human meniscus," *Knee Surg Sports Traumatol Arthrosc*, vol. 7, no. 2, pp. 75–80, 1999.

[132] J. L. Chen, L. Duan, W. Zhu, J. Xiong, and D. Wang, "Extracellular matrix production in vitro in cartilage tissue engineering," *J Transl Med*, vol. 12, p. 88, 2014.

[133] P. Angele, R. Kujat, M. Koch, and J. Zellner, "Role of mesenchymal stem cells in

meniscal repair," *J Exp Orthop*, vol. 1, no. 1, p. 12, 2014.

[134] S. Badylak, K. Kokini, B. Tullius, A. Simmons-Byrd, and R. Morff, "Morphologic study of small intestinal submucosa as a body wall repair device," *J Surg Res*, vol. 103, no. 2, pp. 190–202, 2002.

[135] J. A. Welch, R. D. Montgomery, S. D. Lenz, P. Plouhar, and W. R. Shelton, "Evaluation of small-intestinal submucosa implants for repair of meniscal defects in dogs," *Am J Vet Res*, vol. 63, no. 3, pp. 427–31, 2002.

[136] M. P. Bradley, P. D. Fadale, M. J. Hulstyn, W. R. Muirhead, and J. T. Lifrak, "Porcine small intestine submucosa for repair of goat meniscal defects," *Orthopedics*, vol. 30, no. 8, pp. 650–6, 2007.

[137] J. A. Gastel, W. R. Muirhead, J. T. Lifrak, P. D. Fadale, M. J. Hulstyn, and D. P. Labrador, "Meniscal tissue regeneration using a collagenous biomaterial derived from porcine small intestine submucosa," *Arthroscopy*, vol. 17, no. 2, pp. 151–9, 2001.

[138] J. L. Zitnay, S. P. Reese, G. Tran, N. Farhang, R. D. Bowles, and J. A. Weiss, "Fabrication of dense anisotropic collagen scaffolds using biaxial compression," *Acta Biomater*, vol. 65, pp. 76–87, 2018.

[139] A. F. Steinert, G. D. Palmer, R. Capito, J. G. Hofstaetter, C. Pilapil, S. C. Ghivizzani, M. Spector, and C. H. Evans, "Genetically enhanced engineering of meniscus tissue using ex vivo delivery of transforming growth factor-beta 1 complementary deoxyribonucleic acid," *Tissue Eng*, vol. 13, no. 9, pp. 2227–37, 2007.

[140] Y. Tan, Y. Zhang, and M. Pei, "Meniscus reconstruction through coculturing meniscus cells with synovium-derived stem cells on small intestine submucosa–a pilot study to engineer meniscus tissue constructs," *Tissue Eng Part A*, vol. 16, no. 1, pp. 67–79, 2010.

[141] S. Boeuf and W. Richter, "Chondrogenesis of mesenchymal stem cells: role of tissue source and inducing factors," *Stem Cell Res Ther*, vol. 1, no. 4, p. 31, 2010.

[142] A. C. AufderHeide and K. A. Athanasiou, "Mechanical stimulation toward tissue engineering of the knee meniscus," *Ann Biomed Eng*, vol. 32, no. 8, pp. 1161–74, 2004.

[143] B. D. Elder and K. A. Athanasiou, "Effects of confinement on the mechanical properties of self-assembled articular cartilage constructs in the direction orthogonal to the confinement surface," *J Orthop Res*, vol. 26, no. 2, pp. 238–46, 2008.

[144] B. J. Huang, J. C. Hu, and K. A. Athanasiou, "Cell-based tissue engineering strategies used in the clinical repair of articular cartilage," *Biomaterials*, vol. 98, pp. 1–22, 2016.

[145] S. Inanc, D. Keles, and G. Oktay, "An improved collagen zymography approach for evaluating the collagenases MMP-1, MMP-8, and MMP-13," *Biotechniques*, vol. 63, no. 4, pp. 174–180, 2017.

[146] S. G. Jue, G. W. Dawson, and R. N. Brogden, "Ciclopirox olamine 1% cream. A preliminary review of its antimicrobial activity and therapeutic use," *Drugs*, vol. 29, no. 4, pp. 330–41, 1985.

[147] M. Bohn and K. T. Kraemer, "Dermatopharmacology of ciclopirox nail lacquer topical solution 8% in the treatment of onychomycosis," *J Am Acad Dermatol*, vol. 43, no. 4 Suppl, pp. S57–69, 2000.

[148] M. W. Laschke and M. D. Menger, "Spheroids as vascularization units: from angiogenesis research to tissue engineering applications," *Biotechnol Adv*, vol. 35, no. 6, pp. 782–791, 2017.

[149] T. Maciag, G. A. Hoover, M. B. Stemerman, and R. Weinstein, "Serial propagation of human endothelial cells in vitro," *J Cell Biol*, vol. 91, no. 2 Pt 1, pp. 420–6, 1981.

[150] M. Heiss, M. Hellstrom, M. Kalen, T. May, H. Weber, M. Hecker, H. G. Augustin, and T. Korff, "Endothelial cell spheroids as a versatile tool to study angiogenesis in vitro," *Faseb j*, vol. 29, no. 7, pp. 3076–84, 2015.

[151] C. A. Staton, S. M. Stribbling, S. Tazzyman, R. Hughes, N. J. Brown, and C. E. Lewis, "Current methods for assaying angiogenesis in vitro and in vivo," *Int J Exp Pathol*, vol. 85, no. 5, pp. 233–48, 2004.

[152] M. Raghunath, Y. Sy Wong, M. Farooq, and R. Ge, "Pharmacologically induced angiogenesis in transgenic zebrafish," *Biochem Biophys Res Commun*, vol. 378, no. 4, pp. 766–71, 2009.

[153] R. R. Miller and P. A. Rydell, "Primary culture of microvascular endothelial cells from canine meniscus," *J Orthop Res*, vol. 11, no. 6, pp. 907–11, 1993.

[154] S. H. Lim, C. Kim, A. R. Aref, R. D. Kamm, and M. Raghunath, "Complementary effects of ciclopirox olamine, a prolyl hydroxylase inhibitor and sphingosine 1-phosphate on fibroblasts and endothelial cells in driving capillary sprouting," *Integrative Biology*, vol. 5, no. 12, pp. 1474–1484, 2013.

[155] S. Rey and G. L. Semenza, "Hypoxia-inducible factor-1-dependent mechanisms of vascularization and vascular remodelling," *Cardiovasc Res*, vol. 86, no. 2, pp. 236–42, 2010.

[156] E. Fagiani and G. Christofori, "Angiopoietins in angiogenesis," *Cancer Lett*, vol. 328, no. 1, pp. 18–26, 2013.

[157] M. M. Martino, S. Brkic, E. Bovo, M. Burger, D. J. Schaefer, T. Wolff, L. Gurke, P. S. Briquez, H. M. Larsson, R. Gianni-Barrera, J. A. Hubbell, and A. Banfi, "Extracellular matrix and growth factor engineering for controlled angiogenesis in regenerative medicine," *Front Bioeng Biotechnol*, vol. 3, p. 45, 2015.

[158] C. R. Ozawa, A. Banfi, N. L. Glazer, G. Thurston, M. L. Springer, P. E. Kraft, D. M. McDonald, and H. M. Blau, "Microenvironmental VEGF concentration, not total dose, determines a threshold between normal and aberrant angiogenesis," *J Clin Invest*, vol. 113, no. 4, pp. 516–27, 2004.

[159] I. Jun, T. Ahmad, S. Bak, J. Y. Lee, E. M. Kim, J. Lee, Y. B. Lee, H. Jeong, H. Jeon, and H. Shin, "Spatially assembled bilayer cell sheets of stem cells and endothelial cells using thermosensitive hydrogels for therapeutic angiogenesis," *Adv Healthc Mater*, vol. 6, no. 9, 2017.

[160] M. A. Cleary, G. J. van Osch, P. A. Brama, C. A. Hellingman, and R. Narcisi, "FGF, TGFbeta and Wnt crosstalk: embryonic to in vitro cartilage development from mesenchymal stem cells," *J Tissue Eng Regen Med*, vol. 9, no. 4, pp. 332–42, 2015.

[161] M. Mastrogiacomo, R. Cancedda, and R. Quarto, "Effect of different growth factors on the chondrogenic potential of human bone marrow stromal cells," *Osteoarthritis Cartilage*, vol. 9 Suppl A, pp. S36–40, 2001.

[162] A. Marsano, C. M. Medeiros da Cunha, S. Ghanaati, S. Gueven, M. Centola, R. Tsaryk, M. Barbeck, C. Stuedle, A. Barbero, U. Helmrich, S. Schaeren, J. C. Kirkpatrick, A. Banfi, and I. Martin, "Spontaneous in vivo chondrogenesis of bone marrow-derived mesenchymal progenitor cells by blocking vascular endothelial growth factor signaling," *Stem Cells Transl Med*, vol. 5, no. 12, pp. 1730–1738, 2016.

[163] Y. M. Yoon, C. D. Oh, D. Y. Kim, Y. S. Lee, J. W. Park, T. L. Huh, S. S. Kang, and J. S. Chun, "Epidermal growth factor negatively regulates chondrogenesis of mesenchymal cells by modulating the protein kinase C-alpha, Erk-1, and p38 MAPK signaling pathways," *J Biol Chem*, vol. 275, no. 16, pp. 12353–9, 2000.

[164] S. Grassel and N. Ahmed, "Influence of cellular microenvironment and paracrine signals on chondrogenic differentiation," *Front Biosci*, vol. 12, pp. 4946–56, 2007.

[165] D. A. Yu, J. Han, and B. S. Kim, "Stimulation of chondrogenic differentiation of mesenchymal stem cells," *Int J Stem Cells*, vol. 5, no. 1, pp. 16–22, 2012.

[166] T. Fukumoto, J. W. Sperling, A. Sanyal, J. S. Fitzsimmons, G. G. Reinholz, C. A. Conover, and S. W. O'Driscoll, "Combined effects of insulin-like growth factor-1 and transforming growth factor-beta1 on periosteal mesenchymal cells during chondrogenesis in vitro," *Osteoarthritis Cartilage*, vol. 11, no. 1, pp. 55–64, 2003.

[167] P. Bruckner, I. Horler, M. Mendler, Y. Houze, K. H. Winterhalter, S. G. Eich-Bender, and M. A. Spycher, "Induction and prevention of chondrocyte hypertrophy in culture," *J Cell Biol*, vol. 109, no. 5, pp. 2537–45, 1989.

[168] H. Mertsching, J. Schanz, V. Steger, M. Schandar, M. Schenk, J. Hansmann, I. Dally, G. Friedel, and T. Walles, "Generation and transplantation of an autologous vascularized bioartificial human tissue," *Transplantation*, vol. 88, no. 2, pp. 203–10, 2009.

[169] S. A. Rodeo, "Arthroscopic meniscal repair with use of the outside-in technique," *Instr Course Lect*, vol. 49, pp. 195–206, 2000.

[170] P. Albrecht-Olsen, T. Lind, G. Kristensen, and B. Falkenberg, "Failure strength of a new meniscus arrow repair technique: biomechanical comparison with horizontal suture," *Arthroscopy*, vol. 13, no. 2, pp. 183–7, 1997.

[171] F. A. Barber, M. A. Herbert, and D. P. Richards, "Load to failure testing of new meniscal repair devices," *Arthroscopy*, vol. 20, no. 1, pp. 45–50, 2004.

[172] L. Durselen, J. Schneider, M. Galler, L. E. Claes, and G. Bauer, "Cyclic joint loading can affect the initial stability of meniscal fixation implants," *Clin Biomech (Bristol, Avon)*, vol. 18, no. 1, pp. 44–9, 2003.

[173] C. D. Morgan and S. W. Casscells, "Arthroscopic meniscus repair: a safe approach to the posterior horns," *Arthroscopy*, vol. 2, no. 1, pp. 3–12, 1986.

[174] E. Steck, J. Fischer, H. Lorenz, T. Gotterbarm, M. Jung, and W. Richter, "Mesenchymal stem cell differentiation in an experimental cartilage defect: restriction of hypertrophy to bone-close neocartilage," *Stem Cells Dev*, vol. 18, no. 7, pp. 969–78, 2009.

[175] D. Deponti, A. D. Giancamillo, C. Scotti, G. M. Peretti, and I. Martin, "Animal models for meniscus repair and regeneration," *J Tissue Eng Regen Med*, 2013.

[176] T. Takroni, L. Laouar, A. Adesida, J. A. Elliott, and N. M. Jomha, "Anatomical study: comparing the human, sheep and pig knee meniscus," *J Exp Orthop*, vol. 3, no. 1, p. 35, 2016.

[177] T. G. Koch and D. H. Betts, "Stem cell therapy for joint problems using the horse as a clinically relevant animal model," *Expert Opin Biol Ther*, vol. 7, no. 11, pp. 1621–6, 2007.

[178] J. R. Walmsley, T. J. Phillips, and H. G. Townsend, "Meniscal tears in horses: an evaluation of clinical signs and arthroscopic treatment of 80 cases," *Equine Vet J*, vol. 35, no. 4, pp. 402–6, 2003.

[179] J. P. Walmsley, "Diagnosis and treatment of ligamentous and meniscal injuries in the equine stifle," *Vet Clin North Am Equine Pract*, vol. 21, no. 3, pp. 651–72, vii, 2005.

Appendix A

Supplemental Data

This chapter contains the supplemental data of the experimental work.

A.1. Isotype controls for immunohistochemical stainings

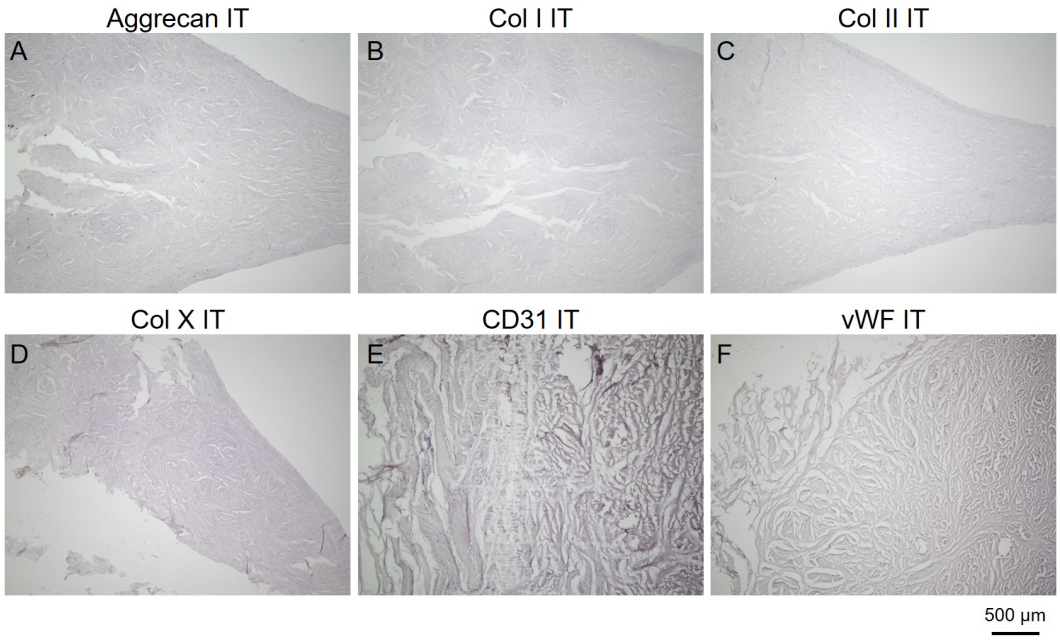

Figure A.1.: Isotype (IT) controls of the used antibodies for immunohistochemical stainings of human medial meniscus sections. Aggrecan IT on hMen67 (**A**), Col I IT on hMen67 (**B**), Col II IT on hMen67 (**C**), Col X IT on hMen67 (**D**), CD31 IT on hMen70 PH (**E**) and vWF IT on hMen70 PH (**F**). IT controls were performed for all stainings and showed no DAB staining. Scale bar as depicted, same magnification for all micrographs.

IT controls (table 2.10) were established and performed for all immunohistochemical stainings (figure A.1). All IT controls were negative and did not show positive DAB staining. Thus, it was confirmed that the used primary antibodies bound specifically to the antigen of interest of each immunohistochemical staining.

A.2. Cell surface markers of hMSCs

Cell surface markers of hMSCs were detected by FCM (figure A.2). HMSCs were positive for CD44, CD73, CD90 and CD105, and negative for CD11b, CD19, CD31, CD34 and CD45.

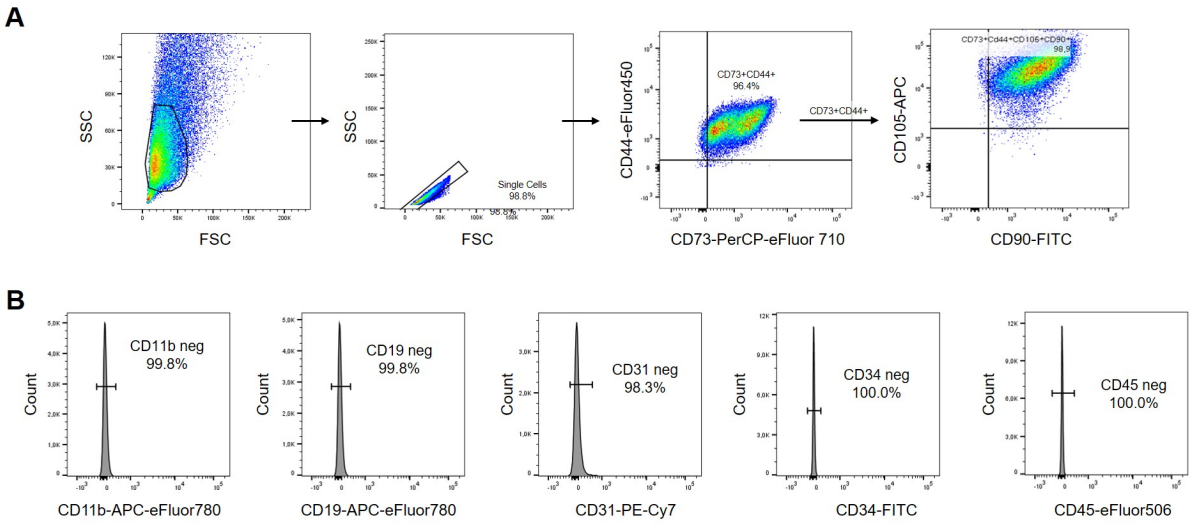

Figure A.2.: FCM analysis of the hMSC pool. **A** Detection of positive MSC surface markers CD44, CD73, CD90 and CD105. **B** Detection of negative MSC surface markers CD11b, CD19, CD31, CD34 and CD45. Adapted from [48] with kind permission.

A.3. Col I antibody reactivity for human Col I

The Col I gels were composed of rat Col I isolated from rat tails. The Col I antibody (table 2.8) was purchased from Abcam. They mentioned that they have preliminary internal testing indicating that this antibody may not react with mouse and rat species. The used Col I antibody with the catalog number ab138492 showed no reactivity for rat Col I as

seen in figure A.3. No positive Col I staining was detected for cell-free Col I gels, whereas hMSC-laden models and native human meniscus showed positive Col I staining. Thus, positive immunohistochemical staining for Col I of hMSC-laden Col I gel models was confirmed to be human Col I newly synthesized by loaded cells such as hMSCs.

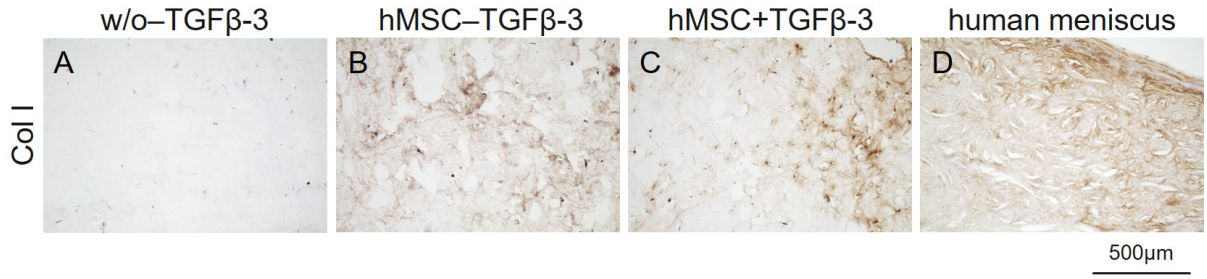

Figure A.3.: The reactivity of the used Col I antibody was proven for human Col I. Col I gel w/o cells cultured in chondrogenic DM without TGFβ-3 on day 21 (**A**), hMSC-laden Col I gel cultured in chondrogenic DM without TGFβ-3 on day 21 (**B**), hMSC-laden Col I gel cultured in chondrogenic DM wih TGFβ-3 on day 21 (**C**) and human meniscus (**D**). The Col I gels were based on Col I isolated from rat tails. The reactivity of the used Col I antibody was confirmed for human Col I, as no positive staining for rat Col I was detected for the Col I gel w/o cells.

Appendix B

List of Publications and Congress Participations

Data presented in this thesis are partially published in peer-reviewed publications, preprinted and presented at international and national conferences as listed in the following.

B.1. Peer-reviewed articles

- **Kremer A**, Wußmann M, Herrmann M, Raghunath M, Walles H. Ciclopirox olamine promotes the angiogenic response of endothelial cells and mesenchymal stem cells. Clin Hemorheol Microcirc, 2019:1-12. doi: 10.3233/CH-190559. Epub 2019 Apr 19, ahead of print.

- **Kremer A**, Ribitsch I, Reboredo J, Dürr J, Egerbacher M, Jenner F, Walles H. Three-Dimensional Coculture of Meniscal Cells and Mesenchymal Stem Cells in Collagen Type I Hydrogel on a Small Intestinal Matrix-A Pilot Study Toward Equine Meniscus Tissue Engineering. Tissue Eng Part A, 2017 May, 23(9-10):390-402. doi: 10.1089/ten.TEA.2016.0317. Epub 2017 Apr 7.

B.2. Further publications

- **Kremer A**, Ribitsch I, Jenner F, Walles H, Reboredo J. Track I. Cellular-, Tissue- and Bioengineering. Biomed Tech (Berl), 2016 Sep 1, 61(s1):81-89. doi: 10.1515/bmt-2016-5007.

B.3. International conferences

- Kremer A, et al. Employment of a prolyl hydroxylase inhibitor to promote vascularization in tissue engineered constructs. Talk, 5th Tissue Engineering and Regenerative Medicine International Society (TERMIS) World Congress 2018, Kyoto, Japan.

- Kremer A, et al. Wedge-shape compression of MSC-laden Col I gel for meniscus tissue engineering. Poster and poster teaser presentation, Orthopedic Research Society (ORS) 2018 Annual Meeting, New Orleans, USA.

- Kremer A, et al. 3D co-culture of mesenchymal stem cells and meniscal cells to build up 3D meniscus models. Talk, ORS Meniscus Scientifc Meeting 2018, New Orleans, USA.

- Kremer A, et al. Influence of mesenchymal stem cell differentiation by 3D co-culturing with meniscal cells in an equine model. Talk, Biomedizinische Technik (BMT) 2016 of Swiss, Austrian and German Societies of Biomedical Engineering, Basel, Switzerland.

- Kremer A, et al. Mutual influence of mesenchymal stem cells and meniscal cells by 3D co-culturing to build up a meniscus model. Talk, 2016 TERMIS Asia Pacific Meeting, Tamsui-Taipeh, Taiwan: **Oral Presentation 1st place**.

B.4. National conferences

- Kremer A, et al. Meniscus 3D model by wedge-shape compression of a MSC-laden Collagen I gel. Talk, Deutscher Kongress für Orthopädie und Unfallchirurgie (DKOU) 2018, Berlin, Germany.

- Kremer A, et al. Wedge-shape compression of MSC-laden Col I gel for meniscus tissue engineering. Poster, 7th KMM-VIN Industrial Workshop (IW7) 2017 'Biomaterials: Key Technologies for Better Healthcare', Erlangen, Germany.

B.5. Other external presentations

- Kremer A, et al. Tissue engineering of a meniscus implant. Talk, May 24, 2018 Department of Experimental Trauma Surgery, University of Regensburg, Germany.

- Kremer A, et al. Meniscus tissue engineering. Talk, Studienstiftung Doktorandenforum 2017, Bad Homburg, Germany.

- Kremer A, et al. Tissue engineering of complex tissues and their application from bench to bedside. Lecture, German-PolyU Innovation and Technology Development Lecture Series 2016: Public Lecture Applied Science Dedicated to Life, The Hong Kong Polytechnic University (PolyU), China.

- Kremer A, et al. Influence of mesenchymal stem cell differentiation by 3D co-culturing with meniscal cells in an equine model. Talk, October 10, 2016, Department of Biomedicine, University Hospital Basel, Switzerland.

Appendix C

Affidavit/Eidesstattliche Erklärung

Affidavit

I hereby confirm that my thesis entitled 'Tissue Engineering of a Vascularized Meniscus Implant' is the result of my own work. I did not receive any help or support from commercial consultants. All sources and/or materials applied are listed and specified in the thesis.

Furthermore, I confirm that this thesis has not yet been submitted as part of another examination process neither in identical nor in similar form.

Place, Date: ..... Signature:.....

Eidesstattliche Erklärung

Hiermit erkläre ich an Eides statt, die Dissertation 'Tissue Engineering eines vaskularisierten Meniskus-Implantates' eigenständig, d.h. insbesondere selbständig und ohne Hilfe eines kommerziellen Promotionsberaters, angefertigt und keine anderen als die von mir angegebenen Quellen und Hilfsmittel verwendet zu haben.

Ich erkläre außerdem, dass die Dissertation weder in gleicher noch in ähnlicher Form bereits in einem anderen Prüfungsverfahren vorgelegen hat.

Ort, Datum: ..... Unterschrift:.....

Appendix D

Acknowledgment

I would like to express my sincere gratitude to **Prof. Dr. Heike Walles** for the opportunity to perform my PhD thesis at the Department Tissue Engineering and Regenerative Medicine (TERM). Thanks for your support, scientific guidance and valuable advice during the whole time of my PhD thesis. In this context, I would also like to thank the **Studienstiftung des deutschen Volkes** for my PhD scholarship.

My gratitude goes also to **Prof. Dr. Michael Raghunath**, **Dr. Jörg Teßmar**, **Dr. Kai Fehske** and **Dr. Iris Ribitsch** as further members of my PhD thesis committee. Thank you all for the critical discussion of my results and sharing your knowledge with me. Special thanks go to Michael for your good ideas and the support on the CPX paper and to Kai for the support regarding meniscal sutures.

As there were a lot of changes during my PhD thesis regarding PostDoc supervision, thanks go to **Dr. Jenny Reboredo**, **Dr. Maria Steinke**, **Dr. Florian Gröber-Becker** and **Dr. Franziska Ehlicke**. Further thanks go to **Dr. Marietta Herrmann** who regularly took the time to critically discuss my experimental plans and results.

I would like to thank **Dr. Andreas Seitz** and **Prof. Dr. Lutz Dürselen** from the Institute of Orthopaedic Research and Biomechanic, Ulm University for the cooperation regarding biomechanical measurements. Thanks for your support to perform the biomechanical measurements in Ulm and the excellent discussions. Furthermore, I would like to thank **Dr. Anke Hoppensack** and **Dr. Marie Weinhart** from the Freie Universität Berlin for the excellent cooperation regarding cell sheet engineering. For providing equine tissue biopsies, I would like to thank the University of Veterinary Medicine in Vienna, particularly **Dr. Iris Ribitsch** for extracting equine tissue biopsies and the excellent cooperation. Furthermore, I would like to thank Iris for proofreading my PhD thesis. Further thanks go to **Werner Stracke** from Fraunhofer ISC for the SEM

support, and to **Prof. Dr. Alma Zernecke with Melanie Schott** from the University Hospital Würzburg to use their polarized light microscope.

Moreover, I express my thanks to **all colleagues of TERM** for the friendly and co-operative atmosphere in the lab. It was a pleasure to work with you all. Special thanks go to my former master student **Maximiliane Wußmann** who did an excellent master thesis and was a big support in the lab. Thank you for the great time in and outside of the lab. I deeply express my thanks to my former lab colleague **Dr. Andrea Schwab** for her friendship. Besides having a great time together in and outside of the lab, she always listened to my ideas and challenges of my research project. Thank you very much. I further want to thank the **skin group**, my final belonging group at TERM and the bioreactor group with **Prof. Dr. Jan Hansmann**, **Marius Gensler**, **Thomas Schwarz**, **Marc Möllmann** and **Dirk Neubauer** for the support regarding wedge-shape compression and biomechanical stimulation.

Last but not least, I would like to thank especially **my family and all my friends** for their mental encouragement. I really appreciate their everlasting trust in me, my research study and future aims. In particular, I owe my deepest gratitude to **my parents**. Thank you for your support throughout my life and all your love.